NOTICE

The quality of this microform is heavily dependent upon the quality of the original thesis submitted for microfilming. Every effort has been made to ensure the highest quality of reproduction possible.

If pages are missing, contact the university which granted the degree.

Some pages may have indistinct print especially if the original pages were typed with a poor typewriter ribbon or if the university sent us an inferior photocopy.

Reproduction in full or in part of this microform is governed by the Canadian Copyright Act, R.S.C. 1970, c. C-30, and subsequent amendments.

AVIS

La qualité de cette microforme dépend grandement de la qualité de la thèse soumise au microfilmage. Nous avons tout fait pour assurer une qualité supérieure de reproduction.

S'il manque des pages, veuillez communiquer avec l'université qui a conféré le grade.

La qualité d'impression de certaines pages peut laisser à désirer, surtout si les pages originales ont été dactylographiées à l'aide d'un ruban usé ou si l'université nous a fait parvenir une photocopie de qualité inférieure.

La reproduction, même partielle, de cette microforme est soumise à la Loi canadienne sur le droit d'auteur, SRC 1970, c. C-30, et ses amendements subséquents.

MODELING OF RADIAL WATER/OIL DISPLACEMENT IN WATER-WET POROUS MEDIA

Nader Agharazi-Dormani

A thesis submitted to the School of Graduate Studies and Research
in partial fulfillment of the requirements for the
degree of
DOCTOR OF PHILOSOPHY
in the Department of Chemical Engineering
University of Ottawa

ISBN 0-315-70512-4

UNIVERSITÉ D'OTTAWA
UNIVERSITY OF OTTAWA

"Rationally, let it be said in a whisper, experience is certainly worth more than theory"

- Amerigo Vespucci

ABSTRACT

The effects of five important operating variables and four dimensionless groups on oil recovery and finger formation during the immiscible radial displacement of oil by water in a consolidated water-wet porous medium were investigated using statistical model building techniques. Two different approaches were used. In the first approach the operating variables studied included: (1) the flow rate (capillary, intermediate and viscous regions, i.e. low, moderate and high flow rates, respectively) of the injection fluid, (2) the radial distance from the injection point, (3) the viscosity difference between the displaced and displacing phases, (4) the permeability of the porous medium, and (5) the oil/water interfacial tension (IFT). The measured responses were the fractional oil recovery and the number of fingers measured at the breakthrough condition. Experiments were carried out according to a central composite design with partial replication over the following operating region:

Flow rate of injection fluid	$0.65 \leq Q \leq 510.00$ (mL/h)
Radius of breakthrough	$2.5 \leq R \leq 7.0$ (cm)
Viscosity difference	$15 \leq \mu_o - \mu_w \leq 152$ (mPa.s)
Permeability	$13.33 \leq K \leq 77.41$ (μm^2)
Interfacial tension	$0.3 \leq \gamma \leq 30.0$ (mN/m)

A second-order polynomial of the general form

$$Y = \beta_o + \sum_{i=1}^{5} \beta_i X_i + \sum_{i=1}^{5} \sum_{j=1}^{5} \beta_{ij} X_i X_j$$

was fitted to the data.

The resulting models were simplified whenever possible and subsequently checked for their adequacy using both qualitative as well as quantitative lack-of-fit tests.

It was found that for water-wet systems, the recovery decreased as the viscosity difference increased and this effect became more significant as the flow rate increased. Conversely, as the breakthrough radius or permeability of the cell increased, the recovery increased. The effect of IFT was negative and also depended on the level of viscosity difference and permeability. In addition, an increase in flow rate, breakthrough radius or the viscosity difference resulted in an increase in the number of fingers, while high permeability reduced the number of fingers. Again the role of IFT was more complex and depended on the value of other operating variables.

In another approach the operating variables were grouped together in dimensionless terms such as the capillary number and the viscosity ratio, and the parameters (β_i's) were estimated for these dimensionless terms according to a second order model of the form:

$$Y = \beta_o + \sum_{i=1}^{4} \beta_i X_i + \sum_{i=1}^{4} \sum_{j=1}^{4} \beta_{ij} X_i X_j$$

over the following operating region:

$$0.09 < B_1 = (Q\mu_w / K\gamma) < 122882.00$$

$$329.6 < B_2 = (h/\sqrt{K}) < 794.3$$

$$8.62 < B_3 = (R/h) < 24.14$$

$$4.9 < B_4 = (\mu_o/\mu_w) < 153.0$$

The recovery was found to be enhanced with an increase in the ratio of breakthrough radius to the cell thickness (R/h). It was, however, reduced as the viscosity ratio increased and this attenuating effect became more significant as the flow rate increased. The effect of ratio of the cell thickness to the square root of the permeability ($h/\sqrt{K}$) and capillary number depended on the value of other variables. The number of fingers increased as any of the above ratios was increased with the exception of ($h/\sqrt{K}$) where the effect was more complex. The analysis of the same data by non-linear parameter estimation methods produced almost similar results. The degree of certainty associated with these results, however, was lower than those obtained by the linear least squares parameter estimation method. In general the results are in agreement with previous work and theory. In considering all five variables and their interactions at the same time, a better understanding of the oil recovery process has been achieved. In addition some previously reported but not fully understood results were explained and further extended. The systematic approach using experimental design and various analysis techniques is new for these types of systems.

ACKNOWLEDGMENTS

I would like to thank my two research supervisors, Drs. V. Hornof and G. Neale, for their invaluable assistance and guidance throughout this work. I would also like to thank Dr. D. McLean of the Department of Chemical Engineering for his valuable advice and assistance.

Equally, I feel that thanks are due to Messrs. G. Gasperetti, L. Tremblay and A. Bonaldo for their technical assistance.

The assistance and financial support of NSERC (National Sciences and Engineering Research Council of Canada) and the University of Ottawa are also greatly appreciated.

In particular, I would like to acknowledge my gratitude for the very valuable comments and recommendations made by the External Examiner (Dr. Ramon G. Bentsen of the University of Alberta, Edmonton) at the final defence examination on August 12, 1991.

TABLE OF CONTENTS

LIST OF TABLES

To the memory of my mother and to my father...

1 - INTRODUCTION

Petroleum is the main energy source in Canada and in almost all other countries. Over 70,000 by-products, of a very wide range, are produced from petroleum. The many interrelationships between petroleum and our everyday life have made us dependent on oil to a very great extent.

Unfortunately, at present rates of consumption, the proven oil reserves of the world recoverable by today's technologies will only provide a 30-40 year supply. The situation in Canada is even less hopeful because Canadian reserves will be depleted by the first decade of the twenty-first century. The geopolitical instability of the oil-rich middle eastern countries makes the future economics and market of oil so uncertain that we must look for alternative sources and recovery technologies. In Canada, tar sands and heavy oils are two such resources. However, economic as well as technological restraints have made the utilization of these sources quite limited. Enhanced oil recovery (EOR) clearly offers one of the best chances for reducing Canada's dependency on foreign oil.

Primary Recovery

Conventional methods of oil production relying on internal reservoir pressure are designated Primary Recovery. In the early stages of oil recovery from a new oil field, much of the pressure required to force the oil to the surface is obtained from the confined fluids (caused by hydrostatic pressure of the surrounding aquifer, and/or the pressure of gases dissolved in the oil). However, continued production results in decreased reservoir pressure to a point where it becomes necessary to use pumps to "lift" the oil from the well to the surface. The primary recovery stage typically produces 10-30% of the original oil-in-place (OOIP) from conventional oil reservoirs (1).

Secondary Recovery

The decreasing force available to drive the oil into the well-bore, as well as the pressure of the gas in the emptied pore space, adversely affect the oil production. To overcome the drop in internal pressure, external energy must be supplied to the reservoir. A technique called "pressure maintenance" will accomplish this task. It consists of injection of large volumes of water (or in some cases gas) through another well, the so-called injection well (Figs. 1-2). The injected fluid will force the oil out of the porous rock towards the production well. It will restore the pressure in the reservoir and help to keep the dissolved gases in solution at the same time (something which will result in maintaining a low oil viscosity). To improve the performance of water flooding, a number of reagents such as acids, alkalis, salts and polymers can be added. These processes are collectively termed secondary recovery processes.

Fig. 3 shows a plane view of some of the patterns in which injection wells are customarily drilled around the production wells. Secondary production techniques may produce anywhere from 10 to 30% additional recovery of the OOIP. In other words, 40-70 percent of OOIP still remains in the reservoir after completion of primary and secondary recovery processes.

Tertiary Recovery

Water flooding works quite well in displacing oil from reservoirs and it is also relatively inexpensive. However, since the early 1970's, the number of prospective North American fields in which water flooding could be applied has been declining. The next step to maintaining oil production is to recover a "third crop" of oil from those fields which have already undergone primary and secondary recoveries. To accomplish this, there are a number of various techniques which are collectively called Tertiary Recovery or Enhanced Oil Recovery (EOR) methods.

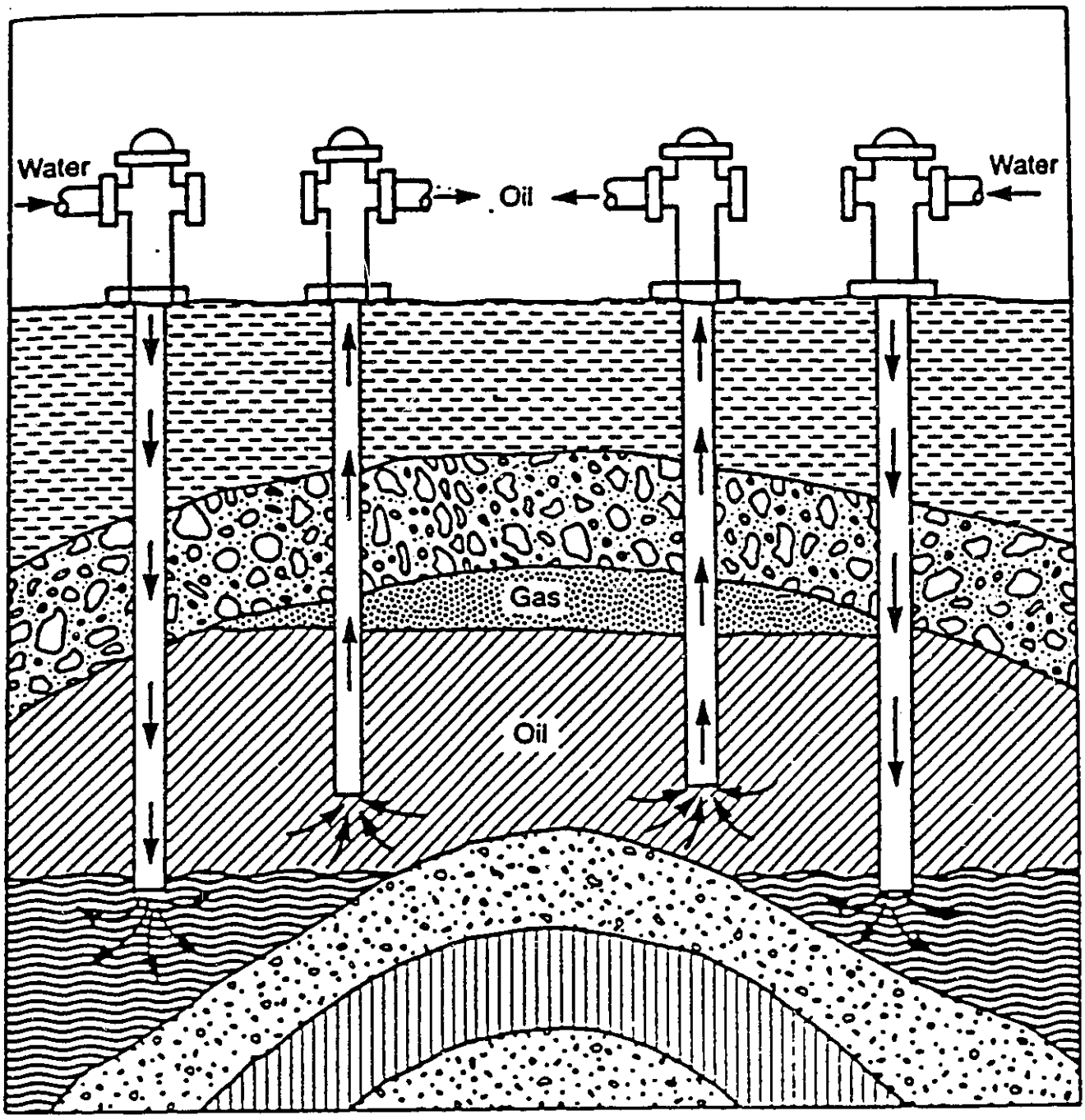

Fig. 1- Water flooding technique (2).

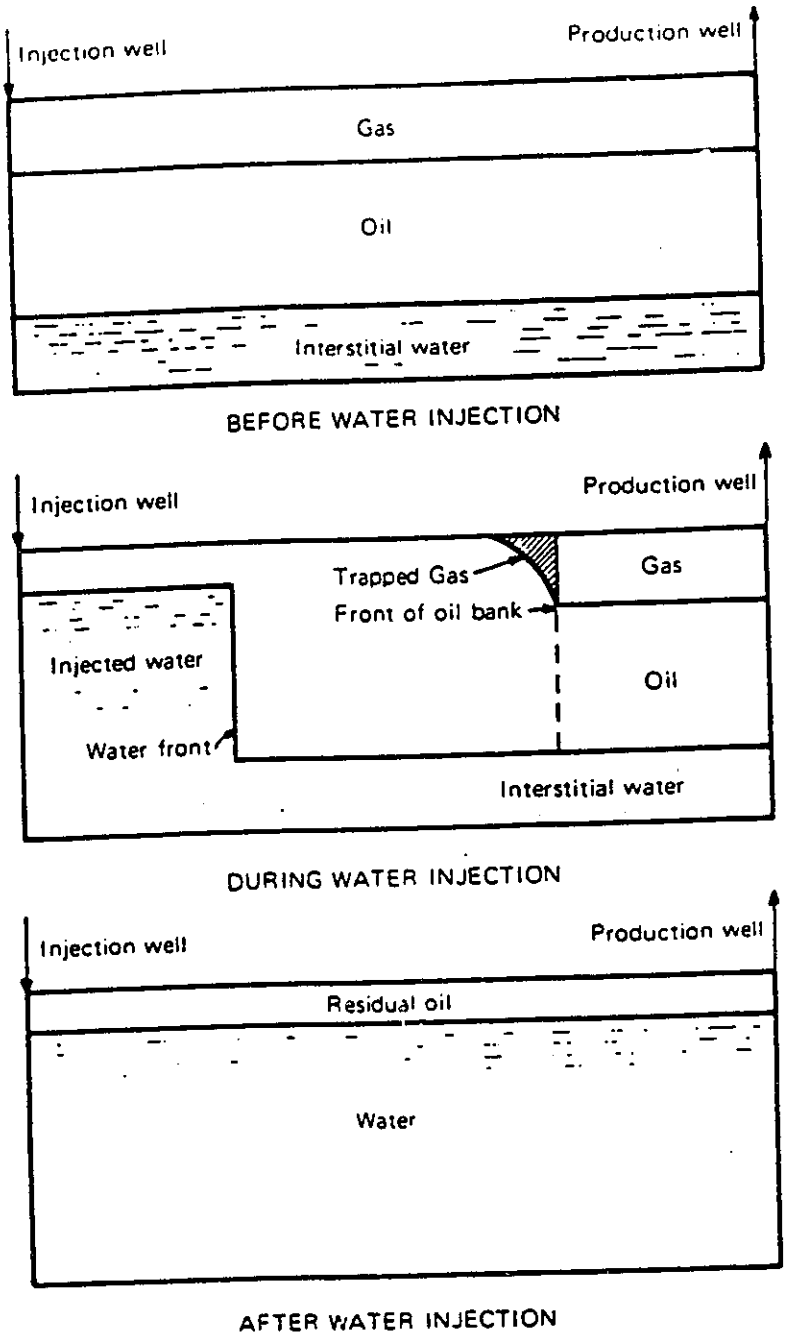

Fig. 2- Various stages of water flooding (3).

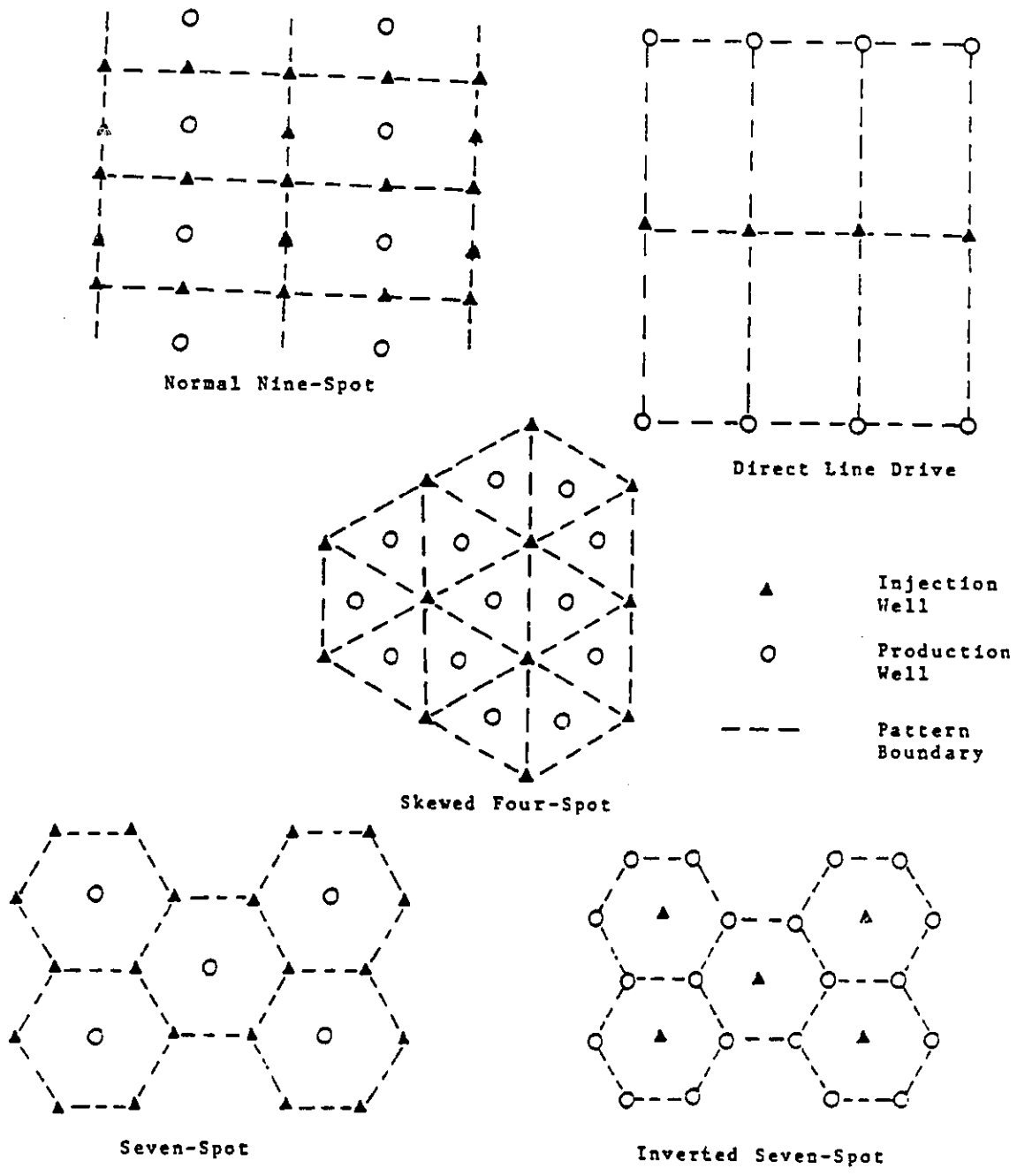

Fig. 3- Some of the patterns in which the injection and production wells are drilled.

Enhanced Oil Recovery (EOR)

Jha (1) has defined EOR as "all the techniques used to increase the amount of oil obtained after primary recovery". A broader definition, which has been adopted by the Alberta Energy Resources Conservation Board, states that "EOR is any oil production via artificial supplementation of natural reservoir energy" (4). By these definitions, EOR methods include:

- Pressure maintenance and waterflooding
- Steam flooding
- CO_2 injection
- Miscible fluid displacement
- Alkaline injection
- In situ combustion
- Steam stimulation
- Polymer injection

Fig. 4 is a classification of these and other related recovery methods (5).

The Potential of EOR

It has been estimated that 5-10 percent of the 640 billion cubic meters (1 m^3 = 6.29 barrels) of the OOIP in the world is recoverable by EOR, making it as important as exploring for new discoveries. In Canada, EOR will add 636 x 10^6 m^3 or 64% to the nation's remaining established light and heavy crude oil reserves of one billion cubic meters. Only about 30% of the light and medium and less than 10% of the heavy OOIP is recovered by primary and secondary recoveries. For the remaining 70 to 90 percent, EOR methods have to be employed (1).

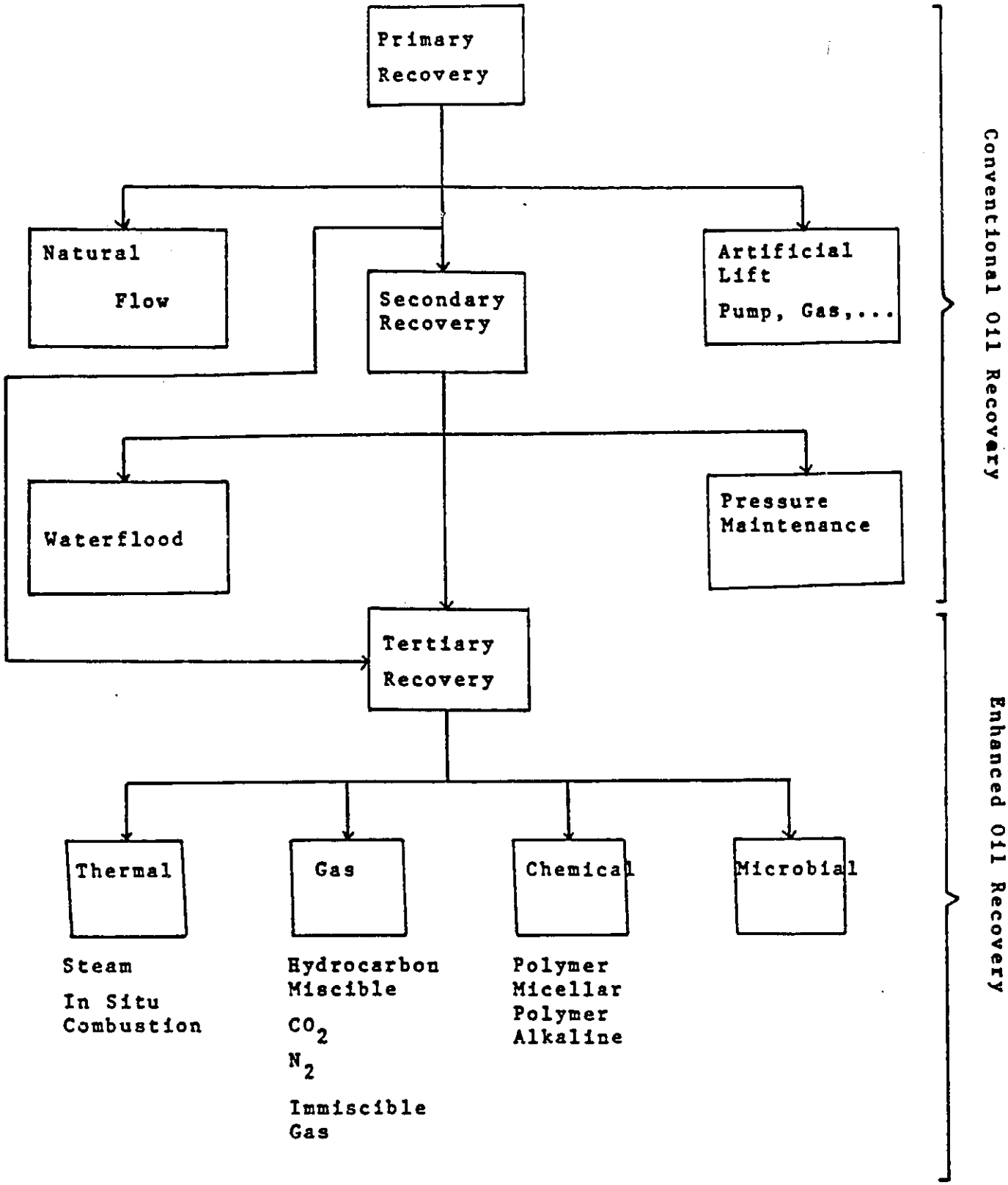

Fig. 4- Classification of recovery methods

In 1980, about 40 percent of the total oil produced in the United States, was recovered using EOR methods (including water flooding). In the U.S. alone, EOR is expected to produce 25-60 billion barrels from an otherwise unrecoverable 300 billion barrels (67% of Original Oil In Place - OOIP) of crude oil. Naturally, this would depend upon further improvements in recovery techniques and, of course, the price of oil. In 1984, EOR production in Canada was 74,400 bbl/day, up 5% from the previous year. Hydrocarbon miscible contributed 82.4% and steam 16.7% with 12,400 bbl/day.

Since EOR processes are high risk ventures, the level of activity will be related to the extent that business climate fosters such activity. Generous tax and royalty incentives are expected to spur additional EOR project activity; that is if the international oil prices do not remain at the present low level for long periods of time.

Of the many EOR schemes, immiscible flooding, including water flooding, is the most widely used. Unfortunately, interfacial instabilities which lead to viscous fingering during oil recovery by means of aqueous fluid injection cause serious losses in recovery. This phenomenon occurs whenever a less viscous fluid displaces a more viscous fluid in a porous medium; generally speaking, whenever the mobility ratio, $M = (k_w/\mu_w)/(k_o/\mu_o)$, is greater than one. The displacing aqueous phase tends to channel or "finger" through the paths of lesser hydrodynamic resistance in the porous rock, thereby leaving large regions of oil uncontacted and hence unrecovered. Typical fingering patterns in experimental cells for two different cases are shown in Figs. 5a,b and 6a,b. This phenomenon is one of the most poorly understood aspects of oil recovery processes in the field.

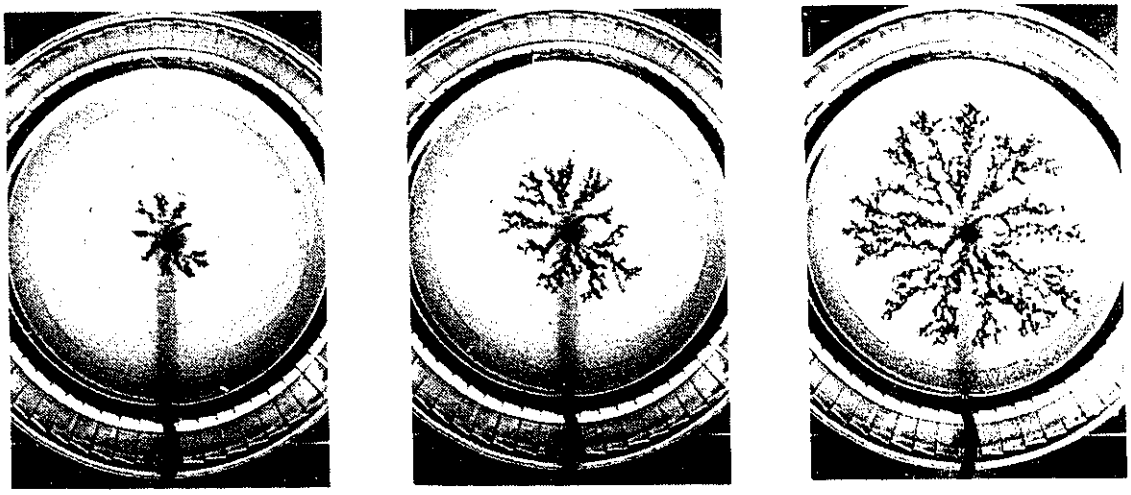

Fig. 5a- Fingering phenomenon for the case of high viscosity difference and high oil/water IFT (water-wet porous medium).

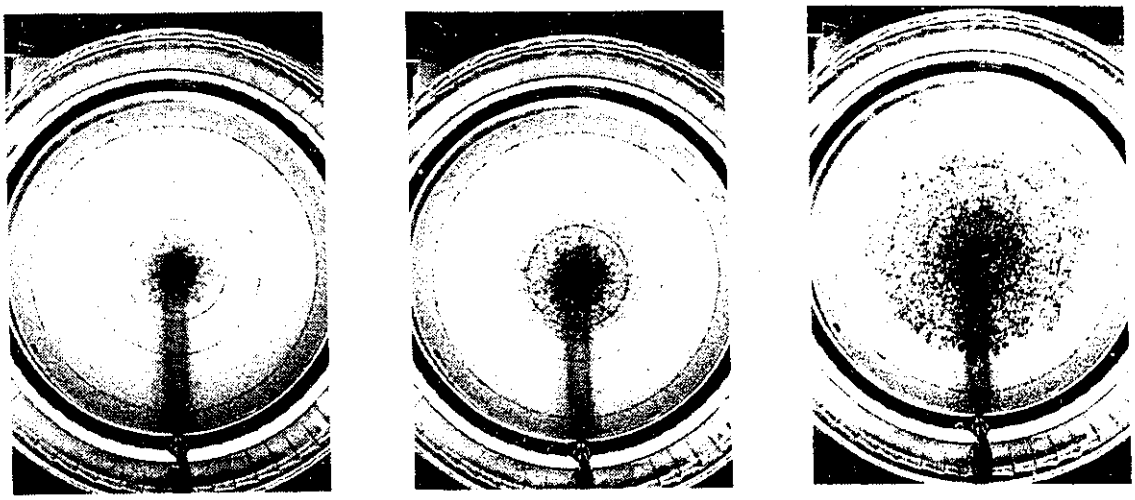

Fig. 5b- Fingering phenomenon for the case of low viscosity difference and low oil/water IFT (water-wet porous medium).

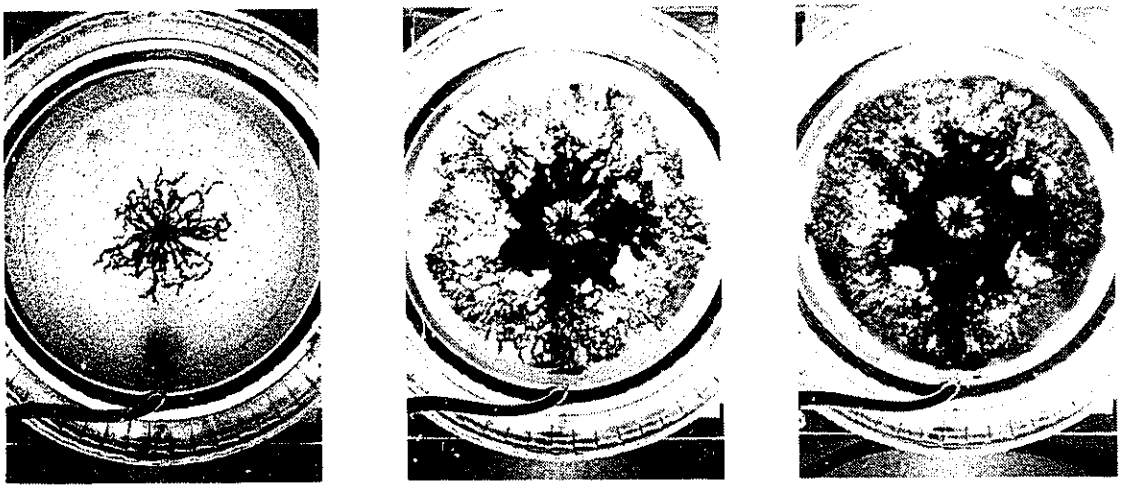

Fig. 6a- Imbibition caused by high P_c (low N_{ca}) followed by end effects (low K, high IFT and low Q).

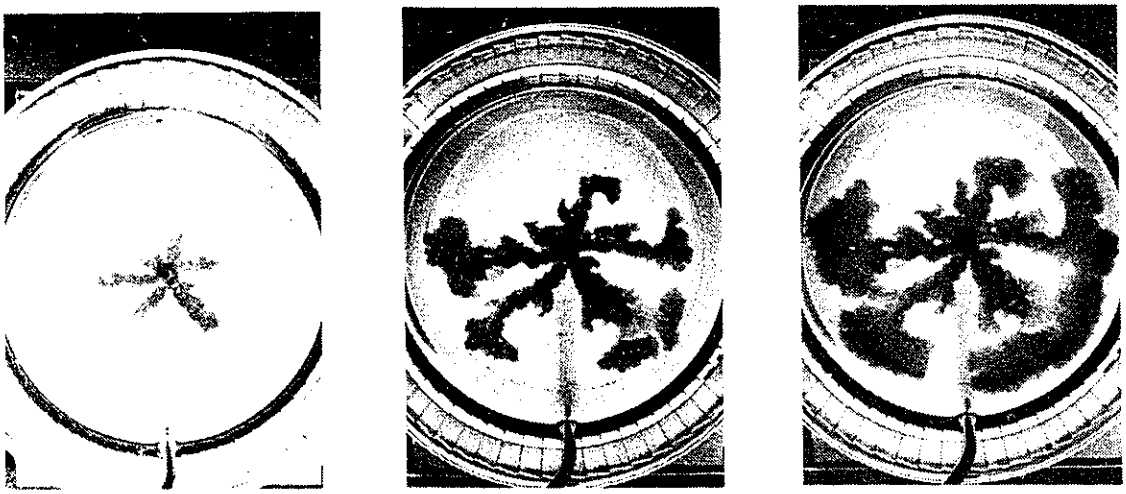

Fig. 6b- Imbibition caused by high P_c (low N_{ca}) followed by end effects (high K, low IFT and low Q).

2 - OBJECTIVES

The principal objective of this work was to determine the single and joint effects of several critical factors and dimensionless groups on finger formation and oil recovery at breakthrough in a water-wet porous medium over a wide range of injection rates. Previous investigators only investigated the main effects of two or three operating variables on the recovery and finger formation and have almost completely ignored the joint effects that these operating variables have on the process. This has led to unexpected results that could not be explained and were considered "strange". One of the objectives was to shed light on some of these so-called unexpected results.

Another important objective of the present work was to compare the results from linear and non-linear parameter estimation methods.

3 - FUNDAMENTAL PRINCIPLES AND CONCEPTS

Surface and Interfacial Tension

The free energy of any system in nature tends to a minimum. Thus, since the molecules at the surface are at a higher energy level than those in the bulk, the surface area of a pure phase will tend to decrease spontaneously. The surface of a liquid is therefore in a state of tension. The force per unit length tending to contract a liquid surface (L-V system) is called the surface tension γ_o. In the case of a L-L system, the interface between the two liquids still possesses a contractible tendency. Here it is called the interfacial tension (IFT) or γ_i.

Antonoff's law relates the interfacial tension of two mutually saturated liquids A and B to their surface tensions.

$$\gamma_{A/B} = |\gamma_{A/air} - \gamma_{B/air}| \qquad (1)$$

Since diffusion processes are often very slow, this mutual saturation could take days to establish.

In 1869 Dupré defined the work of adhesion between say oil and water as:

$$W_{o/w} = \gamma_{o/a} + \gamma_{w/a} - \gamma_{w/o} \qquad (2)$$

This force is a measure of adhesion between adjacent molecules of oil and water. Similarly work of cohesion is a measure of cohesive forces between molecules of a given liquid.

$$W_{oil} = \gamma_{o/a} + \gamma_{o/a} - \gamma_{o/o} \qquad (3)$$

$$= 2\gamma_{o/a}$$

and

$$W_{water} = 2\gamma_{w/a} \quad (4)$$

If attractive forces between oil-water molecules (adhesion) are greater than those between oil-oil and water-water (cohesion), then complete miscibility would be observed.

The Spreading Coefficient of oil on water is a measure of the ability of oil to be spread over (to wet) water and is defined as:

$$S_{o/w} = \gamma_{w/a} - \gamma_{o/a} - \gamma_{w/o} \quad (5)$$
$$= W_{w/o} - W_{oil}$$

Positive values of $S_{o/w}$ implies a decrease in free energy, A, upon spreading (spontaneous spreading).

Spreading will occur if adhesion between oil and water molecules is greater than the cohesion between oil molecules. In other words, spreading is expected when a liquid of lower surface tension is placed on one with higher surface tension ($\gamma_{w/a} > \gamma_{o/a}$).

Contact Angle and Spreading Pressure

The angle between the solid and the liquid/air interface (measured through the liquid) is finite and is called the contact angle θ. A contact angle equal to zero implies complete wetting of the solid where a $\theta = 180°$ implies complete non-wetting of the solid (see Fig. 7). At equilibrium

$$\gamma_{w/o} \cos \theta = \gamma_{s/o} - \gamma_{s/w} \quad (6)$$

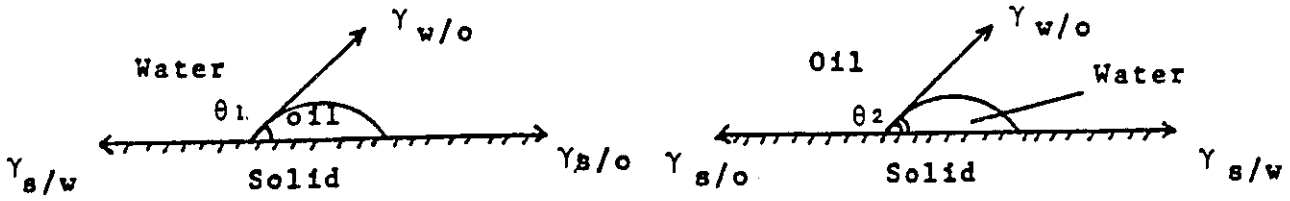

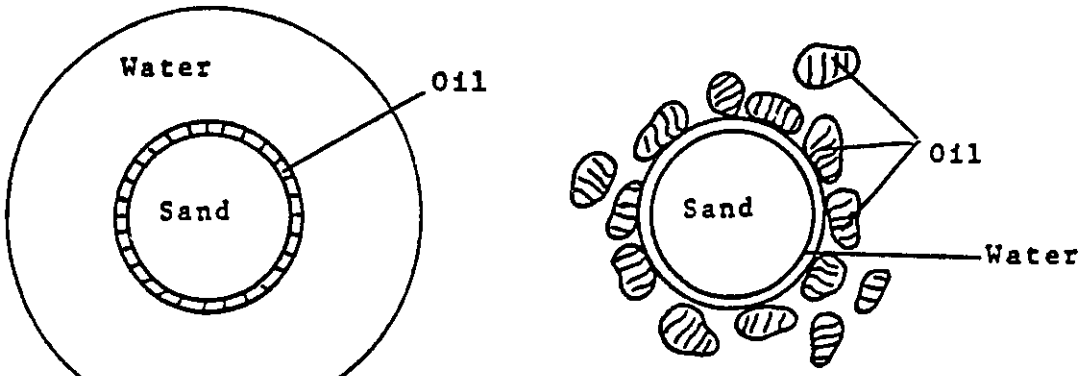

(a)

Oil-wet

$\theta_1 < \theta_2$

(b)

Water-wet

$\theta_1 > \theta_2$

Fig. 7- Oil-wet and water-wet sands

This is the famous Young equation and relates the contact angle to the interfacial tension at the three interfaces.

If sufficient solute is added to a pure liquid phase, an absorbed layer will usually appear at the interface. The thickness of this monolayer at L-V and L-L interfaces is about one molecular diameter. This monomolecular layer will normally reduce the contractile tendency of the interface. This phenomenon is due to the intense repulsive force between the molecules in the monolayer and is called the surface pressure or the spreading pressure and is given by Π. It could be defined as

$$\Pi = \gamma_o - \gamma_{sol} \tag{7}$$

where γ_o is the surface tension of the solvent and γ_{sol} the surface tension of the solutions. The absorbed film pushes back the liquid and therefore would increase θ or decrease cos θ (Fig. 8).

$$\cos\theta = \frac{(\gamma_{s/o} - \Pi) - \gamma_{s/w}}{\gamma_{w/o}} \tag{8}$$

On the other hand, if $\theta < 90°$, the surface is water-wet. A $\theta > 90°$ would represent an oil-wet surface. However, according to Greenkorn (6) the solid surface could be considered to have neutral wettability if $40° < \theta < 140°$. The wettability could be defined as the relative affinity of the coexisting oil and water phases to adhere to the surface of the rock. If the rock is predominantly in contact with water, it is said to be preferentially "water-wet" (PWW) (Fig. 9). If oil covers the rock predominantly, it is referred to as "oil-wet". If a reservoir is oil-wet, the residual oil is generally in the form of a thin layer spread over the reservoir rock (Fig. 7a). Conversely, in a water-wet reservoir, it appears as droplets of oil surrounded by connate water (Fig. 7b). This fundamental difference between oil-wet and water-wet reservoirs leads to two

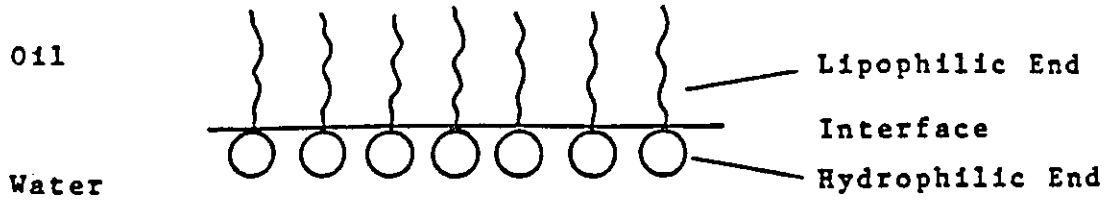

$$\Pi = \gamma_{s/o} - \gamma_{s/w}$$

Π = Surface Pressure of the Adsorbed Film

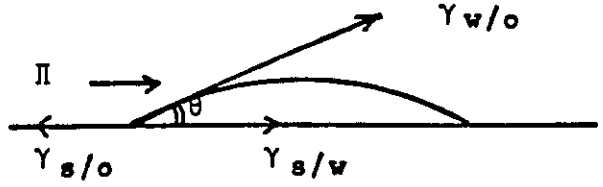

$$\text{Cos } \theta = \frac{(\gamma_{s/o} - \Pi) - \gamma_{s/w}}{\gamma_{w/o}}$$

If Cos θ decreases, θ will increase and so will Π ; This would result in a less water-wet medium.

Fig. 8- Surface pressure and adsorption

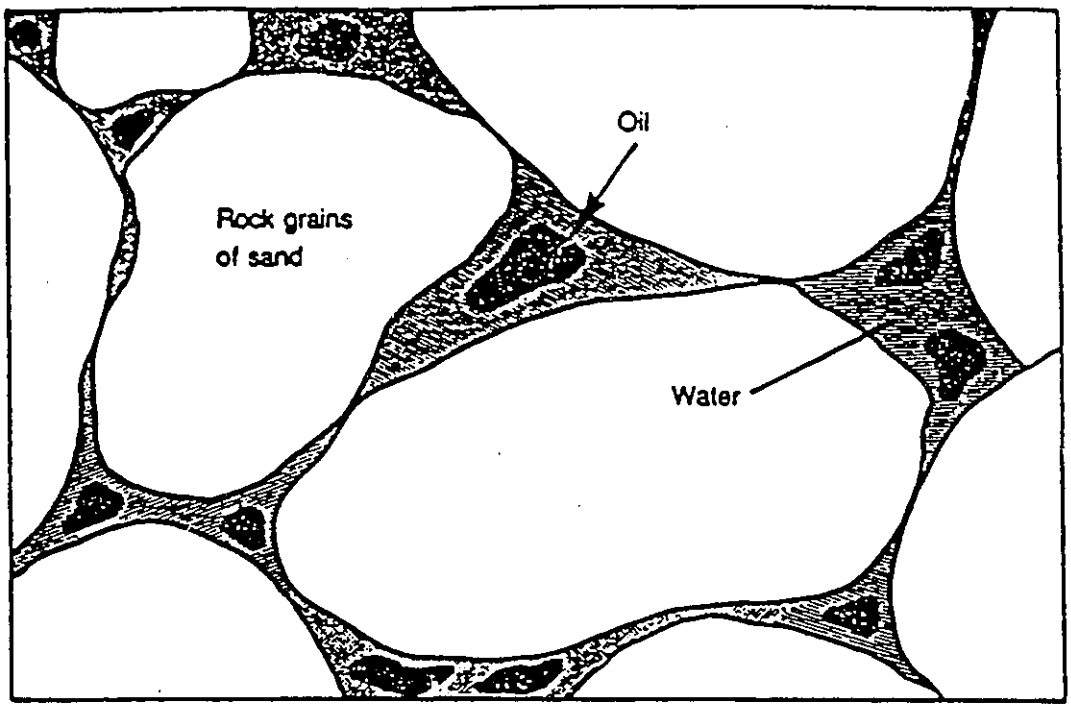

Fig. 9- Water-wet rock(2).

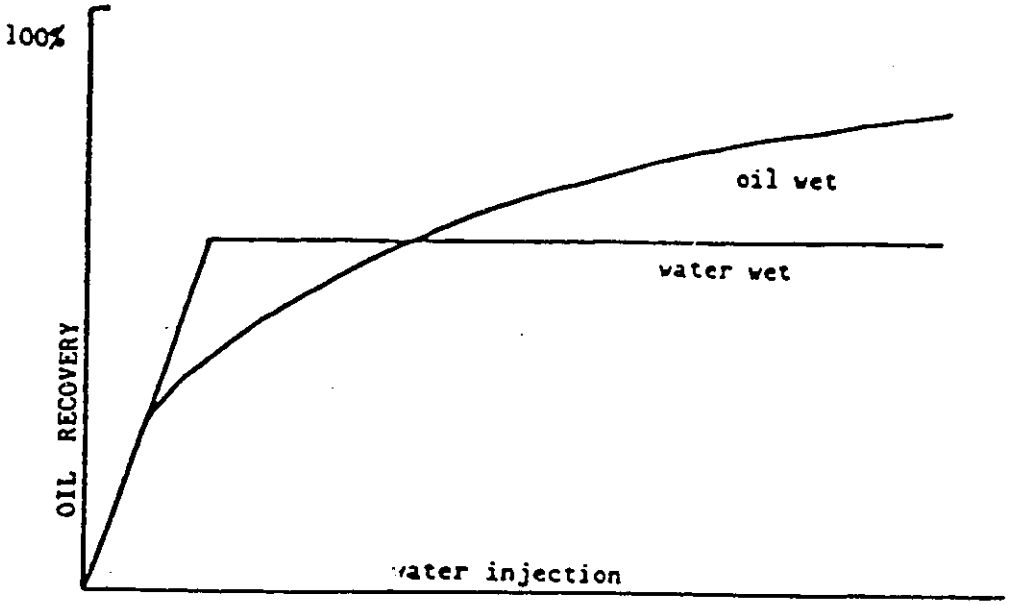

Fig. 10- Production history curve for water-wet and oil-wet porous media (2).

different recovery patterns during waterflooding. In an oil-wet reservoir the amount of oil recovered after breakthrough is considerable whereas in an water-wet reservoir there is virtually no oil recovered after breakthrough (Fig. 10).

In most cases, contact angles exhibit two limiting values rather than a single equilibrium one (contact angle or wettability hysteresis). In other words, the contact angle may be different depending on whether the fluid-fluid interface is moving to the left or the right. The magnitude of the contact angle depends upon the direction of prior movement of the liquid-liquid or oil-water interface. Receding and advancing contact angles, as they are called, are caused by surface roughness and phenomena associated with the adsorption of surface active agents (surfactants). In general the water-advancing contact angle is taken to characterize the reservoir wettability in the case of water displacing oil (Fig. 11).

It should also be noted that reservoir materials often possess various forms of mixed wettability; thus, the concept of uniform wettability (constant θ) is a simplification and idealization.

Capillary Pressure

The pressure difference between the oil and water phases at equilibrium in a pore is called the capillary pressure and is defined by Laplace's equation

$$P_o - P_w = P_c = \gamma_{w/o} R_{wo} \tag{9}$$

where R_{wo} represents the curvature of the interface and depends on the geometry (6).

For a porous medium of low and intermediate permeability (small pore throats) one could assume that the pressure is constant in each of the fluids. Therefore, the

Fig. 11- Advancing and receding contact angles.

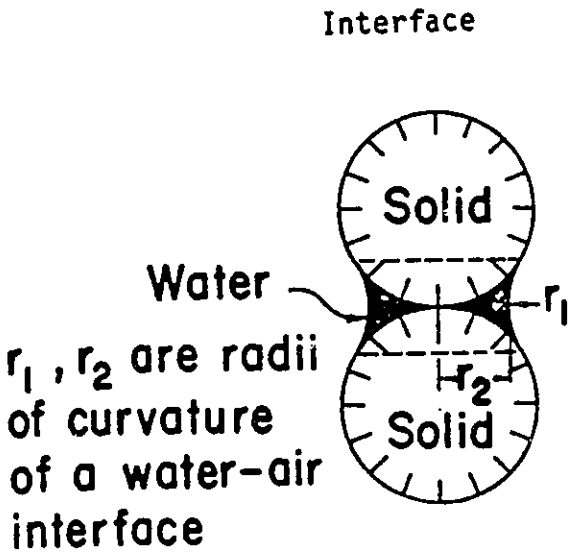

Fig. 12- Equilibrium at a curved interface between two immiscible fluids (liquid-air). (6)

interfacial tension between the two fluids does not depend on the radius of curvature.

Here Laplace's equation may be written in terms of the two principal radii of curvature as follows:

$$P_c = \gamma\left(\frac{1}{r_1} + \frac{1}{r_2}\right) \tag{10}$$

In the case of two flat plates separated by a distance $\frac{h}{2} = r_1 \cos\theta$, r_2 approaches infinity (Fig. 12) and Eqn. (10) becomes

$$P_c = \frac{2\gamma \cos\theta}{h} \tag{11}$$

For capillary tubes r_1 and r_2 could be replaced by their average r/2,

$$P_c = \frac{2\gamma \cos\theta}{r} \tag{12}$$

where r is the radius of the capillary.

For a porous medium saturated with a wetting fluid ($\theta = 0°$) the capillary pressure P_c can be related to the saturation of the displaced fluid S_w by a plot such as the one in Fig. 13. As the displacing (non-wetting) fluid displaces the wetting fluid, the capillary pressure is increased. This is called the drainage or drying.

The reverse case is when the medium is originally saturated by the non-wetting fluid and the wetting fluid imbibes and displaces the non-wetting fluid. This process is called imbibition or wetting and, as can be seen in Fig. 13, the capillary pressure decreases as S_w increases. The hysteresis in the imbibition and drainage curves is due to the instability of certain fluid-fluid interface configurations and to the contact angle hysteresis.

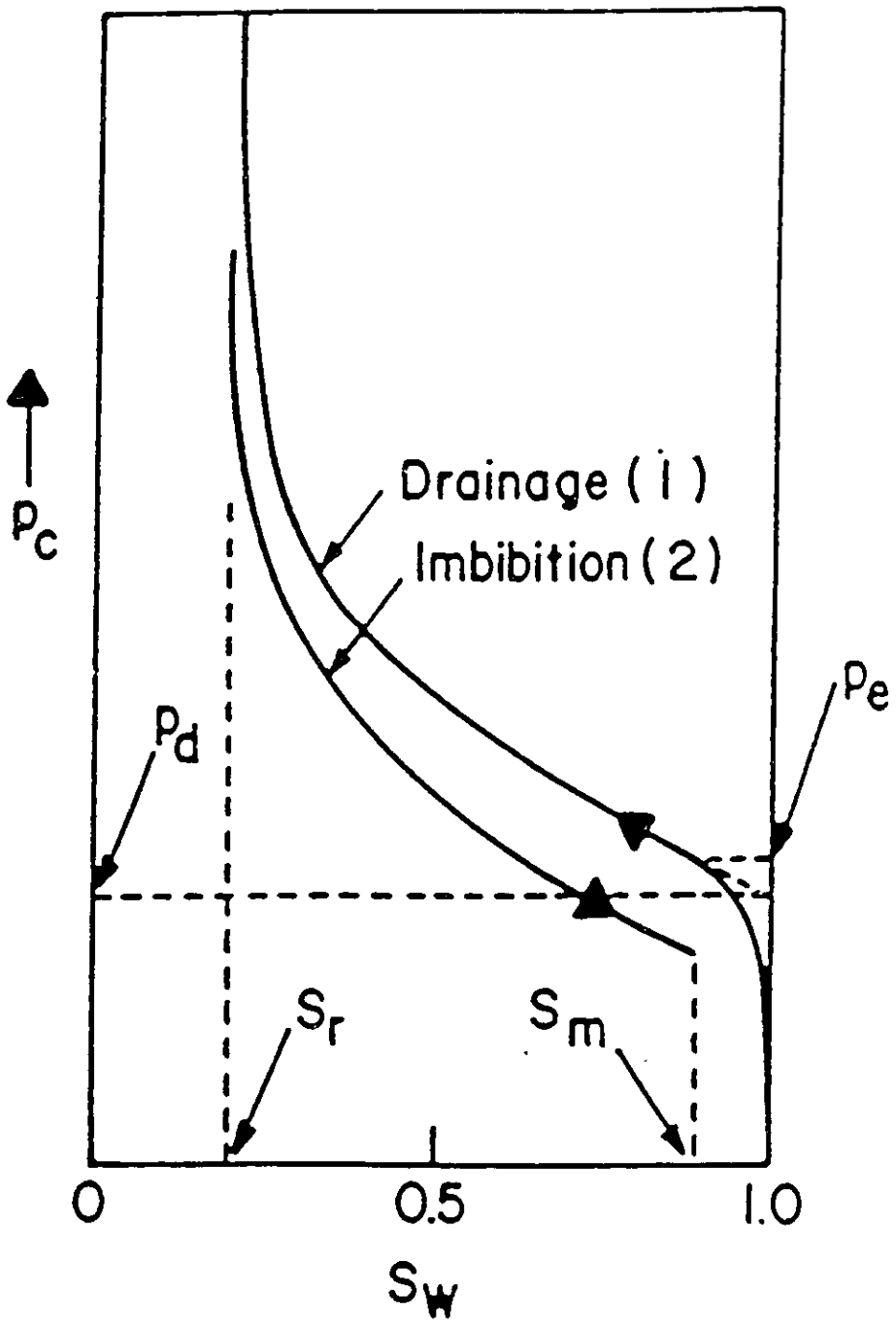

Fig. 13- Capillary pressure as a function of saturation (6).

Fluid-fluid interfaces in a pore may be stable or unstable in certain configurations depending on the geometry of the pores, the saturation and pressure drop across each pore (Fig. 14). The limiting number of stable configurations gives rise to the hysteresis described earlier. However, if the interface takes on an unstable shape, there will be sudden local flow in which one fluid will displace the other. This stuttering flow which restores equilibrium was first observed by Haines in 1930 and is referred to as "Haines jumps".

Morrow (7) performed some experiments with fine capillary glass tubes and showed that the capillary pressure does not rise smoothly and continuously with a decrease in saturation. He suggested the term "rheon" for this irreversible redistribution of fluid which resulted in a reduction of capillary pressure. This phenomenon can be better understood with the aid of a simple experiment such as that shown in Fig. 15. The two interfaces in the two capillaries are stable. However, if, in the left capillary, pressure were applied to push the interface into the bulge, the interface would be unstable and the bulge would immediately drain and come to equilibrium as in the right tube.

The microscopic displacement efficiency E_m is the fraction of the initial oil saturation S_{oi} that is displaced from the reservoir pores and is defined as:

$$E_m = \frac{1 - S_{or} - S_{wi}}{1 - S_{wi}} \tag{13}$$

where

S_{wi} = Irreducible water saturation (the fraction of pore volume containing water at infinite capillary pressure).

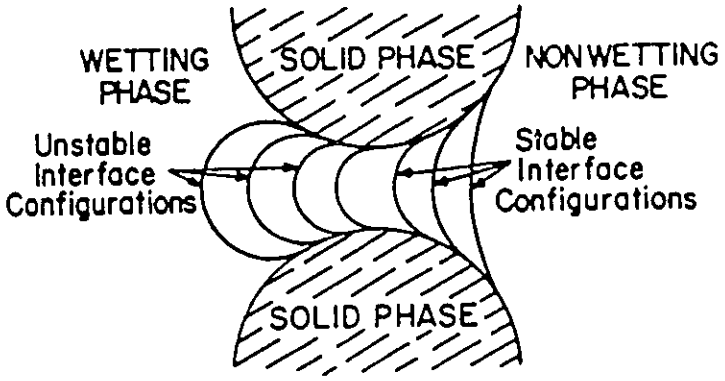

Fig. 14-a - Stable and unstable interface configurations (6).

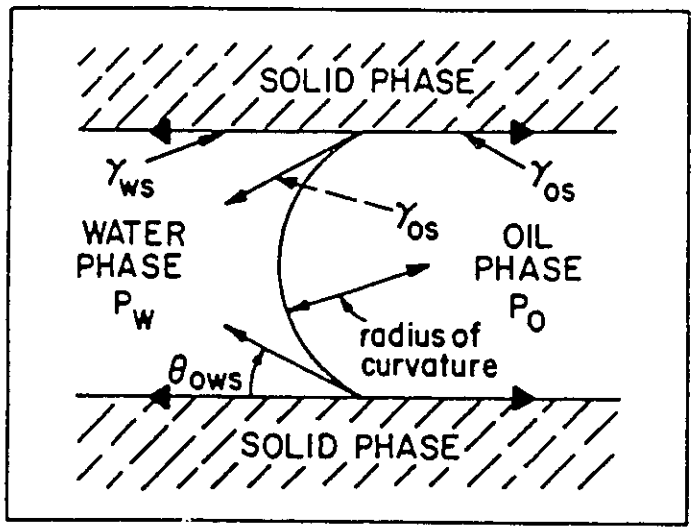

Fig. 14-b - Interfacial forces and contact angle (6).

Capillary Number

A small oil ganglion at rest in a liquid medium in the absence of gravity and other forces will be spherical. This is due to the thermodynamic demands of minimum free energy at equilibrium. In a porous medium, the oil ganglion could occupy most of a single pore space and could extend (if large enough) to fill an interconnecting set of pore spaces. In this case, its shape is determined mainly by the geometry of the pore structure. To move this trapped ganglion from the capillary constriction, a significant pressure is required.

The network nature of pore structure, and capillary forces, are responsible for the entrapment of one phase by another during immiscible displacement in porous media (8). The ratio of viscous to capillary forces is called the capillary number and can be expressed in several forms (9) such as:

$$N_{Ca1} = \frac{V\mu}{\gamma} \qquad (14\text{-a})$$

$$N_{Ca2} = \frac{K\Delta P}{L\gamma} \qquad (14\text{-b})$$

$$N_{Ca3} = \frac{V\mu}{\gamma \cos\theta} \qquad (14\text{-c})$$

$$N_{Ca4} = \frac{V\mu}{\gamma\varepsilon} \qquad (14\text{-d})$$

where $\Delta P/L$ is the imposed pressure gradient across the sample of length L.

Chatzis et al. (8) showed that for water-wet sandstones the capillary number (Eqn. 14-b) needed for complete recovery of residual oil was about 100 times greater than the critical capillary number for the onset of mobilization.

We introduce a new capillary number in this work defined as:

$$N_{Ca} = \frac{Q\mu}{K\gamma} \qquad (15)$$

This capillary number is very similar to Eqn. 14-d but the pore velocity ($V_p = \frac{V}{\varepsilon}$) has been replaced by (Q/K) which is an indication of the velocity if all of the flow, Q, were to occur in a single pore. The advantage of this capillary number is that it remains constant even in the case of radial flow (whereas the traditional capillary numbers that are based on V, the velocity, vary with time for constant Q). Other laboratory studies (9, 10) have shown that residual oil can be recovered if the displacing phase causes viscous forces acting on the residual oil to exceed the capillary retaining forces. Foster (11) found a correlation between the capillary number and the residual oil in porous media (Fig. 16).

At the end of water flooding, the trapped oil in the porous medium is in the form of oil ganglia. At this stage, the capillary number has a typical value of around 10^{-6}. This number has to be increased to 10^{-2} - 10^{-4} in order to remove any additional amount of oil that is trapped due to capillary forces in the rock pore structure (Fig. 17a). This could be done by injection of a surfactant solution. Surfactants lower the oil/water interfacial tension from 20-30 mN/m to 10^{-3} or 10^{-4} mN/m. The displaced oil ganglia will coalesce subsequently to form an oil bank (see Fig. 17b).

This ultra low IFT has to be maintained in order to minimize the entrapment of oil at the trailing edge of the oil bank. In most cases a mobility control polymer slug is also injected after the surfactant (Fig. 17c). The flow of these three fluids in the porous medium causes dispersion of these fluids and usually emulsions are formed at the oil/surfactant interface which will subsequently result in mixing of the polymer and surfactant phases. Another potential problem arises when high viscosity structures are formed in the oil-water-surfactant interfaces. For the above reasons, the choice of the right surfactant in tertiary oil recovery is essential.

The Bond number is the ratio of gravitational to interfacial forces (6) and is defined as

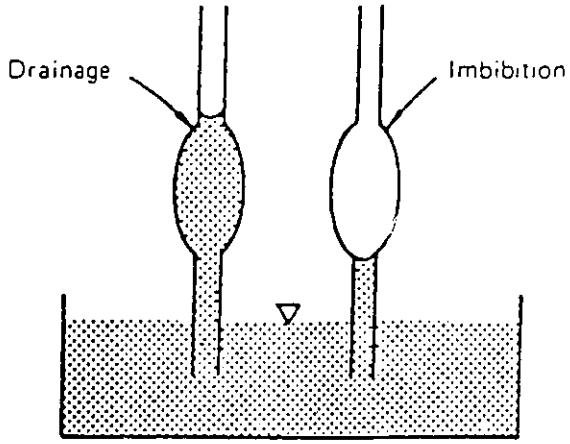

Fig. 15- Capillary hesteresis (6).

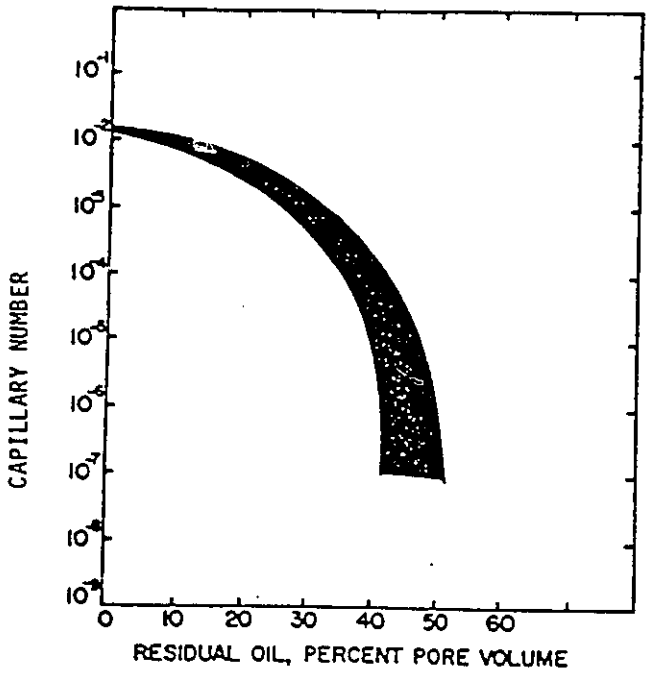

Fig. 16- Dependence of residual oil saturation on capillary number (12).

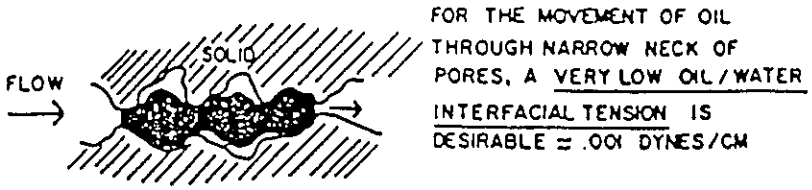

Fig. 17-a - Schematic diagram of the role of low IFT in the surfactant flooding process (12).

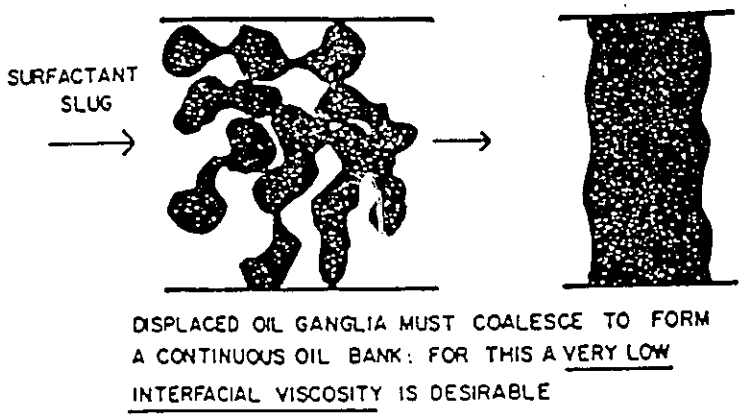

Fig. 17-b - Schematic diagram of the role of low interfacial viscosity in the surfactant flooding process (12).

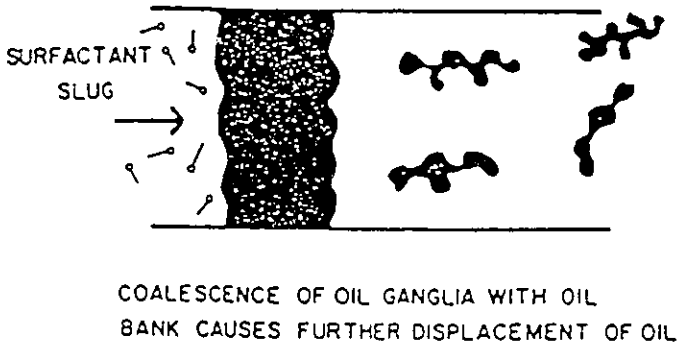

Fig. 17-c - Schematic diagram of the role of coalescence of oil ganglia in the surfactant flooding process (12).

$$N_B = \frac{(\rho_w - \rho_o)gK}{\gamma \varepsilon} \qquad (16)$$

The gravitational forces act in a vertical manner whereas the force exerted by water on the trapped oil is mostly in the horizontal direction. Gravity segregation of oil and water can occur at a Bond number of about 10^{-2}. At this point the water will tunnel through the lower strata of the reservoir. This number, however, has not received much attention in the petroleum industry.

Relative Permeability

The flow of two or more immiscible fluid phases through a porous medium can be described by applying Darcy's law or the concept of permeability to each phase separately where the flow rate of each phase is related to a the pressure drop gradient and the effective permeability for each phase. The effective permeability is defined as

$$k_{ei} = K \cdot k_{ri} \qquad (17)$$

where i denotes either the wetting or the non-wetting phase, k_r is the relative permeability or the ease with which that particular phase passes through the porous medium and K is the absolute permeability. The sum of effective permeabilities is always less than the absolute or single-phase permeability due to mutual interference between fluids flowing through an interconnected pore system. The effective permeabilities depend upon the saturation and saturation history of the phases, pore geometry, wettability and fluid distribution (Figs. 18-a, b). On the other hand, Bear (13) showed that the permeability could be related to the particle diameter by the following empirical relationship.

$$K = 6 \times 10^{-4} d_p^2 \tag{18}$$

Paterson et al. (14) found the lower bound for maximum instability in a porous medium to be

$$\lambda \cong 40\sqrt{K} \tag{19}$$

Spanos (15), however, showed analytically that the lower limit of finger wavelength in porous medium is

$$\lambda \cong \sqrt{3K/2} \tag{20}$$

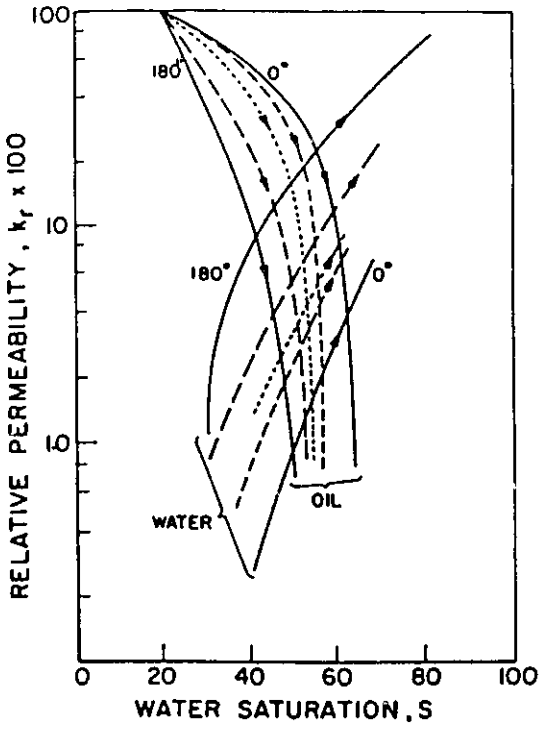

Fig. 18-a - Relative permeabilities for the spectrum of wetting conditions (6).

Displacement in Immiscible Flow

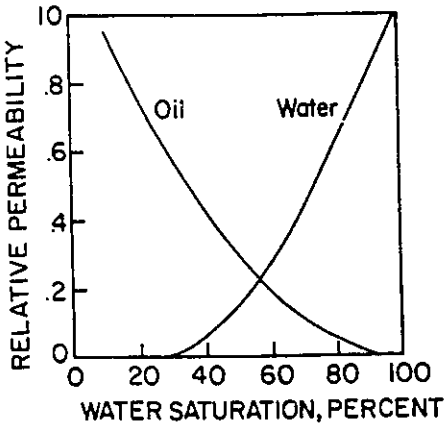

Fig. 18-b - Effect of saturation on relative permeabilities to water and oil in unconsolidated porous medium (6).

4 - LITERATURE SURVEY

Most previous displacement studies concerning viscous fingering have utilized unconsolidated porous media in spite of serious difficulties with respect to reproducibility of such important factors as porosity, permeability, wettability and structural heterogeneity. To avoid these problems, a consolidated porous medium consisting of sintered glass beads sandwiched between two parallel glass plates was used in the present work. Previous investigators (14, 16, 17) who used consolidated porous media studied linear flow situations in which it is very difficult to establish an initial planar displacement front. Furthermore, during EOR in the field, the invading fluid is injected as a point source through a well. Consequently, the initial displacement is in the radial direction. For these reasons radial displacement was employed in this work. There are certain limitations, however, in any laboratory work with regard to the distance from the injection point. On the other hand, large ratios of finger width to the lateral dimensions of the system in the laboratory compared to the same ratio in the field presents another limitation of models such as beadpacks or consolidated porous media (18).

Previous analysis of EOR processes (19, 20) has identified the flow rate of the injection fluid, the difference in viscosities of the displacing and displaced fluids (or their ratio), the permeability of the porous medium, the oil/water interfacial tension, and the breakthrough radius, as the primary operating variables affecting finger formation and recovery. However, the associated mechanisms are not well understood. Investigations to date have been limited to individually examining the influence of only one or two of these variables (21-32). As a result, little information exists as to the joint or interaction effects of all of these important factors. Indeed, the physico-chemical processes involved in EOR suggest that the effect of each factor on finger formation and oil recovery may well depend upon the levels of the other factors.

In 1927, Uren and Fahmy (33) did some rather simple experiments and obtained some general results that are still valid after over sixty years. They investigated the effect of several operating variables, one at a time, and concluded that the conditions for maximum recovery during waterflooding are: high porosity and large and uniform grain size, intermediate wettability, low viscosity, high temperature, slow injection flow rate and low IFT.

Interfacial tension (IFT) has long been known to be one of the most important factors during immiscible oil displacement. The importance of IFT reduction on oil recovery has been recognized since the early 1940's. By then, some companies were starting to produce and commercially sell surfactants (they were commercially known as "wetting-agents" then) as agents for waterflooding efficiency improvement. The laboratory experiments were not, however, very consistent and as Taber (9) reported, in some cases, the recovery was observed to have decreased with the addition of surfactants. Another problem was the adsorption of these surfactants on the surface of the solid rock. Taber (34, 35) recognized this phenomenon and performed some experiments with higher concentrations of surfactants (about 10%) to overcome the adsorption process and actually obtained improved and positive results. Nevertheless, he found that the most sensitive factor in surfactant flooding was the rate of flooding. He also observed that the widely different results obtained with various surfactants and various injection rates could be understood if the experiments were carried out at equivalent values of the ratio of viscous to interfacial forces. In his case, he used the ratio $\Delta P/L\gamma$ ([=] L^{-2}) and performed experiments at various flow rates for systems of different IFT. He found that additional oil recovery was obtained after the critical gradient was exceeded (35). This concept of capillary number or "critical displacement ratio" has been presented by many other workers in the field of surface phenomena and oil recovery (36, 24, 11, 37). Taber (9) has listed most of these workers and the group used by them. In general, almost every-

body agrees that displacement recovery will increase with an increase in the ratio of viscous to capillary forces. This is true if the effects of other variables are not considered (i.e., all other variables stay constant). Taber (9) reported cases where the recovery actually increased as the permeability of the porous rock was reduced even though experiments were carried out at constant values of ($V\mu/\gamma$). This observation underscores the dangers involved in generalizations without consideration of the effects of other variables that influence the oil recovery process. Other examples are common in the literature. Sayyouh et al. (38) found that for very low flow rates (therefore very low N_{Ca}) the recovery actually increased with further decrease in flow rate. The same behavior was observed by Nasr-El-Din et al. (20). Mungan (39) found that for an unconsolidated water-wet core, lowering the interfacial tension or increasing the viscosity of the displacing phase would enhance the recovery. Hornof and Morrow (40) showed that, in a thin water-wet porous medium, high IFT (>1 mN/m) would result in stable displacement with sharp fingers, while lower IFT displacements exhibited considerable degrees of instability which did not necessarily mean lower recoveries. Even lower IFT caused the interface to become fuzzy. They speculated that the instabilities may be due to gravity segregation which occurs if the capillary and viscous forces are not sufficient to overcome the effect of buoyancy forces. Newcombe et al. (41) showed that, for a water-wet porous medium, oil recovery increases as the IFT increases (this is not consistent with results found by Mungan), whereas in the case of an oil-wet system the opposite occurs. Sarma (42) noticed formation of many small fingers at the displacement front as the result of lower IFT in a water-wet porous medium. Chen (43) reported similar findings for Hele-Shaw cells. In general, as fingers grow, the interfacial area also increases but the IFT tends to minimize the surface area thereby acting as a stabilizing factor by inhibiting finger growth.

The flow rate of the displacing fluid has also been found to affect the recovery. Since the velocity in a fluid is proportional to the pressure gradient at any given point of that fluid and because this gradient is higher just ahead of an advancing finger, the growth of that finger is further enhanced. For an oil-wet porous medium Ni et al. (19) found three distinct relationships between flow rate and recovery depending upon the flow rate. At low flow rates recovery increased with flow rate; at intermediate flow rates recovery remained essentially constant; at high flow rates recovery decreased. These three regions were denoted as capillary, intermediate and viscous regions, respectively to reflect the importance of dominant forces acting at that flow rate. On the other hand, they found that the number of fingers increased with injection rate over the entire range of flows studied. Nasr-El-Din et al. (20) used the same concept for a water-wet system; these workers also distinguished three distinct regions and found that in the capillary region (i.e., very low flow rate) the recovery actually decreased with an increase in flow rate. As we will see later, our results from a much greater number of experiments and with the consideration of a wide range of other operating conditions reveal that, in this region, the flow rate does not influence the recovery. A closer examination of Nasr-El-Din's results, including photographs from his experiments, convinced us to conclude that the higher recoveries at the lowest flowrates were caused by mushrooming and imbibition due to end-effects (different from natural imbibition). Moreover, they found virtually no change in recovery with flow rate in the stabilized region. At high injection rates, they observed a decrease in recovery with an increase in flow rate (high degrees of imbibition at lower flow rates resulted in higher recoveries for such a water-wet system).

Reports on the effect of wettability on oil recovery are inconsistent and conflicting. For instance, different investigators have reported both increasing and decreasing oil recovery with an increase in the water-wetness of the porous medium.

The former, however, seems to be a more logical and consistent result because it is supported by the fact that the strong water-wetting preference of the porous medium is associated with strong capillary imbibition forces which in turn enhance the efficiency of oil recovery. In a water-wet medium there is little oil production after breakthrough, while in an oil-wet system the amount of oil produced after breakthrough is significant. Jennings (44) and Mungan (39) discovered that a waterflood in a water-wet porous medium is more efficient than a waterflood in an oil-wet core. In general, as the wettability of a system ranges from water-wet to oil-wet, the breakthrough and residual oil saturations (S_{OR}) increase, resulting in decreased oil recovery (45). As far as the shape of fingers is concerned, Peters and Flock (46) reported that fingers in water-wet porous media were about eight times wider than those in an oil-wet system. Morrow (47) found that an increase in the aging temperature, a decrease in the water saturation and to a lesser extent aging time all tend to make the core less water wet. He also showed that the oil recovery is optimal at neutral wettability ($\theta = 90°$) for a specific crude-oil/brine/rock (COBR) system.

Habermann (48) investigated the role of mobility ratio on the efficiency of miscible displacement and the fingering patterns. He found that fingering starts as soon as M becomes larger than 1 and that the efficiency of the recovery process was reduced as M is increased (degree of fingering increased with an increase in M or $\frac{\mu_o}{\mu_w}$). He also noticed an increase in the number of fingers with an increase in the injection rate. Chen (43) investigated the effect of flow rate on fingering in both rough and smooth Hele-Shaw cells. He observed narrowing of the fingers and more side breaking as flowrate increased. Very recently Tayal and Narayan (49) did experiments similar to those of Nasr-el-Din et al. (20) (linear as opposed to radial displacement). They studied the effect of flow rate on the oil recovery in both homogeneous (spherical glass beads) and non-homogeneous (irregular shaped polystyrene

particles) porous media. Only the injection flow rate was changed. The results were used to calculate the finger wavelengths using the well known Chuoke wavelength equation (50). They, however, used a value of wettability number C = 25, reported earlier by Paterson et al. (14, 16) for an oil-wet porous medium, for both cases without considering the wettability characteristics of the two porous media used. Their final results were similar to those obtained by Ni et al. (19) et Nasr-El-Din et al. (20).

The role of gravity on the oil flow in the reservoir has been investigated by Fayers and Muggeridge (51). In another approach Saffman and Taylor (36) established a criterion for the stability of an immiscible interface (in a gravitation field) in a Hele-Shaw cell. They introduced the concept of finger wavelength. Chuoke et al. (50) improved this theory by considering capillary pressure across the interfacial discontinuity in terms of an additional damping term, the effective interfacial tension-curvature product. These workers started with an equation of motion in the form of Darcy's equation. They considered the curvature of the microscopic interface to be proportional to the pressure drop between the immiscible fluids (incompressible). They concluded that the interfacial instabilities were related to the distance between the two plates, the velocity of the interface, and the viscosities and densities of the displacing or displaced phases. In addition they concluded that fingers with wavelengths less than a critical wavelength would decay and those with wavelengths close to that of the maximum growth would grow. Later on, Rachford (52) modified Chuoke's theory by considering the development of a transition zone behind the interface during the displacement of oil from a water-wet porous medium. In his numerical analysis he found that this zone tends to insulate perturbations of the interface from the high mobility water. More recently, Morrow (53) introduced a dimensionless wave number that correlated the wavelength of the fastest growing finger with pore size of the porous medium.

Spanos (15, 54) used the concept of a critical wavelength to describe the criteria for the onset of fingering. He related such fingering characteristics as the velocity of propagation of the finger and the time of an instability to factors such as the densities and viscosities of the phases and the permeability of the porous medium. Sigmund et al. (28) found that in a rectangular bead-pack, fingering was a function of flowrate and viscosity ratios. Jerauld et al. (55) investigated the capillary effect on the fingering and found that decreasing the capillary number would broaden the saturation front and slow the growth or decay of fingers (increase the finger wavelength) i.e. stabilize a displacement in a porous medium.

Lenormand et al. (21, 23) studied the case of injection of a non-wetting fluid into a two-dimensional porous medium. They showed the existence of three basic domains namely viscous fingering (where viscous forces are dominant), capillary fingering (where capillary forces are acting) and stable displacement within which the patterns remain unchanged. They then mapped the domain of validity of the three different basic mechanisms onto the plane with axes N_{Ca} and viscosity ratio.

In 1968, Bataille (56) investigated the stability of a moving interface in radial flow. Most authors have made use of the perturbation theory and some have calculated the wavelength for the fingers corresponding to maximum growth rate (17, 36, 50). In general, everyone predicted that as IFT tends to zero, the finger wavelength ($\lambda = 2\pi R^*/n$) approached zero. More recently, Paterson et al. (14, 16, 17) investigated the problem in a Hele-Shaw cell. In such cases, the flow is two-dimensional and for slow viscous flow (negligible inertial effects) the pressure drop across the interface is given by the Laplace equation

$$p_w - p_o = \gamma\left(\frac{1}{r} + \frac{2}{h}\right) \qquad (21)$$

where r is the principal radius of curvature of the finger tip (in the plane of the plate), and h is the plate separation. Ni et al. (19) later extended Paterson's work to the case of an oil-wet porous medium where

$$p_w - p_o = \gamma^*\left(\frac{1}{r} + \frac{1}{r'}\right) \tag{22}$$

where r' is the principal radius of curvature (normal to the plate) and γ^* represents an effective IFT. They made the following assumptions:

1) The flow of the displacing phase is two-dimensional (cell thickness is relatively small).

2) Since the microscopic radii of fingers in a porous medium are not known, a macroscopic radius is used in conjunction with the effective IFT.

3) There is no residual saturation effect (permeabilities are absolute permeabilities and the mobility ratio is equal to the viscosity ratio), i.e., displacement in the invaded zone is 100% effective. The second assumption made use of Chuoke's Equation (50), namely

$$\gamma^* = C^*\gamma \tag{23}$$

where C* is the wettability constant and is an indication of the ability of the porous medium to imbibe the displacing fluid (46). For an oil-wet porous medium C* has been reported to be anywhere from 5-8 (14, 19, 46). In the case of a water-wet medium it has been suggested to be around 306 (46) or 151 (20). Since the volumetric flow rate Q remains constant, the flow is pseudo-steady state. The superficial velocity would then be $V = Q/(2\pi hR^*)$ where

$$R^* = \sqrt{R_o^2 + \frac{(Qt)}{(\pi h \varepsilon)}} \tag{24}$$

is the radius of the hypothetical undisturbed interface in the absence of fingering. The mean pore velocity is given by the continuity equation,

$$\nabla . V_{pi} = 0 \tag{25}$$

Furthermore, Darcy's law governs the flow within the two fluid regions

$$V_{pi} = - \frac{K}{(\mu_i \varepsilon)} \nabla p_i \tag{26}$$

where i = w, o represents the displacing and displaced phases, K is the permeability, and ε the porosity. These two equations yield

$$\nabla^2 p_i = 0 \tag{27}$$

where ∇^2 in radial coordinates is:

$$\nabla^2 = \frac{1}{r} \frac{\partial}{\partial r} \left(r \frac{\partial}{\partial r} \right) + \frac{1}{r^2} \frac{\partial^2}{\partial \theta^2} \tag{28}$$

Ni et al. (19) extended Bataille's (56) work to the case of a porous medium and derived the following equation for the rate at which the fingers grow or decay in the radial direction

$$\frac{1}{f_n} \frac{\partial f_n}{\partial t} = \frac{Qn(\mu_o - \mu_w)}{2\pi R^{*2} h \varepsilon (\mu_o + \mu_w)} - \frac{Q}{2\pi R^{*2} h \varepsilon} - \frac{\gamma^* n(n^2 - 1)K}{R^{*3} \varepsilon (\mu_o + \mu_w)} \tag{29}$$

5 - BASIC EQUATIONS

For a Newtonian fluid of constant ρ and μ one can write

$$(\nabla \cdot v) = 0 \qquad \text{Eqn. of continuity} \qquad (30)$$

The equation of motion for a fluid with constant ρ and μ can be written as

$$\rho \frac{Dv}{Dt} = -\nabla p + \mu \nabla^2 v + \rho g \qquad (31)$$

This is the famous Navier-Stokes equation first developed in France by Navier in 1822 by molecular arguments.

It is possible to write these equations in terms of characteristic length, characteristic velocity and dimensionless variables (57).

In 1856 Darcy introduced an empirical equation that related the volumetric flow rate Q to the pressure loss and the permeability of the porous medium. It is often written in differential form as

$$\frac{Q}{A} = q = \frac{-k}{\mu} \frac{dP}{dx} \qquad (32)$$

For an incompressible fluid, Darcy's law can be integrated to yield

1) For a linear case

$$Q = \frac{KA(P_1 - P_2)}{\mu L} \qquad (33)$$

2) For a radial case

$$Q = \frac{2\pi\, Kh(P_1 - P_2)}{\mu \ln(r_1/r_2)} \qquad (34)$$

Eqns. 33 and 34 can be used to calculate the permeability of a porous medium (independent of the fluid properties and dependent on porous structure only). It

could be shown that Darcy's equation is the empirical equivalent of Navier-Stokes (Eqn. 31).

In 1937 Muskat et al. (58) considered Darcy's law for each of the fluids separately, viz:

$$q_1 = -\frac{K\ k_{r1}}{\mu_1} \nabla P_1 \tag{35}$$

and

$$q_2 = -\frac{K\ k_{r2}}{\mu_2} \nabla P_2 \tag{36}$$

where $\underline{\underline{K}}\ k_{r1} = \underline{\underline{K}}_1$ is the effective permeability of the medium to fluid 1 with fluid 2 present. Effective permeability depends on pore structure and the fluids present in the porous medium. It may also depend upon other factors such as viscosity. k_{r1} is called the relative permeability and depends on the wettability and saturation history.

The continuity equation for each fluid is:

$$\varepsilon \frac{\partial \rho_1 S_1}{\partial t} = -(\underline{\nabla} \cdot \rho_1 q_1) \tag{37}$$

and

$$\varepsilon \frac{\partial \rho_2 S_2}{\partial t} = -(\underline{\nabla} \cdot \rho_2 q_2) \tag{38}$$

S_1 and S_2 are fractional saturation of fluids 1 and 2 respectively so that

$$S_w + S_o = S_1 + S_2 = 1 \tag{39}$$

Generally speaking the above equations of change do not have analytical solutions. Their non-linearity results from the relative permeability saturation relationships. Therefore, they have to be solved numerically.

In 1941 Buckley and Leverett (59) simplified the problem by ignoring the capillary pressure across the interface and assumed one-dimensional incompressible flow. This assumption is reasonable for high flow rates or for flow over long distances. For linear displacement of oil by water they wrote:

$$q_w = - \frac{k_w A}{\mu_w} \left(\frac{\partial P_w}{\partial x} + \rho_w \text{ Sin } \alpha \right) \tag{40}$$

$$q_o = - \frac{k_o A}{\mu_o} \left(\frac{\partial P_o}{\partial x} + \rho_o g \text{ Sin } \alpha \right) \tag{41}$$

Since the two fluids are assumed to be incompressible, one can write

$$\varepsilon A \frac{\partial S_w}{\partial t} = - \frac{\partial q_w}{\partial x} \tag{42}$$

and

$$\varepsilon A \frac{\partial S_o}{\partial t} = - \frac{\partial q_o}{\partial x} \tag{43}$$

since $S_o + S_w = 1$

$$\frac{\partial}{\partial x} (q_w + q_o) = 0 \tag{44}$$

Hence, the fractions of water and oil flowing can be defined as

$$f_w = \frac{q_w}{q} \tag{45}$$

$$f_o = \frac{q_o}{q} = 1 - f_w \tag{46}$$

Substitution would yield

$$\frac{\partial S_w}{\partial t} = - \frac{q}{\varepsilon A} \frac{\partial f_w}{\partial x} \tag{47}$$

$$\frac{\partial S_o}{\partial t} = -\frac{q}{\varepsilon A}\frac{\partial f_o}{\partial x} \tag{48}$$

Combination of Eqns. 40 and 41 and assuming small density difference and $\alpha = 0$ and no interfacial tension, one could write

$$f_w = \frac{1}{1 + (k_o\mu_w/k_w\mu_o)} + \frac{k_o A}{q\mu_o}\frac{\left[\frac{dP_c}{dx} - \Delta\rho g \sin\alpha\right]}{1 + \frac{k_o\mu_w}{k_w\mu_o}} \tag{49}$$

The second term in Eqn. 49 can be neglected only when the product $\left[\frac{d P_c}{d S_w}\frac{\partial S_w}{\partial x}\right]$ is small and q is large. This is only the case for saturations greater than the flood front saturation. It is never the case for saturations near S_{wi}. Since k_o and k_w contain relative permeabilities, f_w is a function of saturation.

Using the chain rule and substitution in Eqn. 47 yields,

$$\frac{\partial S_w}{\partial t} = -\left(\frac{q}{\varepsilon A}\frac{df_w}{ds_w}\right)\frac{\partial S_w}{\partial x} \tag{50}$$

Eqn. 50 is a quasi-linear first order differential equation because $\frac{df_w}{ds_w}$ is a function of S_w, not $\frac{\partial S_w}{\partial x}$. Since

$$S_w = S_w(x, t) \tag{51}$$

$$\frac{dS_w}{dt} = \frac{\partial S_w}{\partial x}\frac{dx}{dt} + \frac{\partial S_w}{\partial t} \tag{52}$$

If $x = x(t)$ is chosen to coincide with a fixed S_w; then

$$\frac{dS_w}{dt} = 0 \tag{53}$$

and

$$\left(\frac{dx}{dt}\right)_{S_w} = -\frac{dS_w/dt}{\partial S_w/\partial x} \tag{54}$$

Combination of Eqns. 50 and 54 and elimination of dS_w/dt yields the famous Buckley-Leverett equation. Since S_w is known at the beginning, Eqn. 54 can be integrated to determine saturation at any given $t > 0$.

$$X_{S_w}(t) - X_{S_w}(0) = \frac{Q(t) - Q(0)}{\varepsilon A}\frac{df_w}{ds_w} \tag{55}$$

$$Q(t) = \int_o^{x(t)} \varepsilon[S_w(t) - S_w(0)]A\,dx \tag{56}$$

The same problem was solved for moving boundaries by Muskat (58).

The immiscible displacement of a wetting fluid by a non-wetting fluid in a porous medium can have distinct forms: viscous fingering, capillary fingering and stable displacement. The shape of the interface between the two fluids can be described using three different statistical approaches: the DLA (Diffusion-Limited Aggregation) model for viscous fingering at low viscosity ratio ($M \rightarrow 0$).

The anti-DLA (continuum) model for stable displacement and the invasion percolation model at low capillary numbers for capillary fingering.

A) DLA (Diffusion-Limited Aggregation):

Viscous displacements are governed by the pressure field at the entrance and exit. Therefore, p_i, the pressure in each fluid is a solution of Laplace's equation

$$\nabla^2 p_i = 0 \tag{27}$$

In DLA, a seed particle or line is placed on a lattice and another particle launched from far away moves at random and sticks when it reaches the seed or the line. Then another particle is launched and so on. In other words, in this method, Laplace's equation is solved by letting random walkers wander in the displaced and displacing phases, and stick upon contact with the interface. The absence of random walkers from one phase indicates a negligible pressure gradient in that phase. One of the drawbacks of this type of simulation that needs to be further studied is that the fraction of particles in the cluster will approach zero as the size of the lattice is increased.

B) Anti-DLA model:

The other extreme case is when the viscosity ratio (or M) approaches infinity. In 1984, Paterson et al. (14) suggested a relationship between an Anti-DLA process and a stable displacement in a porous medium. In this case, the displacement cannot be described by a flat interface. In this model, the particle moves at random until it reaches an occupied site. Here the particle (fluid 2) and the site (fluid 1) are removed and a new particle is released.

C) Invasion percolation:

The last two approaches are based on a continuum description of the porous medium and the fingering is due to viscous forces. The invasion percolation

mechanism is related to the capillary forces (microscopic scale) and randomness due to the different sizes of pores in the porous medium. According to this model, capillary forces prevent a non-wetting fluid from spontaneously entering the pores. The wetting fluid can only enter the throat (diameter D_o) if the pressure exceeds the pressure in the wetting fluid by the capillary pressure ($P_c = 4\gamma \cos \theta / D_o$). Therefore, statistically there will be two kinds of ducts (diameter D). Active or conductive bonds ($D > D_o$) and inactive bonds ($D < D_o$). Having the throat size distribution, the fraction of active bonds can be easily calculated. At a given pressure, P_c, the injected fluid invades all the percolation clusters connected to the injection face. Here the interface moves along the paths of least resistance which are present in the largest channels, since they provide the lowest capillary pressure. In this type of displacement the non-wetting fluid forms very thin fingers even if the displacing fluid is more viscous than the fluid filling the network. In addition, during the invasion, the wetting phase will be trapped in the network while the invading non-wetting fluid breaks the continuous path towards the outlet (60).

6 - MODEL FORMULATIONS

In this work empirical models were developed to describe the effects of the aforementioned factors on fingering and recovery. Two approaches were taken. In the first, mechanistic models previously proposed for the system were examined to obtain insight as to the appropriate form for the operating variables, while in the second, dimensional analysis was used.

Consideration of Mechanistic Models

Viscous fingering has been the topic of many research projects during the past three decades. In 1968, Bataille (56) studied the stability of a moving interface in radial flow. More recently, Paterson (14, 16, 17) investigated the problem in a Hele-Shaw cell where the flow is two-dimensional and, for slow viscous flow (negligible inertial effects), the pressure drop across the interface is governed by the Laplace equation.

Ni et al. (19) extended Bataille's (56) work to the case of a porous medium and derived the following equation for the number of fingers growing at maximum rate

$$n_m = \sqrt{\frac{1}{3}\left(1 + \frac{QR^*(\mu_o - \mu_w)}{2\pi h K \gamma^*}\right)} \cong \sqrt{\frac{QR^*(\mu_o - \mu_w)}{6\pi K \gamma^* h}} \qquad (57)$$

This can be linearized by taking logarithms of both sides to give

$$\ln n_m = \frac{1}{2}\{-\ln(6\pi h C^*) + \ln Q + \ln R^* + \ln(\mu_o - \mu_w) - \ln K - \ln \gamma\} \qquad (58)$$

where

$$C^* = \gamma^*/\gamma \qquad (23)$$

and

$$C = 2\pi\sqrt{3C^*} \qquad (59)$$

is called the Chuoke parameter (50).

According to the above model there are six independent process variables that determine the number of fingers growing at the maximum rate. However, as we will see later, it is extremely difficult to calculate the number of fingers at maximum growth in the case of radial displacement. At any given time there will be fingers that are not growing (stable) and there will also exist some fingers that are growing at various rates. On the other hand, a finger could be unstable at one moment and stable at another or vice versa. Therefore, to avoid any erroneous conclusions based on the number of fingers that are growing at the maximum rate (n_m) we considered the total number of fingers, n, in this study. The percentage of fingers that are growing at the maximum rate to the total number of fingers can be calculated and since there is a limit to how fast each finger can grow, this ratio is expected to increase with the flow rate Q. This suggests that a model to describe the total number of fingers n ($> n_m$) might take the form

$$Y = \beta_0 + \beta_1 X_1 + \beta_2 X_2 + \beta_3 X_3 + \beta_4 X_4 + \beta_5 X_5 + \beta_6 X_6 \qquad (60)$$

where

$X_1 = \ln Q$

$X_2 = \ln R^*$

$X_3 = \ln (\mu_o - \mu_w)$

$X_4 = \ln K$

$X_5 = \ln \gamma$

$X_6 = \ln (hC^*)$

$Y = \ln n$

and the β's are constants. In our work, the cell thickness and the wettability of the porous medium were not changed. However, as we will see later, C* depends on other operating variables and cannot be independently calculated; thus, the term $\beta_6 X_6$ was

included in the parameter β_0. It is interesting to note that the logarithmic transformation of the mechanistic model yields a model for which there are no interactions amongst the variables (i.e., the logarithms of the variables in the original model, Eqn. 57). Nonetheless, in light of the assumptions used in its original derivation, it was decided to test a full second-order polynomial,

$$Y = \beta_0 + \sum_{i=1}^{5} \beta_i X_i + \sum_{i=1}^{5} \sum_{j=1}^{5} \beta_{ij} X_i X_j \qquad (61)$$

Should any of the second order terms be found significant this would provide evidence of the inadequacy of Eqn. 58 and also some indication as to the nature of the inadequacy. Since recovery can reasonably be expected to depend upon the same factors as the number of fingers, Eqn. 61, with Y = ln(Rec%) was also fitted to the recovery data.

Dimensional Analysis

An alternate approach, based on dimensional analysis, was also used to develop empirical models for the recovery (Rec%) and total number of fingers (n). To accomplish this it was assumed that

$$\text{Rec\%} = f(Q, R, \mu_o, \mu_w, K, \gamma) \qquad (62\text{-a})$$

and

$$n = g(Q, R, \mu_o, \mu_w, K, \gamma) \qquad (62\text{-b})$$

Here R is the radius of the finger at breakthrough, i.e., the distance of the tip of the longest finger from the injection point (or the length of the longest finger) and not the traditional mean radius of displacement, R* (radius of displacement front in the absence of fingering). Since R* is not an independent variable (it is a function of Q,

see Eqn. 24) it cannot be used in any statistical design as an operating variable. Therefore, we replaced it by R. Moreover, to avoid any imbibition and high recoveries due to the end-effects, the largest R (R_3) was chosen to be 7.5 cm (cf. the cell radius was 8.15 cm). This is approximately where end-effects started. Therefore, our results do not include recoveries that are due to unnatural imbibition caused by end-effects (i.e. the presented models are not valid when $R \approx R_{cell}$). The decision to exclude end-effects was made despite the fact that similar end-effects exist in real (water wet) field situations in the vincinity of the recovery well because it was the only comprehensive way to attain our objectives (see Chapter 2).

Application of Buckingham's Π-theorem to Eqns. 62-a, 62-b yields

$$Rec\% = \phi_o B_1^{\phi_1} B_2^{\phi_2} B_3^{\phi_3} B_4^{\phi_4} \tag{63}$$

and

$$n = \lambda_o B_1^{\lambda_1} B_2^{\lambda_2} B_3^{\lambda_3} B_4^{\lambda_4} \tag{64}$$

where $B_1 = (Q\mu_w/K\gamma)$ is the capillary number of the displacing phase and represents the ratio of viscous to capillary forces,

$B_2 = (h/\sqrt{K})$ is the ratio of cell thickness to the square root of the permeability,

$B_3 = (R/h)$ is the ratio of the cell radius to the cell thickness,

$B_4 = (\mu_o/\mu_w)$ is the ratio of viscosities of the oil and water phases.

and the ϕ's and λ's are parameters to be estimated. The dimensionless terms, B_i, are not unique and may be multiplied or divided by each other to yield new (but not independent) dimensionless variables. However, the terms used in Eqns. 63 and 64 were felt to be of significant interest to petroleum engineers. It is important to note

that B_1 is not the traditional definition of the capillary number, i.e. $\left(\frac{V\mu}{\gamma\varepsilon}\right)$. Here the pore velocity $\left(V_p = \frac{V}{\varepsilon}\right)$ has been replaced by (Q/K) which is an indication of the velocity if all of the flow rate, Q, were to occur in a single pore (since the cross-sectional area of a pore is of order K). As mentioned earlier, this capillary number remains constant for both linear and radial displacements. Thus, it will be many orders of magnitude larger than the traditional values. In this study, the values of B_1 varied from 0.09 to 122,882 whereas the traditional N_{Ca} (Eqn. 14-d) of the displacing phase would be between 1.90×10^{-8} to 5.37×10^{-2}. This gives rise to a Reynolds number $\left(Re = \frac{\rho d_p V}{\mu\varepsilon}\right)$ of 1.74×10^{-5} to 2.98. Therefore, the flow can be considered as creeping flow and Darcy's law can be applied.

Eqns. 63 and 64 suggest first-order models in terms of the logarithms of the dimensionless variables. However, when analyzing the data, complete second-order polynomials of the form

$$Y = \beta_o + \sum_{i=1}^{4} \beta_i X_i + \sum_{i=1}^{4} \sum_{j=1}^{4} \beta_{ij} X_i X_j \qquad (65)$$

were employed. In this case $X_i = \ln B_i$, Y is either ln(Rec%) or ln(n), and the β's are parameters to be estimated (with $\beta_i = \phi_i$ or λ_i). Inclusion of the second-order terms provided a means to check the need for a more complex relationship.

Bentsen and Sarma (61) have used inspectional analysis in almost the same way we have used dimensional analysis and have come up with similar dimensionless groups which are subsequently used to predict the onset of unstable behavior. They modified the previous theory and included a linear time function. They concluded that when the combined forces of gravity and capillarity are greater than the viscous forces, the displacement will be stable.

Experimental Design

In order to efficiently obtain estimates for the parameters in the second-order polynomial given by Eqn. 61 a modified central composite experimental design was followed (62). To improve the numerical accuracy of the estimation and to achieve low (ideally zero) correlations between parameter estimates, the operating variables were centered and scaled according to

$$X_i = (x_i - \bar{x}_i)/[0.5(x_i^U - x_i^L)] \qquad (66)$$

where $\bar{x}_i = 0.5(x_i^U + x_i^L)$ is the midpoint of the range of values for x_i in the factorial part of the central composite design; x_i^U and x_i^L are respectively the upper and lower values of x_i in the factorial part of the design. This coding yields values of X_i of 1 or -1 for two-level factorial designs.

The central composite design consisted of a 2^{5-1} fractional factorial design (consisting of 16 runs at various combinations of two levels of each of the five operating variables), 10 axial points and 8 centre point replicates. The 2^{5-1} factorial design had the defining relation $I = X_1X_2X_3X_4X_5$ yielding a Resolution V design (62). Assuming that third and higher order interactions (i.e., terms consisting of products of 3 or more coded operating variables) are insignificant, this component of the design allows us to obtain unconfounded estimates of the main effects, and 2-factor interactions. Optimal settings for the axial points are at ± 2.0 coded units. However, as a result of difficulties in running at more than 3 levels of each operating variable in this work, the axial points were located at ± 1, corresponding to the upper and lower values.

Another deviation from the strictly optimal central composite design involved replication of additional experiments at the centre-points along with replications of several other run conditions. In addition, since it was difficult to set the operating

variables exactly; that is, the settings for the operating variables deviated slightly from their optimal coded values of -1, 0, and 1. The resulting designs in terms of coded variables are given in Tables 1, 3 and 5 for the capillary, intermediate and viscous regions, respectively. The total of (55 + 64 + 40 = 159) runs was carried out in random order. The actual values of the operating variables for X_i = 1, 0, and -1 are given in Tables 2, 4 and 6 for each of the respective regions.

The experimental design with respect to the dimensionless variables in Eqn. 65 did not follow a central composite design since the value of the dimensionless variables were those resulting from the central composite design in terms of the operating variables in Eqn. 61.

Table 1

Summary of Run Locations and Observed Responses for Capillary Region

Design	Run Order	CODED $X_i = \ln x_i$					$\ln y_j$		CODED $X_i = \ln B_i$			
		X_1	X_2	X_3	X_4	X_5	Y_1	Y_2	X_1	X_2	X_3	X_4
2^{5-1}	5	-1	-1	-0.86	-1	0.91	1.44	1.39	-0.60	1	-1	-0.28
Fractional	8	-1	-1	-0.86	-1	0.91	0.52	1.39	-0.60	1	-1	-0.28
Factorial	11	-1	-1	-0.86	-1	0.91	0.63	1.10	-0.60	1	-1	-0.28
	51	-1	-1	-0.86	-0.64	0.95	0.70	1.79	-0.68	0.64	-1	-0.28
	2	1	-1	-1	-1	-1	3.08	2.20	1	1	-1	-1
	20	-1	1	-0.96	-1	-1	4.22	2.83	0.55	1	1	-0.98
	24	1	1	-0.86	-1	1	4.17	2.64	-0.19	1	1	-0.28
	45	1	1	-0.86	-0.64	0.94	4.08	2.89	-0.23	0.641	1	-0.28
	46	1	1	-0.86	-0.64	0.88	3.10	3.26	-0.20	0.64	1	-0.28
	53	-1	-1	0.99	-0.64	-1	1.77	2.48	0.49	0.64	-1	-0.28
	28	1	-1	1	-1	0	1.74	2.64	0.34	1	-1	0.82
	35	-1	1	1	-1	1	3.00	3.00	-0.64	1	1	1
	31	1	1	0.99	-1	-1	3.40	3.89	1	1	1	-0.28
	34	-1	-1	-1	1	-1	3.53	2.20	0.19	-1	-1	-1
	17	-1	-1	-1	1	-1	3.47	2.30	0.19	-1	-1	-1
	19	-1	-1	-1	1	-1	3.68	2.20	0.19	-1	-1	-0.98
	12	1	-1	-0.86	1	0.91	2.29	2.08	-0.51	-1	-1	-0.28
	37	-1	1	-0.86	1	1	4.23	3.22	-1	-1	1	-0.28
	32	-1	1	-0.86	1	1	4.01	3.22	-1	-1	1	-0.28
	26	1	1	-1	1	-1	4.20	2.71	0.64	-1	1	-1
	9	-1	-1	1	1	0.91	2.09	2.20	-0.96	-1	-1	1
	15	1	-1	0.96	1	-1	2.26	2.77	0.64	-1	-1	-0.28
	54	1	-1	0.99	1	-1	2.65	2.89	0.64	-1	-1	-0.28
	3	-1	1	0.99	1	-1	3.31	2.89	0.19	-1	1	-0.28
	50	-1	1	0.99	1	-1	3.10	2.83	0.20	-1	1	-0.28
	52	-1	1	0.99	1	-1	3.15	2.77	0.20	-1	1	-0.28
	6	1	1	1	1	0.91	3.08	3.43	0.51	-1	1	1
Centre	30	0.03	0	0.05	0.54	0	3.09	3.00	-0.15	-0.54	0	0.16
points	16	0.03	0	0.05	0.54	0	2.71	3.00	-0.16	-0.54	0	0.16
	4	0.03	0	0.05	0.54	-0.12	2.40	2.89	-0.09	-0.54	0	0.16
	43	0.03	0	0.05	0.54	0	3.09	2.94	-0.16	-0.54	0	0.16

Table 1 (Cont'd)

Design	Run Order	CODED $X_i = \ln x_i$					$\ln y_i$		CODED $X_i = \ln B_i$			
		X_1	X_2	X_3	X_4	X_5	Y_1	Y_2	X_1	X_2	X_3	X_4
Centre	1	0.03	0	0.05	0.54	-0.12	2.48	3.00	-0.09	-0.54	0	0.16
points	7	0.03	0	0.05	0.54	0.05	2.64	3.09	-0.18	-0.54	0	0.16
	25	0.03	0	0.05	0.54	0	3.26	2.94	-0.15	-0.54	0	0.16
	27	0.03	0	0.05	0.54	0	2.90	2.00	-0.15	-0.54	0	0.16
Axial	14	1	0	0.05	0.54	0	2.36	3.30	0.07	-0.54	0	0.16
Points	10	-1	0	0.05	0.54	1	2.36	2.40	-0.85	-0.54	0	0.16
	33	0.03	1	0.05	0.54	0	4.03	3.56	-0.16	-0.54	1	0.16
	44	0.03	-1	0.05	0.54	0	2.84	2.56	-0.16	-0.54	-1	0.16
	18	0.03	0	1	0.54	0	2.28	3.18	-0.16	-0.54	0	0.82
	40	0.03	0	1	0.54	0	2.88	3.30	-0.16	-0.54	0	0.82
	38	0.03	0	-0.86	0.54	0	3.75	2.71	-0.22	-0.54	0	-0.28
	29	0.03	0	0.05	1	0	3.74	2.71	-0.24	-1	0	0.16
	41	0.03	0	0.05	1	0	3.14	2.77	-0.24	-1	0	0.16
	13	0.03	0	0.05	-1	0	2.42	2.20	0.13	1	0	0.16
	42	0.03	0	0.05	-1	0	2.01	2.40	0.13	1	0	0.16
	23	0.03	0	0.05	0.54	1	2.24	2.77	-0.69	-0.54	0	0.34
	36	0.03	0	0.06	0.54	1	2.20	2.83	-0.69	-0.54	0	0.34
	21	0.03	0	0.01	0.54	-1	2.18	3.30	0.50	-0.54	0	-0.38
Others	22	1	-1	1	1	1	2.17	2.48	-0.55	-1	-1	1
	39	-1	1	-0.86	-1	1	3.80	2.83	-0.64	1	1	-0.28
	47	0.03	1	-0.86	-0.64	0.96	3 53	3.09	-0.46	0.64	1	-0.28
	48	1	1	0.99	-1	-1	3.44	3.40	0.64	-1	1	0.28
	49	0.03	1	0.99	1	-1	2.93	3.18	0.42	-1	1	0.28
	55	0.03	1	0.99	1	-1	2.99	3.30	0.42	-1	1	0.28

Table 2

Relationship Between Coded and Actual Values of the Operating Variables for Capillary Region

Variable	Coded Value*		
	-1	0**	1
Q(mL/h)	0.65	2.00	5.80
R (cm)	2.50	4.18	7.00
μ_o-μ_w (mPa.s)	14.30	47.30	151.90
K (μm^2)	13.33	51.70	77.41
γ (mN/m)	0.30	3.00	30.00
B_1 (dimensionless)	0.09	15.60	1490.65
B_2 (dimensionless)	329.60	403.50	794.30
B_3 (dimensionless)	8.62	14.41	24.14
B_4 (dimensionless)	4.90	34.00	153.00

* Coding was performed using Eqn. (66).
** The mid-value '0' is approximate.

Table 3

Summary of Run Locations and Observed Responses for Intermediate Region

Design	Run Order	CODED $X_i = \ln x_i$					$\ln y_j$		CODED $X_i = \ln B_i$			
		X_1	X_2	X_3	X_4	X_5	Y_1	Y_2	X_1	X_2	X_3	X_4
2^{5-1}	7	-1	-1	-0.84	-0.59	0.93	2.60	3.09	-0.68	0.59	-1	-0.23
Fractional	37	-1	-1	-0.84	-1	0.95	2.62	3.26	-0.61	1	-1	-0.23
Factorial	31	1	-1	-0.97	-1	-0.98	3.48	3.30	1	1	-1	-0.97
	56	1	-1	-0.97	-1	-0.82	3.54	3.26	0.91	1	-1	-0.97
	39	-1	1	-0.97	-1	-0.99	3.81	4.23	0.69	1	1	-0.97
	6	1	1	-0.84	-0.64	0.95	2.71	4.42	-0.37	0.64	1	-0.23
	9	1	1	-0.84	-0.59	0.96	2.87	4.39	-0.38	0.59	1	-0.23
	41	-1	-1	0.99	-1	-0.99	2.40	3.50	0.69	1	-1	0.27
	47	1	-1	1	-1	0.95	2.20	3.33	-0.30	1	-1	1
	35	-1	1	1	-1	0.95	2.56	4.61	-0.61	1	1	1
	50	-1	1	1	-1	0.95	2.66	4.38	-0.61	1	1	1
	61	-1	1	1	-1	0.95	2.30	4.49	-0.61	1	1	1
	44	1	1	0.99	-1	-0.78	2.64	4.61	0.89	1	1	0.27
	54	1	1	0.99	-1	-0.81	2.71	4.70	0.91	1	1	0.27
	15	-1	-1	-0.98	1	-0.97	3.18	3.00	0.30	-1	-1	-1
	40	-1	-1	-0.97	1	-0.99	3.38	2.71	0.30	-1	-1	-0.97
	13	1	-1	-0.84	1	0.98	2.89	2.94	-0.70	-1	-1	-0.23
	51	1	-1	-0.84	1	0.95	3.19	3.09	-0.69	-1	-1	-0.23
	27	-1	1	-0.84	1	0.95	3.22	3.66	-1	-1	1	-0.23
	58	-1	1	-0.84	1	0.95	3.48	3.76	-1	-1	1	-0.23
	42	1	1	-0.97	1	-0.99	3.33	3.76	0.62	-1	1	-0.97
	64	1	1	-0.97	1	-0.82	3.59	3.95	0.53	-1	1	-0.97
	29	-1	-1	1	-1	0.95	2.47	2.89	-1	-1	-1	1
	49	-1	-1	1	-1	0.95	2.35	3.00	-1	-1	-1	1
	10	1	-1	0.98	1	-0.93	2.12	3.47	0.60	-1	-1	0.23
	20	1	-1	0.99	1	-0.81	2.21	3.02	0.52	-1	-1	0.27
	46	1	-1	0.99	1	-0.78	2.43	3.30	0.51	-1	-1	0.27
	3	-1	1	0.99	1	-0.88	2.92	3.87	0.20	-1	1	0.40
	8	-1	1	0.98	1	-0.92	2.59	3.78	0.30	-1	1	0.19
	23	-1	1	0.99	1	-0.93	2.94	3.74	0.27	-1	1	0.27
	32	1	1	1	-1	1	2.59	3.71	-0.67	-1	1	1

Table 3 (Cont'd)

Design	Run Order	CODED $X_i = \ln x_i$					$\ln y_j$		CODED $X_i = \ln B_i$			
		X_1	X_2	X_3	X_4	X_5	Y_1	Y_2	X_1	X_2	X_3	X_4
	59	1	1	1	-1	1	2.71	3.81	-0.69	-1	1	1
Centre	21	0.03	0	0.04	0.04	-0.14	2.56	3.76	0.02	-0.04	0	0.12
Points	16	0.03	0	0.04	0.04	0.19	2.58	3.50	-0.16	-0.04	0	0.12
	24	0.03	0	0.04	0.04	-0.13	2.26	3.26	0	-0.04	0	0.12
	55	0.03	0	0.04	0.45	0.01	2.40	3.40	-0.14	-0.45	0	0.12
	28	0.03	0	0.04	0.04	-0.12	2.30	3.30	0	-0.04	0	0.12
	52	0.03	0	0.04	0.45	0.01	2.48	3.40	-0.14	-0.45	0	0.12
	60	0.03	0	0.04	0.45	-0.07	2.43	3.43	-0.10	-0.45	0	0.12
	26	0.03	0	0.04	0.04	-0.13	2.25	3.43	0	-0.04	0	0.12
	19	0.03	0	0.04	0.04	-0.09	2.50	3.64	0	-0.04	0	0.12
	22	0.03	0	0.04	0.04	-0.14	2.53	3.58	0.02	-0.04	0	0.12
	18	0.03	0	0.04	0.04	0.20	2.58	3.64	-0.17	-0.04	0	0.12
Axial	48	1	0	0.04	0.45	0.07	2.56	3.76	-0.02	-0.45	0	0.12
Points	43	-1	0	0.04	0.45	0.08	2.71	3.22	-0.34	-0.45	0	0.12
	57	0.03	1	0.04	0.45	-0.07	2.56	3.85	-0.10	-0.45	1	0.12
	62	0.03	-1	0.04	0.45	-0.07	2.44	2.83	-0.10	-0.45	-1	0.12
	30	0.03	0	1	0.04	0.12	2.08	3.43	-0.12	-0.04	0	0.76
	63	0.03	0	1	0.45	-0.07	2.20	3.50	-0.10	-0.45	0	0.76
	45	0.03	0	-0.86	0.45	0.07	2.74	3.30	-0.17	-0.45	0	-0.47
	38	0.03	0	0.04	1	0.07	3.13	3.14	-0.28	-1	0	0.12
	53	0.03	0	0.04	1	0.01	2.83	3.30	-0.25	-1	0	0.12
	17	0.03	0	0.05	-0.59	0.20	2.56	3.87	-0.13	0.60	0	0.36
	12	0.03	0	0.05	0.10	0.98	2.32	3.69	-0.68	-0.10	0	0.36
	14	0.03	0	0.05	0.04	1	2.20	3.47	-0.68	-0.04	0	0.36
	36	0.03	0	0.05	0.04	0.95	2.20	3.47	-0.65	-0.04	0	0.36
	34	0.03	0	0	0.04	-0.98	2.56	3.69	0.65	-0.04	0	-0.38
Others	1	1	1	1	1	-0.83	2.82	4.26	0.48	-1	1	0.40
	2	0.03	1	1	1	-0.86	2.48	3.89	0.34	-1	1	0.40
	4	-1	1	-0.84	-0.64	0.96	3.00	4.09	-0.69	0.64	1	-0.23
	5	0.03	1	-0.84	-0.64	0.96	2.71	4.09	-0.53	0.64	1	-0.23
	11	0.03	1	1	1	0.99	2.74	2.73	-0.86	-1	1	1
	25	-1	-1	-0.84	1	0.95	3.13	3.14	-1	-1	-1	-0.23
	33	0.03	-1	0	0.04	-0.99	2.56	3.22	0.65	-0.04	-1	-0.38

Table 4

Relationship Between Coded and Actual Values of the Operating Variables for Intermediate Region

Variable	Coded Value*		
	-1	0**	1
Q(mL/h)	13.20	27.60	55.20
R (cm)	2.50	4.18	7.00
μ_o-μ_w (mPa.s)	15.20	47.50	152.00
K (μm^2)	13.33	33.36	77.41
γ (mN/m)	0.30	3.00	30.00
B_1 (dimensionless)	1.90	182.40	16,775.00
B_2 (dimensionless)	329.61	502.09	794.30
B_3 (dimensionless)	8.62	14.41	24.14
B_4 (dimensionless)	5.10	34.00	153.00

* Coding was performed using Eqn. (66).

** The mid-value '0' is approximate.

Table 5

Summary of Run Locations and Observed Responses for Viscous Region

Design	Run Order	CODED $X_i = \ln x_i$					$\ln y_j$		CODED $X_i = \ln B_i$			
		X_1	X_2	X_3	X_4	X_5	Y_1	Y_2	X_1	X_2	X_3	X_4
2^{5-1}	5	-1	-1	-0.86	-1	1	2.87	3.61	-0.59	1	-1	-0.27
Fractional	25	-1	-1	-0.86	-1	1	3.16	3.58	-0.59	1	-1	-0.27
Factorial	20	1	-1	-1	-1	-1	3.34	3.69	1	1	-1	-1
	15	-1	1	-1	-1	-1	3.43	4.47	0.75	1	1	-1
	17	-1	1	-1	-1	-1	3.27	4.42	0.75	1	1	-1
	32	1	1	-0.86	-1	1	3.03	4.13	-0.34	1	1	-0.27
	9	-1	-1	0.99	-1	-1	2.37	4.08	0.75	1	-1	0.27
	35	1	-1	1	-1	1	1.61	3.53	-0.34	1	-1	1
	23	-1	1	1	-1	1	1.96	4.44	-0.59	1	1	1
	1	1	1	0.99	-1	-1	2.91	5.14	1	1	1	0.27
	28	1	1	0.99	-1	-1	2.61	5.11	1	1	1	0.27
	18	-1	-1	-1	1	-1	3.51	2.89	0.34	-1	-1	-1
	26	1	-1	-0.86	1	1	2.71	2.89	-0.75	-1	-1	-0.27
	21	-1	1	-0.86	1	1	3.23	3.09	-1	-1	1	-0.27
	36	-1	1	-0.86	1	1	3.52	3.00	-1	-1	1	-0.27
	12	1	1	-1	1	-1	3.79	2.83	0.59	-1	1	-1
	24	-1	-1	1	1	1	1.35	3.40	-1	-1	-1	1
	8	1	-1	0.99	1	-1	1.33	3.81	0.59	-1	-1	0.27
	30	1	-1	0.99	1	-1	2.20	3.76	0.59	-1	-1	0.27
	2	-1	1	0.99	1	-1	2.35	4.42	0.34	-1	1	0.27
	6	1	1	1	1	1	1.42	4.17	-0.75	-1	1	1
	33	1	1	1	1	1	1.75	4.20	-0.75	-1	1	1
Centre	10	-0.22	0	0.03	0.54	-0.14	2.75	4.06	-0.13	-0.54	0	0.15
points	7	-0.22	0	0.03	0.45	-0.14	2.21	3.95	-0.11	-0.45	0	0.15
	3	-0.22	0	0.03	0.45	-0.14	2.03	4.06	-0.11	-0.45	0	0.15
	39	-0.22	0	0.03	0.54	-0.14	2.53	3.53	-0.13	-0.54	0	0.15
	40	-0.22	0	0.03	0.54	-0.14	2.58	3.58	-0.13	-0.54	0	0.15
	16	-0.22	0	0.03	0.54	-0.14	2.34	3.61	-0.13	-0.54	0	0.15
	13	-0.22	0	0.03	0.54	-0.14	2.47	3.85	-0.13	-0.54	0	0.15
	19	-0.22	0	0.03	0.54	-0.14	2.84	3.64	-0.13	-0.54	0	0.15

Table 5 (Cont'd)

Design	Run Order	CODED $X_i = \ln x_i$					$\ln y_j$		CODED $X_i = \ln B_i$			
		X_1	X_2	X_3	X_4	X_5	Y_1	Y_2	X_1	X_2	X_3	X_4
Axial	31	-1	0	0.03	0.54	-0.14	1.97	3.76	0.02	-0.54	0	0.15
Points	27	-1	0	0.03	0.54	-0.14	2.46	3.53	-0.23	-0.54	0	0.15
	38	-0.22	1	0.03	0.54	-0.14	2.89	4.14	-0.13	-0.54	1	0.15
	37	-0.22	-1	0.03	0.54	-0.14	2.12	3.37	-0.13	-0.54	-1	0.15
	4	-0.22	0	1	0.45	-0.14	0.94	4.06	-0.11	-0.45	0	0.81
	34	-0.22	0	-0.88	0.54	-0.14	3.23	3.40	-0.13	-0.54	0	-0.46
	14	-0.22	0	0.03	1	-0.14	2.53	2.83	-0.23	-1	0	0.15
	11	-0.22	0	0.03	-1	-0.14	2.16	4.17	0.18	1	0	0.15
	22	-0.22	0	0.03	0.54	1	2.10	3.64	-0.81	-0.54	0	0.34
	29	-0.22	0	-0.01	0.54	-1	2.79	3.93	0.53	-0.54	0	-0.39

Table 6

Relationship Between Coded and Actual Values of the Operating Variables for Viscous Region

Variable	Coded Value*		
	-1	0**	1
Q(mL/h)	174.00	264.00	510.00
R (cm)	2.50	4.18	7.00
μ_o-μ_w (mPa.s)	15.00	49.90	151.90
K (μm^2)	13.33	47.55	77.41
γ (mN/m)	0.32	2.25	30.00
B_1 (dimensionless)	22.90	1829.00	122882.00
B_2 (dimensionless)	329.60	420.60	794.30
B_3 (dimensionless)	8.62	14.41	24.14
B_4 (dimensionless)	5.10	34.00	153.00

* Coding was performed using Eqn. (66).
** The mid-value '0' is approximate.

7 - PARAMETER ESTIMATION

In general, any process model may be expressed in the form (62, 63, 64)

$$\eta = f(\underline{\xi}, \underline{\theta}) \tag{67}$$

where

η is the expected response (E(y))

y is the measured response value

$\underline{\xi}$ is the vector of corresponding values of the operating variables

$\underline{\theta}$ is the vector of the parameters

and f is the response function

In any experimental run carried out at operating conditions $\underline{\xi}_u$, a measured value of the response, y_u, will be obtained where

$$\begin{aligned} y_u &= \eta_u + \varepsilon_u \\ &= f(\underline{\xi}_u, \underline{\theta}) + \varepsilon_u \end{aligned} \tag{68}$$

where ε_u is the random error.

Linear Least Squares Estimation

The least squares estimates of the parameters $\underline{\theta}$ in Eqn. 68 fitted to data $(\underline{\xi}_u, y_u)$, u = 1, 2 ..... n, are those values $\hat{\underline{\theta}}$ for which the sum of squares (65)

$$S(\underline{\theta}) = \sum_{u=1}^{n} \{y_u - f(\underline{\xi}_u, \underline{\theta})\}^2 \tag{69}$$

is minimized.

Parameters in the various models were estimated using the linear least squares procedure REG contained in SAS (66). Ninety-five percent confidence intervals for the true values of the parameters were examined to determine the need to include them in the model. If the interval (for any parameter contained zero, the corresponding term was omitted from the model and the adequacy of the model re-evaluated. Retention of insignificant terms in the model leads to inflated variances for model predictions.

The models were examined for lack of fit using plots of residuals and a quantitative lack of fit test (63). Residuals (i.e., observed minus predicted values of the responses) were plotted against the predicted value of the response, values of the operating variables and run order to ensure that no trends were evident. In the quantitative test for lack-of-fit the ratio

$$R = \frac{(SSR - \nu_p\widehat{\sigma}_p^2)/(N - N_p - \nu_p)}{\widehat{\sigma}_p^2} \qquad (70)$$

was compared with the upper 5% abscissa value of F_{v,ν_p} distribution where ν_p is the number of degrees of freedom associated with $\widehat{\sigma}_p^2$, the pooled estimate of variance. This ratio was then compared to $F_{v,\nu_p,0.05}$ ($v = N - N_p - \nu_p$) and if R was smaller than $F_{v,\nu_p,0.05}$, no lack-of-fit was indicated (67, 68).

For each run, both the recovery and number of fingers were measured at each of the three values of ln(R), namely -1, 0 and +1. Consequently, for each experiment we measured two sets of three responses (3 values of recovery and 3 values of number of fingers). These observations are correlated within each set for any particular run but are not correlated with observations from other runs. The two sets of responses had the following characteristics:

1) They were measured independently, i.e.

$$a_1Y_1 + a_2Y_2 \neq a_0 \tag{71}$$

where a_0 is a constant vector and a_1 and a_2 are scalar constants.

2) There was no linear relationship between the expected values of the responses, viz

$$b_1E(Y_1) + b_2E(y_2) \neq b_0 \tag{72}$$

where b_0 is a vector of constants.

In this part the data were analyzed using the SAS single response linear least squared parameter estimation routine, in which the likelihood function is

$$l(\beta,\sigma|y)\alpha\sigma^{-N}\exp\left\{\frac{-||y - x\beta||^2}{2\sigma^2}\right\} \tag{73}$$

This likelihood is maximized with respect to β when the residual sum of squares $S(\beta) = ||y - x\beta||^2$ is a minimum.

Therefore the maximum likelihood estimates are the values of β which minimize $S(\beta)$. The least squares estimates $\hat{\beta}$ are thus

$$\hat{\beta} = \left(X^TX\right)^{-1}X^Ty \tag{74}$$

In using this method, it is assumed that (63):

1- The expectation function is correct: $E(\varepsilon_u) = 0$

2- The response is the expectation function plus disturbance.

3- The disturbance is independent of the expectation function.

4- Each disturbance has a normal distribution.

5- Each disturbance has a zero mean.

6- The disturbances have equal variances (same reproducibility): $V(\varepsilon_u) = \sigma^2$.

7- The disturbances are independently distributed: $E(\varepsilon_u \varepsilon_v) = 0$

(no systematic association).

As we will see later on, the response and residual plots are an effective way of verifying these assumptions.

In general, 95% confidence intervals for the parameters were calculated to evaluate the precision of the parameter estimates. If the confidence interval contained zero, that parameter was omitted from the Eqns. 61 or 65. This resulted in a few plausible models for each of the responses. The need for additional parameters was also determined by evaluating the extra sum of squares ratio (63):

$$Q = \frac{1}{\hat{\sigma}^2} \frac{(SSR_B - SSR_A)}{(N_{PB} - N_{PA})} \tag{75}$$

where,

$$\hat{\sigma}^2 = \frac{SSR_B}{(N - N_{PB})} \tag{76}$$

SSR = Sums of squares of residuals (A and B refer to the models containing the least and most parameters, respectively)

N_P = Number of parameters

N = Number of runs.

This Q ratio was then compared to $F_{v1,v2,\ 0.05}$, where $v_1 = N_{PB} - N_{PA}$ and $v_2 = N - N_B$. If $F_{v1,v2,\ 0.05}$ was smaller than the Q, the extra parameter was significant and thus its addition was justified.

Non-Linear Parameter Estimation

Here our strategy consisted of using non-linear single response, as well as, multiresponse parameter estimation (MPE) techniques to estimate the parameters of the non-linear models that predict the recovery and the number of fingers.

A: Non-Linear Single Response Parameter Estimation

An iterative optimization program based on the Levenberg-Marquardt method (65) was written and used to determine values of the parameters which minimize the sum of squares of residuals. Here, the following two models were fitted to the data

$$Y = \theta_0 Q^{\theta_1} R^{\theta_2} (\mu_0 - \mu_w)^{\theta_3} K^{\theta_4} \gamma^{\theta_5} \qquad (77)$$

and

$$Y = \theta_0 B_1^{\theta_1} B_2^{\theta_2} B_3^{\theta_3} B_4^{\theta_4} \qquad (78)$$

Since any interaction term would simply be a multiplication of two operating variables, direct inclusion of any interactions would make X^TX and subsequently Hessian matrices singular, models of the general form of Eqns. 77 and 78 should be fitted to the data. It should be noted, however, that in the presence of an interaction $(K\gamma)^{\theta_6}$, between K and IFT for instance, the effect of θ_6 would be included in the parameters θ_4 and θ_5.

B: Multiresponse Parameter Estimation

In general, one can deal with MPE using two different criteria:

1- Maximum likelihood, in which the likelihood function would be:

$$L(\theta, \Sigma(\theta)) = k^* - \frac{N}{2} \ln |Z^TZ| \qquad (79\text{-a})$$

Maximum likelihood estimates are obtained by minimizing $|Z^TZ|$ with respect to θ.

2- Bayesian approach (64, 69) where the marginal posterior density is

$$P(\theta|Y) \alpha |Z^TZ|^{-N/2} \tag{79-b}$$

Again, to maximize the posterior density one has to minimize the determinant. Eqns. (79-a) and (79-b) are general results and they do not depend on whether the expectation function is linear or non-linear. Neither are they influenced by the number of common parameters, nor by a scale change on any of the responses (63, 67). In 1973 Box and Draper (69) used a Bayesian approach to show that the parameter estimates had to be chosen to minimize

$$d(\theta) = |Z^TZ| \tag{80}$$

the determinant of the M x M dispersion matrix Z^TZ. Here they assumed that:

$$E[Z_{nm}] = 0 \tag{81}$$

and

$$E[Z_{nm}Z_{ri}] = \begin{cases} \Sigma_{mi} & \text{for } n = r \\ 0 & \text{for } n \neq r \end{cases} \tag{82}$$

where Σ is a fixed M x M covariance matrix.

In other words, it was assumed that the measurements from different experiments were independent but measurements from the same experiments were corre-

lated. Three sets of data for recoveries at each R (therefore, R was kept constant within each set) were analyzed. The following models were assumed for each response

$$Y_1 = \theta_1(B_1)^{\theta_2}(B_2)^{\theta_3}(B_{31})^{\theta_4}(B_4)^{\theta_5} \tag{83}$$

$$Y_2 = \theta_6(B_1)^{\theta_2}(B_2)^{\theta_3}(B_{32})^{\theta_4}(B_4)^{\theta_7} \tag{84}$$

$$Y_3 = \theta_8(B_1)^{\theta_2}(B_2)^{\theta_3}(B_{33})^{\theta_4}(B_4)^{\theta_9} \tag{85}$$

where Y_i are the observed responses at each R. Unfortunately, since B_{3i} is a constant for each model, θ_4 will be highly correlated with and included in θ_1, θ_6 and θ_8. Therefore, θ_4 cannot be estimated separately. The decision to keep θ_2 and θ_3 constant for all three models was based on the results from linear LSE and non-linear single response estimation. IMSL subroutines were used to minimize the determinant and calculate the Hessian. Initial estimates of parameters were taken from single response linear least squares and single response non-linear analysis of the data. In brief, we expected the multiresponse estimates to provide more precise estimates of the common parameters than the non-linear single response method.

8 - EXPERIMENTAL

In choosing the ranges of the operating variables, both practicality and manufacturing limitations were considered. In the case of flow rate, the ranges were based on previous data reported by Ni et al. (19) and Nasr-El-Din et al. (20).

The experiments were conducted in consolidated porous media with permeabilities in the range of 13.33-77.41 μm^2. The medium consisted of sintered glass beads (30-100 U.S. Mesh, $150 < d_p < 600$ microns) sandwiched between two glass plates. The cell was circular (thus resulting in a symmetrical pressure drop profile) with a constant thickness of 2.9 mm and diameter of 16.4 cm. The porosity ranged from 0.31 to 0.40. Great care was taken to ensure a constant thickness and to prevent any heterogeneities (16, 50, 70). Each cell was subjected to a heterogeneity detection test as described by Nasr-El-Din (20). Three circles (with radii of 2.50, 4.18 and 7.00 cm) were engraved on the upper glass plate. This enabled us to see and photograph the displacement pattern at each level of breakthrough radius (X_i = -1, 0 and +1).

The resident fluids were three different mixtures of paraffin oil (density range of 0.87-0.91 g/cm^3) with viscosities of 18.7, 51.0 and 154.0 mPa.s. The invading fluids consisted of pure water or fresh solutions of a surfactant (Petrostep-420 petroleum sulfonate) in distilled water (density ranged from 1.04 to 1.07 g/cm^3). These solutions had a wide range of interfacial tension (71) (IFT = 0.3 - 30.0 mN/m) and had a viscosity of 1-4 mPa.s. All measurements and experiments were conducted at a room temperature of 24.0 ± 1.0°C. To ensure a visual contrast between the two liquid phases, a small amount of dye (0.04% of Malachite Green) was added to the aqueous displacing fluid. These fluids were then filtered to prevent any pore blockage. Immersion of the oil-saturated cell into a water bath resulted in rapid imbibition of water into the porous medium. This indicated the preferential water-wettability of the porous medium.

Prior to each experiment, both fluids were deaerated to avoid air bubble formation and the cell alignment was checked to ensure a horizontal mode. The cell was then filled with a paraffin oil under vacuum (complete initial oil saturation, S_{oi} = 100%). The displacing fluid was injected into the cell at various constant flow rates (0.65-510.00 mL/h) through a small inlet port at the bottom center of the cell by means of a precision syringe pump (Fig. 19).

At each radius, the breakthrough time and fractional recovery were recorded and a photograph was taken. These photographs were later used to count the number of fingers and to examine the displacement pattern. Recovery was calculated as the ratio of the volume of the oil displaced (equal to the volume of the fluid injected) to the total initial volume (or volume of the pore space), such that

$$\text{Rec\%} \equiv \frac{Qt}{\pi R^2 h \varepsilon} \times 100 \qquad (86)$$

where t is the time when the first finger reaches radius R. Each experiment was continued until breakthrough of the displacing phase occurred at the outer edge. After this, no further paraffin oil could be recovered. To ensure reproducibility of the wettability characteristics of the porous medium, the cell was subjected to a predetermined sequence of cleaning and drying operations at the end of each run. The details of these procedures are given elsewhere (20).

In laboratory scale experiments, inlet and outlet effects can greatly influence recovery and saturation measurements. The outlet end effect (Figs. 6a, b) is due to the accumulation of the wetting phase at the outlet and is caused by local capillary forces. In a water-wet system the capillary pressure, $p_c = p_o - p_w$, is positive in the interior of the porous medium (oil pressure is larger than the water pressure). On the other hand, since the oil-water interface is almost flat outside the medium, the

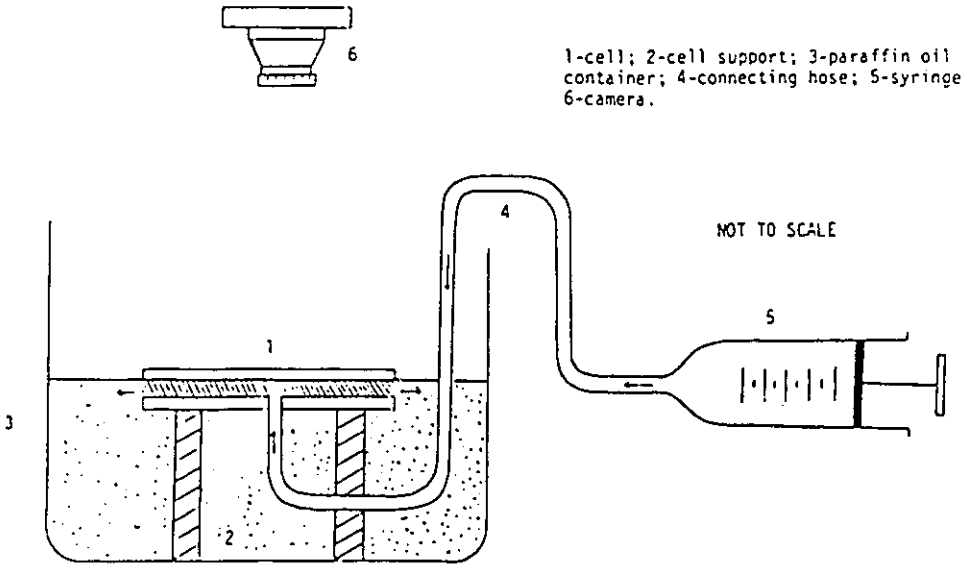

Fig. 19- Experimental set up.

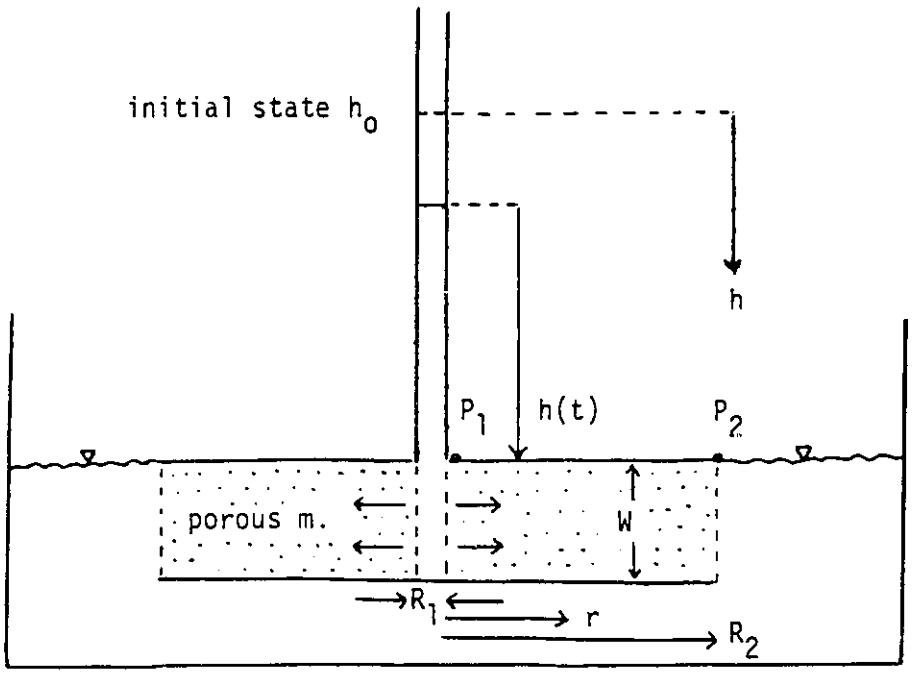

Fig. 20- Experimental set up for permeability measurement.

capillary pressure outside the porous medium is zero (45). When water initially reaches the outlet, its pressure is lower than the pressure of the oil surrounding the outlet face; therefore, no water can be produced, causing its accumulation near the outlet and thereby allowing the capillary pressure to decrease until it equals the capillary pressure outside the porous medium (zero). At this moment breakthrough occurs. Since this phenomenon is more pronounced at low flow rates, one could minimize this effect by increasing the injection rate and/or the core length (radius). During the present work, effects that are in agreement with this explanation were noted. Increasing the flow rate in strongly water-wet systems will enhance the spontaneous imbibition of water into the porous medium and, consequently, a simultaneous counterflow of oil out of the medium. This inlet end-effect is more obvious in short cores and at high flooding rates.

During the present work, much effort was given to differentiating between natural imbibition and imbibition due to end-effects. This was the primary motivation behind our selection of R_3 as the final recovery stage and not the edge of the cell as other researchers have done.

Porosity Measurement

The glass plates for each cell were weighed before glass beads were packed between them. The packed cell was then put in the oven and heated up gradually to 700°C. A few hours later the oven temperature was very slowly reduced (sharp increase or reduction of temperature would result in cracking of the cell). After the cell temperature became equal to that of the room, the cells were taken out and weighed again. The difference was the weight of the glass beads and since the thickness of cell was virtually constant, the pore volume (PV) and porosity could then be easily calculated using the following relationship:

$$\varepsilon = \frac{V_{cell} - V_{solid}}{V_{cell}} \times 100 \qquad (87)$$

where

$$V_{solid} = m_{solid}/\rho_{solid} \qquad (\rho_{solid} = 2.50 \text{ g cm}^{-3}) \qquad (88)$$

Permeability Measurement

The absolute permeability of each cell was measured using the following relationship developed for radial flow in a cylindrical porous medium (see Appendix B).

$$K = \frac{R_1^2 \mu}{2tw\rho g} \ln\left(\frac{h_o}{h(t)}\right) \ln\left(\frac{R_2}{R_1}\right) \qquad [=] L^2 \qquad (89)$$

The fluid used was pure water. The time t for the liquid height to be reduced from h_o to h(t) was measured for 10 equal intervals and the average absolute permeability was calculated in μm^2 (Fig. 20).

IFT Measurement

IFT measurements were carried out using a University of Texas spinning drop tensiometer. A detailed description of this method has been given by Cayias et al. (71). A standard capillary tube is filled up with the connate water and then a small droplet of crude oil is introduced. The cell is placed in a slot on a shaft of a rotor assembly. It is spun for 1-6 hours (sometimes longer) at speeds ranging from 1200-24000 rpm. Keeping the temperature constant at 25°C, the droplet width is measured at constant intervals until an equilibrium is reached. To calculate the IFT the following formula is used:

$$\gamma = 0.522\ \Delta\rho\ (d^3/T^2) \qquad (90)$$

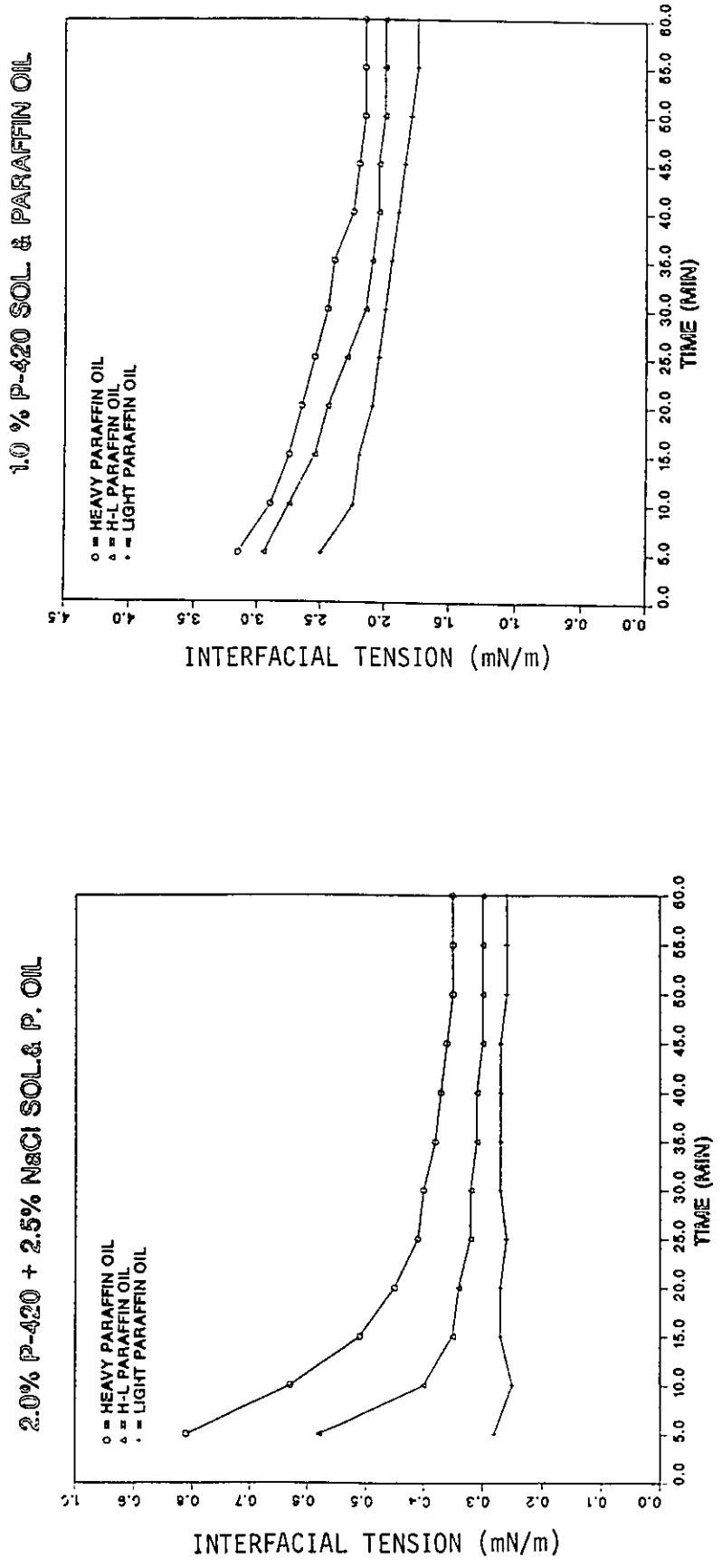

Fig. 21- Interfacial tension VS. Time for heavy, mixed and light paraffin oil.

where:

γ = interfacial tension (mN/m)

$\Delta\rho$ = density difference between the oil and water (g/cm^3)

d = the diameter of the droplet (cm)

T = the inverse of the angular velocity (sec)

Fig. 21 shows the IFT measurement results for six different situations in the presence of surfactant (Petrostep-420). It should be noted that without the surfactant the oil/water IFT was about 30.0 mN/m and therefore had to be measured by the classic du Nouy ring method.

Viscosity Measurement

The viscosity was measured using a Brookfield viscometer with a U.L. adapter (provided by Brookfield Engineering Laboratories). This viscometer operates by measuring the torque necessary to overcome the viscous resistance to the induced movement. The accuracy of this viscometer is about 1-2% of the full scale range employed. Sixteen mililitres of the solution were placed in the stainless steel tube of the U.L. adapter and then the precision cylindrical spindle was introduced into the cylinder. This assembly was then attached to the viscometer. The measurements were taken after equilibrium was reached.

Density Measurement

The density measurements were made using a 25 ml specific gravity bottle at room temperature of 24.0 ± 1.0°C.

9 - RESULTS AND DISCUSSION

As a first step, two sets of distinct qualitative experiments were performed. In the first set a less viscous fluid (water or/and surfactant solution) was used to displace a more viscous fluid (paraffin oils having different viscosities). Here the mobility ratio was greater than one and therefore, depending on the operating variables, different patterns of fingering were observed and naturally the recovered oil was much less than 100% (Figs. 6-a, 6-b). In another approach, the process was reversed, i.e. paraffin oil was used to displace pure water. In this case M, the mobility ratio was, less than one and, as can be seen in Figs. 22-23 the interfacial front looks quite stable and uniform and no macroscopic fingers are formed. Thus the oil recoveries obtained are much closer to 100% (favorable mobility ratio). Here mobility ratios of 1/18 and 1/154 were used and no significant visual effect of viscosity on the fingering pattern was observed. However, when very low injection flowrates (Q = 2.9 ml/h) were used, we observed the formation of very small microscopic finger-like instabilities at the oil-water interface (Fig. 23). These instabilities are the already discussed Haines jumps that occur at drainage or drying conditions (since the invading fluid is a non-wetting fluid there was no imbibition). At higher flow rates (Q = 348 ml/h) the interface moved so fast that the Haines jumps could not be detected by the naked eye, even though they exist and are probably 1-3 pores in length.

Lenormand et al. (23) have also observed similar results, but have incorrectly called these instabilities "fingers" and have concluded that the number of fingers at favorable mobility ratio conditions increases with a decrease in flow rate.

Since a favorable mobility ratio displacement ($M < 1$) has little practical importance in petroleum industry, we focussed our efforts on the unfavorable mobility ratio ($M > 1$) displacement process and various experiments were performed where a less viscous fluid displaced a more viscous non-wetting oil, as discussed in previous sections.

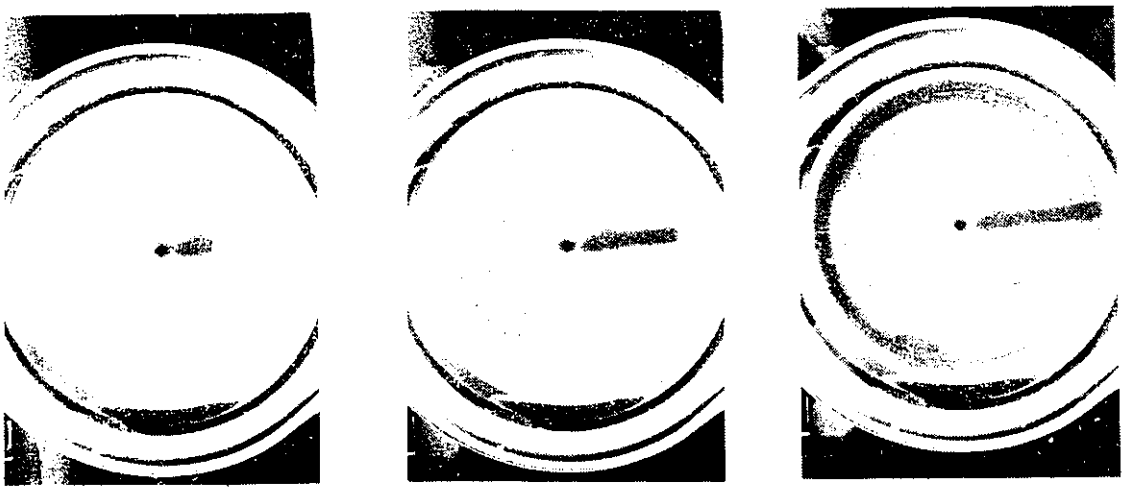

Fig. 22- Heavy paraffin oil displacing water at high flowrate (M - 1/154).

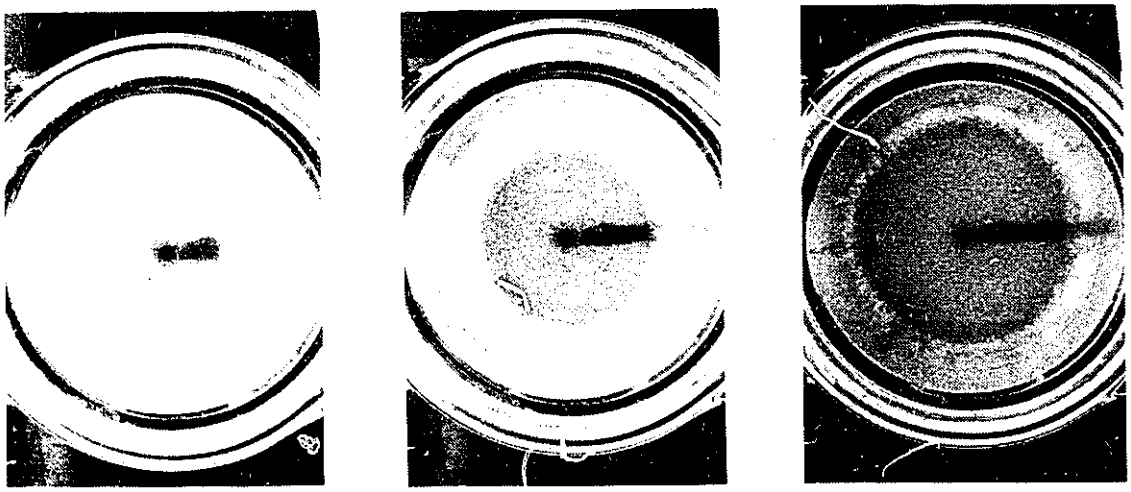

Fig. 23- Heavy paraffin oil displacing water at low flowrate (M - 1/154).

Complete listings of the results are given in Tables 1, 3 and 5. The results of fitting second order polynomials (i.e., Eqns. 61 and 65) to the observed data are presented in Tables 7 to 12. The significant parameters, and their precision and pertinent statistics for judging model adequacy, are also presented.

A few results yielded unusually large residuals during the initial fitting of the models. Closer examination of these outliers revealed unusual patterns of fingering and flow, most probably due to poor cleaning of the cell. In some cases, end effects (very low N_{Ca}) produced early imbibition and mushrooming resulting in abnormally high recoveries and fewer fingers (Figs. 6-a, 6-b). This very important effect has been ignored by many investigators. In yet other cases it was very difficult to accurately count the number of fingers. When re-examination of the results indicated such anomalies in analysis, they were either eliminated from the model building process or were repeated. The results listed in Tables 1, 3 and 5 exclude any such outliers.

Each model was found to adequately represent the data and to explain most of the variability in the data as indicated by the lack of fit ratios and R^2_{adj}-values in Tables 7-12. As well, plots of the residuals did not reveal any undesirable trends. Observed versus predicted values of the responses are plotted in Figs. 57-74 along with plots of the residuals versus run order and predicted value of the response. No unexpected trends are evident. (see Appendix A).

It is very important to note that other investigators have based their experimental and analytical work (including computation of the wettability number C*) on the number of fingers at maximum growth rate (n_m) which is extremely difficult to measure during a radial displacement. Contrary to linear displacement, where the number of fingers is limited by the cell width, the number of fingers increases with the finger length in radial displacement. In a radial cell the expanding circular front will eventually split while the fingers in a linear cell can remain stable, even

at low flow rates. Thus, in order to avoid errors resulting from misjudgment about which fingers are at maximum growth rate, the total number of fingers (n), representing all interfacial perturbations, were measured in the present work. Consequently, our models will predict a higher number of fingers than those proposed by previous theoretical work (19-20). Ni et al. (19) and Nasr-El-Din et al. (20) used R*, the macroscopic mean radius (the radius of the front in the absence of fingering), in their work. In this study R, the radius at breakthrough, which is actually the distance from the inlet point at breakthrough, or the length of the largest finger at breakthrough, has been used.

I) "Mechanistically-Based" Linear Models

Evaluation of Equation 61

The results of fitting the "mechanistically based" models given by Eqn. 61 to the experimental data for both the recovery and the total number of fingers are given in Tables 7, 9 and 11. Only those parameters found to contribute significantly to the fit and pertinent statistics are reported. Other terms were omitted because they were not found to be significantly different from zero nor to contribute significantly to the adequacy of the model fit. Correlations between estimates of the parameters were small as the result of the experimental design employed. Consequently, reliable inferences about individual parameters could be made without the need to consider the values of other parameters.

II) Models Based on Dimensionless Variables

A model based on dimensional analysis of the system, given by Eqn. 65 was also fitted to the data for both the recovery and number of fingers. The parameter estimates and pertinent statistics are listed in Tables 8, 10 and 12. Only those parameters that were found to significantly improve the fit are reported.

1 - CAPILLARY REGION

Recovery Model (Model A - Table 7)

The fitted model for oil recovery in the capillary region is

$$\begin{aligned} Ln(Rec\%) = {} & 2.794 + 0.814\ X_2 - 0.371\ X_3 + 0.301\ X_4 - 0.360\ X_5 \\ & - 0.260\ X_2X_4 + 0.286\ X_2X_5 + 0.177\ X_3X_5 \end{aligned} \qquad (91)$$

The model predicts that all the operating variables with the exception of flow rate, X_1, have a significant effect on the recovery. This contradicts the results of Nasr-El-Din et al. (20) and Sayyouh et al. (38) who found that, in the capillary region, recovery increased as the flowrate decreased. Examination of the results and the photographs from the experiments performed by Nasr-El-Din et al. (20) showed that, since they measured the recovery at the edge of the cell (i.e. $R = R_{cell}$), end-effects and the subsequent mushrooming and imbibition resulted in abnormally high recoveries. This phenomenon is more obvious at lower capillary numbers (lower flowrates) and explains the higher recoveries obtained by them at lower flowrates. The large data set and the experimental design employed in the present study ensures the validity of our finding over a wide range of values for the other operating variables.

The coded radius of breakthrough X_2, has a rather complex effect on the recovery. This effect depends on the values of coded permeability, X_4, and IFT, X_5. For low values of X_4 and high values of X_5, an increase in the distance from the injection point causes a large increase in recovery. At $(X_4, X_5) = (-1, 1)$ the logarithm of percent recovery increases by 2.72 as X_2 increases from -1 to 1; this yields a relative increase in percent recovery of 14.22 (1422%). At $(X_4, X_5) = (1, -1)$ the logarithm of percent recovery increases by only 0.54 as X_2 increases from -1 to 1. This translates into an increase in percent recovery of 71%. The minimum predicted (by Eqn. 91)

Table 7

Parameter Estimates and Pertinent Statistics for Models Based on Eqn. 61 (Models A & B)

Response	Significant Parameters	Parameter Values	Standard Error	$\frac{SSR}{(n-p)}$	$\hat{\sigma}_p^2$	lack of fit ratio (eqn. 70)	$F_{0.05}$	R^2_{adj}
ln(Rec%) N = 55 Np = 8 Model A	β_0	2.794	0.057	0.145	0.103	1.814	2.01	0.813
	β_2	0.814	0.067					
	β_3	-0.371	0.075					
	β_4	0.301	0.070					
	β_5	-0.360	0.070					
	β_{24}	-0.260	0.077					
	β_{25}	0.286	0.076					
	β_{35}	0.177	0.082					
ln (n) N = 55 Np = 12 Model B	β_0	3.053	0.047					
	β_1	0.145	0.027	0.020	0.023	0.737	2.03	0.932
	β_2	0.496	0.025					
	β_3	0.219	0.029					
	β_4	0.094	0.026					
	β_5	-0.143	0.028					
	β_{44}	-0.454	0.060					
	β_{13}	0.147	0.029					
	β_{24}	-0.073	0.028					
	β_{25}	0.133	0.029					
	β_{34}	-0.069	0.032					
	β_{45}	0.125	0.030					

value of the logarithm of percent recovery is found at X_2 = -1 and (X_4, X_5) = (1, -1). The ratio of maximum to minimum recovery is 19.16. In general, for the capillary region, as the distance from the injection point increases, the oil recovery also increases (Figs. 24, 25). This seems quite logical because in radial displacement, the velocity decreases as R increases. Therefore, imbibition is expected to increase with an increase in R, causing higher recoveries.

The effect of the logarithm of viscosity difference, X_3, on the recovery depends on the level of IFT. The lowest recovery is obtained at (X_3, X_5) = (1, 1) and the highest at (X_3, X_5) = (-1, -1). The ratio of predicted maximum to minimum recovery is 4.31 (Fig. 26). This finding is consistent with theory and previous research (39) as well as practice which predicts higher oil recoveries from reservoirs containing lighter oil by floods that produce lower oil/water IFT.

The effect of the logarithm of the permeability of the porous medium, X_4, depends on the value of the logarithm of the radius at breakthrough as mentioned earlier. The recovery increases with permeability, the increase being greater as the radius increases. This interaction is shown in Fig. 24.

The effect of X_5, the coded form of the IFT, on the logarithm of recovery is complex and depends on the values of X_2 and X_3. At (X_2, X_3) = (-1, 1) the logarithm of recovery decreases by 0.94 as the coded value of IFT increases from -1 to 1. This would mean a relative decrease of 61% in oil recovery. On the other hand, at (X_2, X_3) = (1, -1), the logarithm of recovery is decreased by 0.5 (39%) as the coded value of IFT increases from -1 to 1. The highest recovery is obtained at (X_2, X_3) = (1, -1) and the lowest value of IFT. The minimum recovery occurs at (X_2, X_3) = (-1, 1) and X_5 = 1. These findings are quite consistent with theory and confirm the results obtained by Mungan (39) and Uren and Fahmy (33). The ratio of maximum to minimum recovery is 21.98 (see Figs. 25-26).

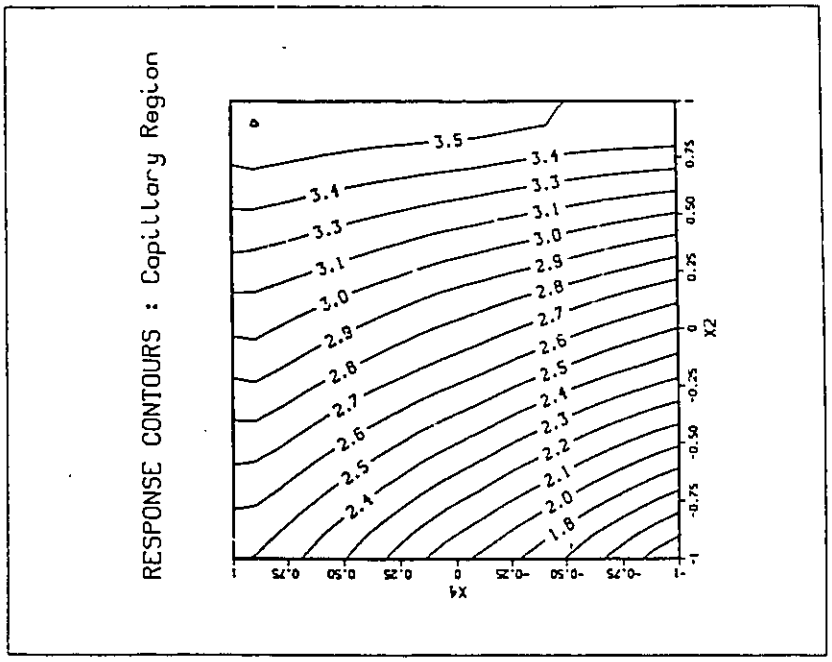

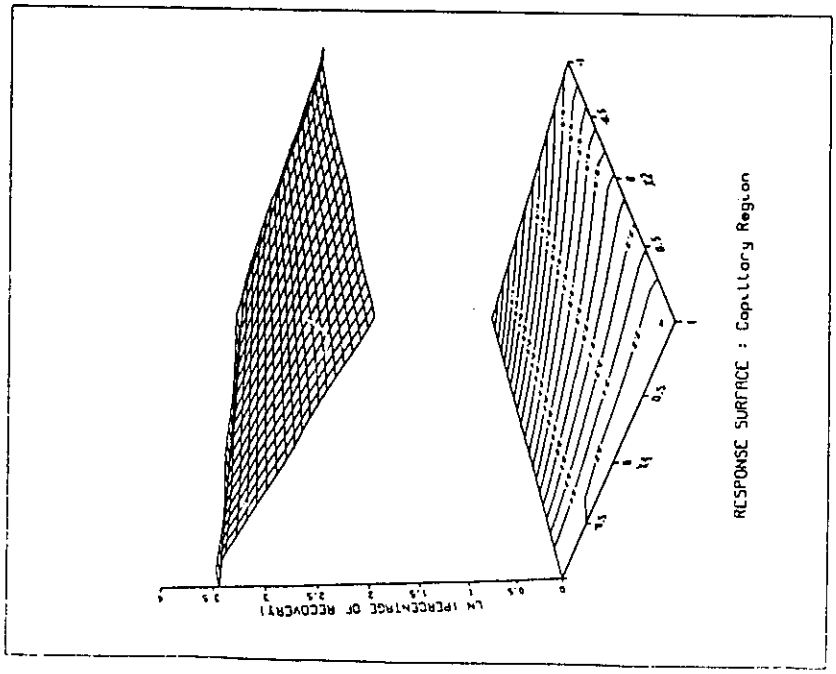

Fig. 24- Response surface and contours for model A.

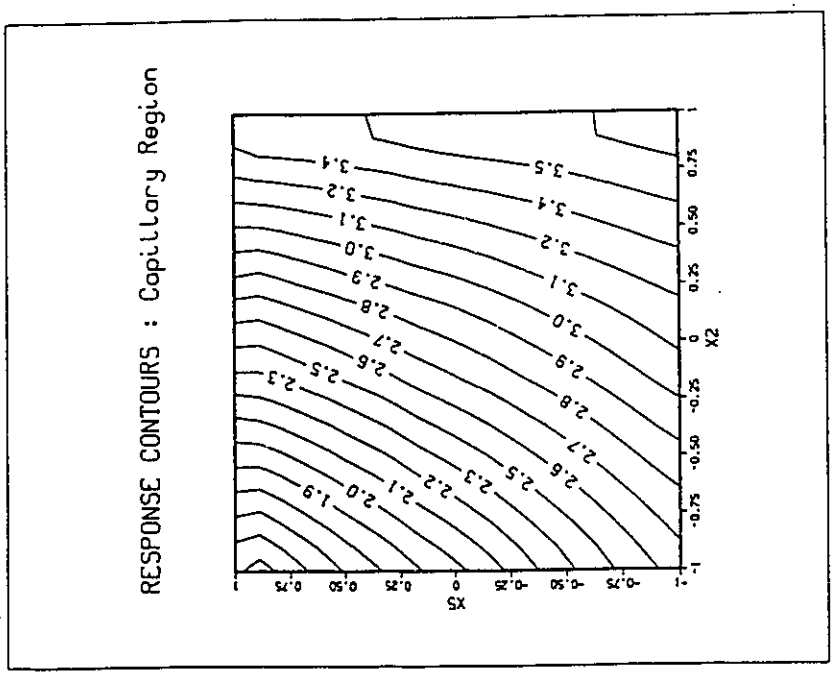

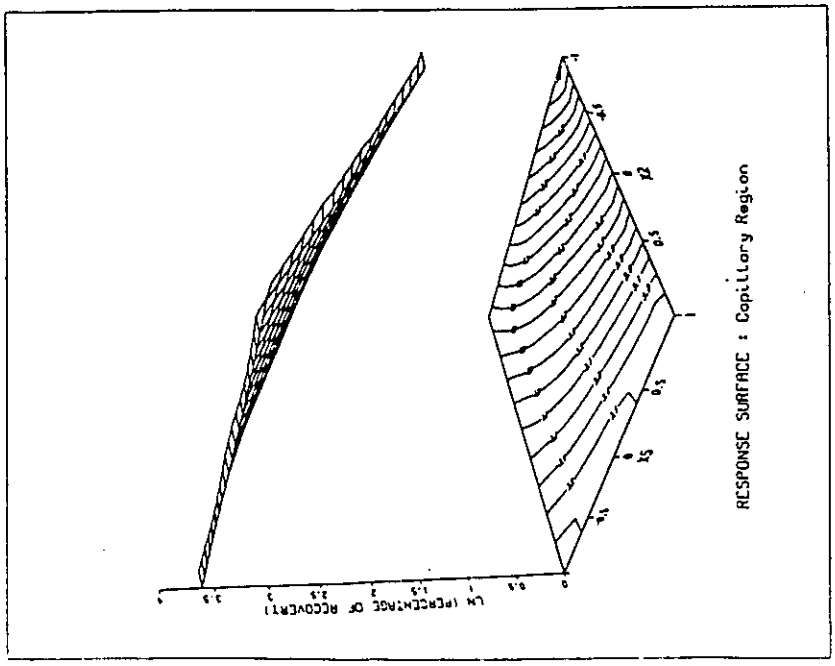

Fig. 25- Response surface and contours for model A.

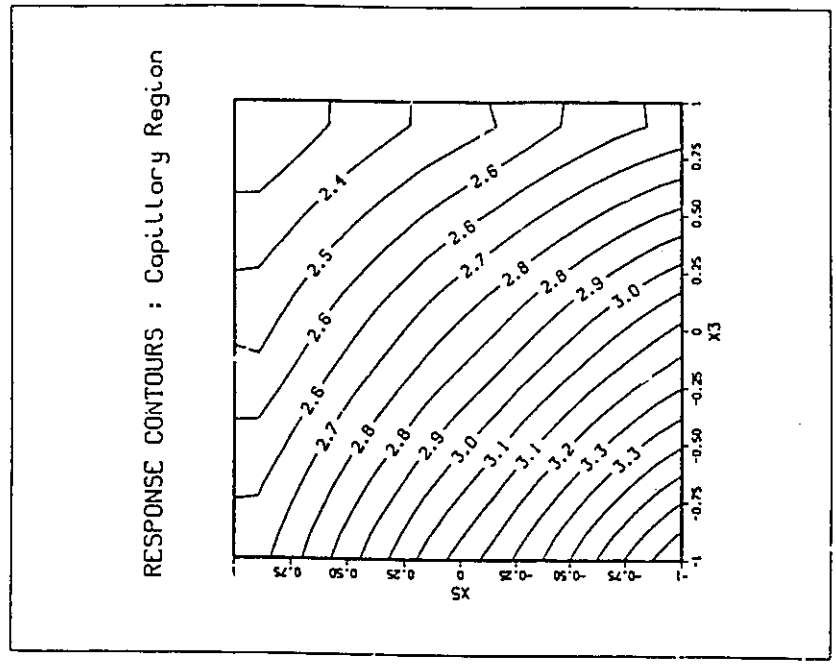

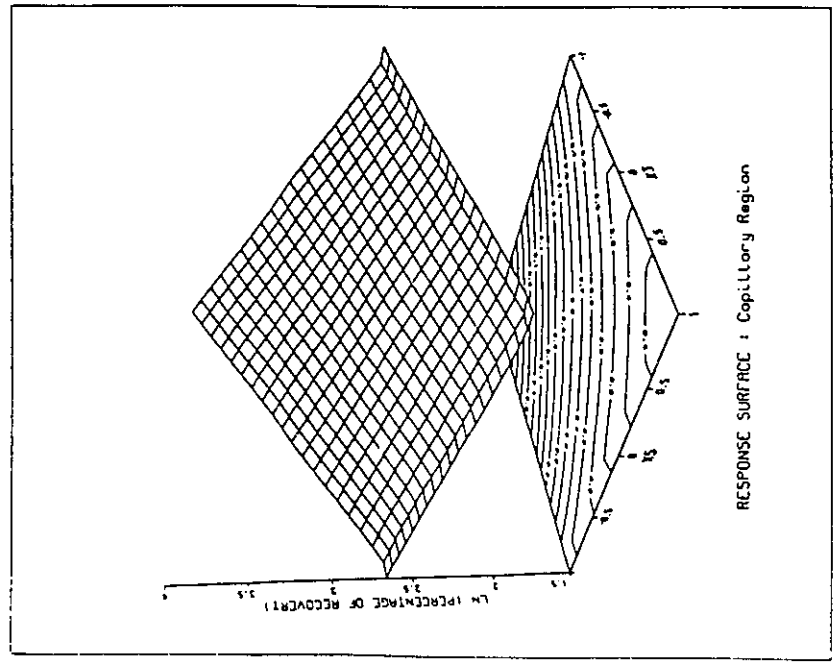

Fig. 26- Response surface and contours for model A.

Model for Number of Fingers (Model B - Table 7)

The fitted model relating the total number of fingers to various operating variables is

$$\begin{aligned} Ln(n) = {} & 3.053 + 0.145\ X_1 + 0.496\ X_2 + 0.219\ X_3 + 0.094\ X_4 - 0.143\ X_5 - 0.454\ X_4^2 \\ & + 0.147\ X_1X_3 - 0.073\ X_2X_4 + 0.133\ X_2X_5 - 0.069\ X_3X_4 + 0.125\ X_4X_5 \end{aligned} \quad (92)$$

The number of fingers depends on all the factors studied. Unlike the recovery, the coded value of flowrate was found to affect the number of fingers. Generally speaking, since there is a limit to how fast a finger can grow or absorb an increase in flowrate, new fingers are formed as the injection rate reaches a certain value. Thus, increased flow rate should in theory result in a higher number of fingers. The interaction term $\beta_{13}X_1X_3$ indicates that the effect of flowrate depends upon the value of X_3, the coded viscosity difference. At low levels of viscosity difference, the number of fingers increases with flowrate. At high levels of viscosity difference, this increase in the number of fingers with flowrate intensifies (Fig. 27). This phenomenon is due to the increased mobility ratio, (M) at high viscosity differences.

The effect of the coded value of radius at breakthrough, X_2, depends upon the level of permeability, X_4, and IFT, X_5. At (X_4, X_5) = (-1, 1) the logarithm of the number of fingers increases by 1.40, a 307% increase in the number of fingers as X_2 increases from -1 to 1. At X_2 = 1 the maximum occurs at X_4 = 0.02 and at X_2 = -1 it happens at X_4 = 0.18 (Fig. 28). As X_2 increases from -1 to 1, at (X_4, X_5) = (1, -1), the recovery increases by 0.79. In general, the number of fingers steadily increases as the distance from the injection point is increased. This is due to the increasing surface area of the oil/water interface which enhances the possibility of instabilities. At X_4 = 0 the maximum number of fingers occurs at (X_2, X_5) = (1, -1) and is equal to 35.13 (Fig. 29).

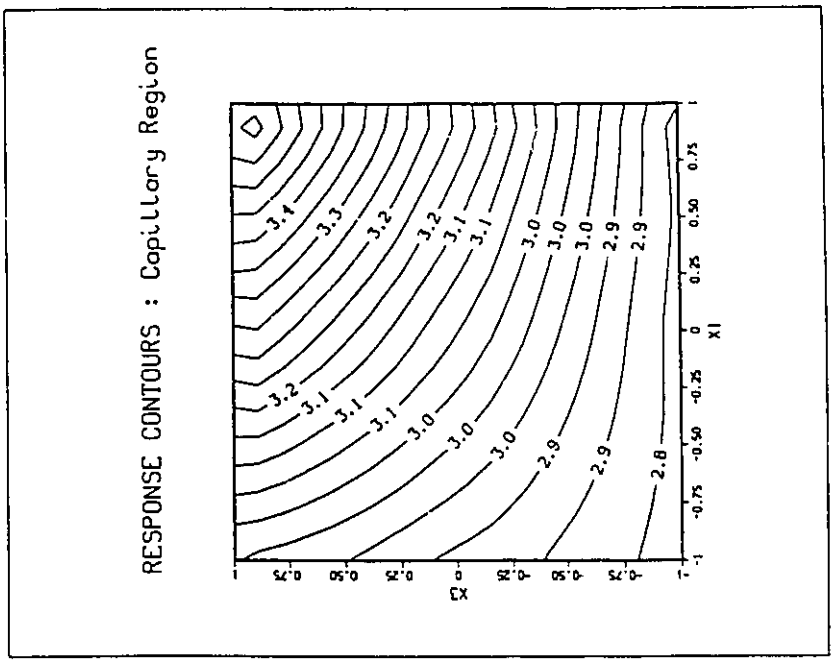

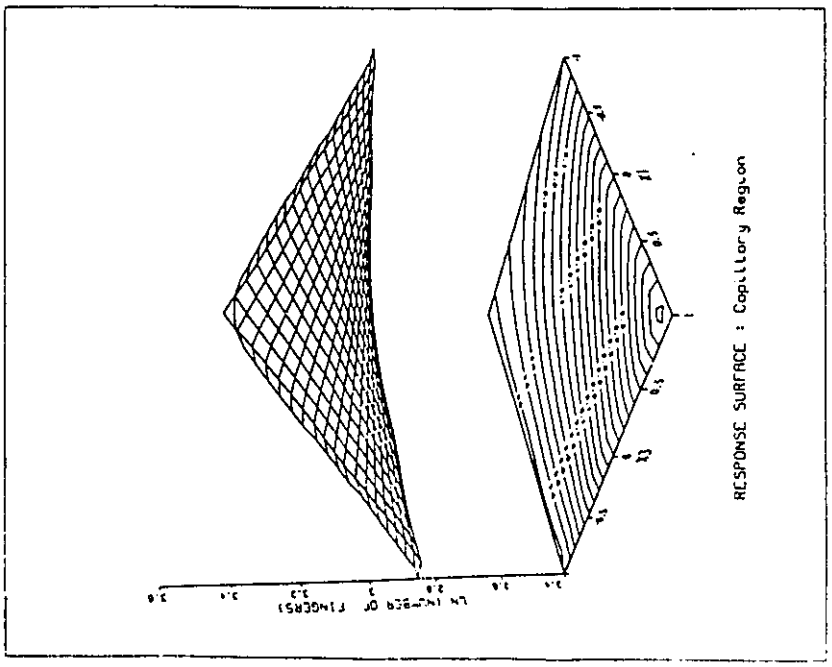

Fig. 27- Response surface and contours for model B.

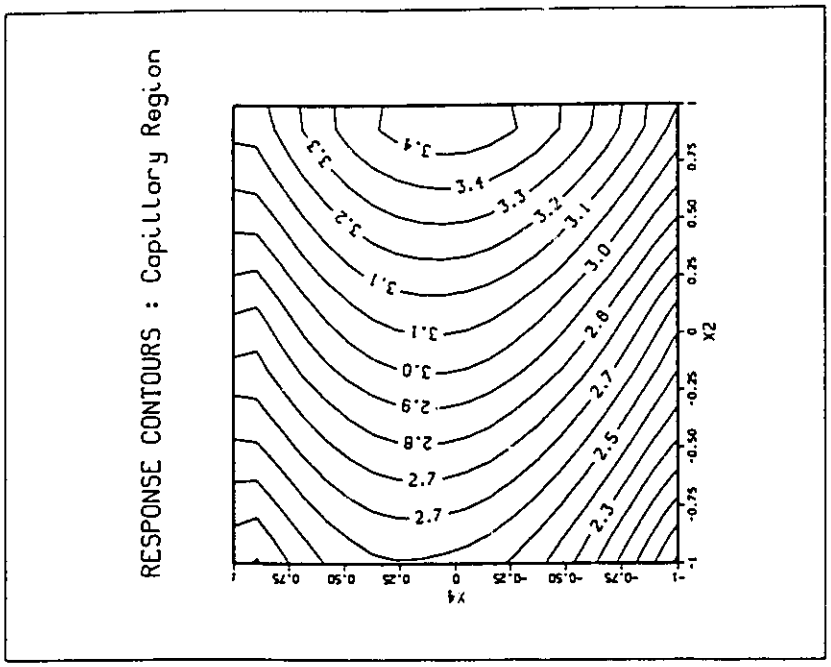

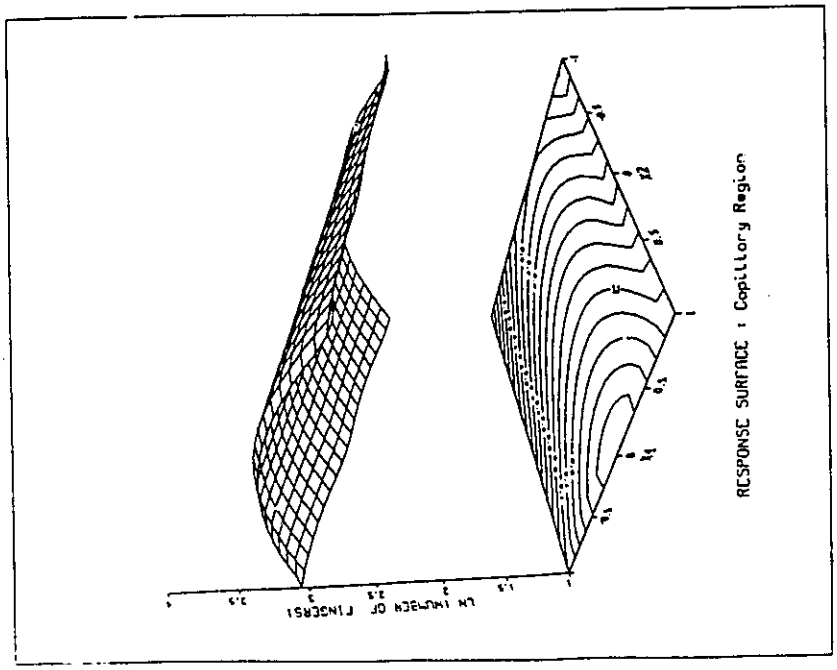

Fig. 28- Response surface and contours for model B.

The effect of viscosity difference is also dependent on other operating variables. At (X_1, X_4) = (-1, 1), as the coded viscosity difference varies from -1 to 1, the logarithm of the number of fingers is slightly increased by a factor of 0.08. At (X_1, X_4) = (1, -1) the increase is 0.96 corresponding to a doubling of the number of fingers. This indicates the enhancing effect that flowrate has on the number of fingers. At X_3 = 1, there is a maximum at X_4 = 0.03 and this maximum shifts to X_4 = 0.18 as X_3 is reduced to -1 (Fig. 30).

The effect of permeability on the logarithm of the number of fingers appears in linear, quadratic and interaction terms. As Figures 28, 29 and 30 show, the response surface for the logarithm of the number of fingers passes through a maximum. At X_2 = 1, X_3 = 1 and X_5 = 1, this maximum occurs at X_4 = 0.08 while at X_2 = -1 and X_3 = -1 and X_5 = -1 this maximum occurs at X_4 = 0.12.

IFT also affects the fingering pattern in a complex fashion Its effect depend on the values of coded distance and coded permeability (see Table 7). Figure 29 shows that the number of fingers increases at a higher rate at low values of X_2 than at high values as the IFT is reduced from 1 to -1. At (X_2, X_4) = (-1, 1), the logarithm of the number of fingers decreases by a factor of 0.30 as the coded IFT increases from -1 to 1. At (X_2, X_4) = (1, -1) the decrease is 0.27. The lowest number of fingers corresponds to (X_2, X_4) = (-1, 1) and X_5 = 1. The maximum number of fingers is obtained at (X_2, X_4) = (1, 1) and X_5 = -1. The ratio of maximum to minimum number of fingers is 7.26.

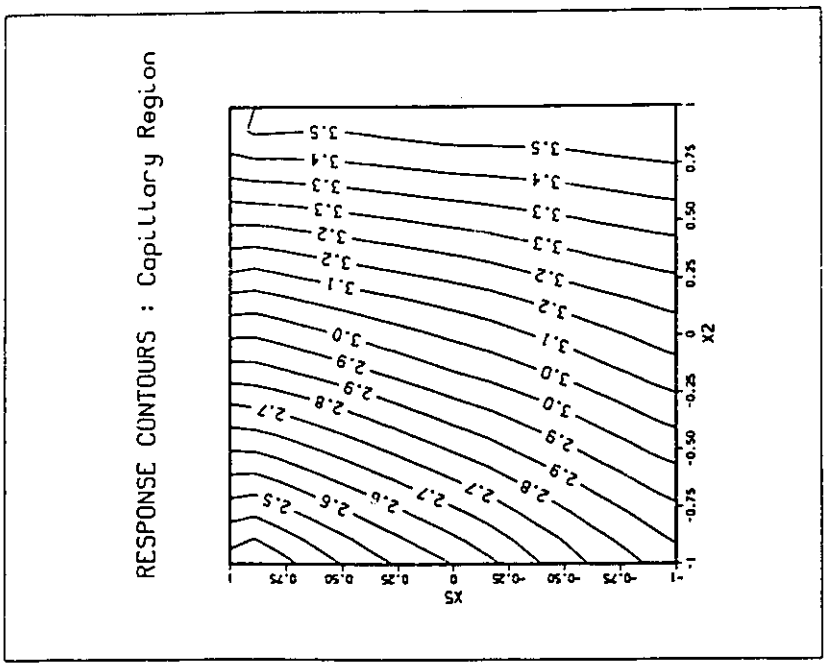

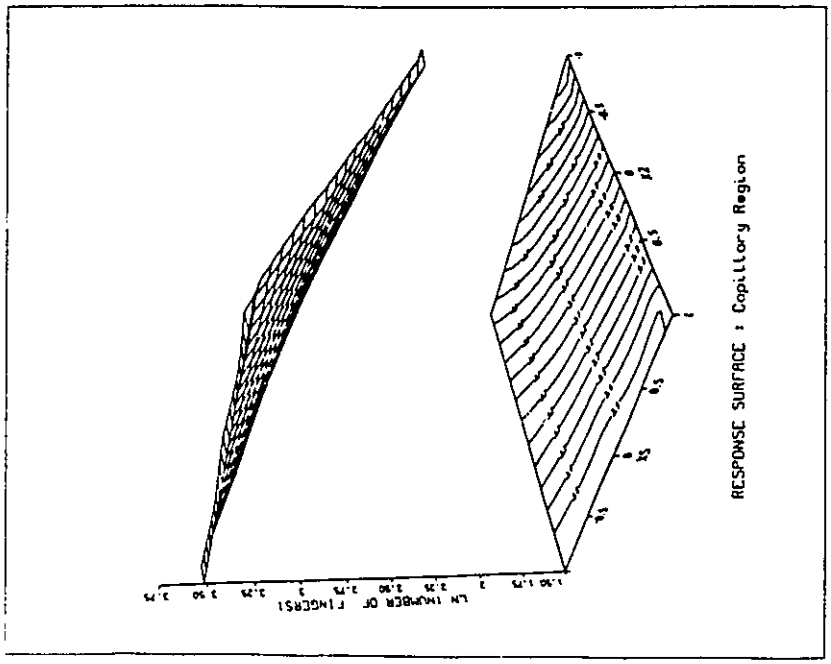

Fig. 29- Response surface and contours for model B.

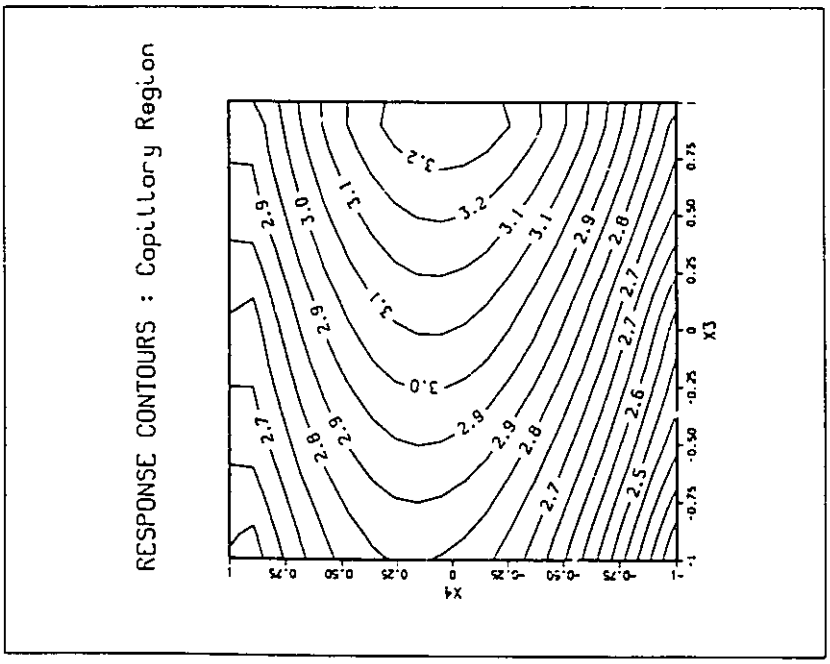

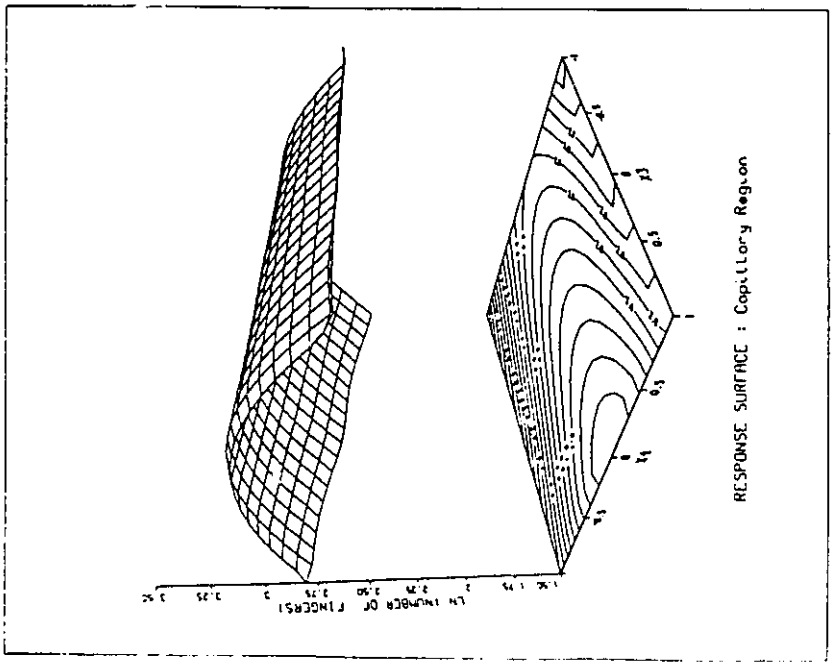

Fig. 30- Response surface and contours for model B.

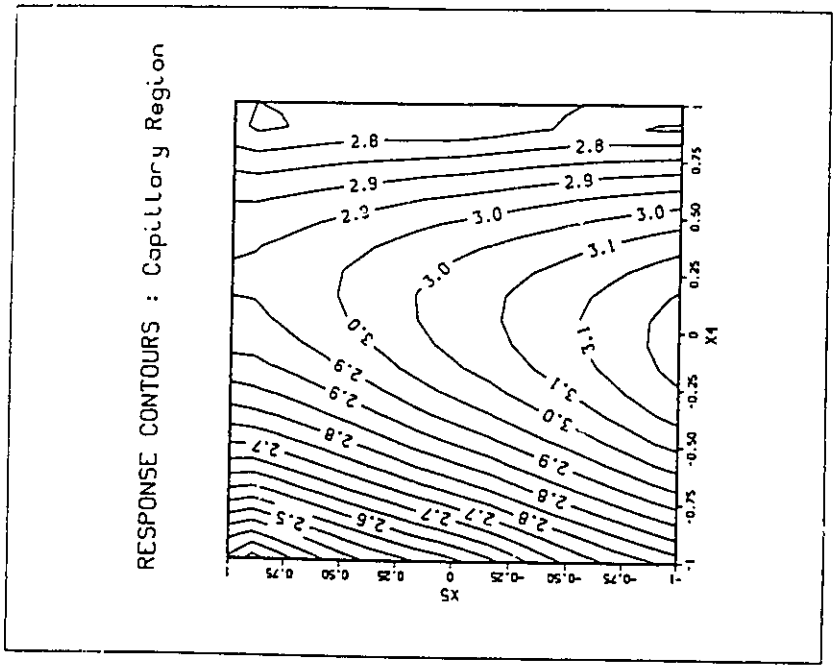

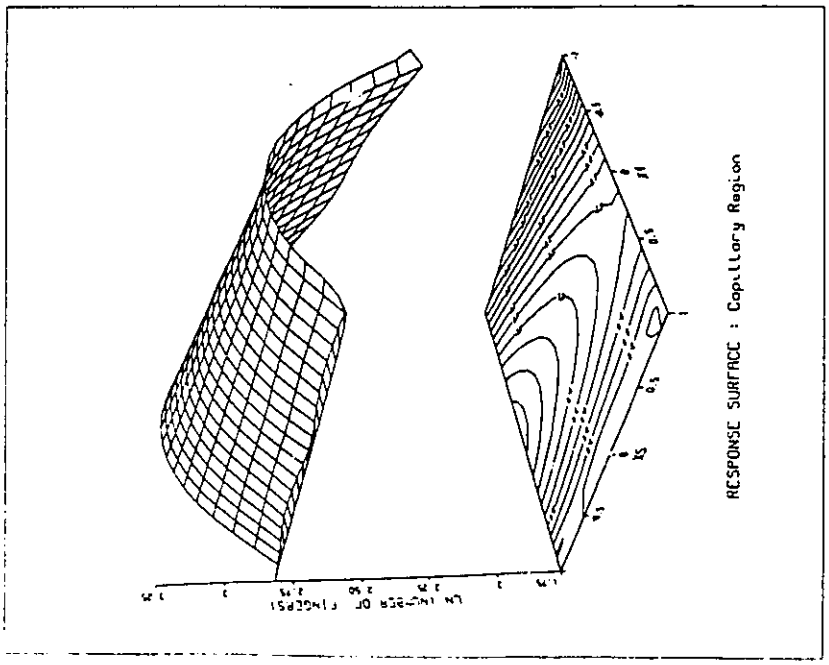

Fig. 31- Response surface and contours for model B.

Recovery Model (Model C - Table 8)

In terms of coded dimensionless variables, the estimated parameters and pertinent statistics from fitting the data obtained in the capillary region are listed in Table 8. Recovery is described by:

$$\begin{aligned} \text{Ln(Rec\%)} = {} & 2.795 + 0.314\,X_1 - 0.349\,X_2 + 0.758\,X_3 - 0.619\,X_4 \\ & + 0.334\,X_1X_2 - 0.422\,X_1X_3 + 0.363\,X_2X_3 \end{aligned} \qquad (93)$$

All dimensionless variables have an effect on the oil recovery. The coded capillary number X_1, has a linear effect on the logarithm of recovery which depends on the value of X_2 and X_3. At $(X_2, X_3) = (-1, 1)$, the model predicts a decrease in the logarithm of recovery by 0.88 which, in terms of real recovery, is a 58.68% decrease as X_1 increases from -1 to 1. The maximum recovery of 77.01% occurs at $(X_2, X_3) = (-1, 1)$ and $X_1 = -1$. This is a good example of the danger involved in generalizing conclusions from experimental work without looking at the interactions between the independent variables. Considering the capillary number alone, the highest recovery is expected at the highest value of capillary number but because of the interactions, the maximum recovery occurs at the lowest value of X_1.

On the other hand, at $(X_2, X_3) = (1, -1)$ the logarithm of recovery increases by 2.14 representing an increase in recovery by a factor of 7.48 as the coded value of capillary number, X_1, increases from -1 to 1. Under these conditions, minimum and not maximum recovery occurs at $X_1 = -1$. The ratio of maximum to minimum predicted recoveries is large namely 77/1.9 = 40.5. Figures 32 and 33 depict the predicted recovery contours for the X_1X_2 and X_1X_3 interactions, respectively. The values of X_3 and X_2 are held at zero respectively, for each case. Considering only the main and particular interaction effect, the recovery increases as the coded capillary number, X_1, increases from -1 to 1. This is consistent with the theory that predicts an increase in

Table 8

Parameter Estimates and Pertinent Statistics for Models Based on Eqn. 65 (Models C & D)

Response	Significant Parameters	Parameter Values	Standard Error	$\frac{SSR}{(n-p)}$	$\tilde{\sigma}_p^2$	lack of fit ratio (eqn. 70)	$F_{0.05}$	R^2_{adj}
ln(Rec%) N = 55	β_0	2.795	0.054	0.141	0.103	1.729	2.01	0.818
$N_p = 8$	β_1	0.314	0.107					
	β_2	-0.349	0.064					
Model C	β_3	0.758	0.065					
	β_4	-0.619	0.104					
	β_{12}	0.334	0.115					
	β_{13}	-0.422	0.114					
	β_{23}	0.363	0.069					
ln (n) N = 55	β_0	3.024	0.051					
$N_p = 12$	β_1	0.451	0.045	0.023	0.023	1.040	2.03	0.921
	β_2	-0.179	0.026					
	β_3	0.467	0.027					
	β_4	0.326	0.043					
Model D	β_{11}	0.281	0.090					
	β_{22}	-0.625	0.077					
	β_{44}	0.336	0.101					
	β_{12}	0.167	0.054					
	β_{13}	-0.184	0.047					
	β_{14}	0.544	0.125					
	β_{23}	0.144	0.029					

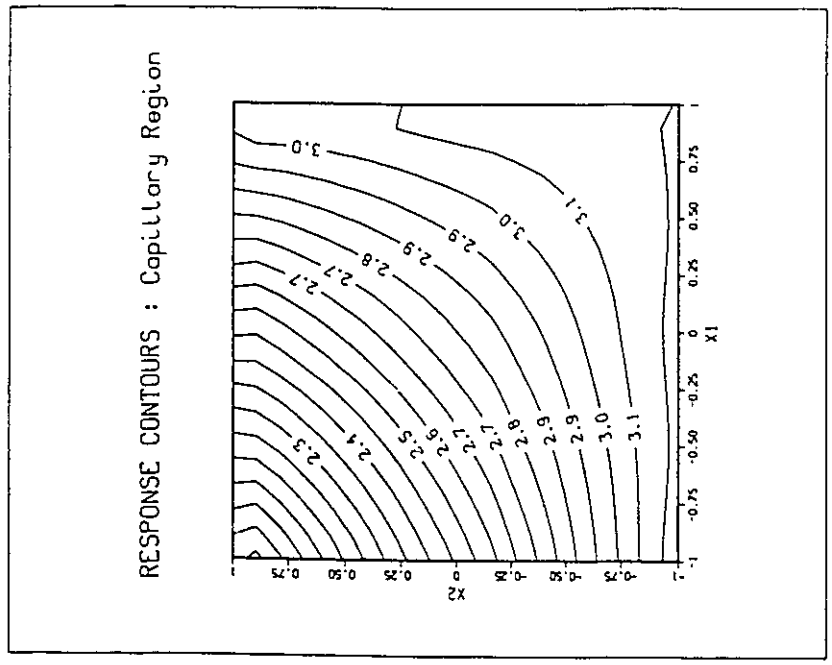

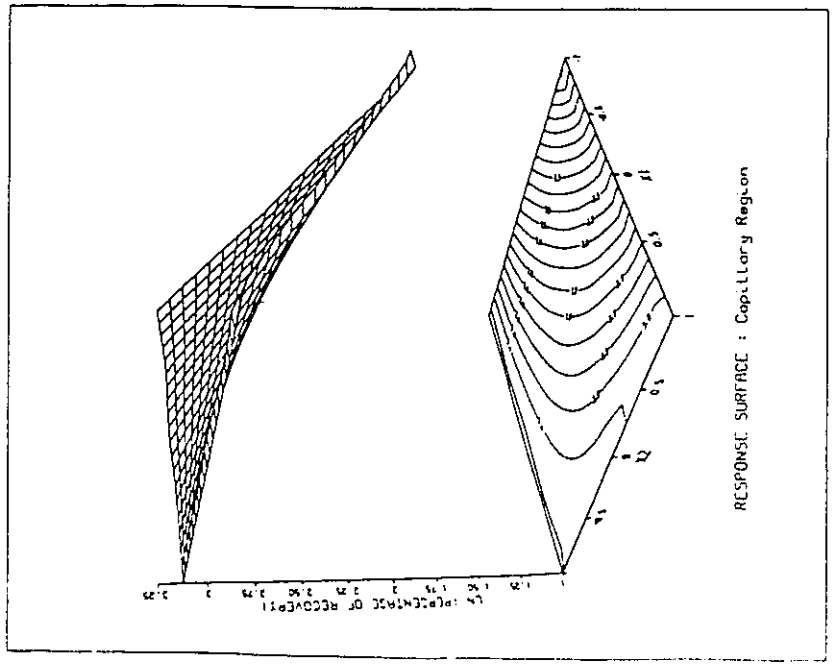

Fig. 32- Response surface and contours for model C.

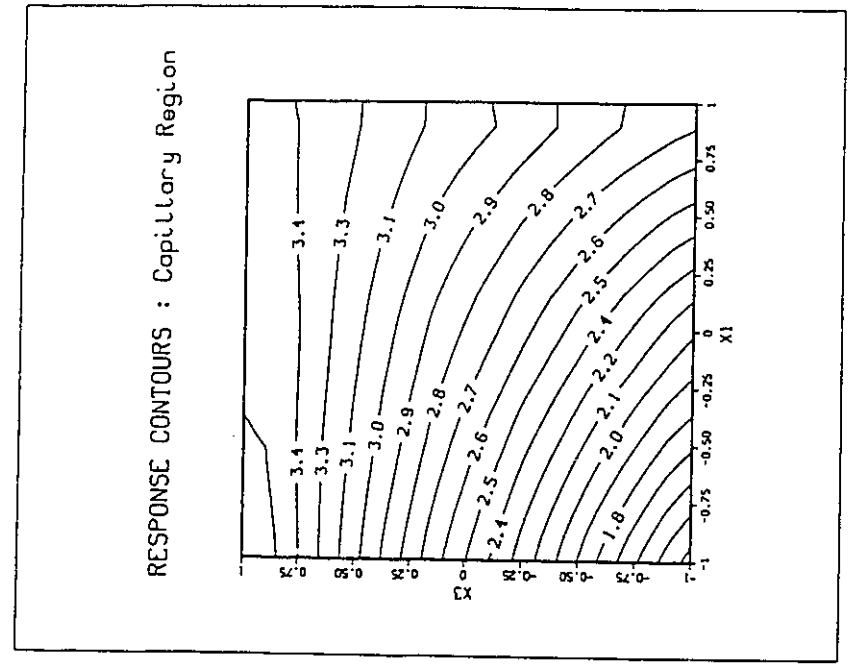

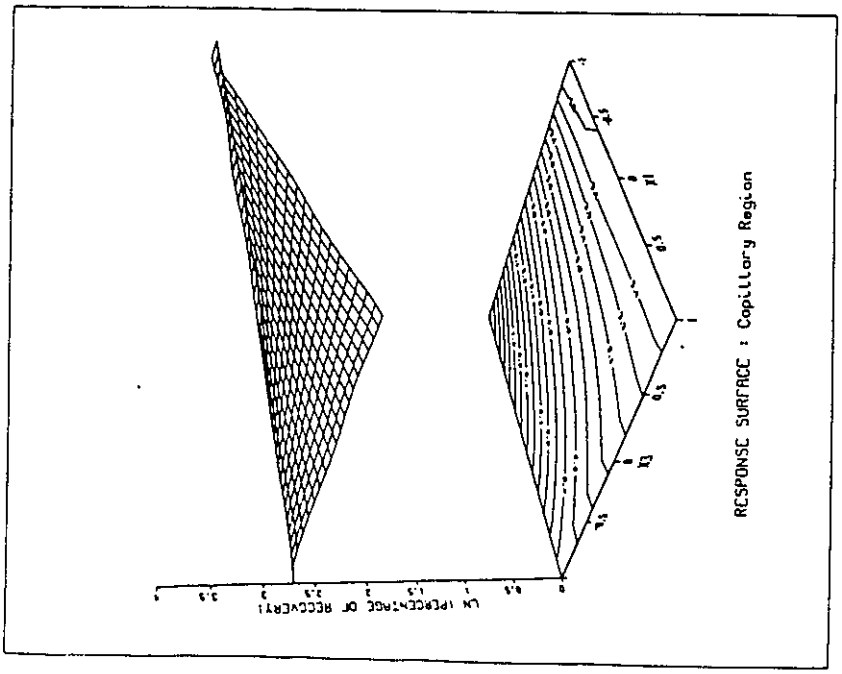

Fig. 33- Response surface and contours for model C.

the recovery with an increase in the capillary number, N_{Ca}. However, as we saw earlier, this is not true if all interactions are considered.

The coded form of h /$\sqrt{K}$, X_2, affects recovery as a main effect as well as through the interaction terms, X_1X_2 and of X_2X_3 (Table 8). At (X_1, X_3) = (-1, 1) the predicted logarithm of recovery decreases by 0.64 as X_2 increases from -1 to 1. This represents a relative decrease in the recovery percent by a factor of 0.47. At (X_1, X_3) = (1, -1), increasing X_2 from -1 to 1 results in a decrease in the logarithm of recovery by 0.76 which represents a predicted decrease in real recovery by a factor of 0.47. The maximum predicted recovery occurs at (X_1, X_2, X_3) = (-1, -1, 1), the lowest capillary number, highest permeability and highest radius and the minimum recovery (1.29%) is at (X_1, X_2, X_3) = (-1, 1, -1). The ratio of maximum to minimum recovery is large, being 41.52. Fig. 32 shows that, when considering X_1 and X_2, the recovery increases as the coded capillary number X_1, increases (with the exception of at X_2 = -1) and it decreases as X_2 increases. Fig. 34 also shows that the recovery decreases as X_2 increases and it increases as X_3, the coded R/h, increases. This means that, at low flowrates, an increase in the permeability results in an increase in the recovery. This increase is much less considerable at high X_3 (Fig. 34) values. Considering the increased possibility of imbibition (and therefore higher recoveries) at higher X_3, the coded form of R/h, this seems very logical.

As far as the coded value of R/h, X_3, is concerned, its effect depends upon X_1 and X_2. Keeping the coded capillary number, X_1, equal to zero means that for any permeability, the predicted recovery increases as X_3 is increased (Fig. 34). This is due to increased imbibition at higher R values. On the other hand, at X_2 = 0 (moderate permeabilities), an increase in the capillary number or the radius results in higher (except at high X_3 values) recoveries (Fig. 33). This is consistent with theory and previous research.

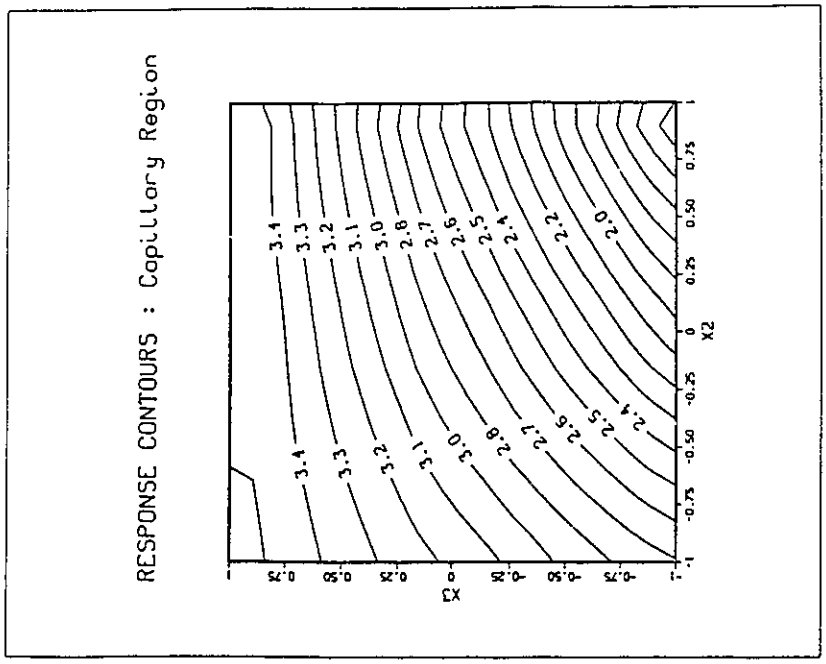

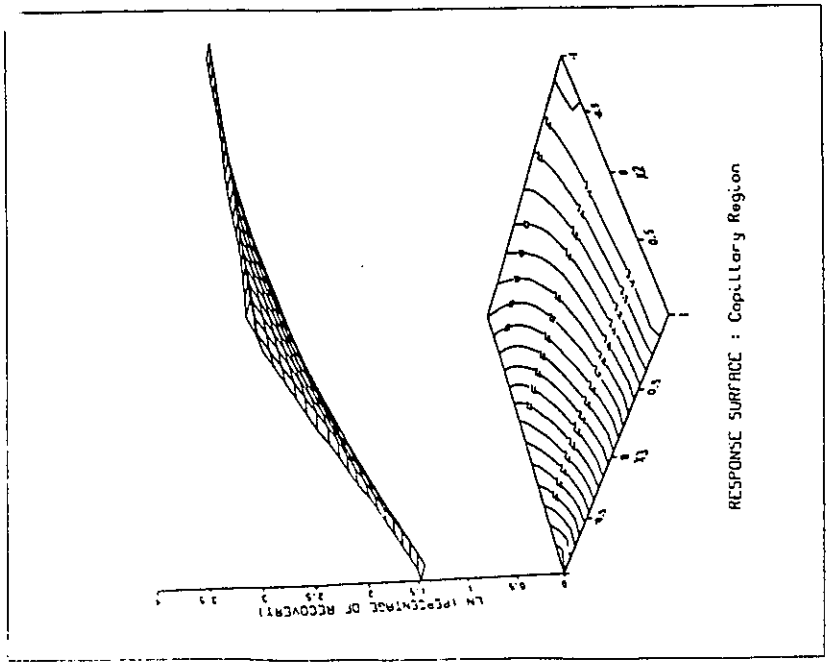

Fig. 34- Response surface and contours for model C.

The coded viscosity ratio, X_4, has a large linear negative effect on the recovery. As the viscosity difference is increased from -1 to 1, the recovery is decreased by a factor of $0.29 = e^{-1.238}$. This is in agreement with theory and can be explained by higher mobility ratios which in turn produce more fingers and cause the recovery to be reduced. This phenomenon is encountered during oil recovery from heavy oil fields.

Model for Number of Fingers (Model D - Table 8)

In terms of coded dimensionless variables (Eqn. 65) the fitted model for the number of fingers was found to be

$$\begin{aligned} \mathrm{Ln}(n) = {} & 3.024 + 0.451\,X_1 - 0.179\,X_2 + 0.467\,X_3 + 0.326\,X_4 + 0.281\,X_1^2 - 0.625\,X_2^2 \\ & + 0.336\,X_4^2 + 0.167\,X_1X_2 - 0.184\,X_1X_3 + 0.544\,X_1X_4 + 0.144\,X_2X_3 \end{aligned} \qquad (94)$$

The model predicts that each of the coded dimensionless variables has a significant effect on the number of fingers in the capillary region (Table 8).

The coded capillary number X_1, influences the fingering pattern in a complex fashion. Its effect appears in both linear and quadratic terms as well as in interaction form with X_2, X_3 and X_4. The maximum number of fingers (the least desirable condition) occurs at $X_1 = X_2 = X_3 = X_4 = 1$. The minimum number of fingers is obtained at $(X_1, X_3) = (-1, -1)$ and $(X_2, X_4) = (1, 1)$. The ratio of maximum to minimum number of fingers is 34.68. The above conclusions are consistent with theory. Fig. 35 shows the response surface and contours for the X_1X_2 interaction with $X_3 = X_4 = 0$. The response surface is a saddle. At $X_1 = 1$ the maximum is at $X_2 = -0.01$ and at $X_1 = -1$ the maximum is at $X_2 = -0.28$. Consideration of X_1 and X_3 alone reveals that the number of fingers increases steadily as X_1 and X_3 increase from -1 to 1. This increase is larger at low values of R/h (Fig. 36). Fig. 37 shows that the maximum number of fingers is pre-

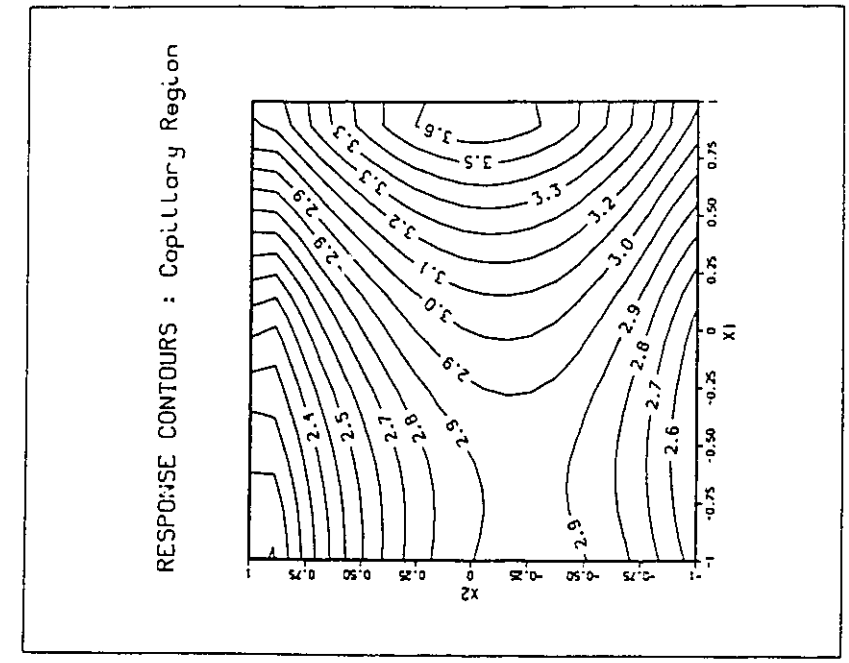

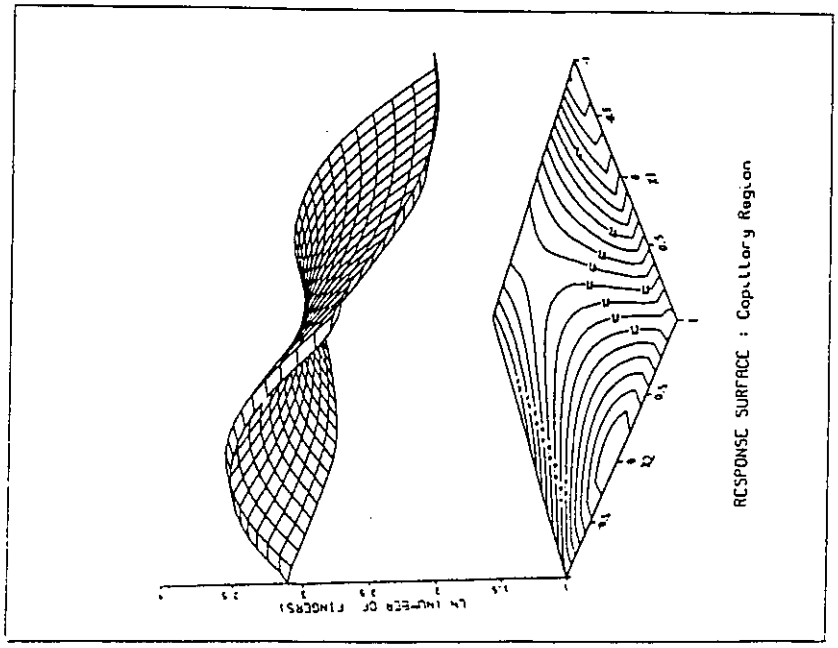

Fig. 35- Response surface and contours for model D.

dicted at high values of X_1 and X_4. Again this is consistent with theory. At $X_2 = X_3 = 0$, the minimum number of fingers is on the line $X_1 = (-0.451 - 0.544\ X_4)/0.562$.

The effect of the coded dimensionless term h $/\sqrt{K}$, X_2, on the logarithm of number of fingers also appears as linear, quadratic and interaction terms. At $(X_1, X_3) = (-1, 1)$, as coded h $/\sqrt{K}$ increases from -1 to 1, the logarithm of number of fingers is decreased by 0.40, a 33.2% decrease in the number of fingers. At the other extreme, namely $(X_1, X_3) = (1, -1)$, however, the logarithm of number of fingers decreases as X_2 is increased from -1 to 1. This is a decrease of 0.31, a 27.27% decrease in the number of fingers. Fig. 35 shows the response surface and contours for the X_1X_2 interaction (all the other variables have been kept constant at their zero level). In general, the location of the maximum is at $X_2 = (-0.179 + 0.167\ X_1 + 0.144\ X_3)/1.25$ or at $X_1 = -(0.451 + 0.167\ X_2 - 0.184\ X_3 + 0.544\ X_4)/0.562$. Fig. 38 shows that when considering X_2 and X_3 alone, the number of fingers constantly increases as X_3 is increased from -1 to 1 for all values of X_2. For $X_1 = 0$ (moderate capillary numbers) this maximum occurs at $X_2 = -0.26$ for $X_3 = -1$ and at $X_2 = -0.03$ for $X_3 = 1$ (see Fig. 38).

The effect of X_3, depends on the value of X_1 and X_2. At $(X_1, X_2) = (-1, 1)$ as the coded R/h increases from -1 to 1, the logarithm of number of fingers increases by 1.59, a 390.56% relative increase in the number of fingers. At the other extreme, namely at $(X_1, X_2) = (1, -1)$, this increase is only by 0.28, a relative increase of 32%. This means that any increase in the number of fingers due to increased radius is more considerable at low capillary numbers (e.g. low flow rates) and low permeabilities. At $X_3 = -1$, the minimum number of fingers is equal to 2.97 at $(X_1, X_2) = (-1, 1)$ and, at $X_3 = 1$ the maximum (26.26%) is at $(X_1, X_2) = (1, -1)$. The ratio of maximum to minimum is 8.96 (also see Fig. 36, 38). The maximum or minimum could be generally found at $X_3 = (0.179 - 0.167\ X_1 + 1.25\ X_2)/0.144$.

The effect of X_4, coded viscosity ratio appears in linear, quadratic and interaction term with X_1. As discussed earlier, Fig. 37 shows that response surface passes

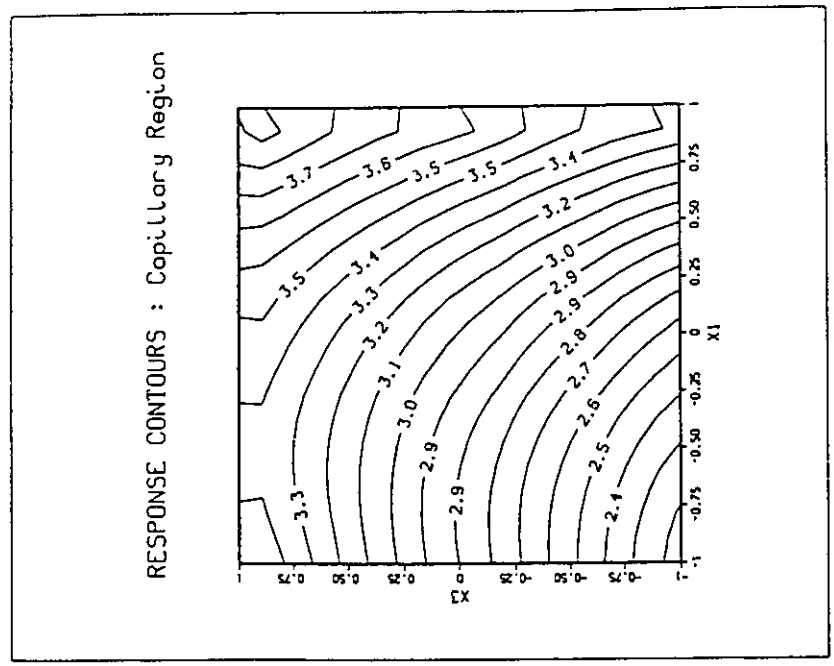

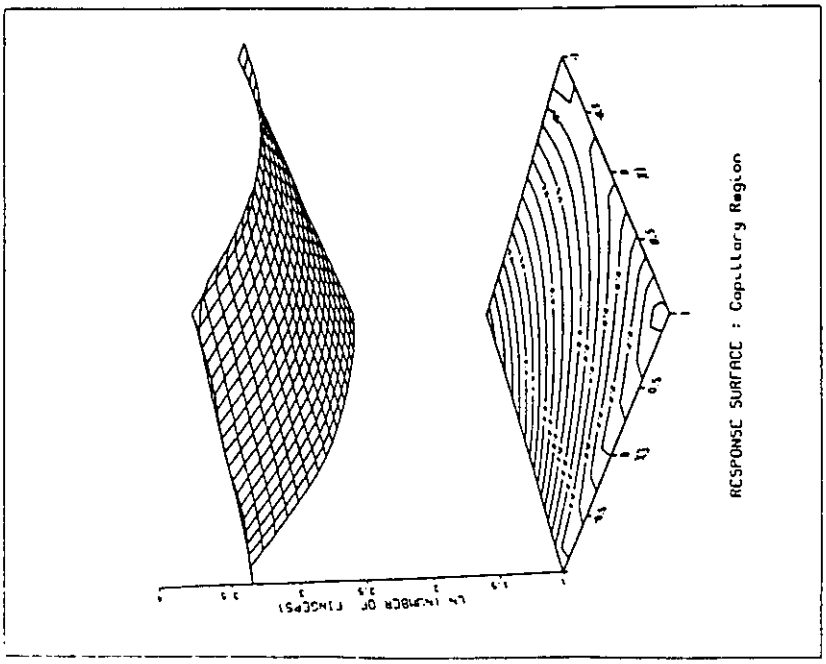

Fig. 36- Response surface and contours for model D.

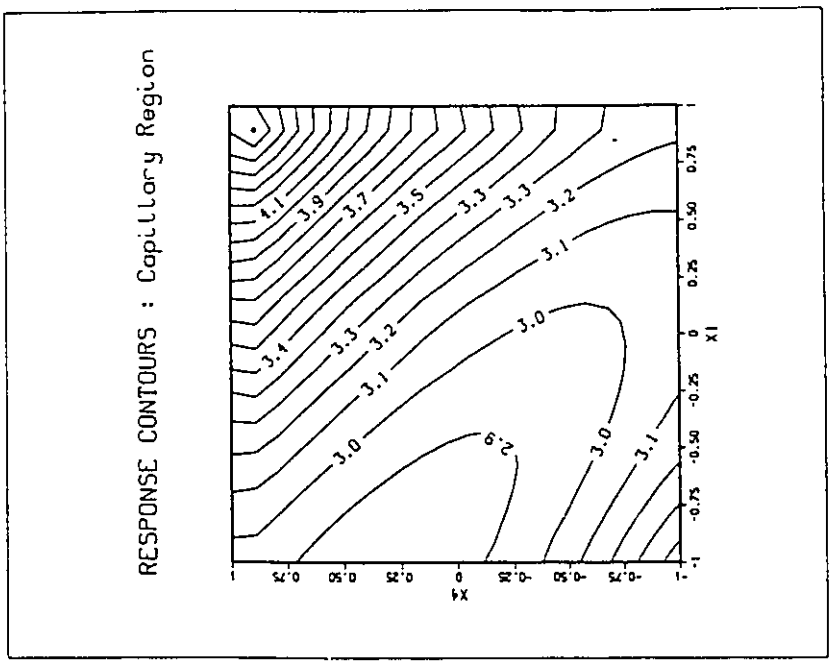

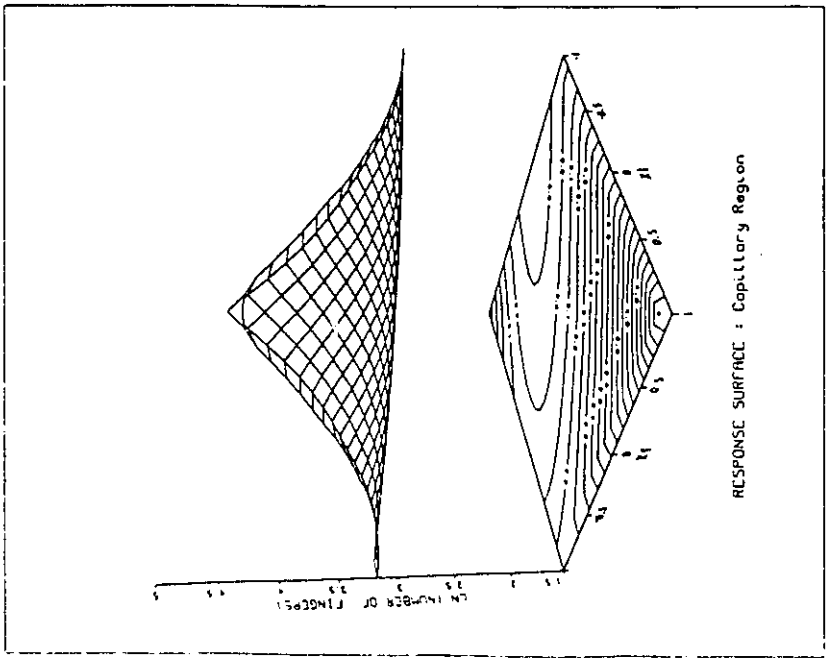

Fig. 37- Response surface and contours for model D.

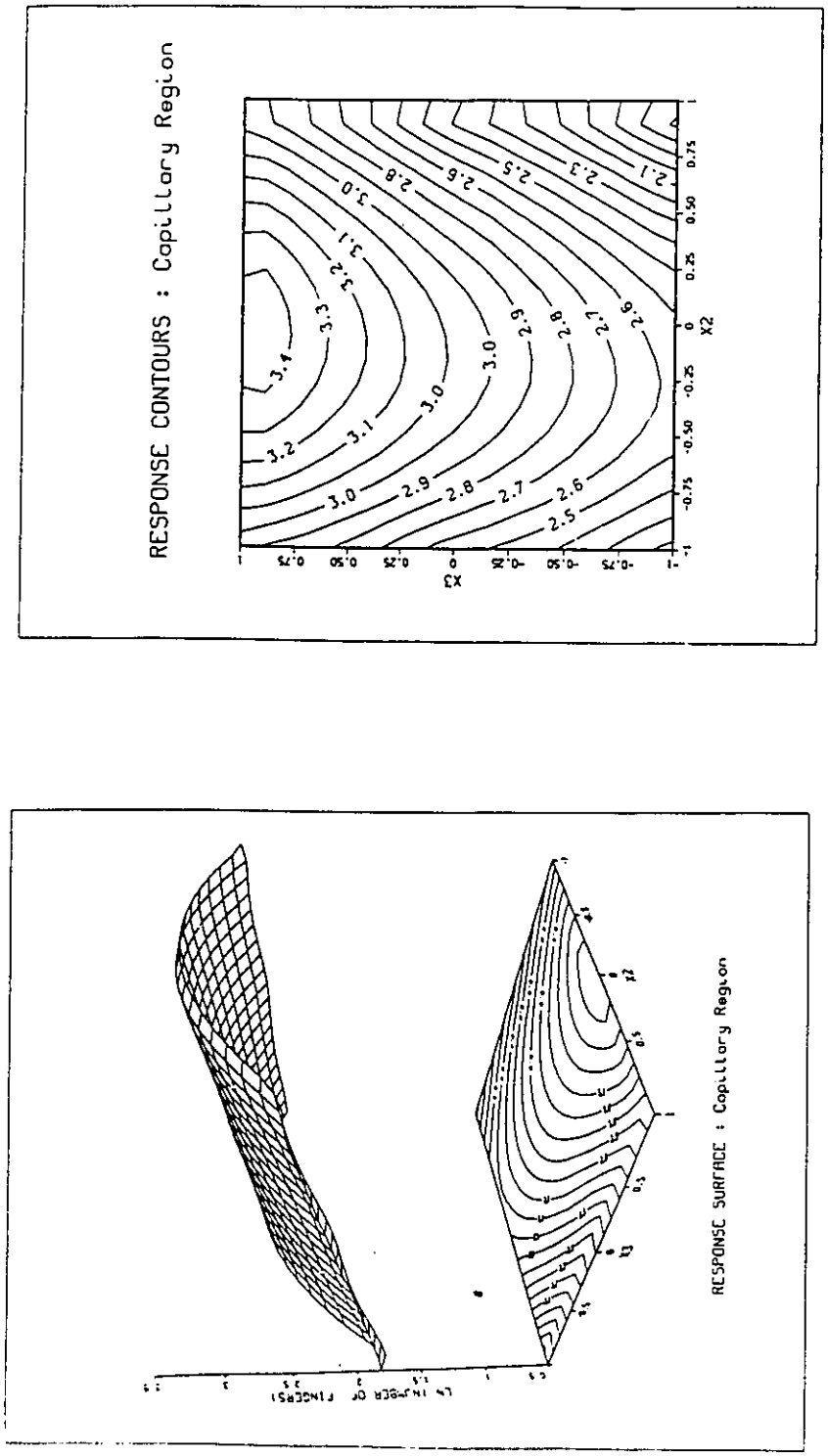

Fig. 38- Response surface and contours for model D.

through a minimum at $X_4 = (-0.326 - 0.544\ X_1)/0.672$. For example at $X_1 = -1$ this minimum is at $X_4 = 0.32$. The highest number of fingers is obtained at $(X_1, X_4) = (1, 1)$, which is quite consistent with the accepted fact that at high capillary number (high Q or low γ or high μ_w) and high viscosity ratio (high mobility ratio M) the number of fingers is the highest.

2 - INTERMEDIATE REGION

Recovery Model (Model E - Table 9)

The fitted model for recovery is

$$\text{Ln (Rec\%)} = 2.433 + 0.144X_2 - 0.396X_3 + 0.484X_4^2 - 0.141X_5 + 0.116X_4X_5 \qquad (95)$$

The model indicates that each of the operating variables, with the exception of the coded flowrate, X_1, has a significant effect on the logarithm of the recovery. The lack of any dependence on flowrate is not surprising and corroborates the results reported elsewhere (20) which indicated that recovery is independent of flowrate in the "intermediate region" over which these data were collected. Our results extend the validity of this conclusion to cover a range of values for the other operating variables. Moreover, the larger data set and experimental design employed in this work provide a more sensitive test of this behaviour.

The coded distance from the injection point, X_2, has a relatively small positive effect on recovery and this effect holds over the range of values studied for the other operating variables. The model predicts an increase in recovery by a factor of 1.33 as X_2 increases from -1 to 1. In radial displacement, superficial velocity (different from the instantaneous local pore velocity) decreases with R ($V \equiv Q/2\pi R^*h = \varepsilon V_p$), thereby increasing the possibility of imbibition and enhancing recovery.

The viscosity difference, X_3, has a major negative effect on recovery which is, again, independent of the levels of the other operating variables. The model predicts a decrease in recovery by a factor of 0.45 from the lowest to the highest viscosity difference. This result is expected and is consistent with that found by Mungan (39) and explains the lower recoveries obtained from heavy oil fields (increased mobility ratio).

The model shows that the permeability of the cell, X_4, has a quadratic effect on the recovery which depends upon the value of the interfacial tension as indicated by the interaction term, $\beta_{45}X_4X_5$. Such interaction is not unexpected since, in the absence of wettability effects, both permeability and interfacial tension determine the extent of imbibition. From a physical point of view, both permeability and IFT are surface dependent and thus this kind of relationship would be expected. At a low level of IFT a minimum in the recovery occurs at $X_4 = 0.12$ while at a high level of IFT the minimum occurs at $X_4 = -0.12$. In the former case, the predicted maximum recovery is at the lowest permeability while in the latter, it is at the highest permeability. In either situation, the ratio of maximum to minimum recovery is 1.8 (Fig. 39).

The effect of coded IFT, X_5, depends upon the level of permeability. At low levels of permeability, the effect of IFT on recovery is moderate and negative, while at high levels of permeability the effect of IFT remains negative but is not significant. Over the range of values for IFT, the predicted recovery decreases by a factor of 0.6 at the lowest level of permeability (Fig. 39). This inverse relationship is contrary to that reported by Newcombe (41), but consistent with the findings of Mungan (39) and Uren and Fahmy (33).

The fitted model can be used to predict recoveries or to determine optimal operating conditions for a particular system. For example, the fitted model for recovery indicates that the maximum recovery will be attained at the highest levels of the distance from injection point, X_2, and the lowest levels of viscosity difference, X_3. To determine the levels of permeability, X_4, and IFT, X_5, that yield optimal recoveries is more difficult, since these factors must be considered jointly. Analysis of the model in the X_4 - X_5 plane shows that the maximum recovery is attained at the lowest values of both X_4 and X_5 in the operating region. A minimum exists at $X_4 = -0.12$ and $X_5 = 1$, the surface being a slowly sloping valley along $X_5 = -8.3\ X_4$.

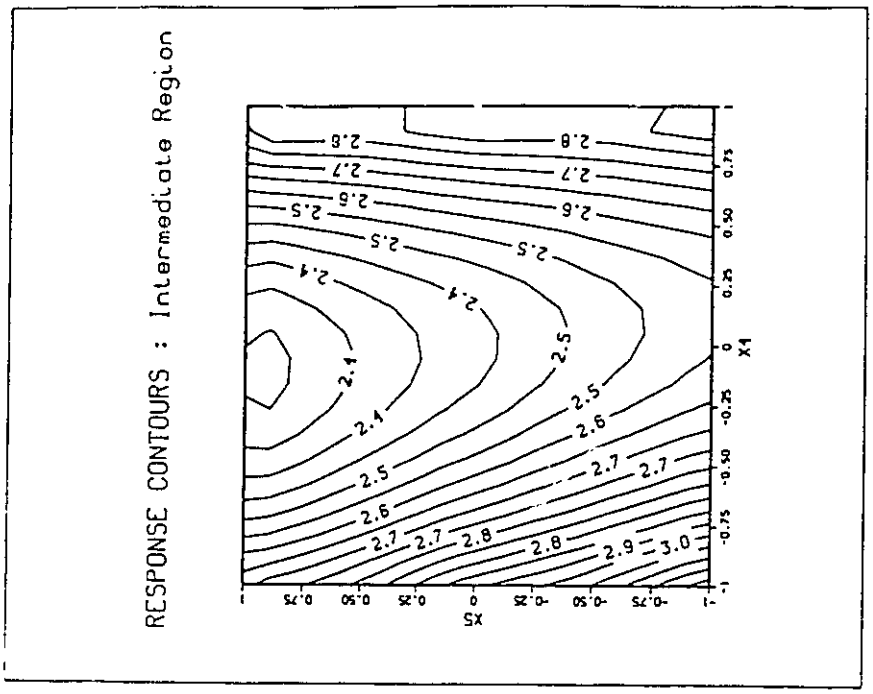

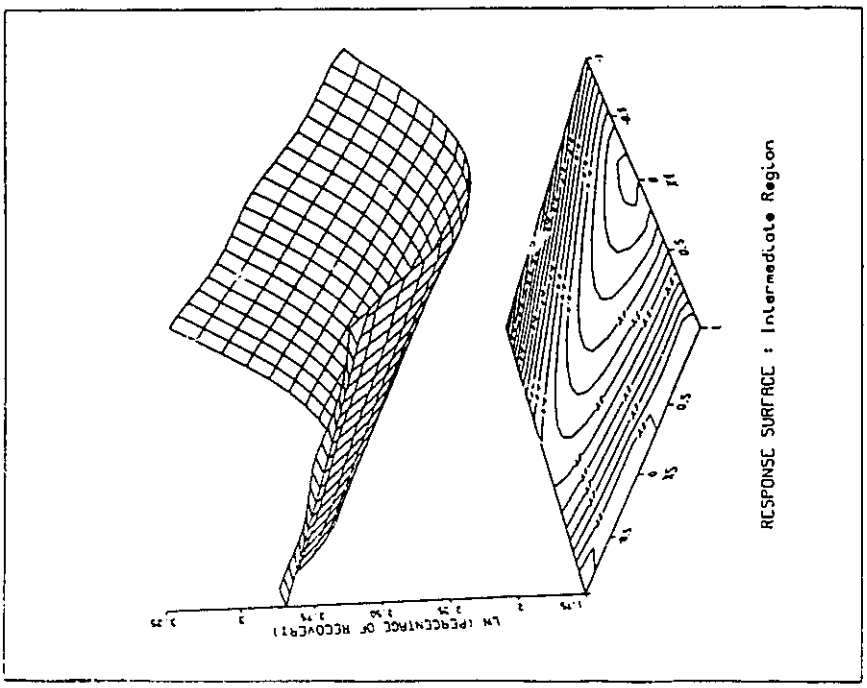

Fig. 39- Response surface and contours for model E.

Table 9

Parameter Estimates and Pertinent Statistics for Models Based on Eqn. 61 (Models E & F)

Response	Significant Parameters	Parameter Values	Standard Error	$\frac{SSR}{(n-p)}$	$\widehat{\sigma}_p^2$	lack of fit ratio (eqn. 70)	$F_{0.05}$	R^2_{adj}
ln(Rec%) N = 64	β_0	2.433	0.032	0.022	0.019	1.43	1.86	0.86
$N_p = 6$	β_2	0.144	0.024					
	β_3	-0.396	0.025					
Model E	β_5	-0.141	0.025					
	β_{44}	0.484	0.043					
	β_{45}	0.116	0.028					
ln (n) N = 64	β_0	3.507	0.030					
$N_p = 9$	β_1	0.098	0.022	0.017	0.017	1.00	1.88	0.92
	β_2	0.474	0.022					
	β_3	0.090	0.022					
Model F	β_4	-0.229	0.022					
	β_{55}	0.157	0.040					
	β_{15}	-0.053	0.024					
	β_{24}	-0.093	0.023					
	β_{35}	-0.064	0.024					

Model for Number of Fingers (Model F - Table 9)

The fitted model relating the total number of fingers to the various operating variables is

$$Ln(n) = 3.507 + 0.098X_1 + 0.474X_2 + 0.090X_3 - 0.229X_4 + 0.157X_5^2$$
$$- 0.053X_1X_5 - 0.093X_2X_4 - 0.064X_3X_5 \qquad (96)$$

The number of fingers depends on all the factors studied. Unlike the recovery, the number of fingers depends on the flowrate. The nature of this effect hinges upon the IFT as indicated by the interaction term, $\beta_{15}X_1X_5$, although the importance of this interaction is only marginally significant. At the low levels of IFT the number of

fingers increases with flowrate, while at the high levels of IFT the number of fingers increases with flowrate but at about one third the rate (Fig. 40). Our preliminary study of the IFT behavior revealed that it drops with time until an equilibrium is established (Fig. 21). This phenomenon is due to the fact that the solutions have not been pre-equilibrated, so mass transfer processes take place at the interface. Therefore, the lower the flowrate, the longer the oil/water contact time, resulting in a lower IFT.

Increasing the distance from the injection point, X_2, leads to a large increase in the number of fingers. As the distance from the injection point increases, the surface area of the interface between the displacing and displaced fluids increases rapidly, thereby increasing the probability of finger formation. This effect again depends on the level of another factor, in this case the permeability, X_4. At $X_4 = -1$, the increase in the number of fingers is by a factor of 3.1, while at $X_4 = 1$ the increase is by a factor of 2.1. As might be expected, at high levels of permeability, the effect of the distance from injection point is less than at low permeabilities (Fig. 41). This can be explained by the fact that, at high values of K, the oil/water contact area (interface) and, therefore, the possibility of finger formation is much smaller than is the case for low permeability.

An increase in the viscosity difference results in a moderate increase in the predicted number of fingers; the extent of its effect depending on the IFT as indicated by the interaction term, $\beta_{35}X_3X_5$. The number of fingers increases by a factor of 1.05 over the range of values for X_3 at the highest level of IFT. At low IFT the effect of viscosity difference is to increase the number of fingers by a factor of about 1.4. The response surface is a slightly sloping valley (Fig. 42).

The fitted model reveals that the number of fingers decreases with increasing permeability of the medium, X_4; the extent of this decrease grows with the distance from the injection point. At $X_2 = -1$ the model predicts a decrease in the number of

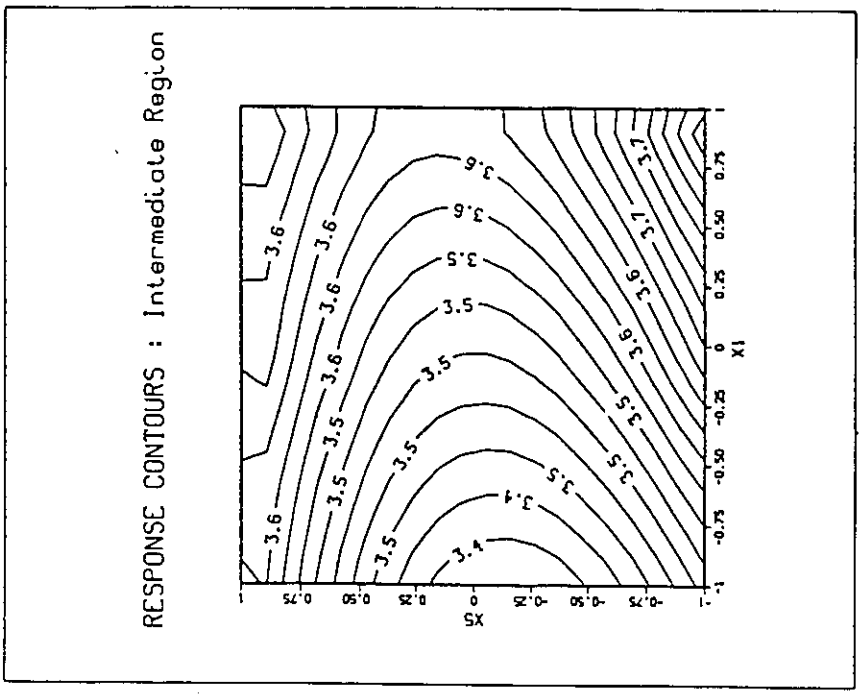

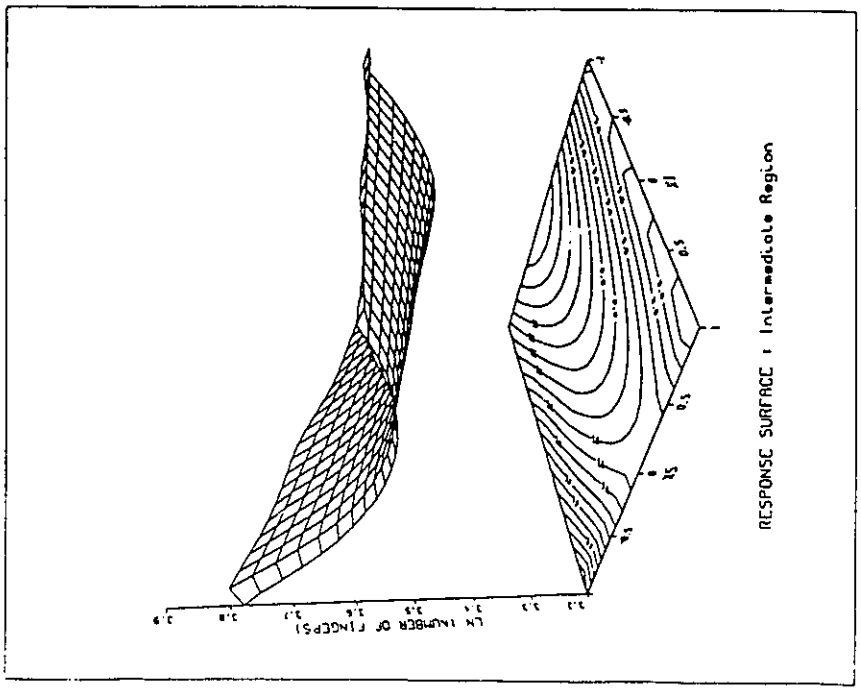

Fig. 40- Response surface and contours for model F.

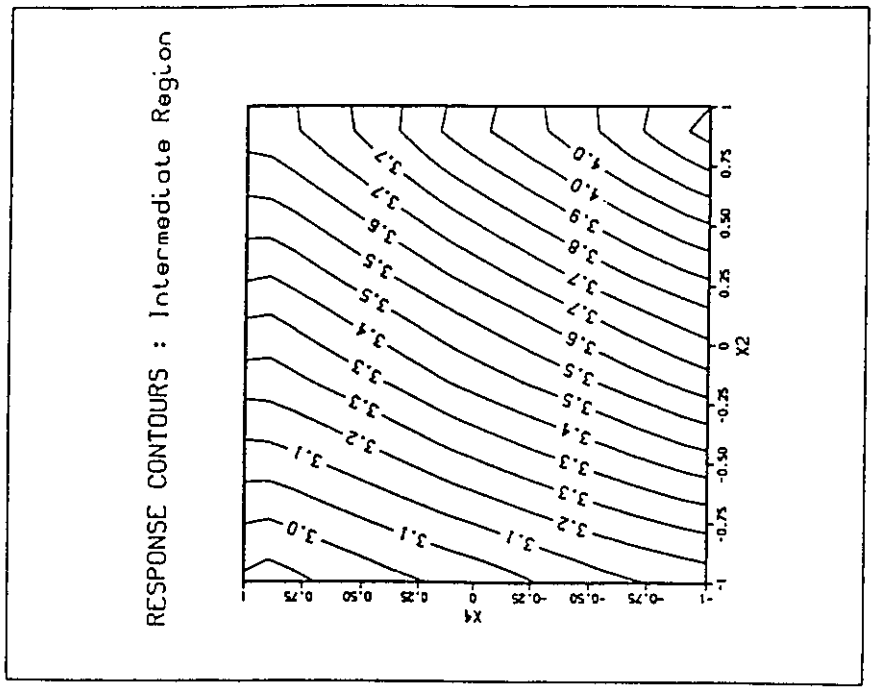

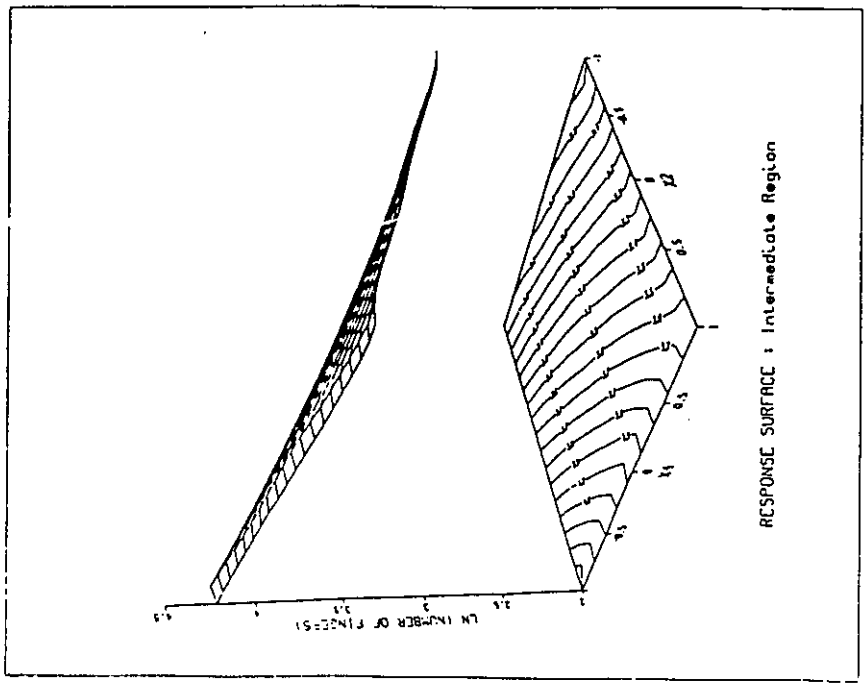

Fig. 41- Response surface and contours for model F.

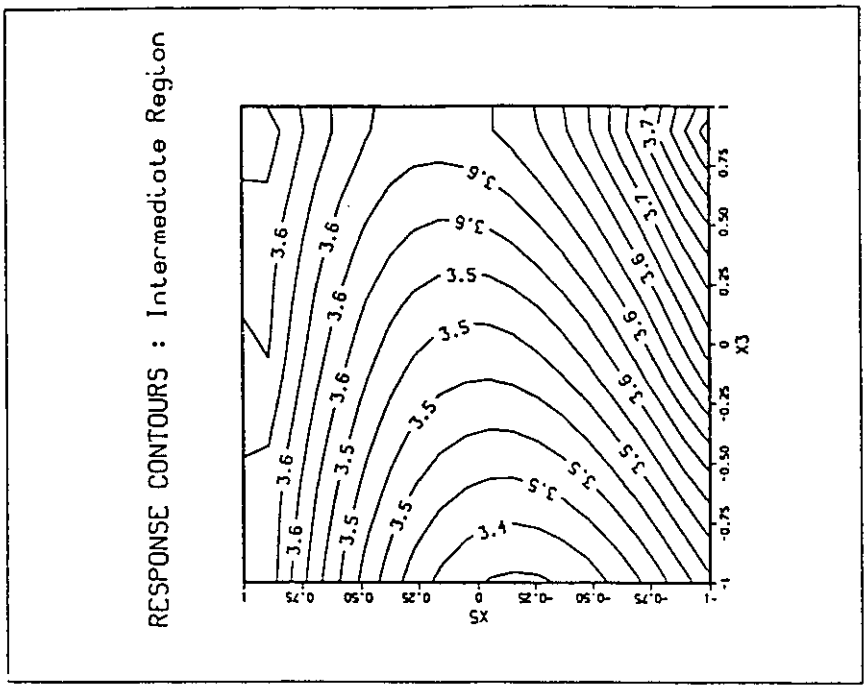

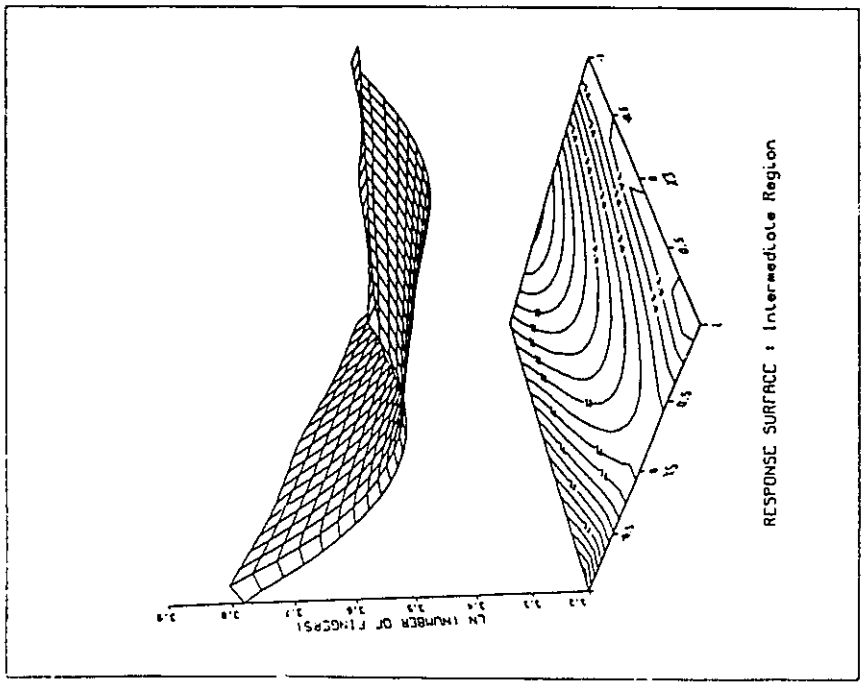

Fig. 42- Response surface and contours for model F.

fingers by a factor of 0.76 as the coded permeability, X_4, increases from -1 to 1; at X_2 = 1, the predicted number of fingers decreases by a factor of 0.53 (Fig. 41).

The IFT, X_5, has a rather complex quadratic effect on the number of fingers that depends on the flowrate and viscosity difference. At (X_1, X_3) = (-1, -1) the predicted number of fingers passes through a minimum at X_5 = -0.37 and reaches a maximum at X_5 = 1. The ratio of maximum to minimum number of fingers is 1.23. At (X_1, X_3) = (1, 1) the predicted number of fingers passes through a minimum at X_5 = 0.37 and has a maximum at X_5 = -1. The ratio of maximum to minimum number of fingers is again 1.23 (Figs. 40, 42).

These results show that the conclusions of Sarma (42) and Chen (43) as to the enhancing effect of lower IFT on the number of fingers are not general and depend on the level of flowrate and viscosity difference (or ratio). Figures 5-a and 5-b demonstrate this rather clearly.

The fitted model for number of fingers can also provide useful information on the validity and applicability of the theoretical model on which it is based. In this case, the results indicate several deviations from the theoretical model proposed by Ni et al. (19). If the model proposed by Ni et al. (19) were strictly valid, there should be no interaction or quadratic terms, and each of the parameters associated with the main effects in the uncoded form of the model should be equal to 0.5. Neither of these conditions holds for the present model. However, one should not forget that in previous theoretical developments (e.g. 19, 20) many assumptions were made that were not necessarily attained in the present experimental study. One good example is the assumption of perfect two-dimensional flow. Another example is the extension of the Hele-Shaw cell theory to a porous medium. The use of macroscopic continuum equations and boundary conditions involving pressure at the interface to describe interfacial effects, which obviously take place at a microscopic level, is questionable.

Recovery Model (Model G - Table 10)

In terms of coded dimensionless variables (see Eqn. 65), the fitted model for the percent recovery was found to be

$$\ln(\text{Rec}\%) = 2.487 - 0.144X_1 + 0.146X_3 - 0.626X_4 - 0.228X_1^2 + 0.434X_2^2 + 0.220X_1X_2 - 0.200X_1X_4 \quad (97)$$

As in the case of capillary region, all of the dimensionless numbers have an effect on the recovery.

The capillary number is the ratio of viscous to capillary forces. Its effect on the recovery is quite complex, being found in linear, quadratic and interaction terms in the model. The existence of interaction terms $\beta_{12}X_1X_2$ and $\beta_{14}X_1X_4$ means that the effect of X_1 depends on the values of X_2 and X_4, the coded forms for the dimensionless numbers $h/\sqrt{K}$ and μ_o/μ_w, respectively. For low values of X_2 and high values of X_4 an increase in the capillary number causes a large decrease in the recovery while at high values of X_2 and low values of X_4 an increase in capillary number causes a small increase in recovery. The extent of these changes can be calculated by evaluating the change in recovery over the extremes of the operating region for X_1 (i.e., $-1 \le X_1 \le 1$) at the two extreme conditions of X_2 and X_4, namely (-1, 1) and (1, -1). At $(X_2, X_4) = (-1, 1)$ the logarithm of percent recovery decreases by 1.13 as X_1 increases from -1 to 1; this yields a relative decrease in percent recovery of 0.68. On the other hand, at (1, -1) the logarithm of percent recovery passes through a maximum at $X_1 = 0.61$. The minimum value of the logarithm of percent recovery is found at $X_1 = -1$. The increase in the logarithm of percent recovery from minimum to maximum is 0.59 which represents a ratio of maximum to minimum recovery of 1.8 (Figs. 43-44). The effect of capillary number on recovery is clearly very different from one set of values for

X_2 and X_4 to another. This demonstrates the danger in generalizing conclusions from studies where only one variable at a time is investigated.

The effect of X_2 on the logarithm of recovery is quadratic and also depends on the value of X_1. At the lowest value of capillary number, the ratio of the maximum recovery (obtained at $X_2 = -1$) to the minimum recovery (obtained at $X_2 = 0.25$) is 2.0. At the highest value of capillary number the relationship between ln(Rec%) and X_2 mimics that found for $X_2 = -1$ except that the location of the minimum has shifted to $X_2 = -0.25$. Consequently, the maximum recovery is attained at either the highest or lowest value of $h/\sqrt{K}$ depending upon the value of the capillary number (Fig. 43). This could shed some light on the results reported by Taber (9) and again emphasizes the importance of considering all operating variables together.

The effect of X_3, the coded form of the dimensionless variable R/h, on the logarithm of the recovery is linear and independent of the levels of other variables. An increase in X_3 from -1 to 1 results in an increase in recovery by a factor of 1.34.

The coded form of the viscosity ratio (μ_o/μ_w), X_4, has a linear effect on the logarithm of percent recovery which depends on the capillary ratio. At a low level of X_1 an increase in X_4 from -1 to 1 yields a decrease in recovery by a factor of 0.43, whereas at a high level of capillary number a decrease in recovery by a factor of 0.19 is obtained (Fig. 44). This is consistent and further extends the results obtained by Habermann (49) and explains lower recoveries obtained from heavy oil reservoirs.

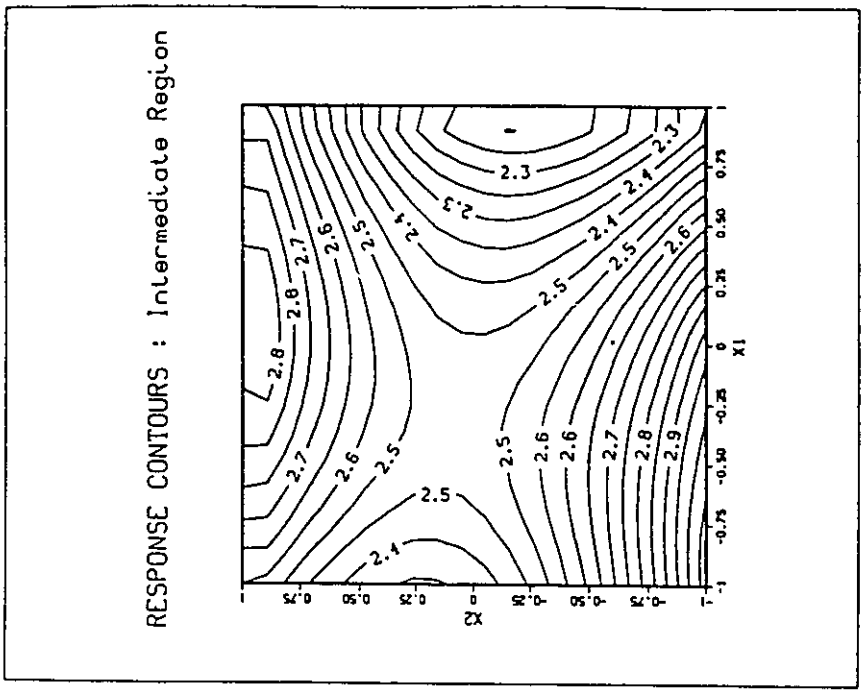

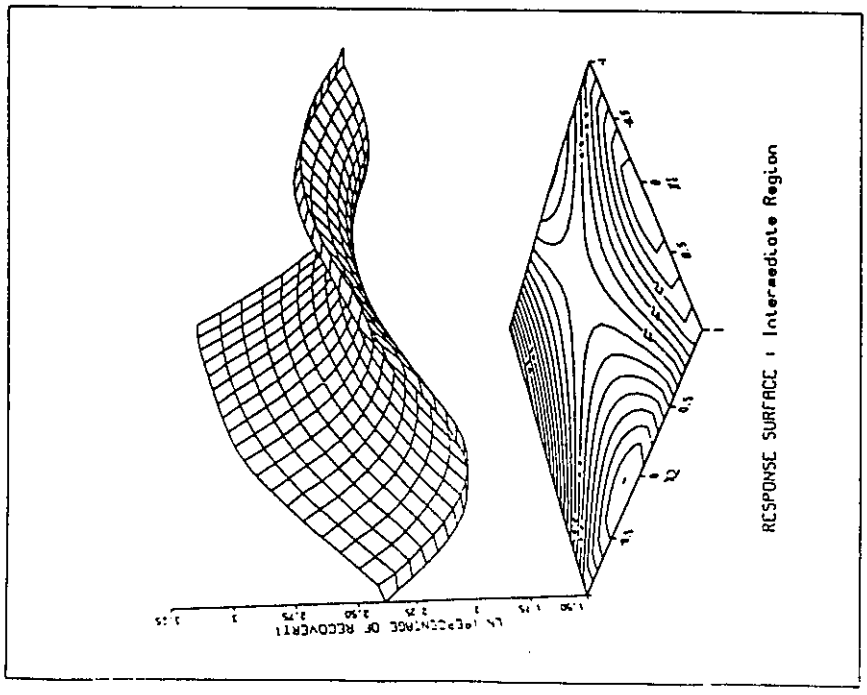

Fig. 43- Response surface and contours for model G.

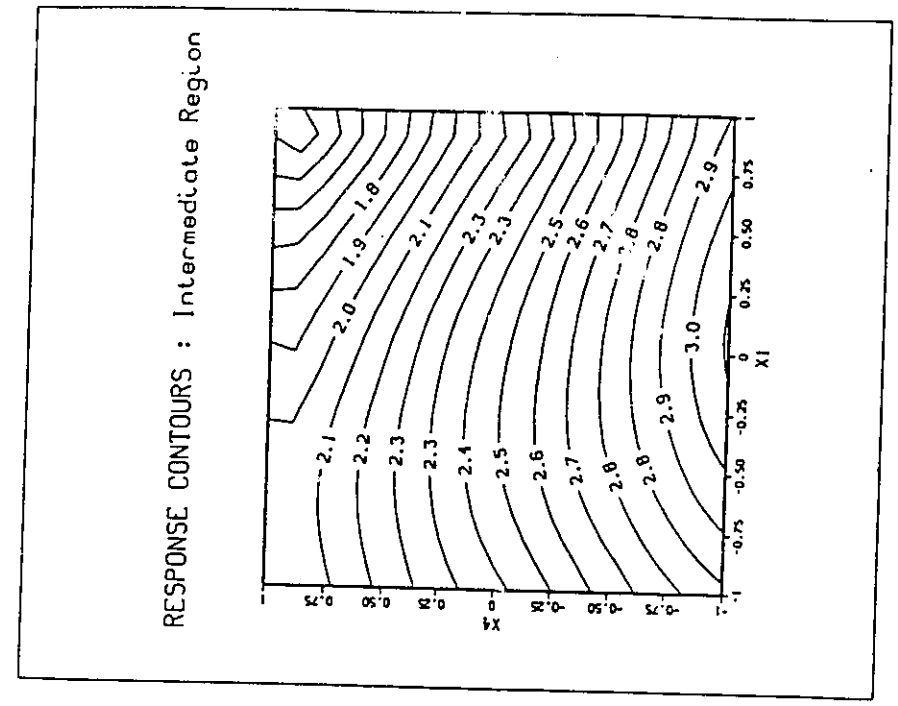

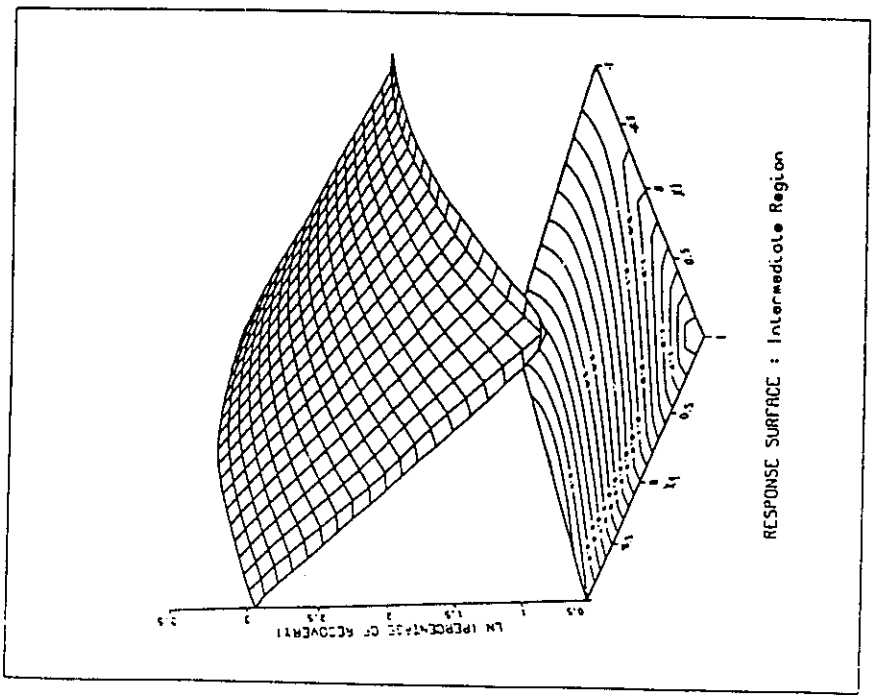

Fig. 44- Response surface and contours for model G.

Table 10

Parameter Estimates and Pertinent Statistics for Models Based on Eqn. 65 (Models G & H)

Response	Significant Parameters	Parameter Values	Standard Error	$\frac{SSR}{(n-p)}$	$\tilde{\sigma}_p^2$	lack of fit ratio (eqn. 70)	$F_{0.05}$	R^2_{adj}
ln (Rec %) N = 64 $N_p = 8$ Model G	β_0	2.487	0.031	0.019	0.019	1.077	1.87	0.88
	β_1	-0.144	0.037					
	β_3	0.146	0.022					
	β_4	-0.626	0.037					
	β_{11}	-0.228	0.089					
	β_{22}	0.434	0.048					
	β_{12}	0.220	0.046					
	β_{14}	-0.200	0.054					
ln (n) N = 64 $N_p = 8$ Model H	β_0	3.522	0.030	0.021	0.017	1.46	1.87	0.90
	β_1	0.178	0.038					
	β_2	0.190	0.025					
	β_3	0.482	0.024					
	β_4	0.135	0.037					
	β_{11}	0.327	0.078					
	β_{12}	-0.138	0.048					
	β_{23}	0.097	0.026					

Model for Number of Fingers (Model H - Table 10)

In terms of the coded dimensionless variables the number of fingers is well described by the model

$$\ln(n) = 3.522 + 0.178X_1 + 0.190X_2 + 0.482X_3 + 0.135X_4 + 0.327X_1^2 - 0.138X_1X_2 + 0.097X_2X_3 \quad (98)$$

Again, all the dimensionless variables have an effect on the number of fingers.

The effect of the coded capillary number, X_1, on ln(n) is quadratic in form having a minimum whose location depends upon the value of X_2, the coded form of the dimensionless variable $h/\sqrt{K}$. At $X_2 = -1$, the minimum occurs at $X_1 = -0.48$ while at $X_2 = 1$ the minimum is located at $X_1 = -0.06$. In both cases the maximum number of fingers is encountered at the maximum value of X_2. (lowest K). However, at $X_2 = 1$, the predicted number of fingers at $X_1 = -1$ does not differ significantly from the maximum at $X_1 = 1$. The extent of the effect of capillary number on the number of fingers can be predicted by comparing the number of fingers at the minimum and the maximum. At $X_2 = -1$ the ratio of the maximum number of fingers to the minimum over the operating region is 2.1 while at $X_2 = 1$ the ratio is 1.4. The magnitude of the effect of capillary number is thus significant. The existence of a minimum in the number of fingers with respect to capillary number is interesting as is the dependency on the dimensionless number associated with permeability (Fig. 45).

The effect of the dimensionless variable involving permeability, $h/\sqrt{K}$, is linear with respect to its coded form, X_2, but depends on the values of the coded variables X_1 and X_3. At $(X_1, X_3) = (-1, 1)$, the model predicts an increase in the number of fingers by a factor of 2.3 as X_2 increases from -1 to 1. At $(X_1, X_3) = (1, -1)$, the model predicts a small decrease in the number of fingers by a factor of 0.9. An increase in the number of fingers with a decrease in permeability was expected but the predicted decrease when $(X_1, X_3) = (1, -1)$ was somewhat surprising (Figs. 45-46).

The effect of X_3, the coded form of the dimensionless variable R/h, on the logarithm of the number of fingers is linear and depends on the value of X_2. At the highest value of X_2 the predicted number of fingers increases by a factor of 3.2 over the range of X_3, while at the lowest value of X_2, the increase is only by a factor of 2.2 (Fig. 46).

The effect of X_4, the coded form of the dimensionless variable μ_o/μ_w, on ln(n) is linear and independent of the other variables. This positive effect of viscosity ratio

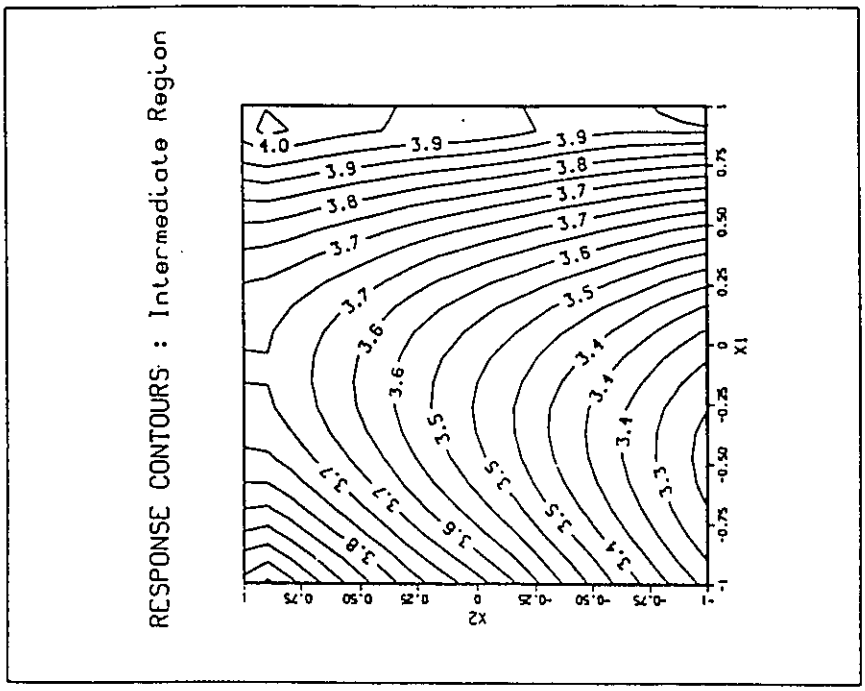

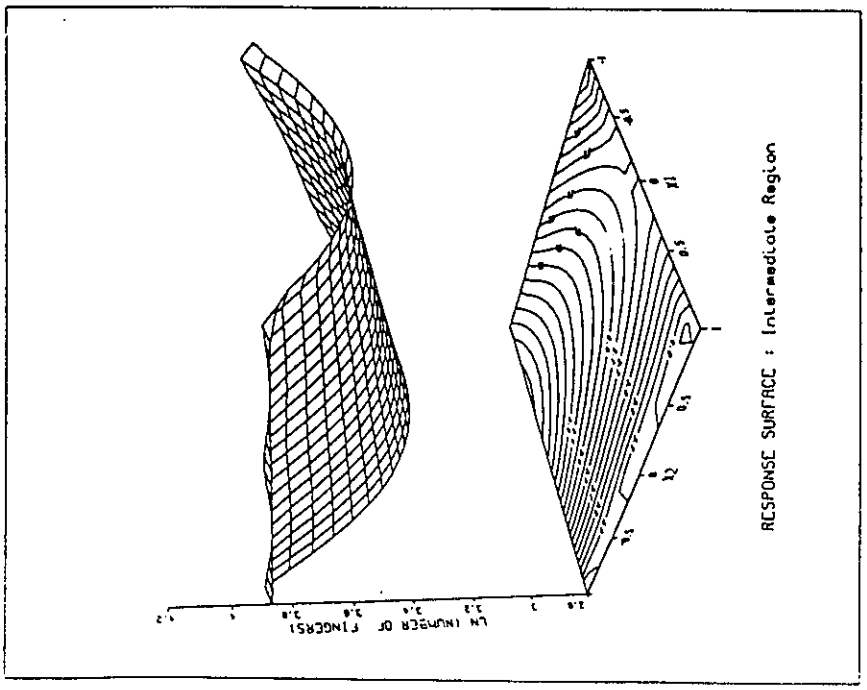

Fig. 45- Response surface and contours for model H.

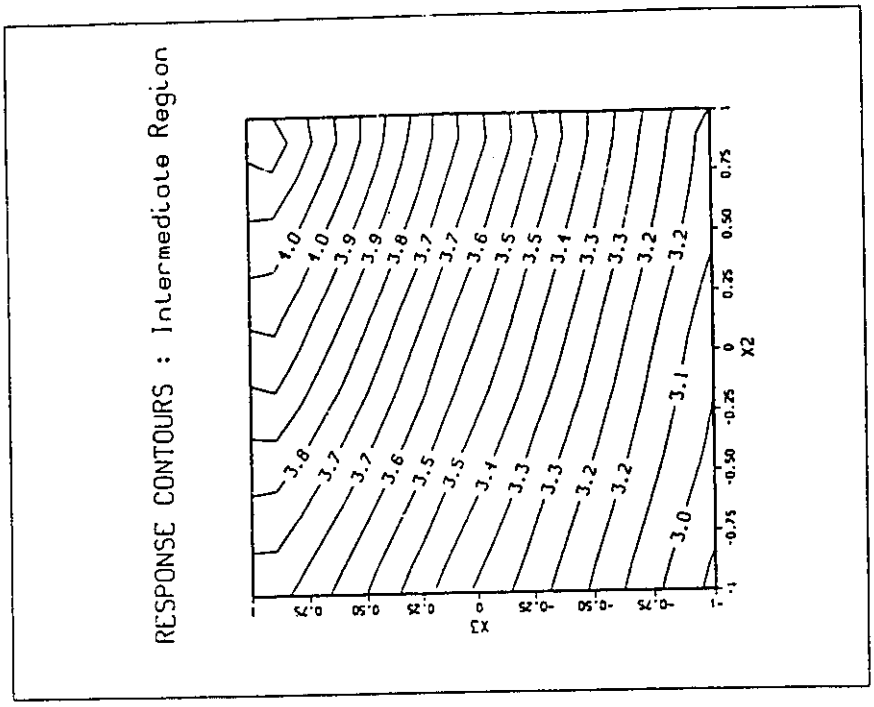

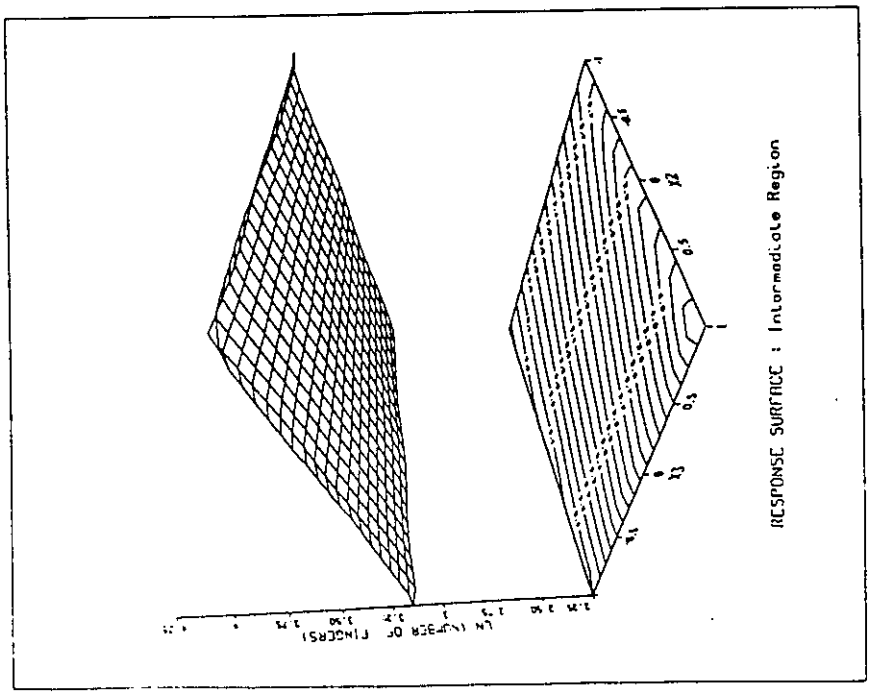

Fig. 46- Response surface and contours for model H.

on the number of fingers is expected and corroborates previous research (48). The higher the viscosity ratio, the higher the mobility ratio M, and thus, there will be more fingering. The model predicts an increase in the number of fingers by a factor of 1.3 as X_4 changes from -1 to 1. This is a relatively small effect considering that the viscosity ratio varied from 5.1 to 153.0.

In summary, all of the dimensionless quantities have a significant effect on the recovery and the number of fingers. The nature of these effects is complex; however, the fitted models allow the effects to be analyzed and the overall nature of the response surfaces to be assessed. The interpretation of the results in terms of these models is more difficult than for the "mechanistically based" models described earlier since the independent variables in the dimensionless models are themselves functions of the operating variables. This makes it difficult to determine how the operating variables actually affect the recovery and number of fingers. On the other hand, use of the dimensionless quantities provides a model in terms of more traditional variables.

3 - VISCOUS REGION

Recovery Model (Model I - Table 11)

The fitted model relating the logarithm of recovery to various operating variables is

$$\text{Ln(Rec \%)} = 2.366 + 0.167\ X_2 - 0.721\ X_3 - 0.245\ X_5 + 0.271\ X_2^2 - 0.194\ X_3X_4 \qquad (99)$$

The model predicts that each of the independent operating variables has a significant effect on the logarithm of the recovery except X_1, the coded flow rate (Table 11). Recalling that this behaviour was also observed in capillary and intermediate regions, it can be concluded that flowrate, Q, does not influence the oil recovery at all and that this conclusion is valid over a wide range of values for other operating variables. As mentioned earlier, the same result was observed only in the intermediate region by Ni et al. (19) for an oil-wet system (although he did not have enough data points to conclusively prove this) and by Nasr-El-Din et al. (20) for a water wet porous medium.

In addition, we concluded that the increased recoveries that Nasr-El-Din et al. (20) observed at low flowrates, were due to end-effects and subsequent mushrooming and not natural imbibition caused by a low capillary number.

The effect of coded radius X_2, on the logarithm of percent oil recovery is both linear and quadratic and is independent of the other operating variables. The minimum recovery is obtained at $X_2 = -0.31$ and the maximum at $X_2 = 1$. Since there is no imbibition in this region, and since this effect is not dependent on other variables, this phenomenon could only be explained through better sweep efficiency at higher radii.

The effect of coded viscosity difference X_3, depends on the value of permeability. The model predicts a reduction in the logarithm of percent recovery as X_3, the coded viscosity difference increases. This decrease becomes more significant as X_4 increases from -1 to 1 (Fig. 47). Therefore, the minimum recovery is attained at (X_3, X_4) = (1, 1) and, conversely, the maximum recovery is obtained at (X_3, X_4) = (-1, 1). This result is consistent with theory, Mungan's findings (39) and the higher recoveries obtained from light oil fields.

The effect of coded permeability, X_4, is dependent on the value of the X_3, coded viscosity difference. The maximum recovery is obtained at X_4 = 1 and X_3 = -1. On the other hand, the recovery constantly decreases as X_3, coded viscosity difference, is increased from -1 to 1 (Fig. 47).

The ratio of highest recovery to minimum recovery is 6.23, a relative decrease of 84%. Therefore, it can be concluded that within viscous region, no matter what the viscosity difference, the recovery is always greater for more permeable reservoirs and this is due to a lower resistance to the flow of the displacing phase and a better sweep efficiency. This can also be explained by the fact that in the absence of imbibition (flow is too fast within this region, therefore, capillary forces do not have enough time to cause imbibition) the recovery would be higher if the pores were larger and therefore more accessible to the displacing fluid. This is the case for high permeability porous media.

The effect of coded IFT, X_5, on the logarithm of percent recovery is linear negative, and is independent of other variables. The highest recovery is attained at X_5 = -1 and constantly decreases as IFT is increased. This is quite consistent with theory and previous research (33, 39). The ratio of maximum to minimum recovery is 1.63, a relative decrease of 39%.

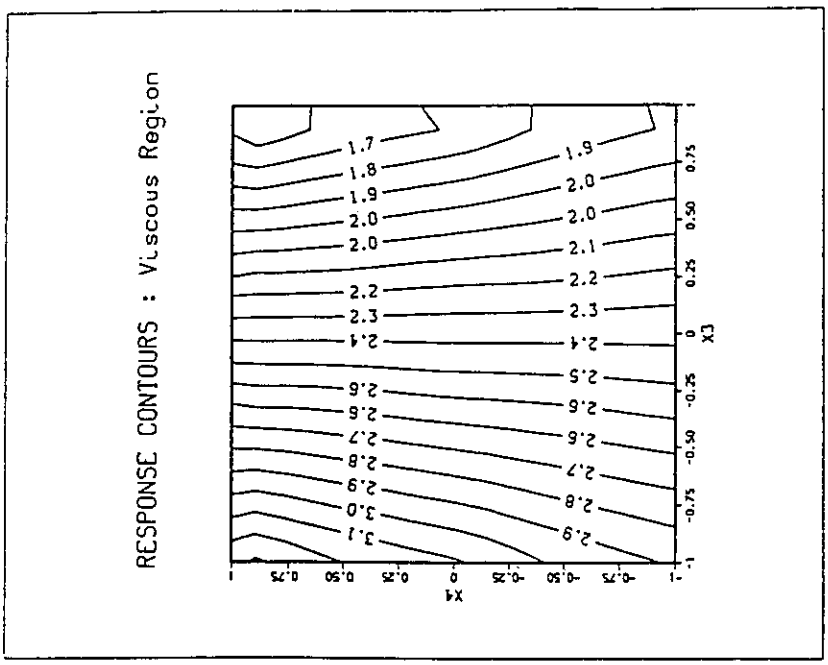

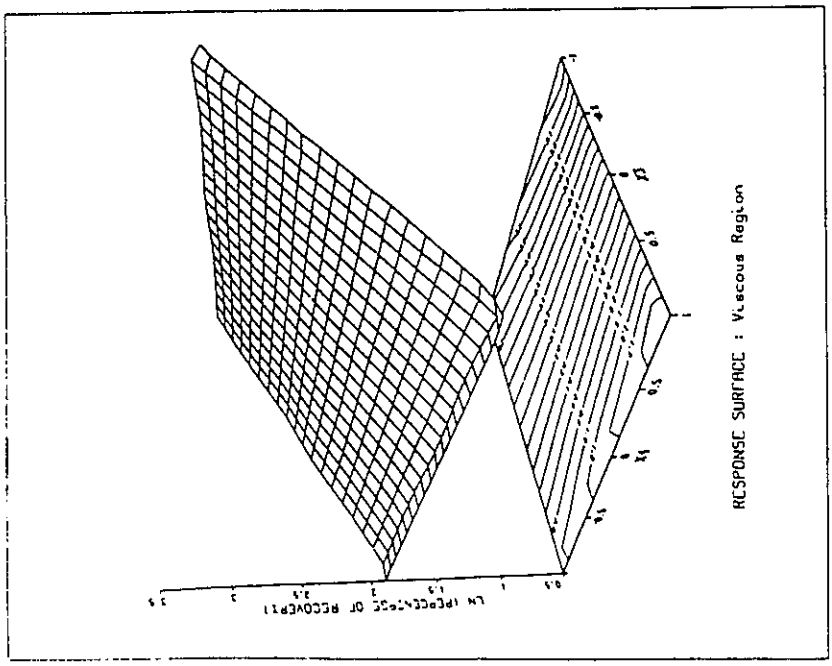

Fig. 47- Response surface and contours for model I.

Table 11

Parameter Estimates and Pertinent Statistics for Models Based on Eqn. 61 (Models I & J)

Response	Significant Parameters	Parameter Values	Standard Error	$\frac{SSR}{(n-p)}$	$\tilde{\sigma}_p^2$	lack of fit ratio (eqn. 70)	$F_{0.05}$	R^2_{adj}
ln(Rec%) N = 40	β_0	2.366	0.071	0.079	0.083	0.918	2.45	0.825
$N_p = 6$	β_2	0.167	0.058					
	β_3	-0.721	0.060					
Model I	β_5	-0.245	0.057					
	β_{22}	0.271	0.091					
	β_{34}	-0.194	0.062					
ln (n) N = 40	β_0	4.032	0.063					
$N_p = 12$	β_2	0.312	0.034	0.026	0.027	0.926	2.53	0.914
	β_3	0.340	0.035					
	β_4	-0.384	0.033					
	β_5	-0.142	0.034					
Model J	β_{44}	-0.467	0.120					
	β_{55}	0.204	0.087					
	β_{23}	0.129	0.036					
	β_{24}	-0.097	0.035					
	β_{34}	0.189	0.036					
	β_{35}	-0.089	0.036					
	β_{45}	0.073	0.035					

Model for Number of Fingers (Model J - Table 11)

In terms of coded operating variables, the logarithm of total number of fingers is predicted by the model (see Eqn. 61).

$$Ln(n) = 4.032 + 0.312\ X_2 + 0.340\ X_3 - 0.384\ X_4 - 0.142\ X_5 - 0.467\ X_4^2 + 0.204\ X_5^2$$
$$+ 0.129\ X_2X_3 - 0.097\ X_2X_4 + 0.189\ X_3X_4 - 0.089\ X_3X_5 + 0.073\ X_4X_5 \qquad (100)$$

The model indicates that for viscous region, the logarithm of total number of fingers is dependent on all operating variables with the exception of flow rate. As we saw earlier in sections 1 and 2 of this chapter, at capillary and intermediate regions, the number of fingers generally increased as the flow rate was increased. Here, at $X_1 = -1$, the flow rate is 174.0 mL/h (see Table 6). Since this injection rate is already rather high, the further increases of it at $X_1 = 0$ and $X_1 = 1$ (264.0 mL/h and 510.0 mL/h, respectively) do not affect significantly the number of fingers. This could mean that the existing fingers are capable of absorbing (conducting) the increased flowrates; thus there is no need for the number of fingers to increase.

The effect of coded distance, X_2, depends on the value of X_3, the coded viscosity difference and X_4, the coded permeability. At $(X_3, X_4) = (-1, 1)$, as the value of X_2 increases from -1 to 1, the logarithm of number of fingers increases by 0.20 (the number of fingers increases by a relative 22%). At $(X_3, X_4) = (1, -1)$ this increase is by 1.08, a relative 193% increase. The ratio of maximum to minimum number of fingers is 7.94. Fig. 48 shows the response surface and contours for the X_2X_3 interaction. The logarithm of the number of fingers steadily increases as X_2 (or X_3) is increased. The highest number of fingers is obtained at $(X_2, X_3) = (1, 1)$ This is consistent with theory and as mentioned earlier, is due to increased oil/water interface surface area and to increased M, mobility ratio, respectively. Fig. 49 depicts the response surface and contours for the X_2X_4 interaction (keeping $X_3 = 0$). The logarithm of number of fingers constantly increases as X_2 is increased from -1 to 1. On the other hand, logarithm of number of fingers passes through maximums as X_4 is increased from -1 to 1. The location of this maximum is at $X_4 = -(0.384 + 0.097\ X_2)/0.934$ i.e., $X_4 = -0.51$ at $X_2 = 1$ and $X_4 = -0.27$ at $X_2 = -1$ is a maximum (see Fig. 49).

The effect of coded viscosity difference, X_3, depends on X_2, X_4 and X_5. At $(X_2, X_4, X_5) = (-1, 1, 1)$ an increase in coded viscosity difference, X_3, from -1 to 1 results in an increase of 0.43 in the logarithm of the number of fingers. This corresponds to a

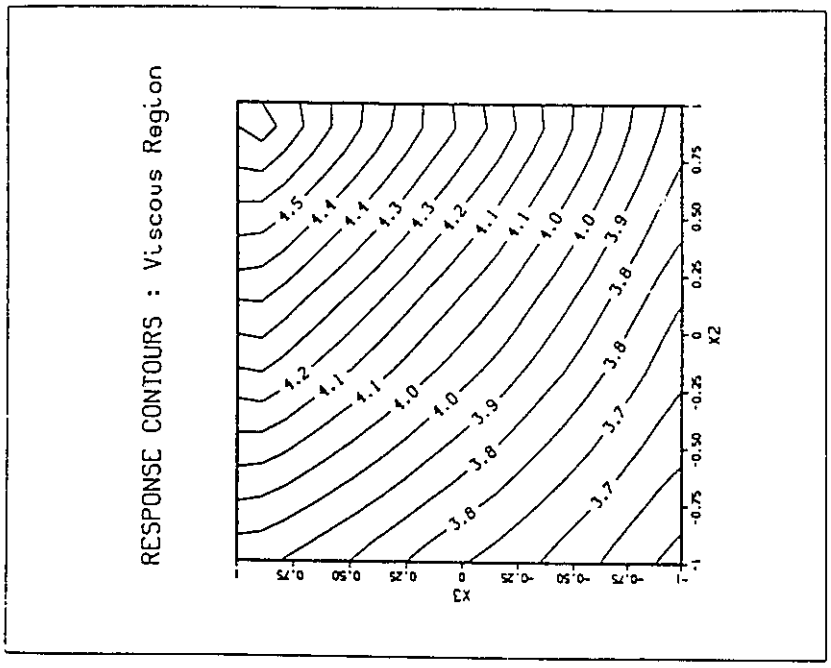

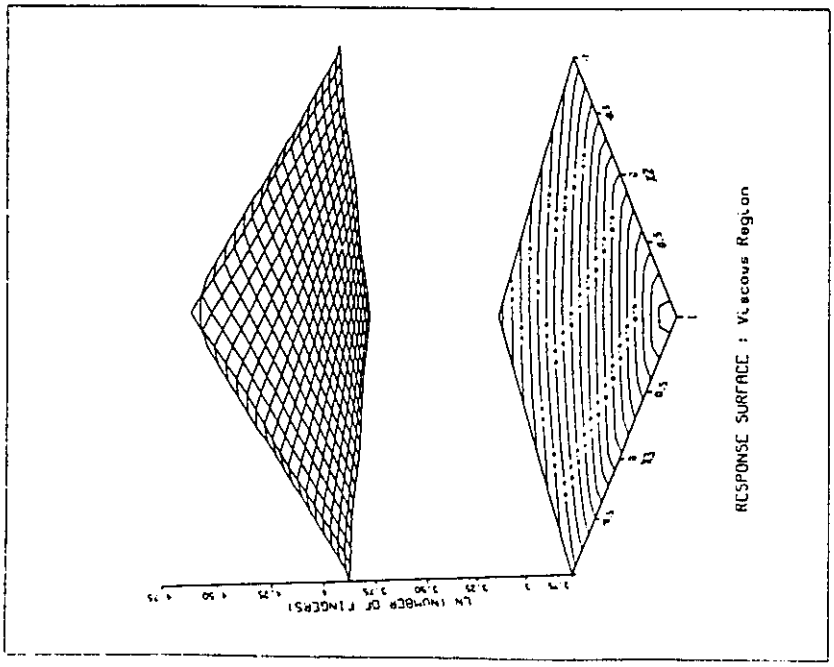

Fig. 48- Response surface and contours for model J.

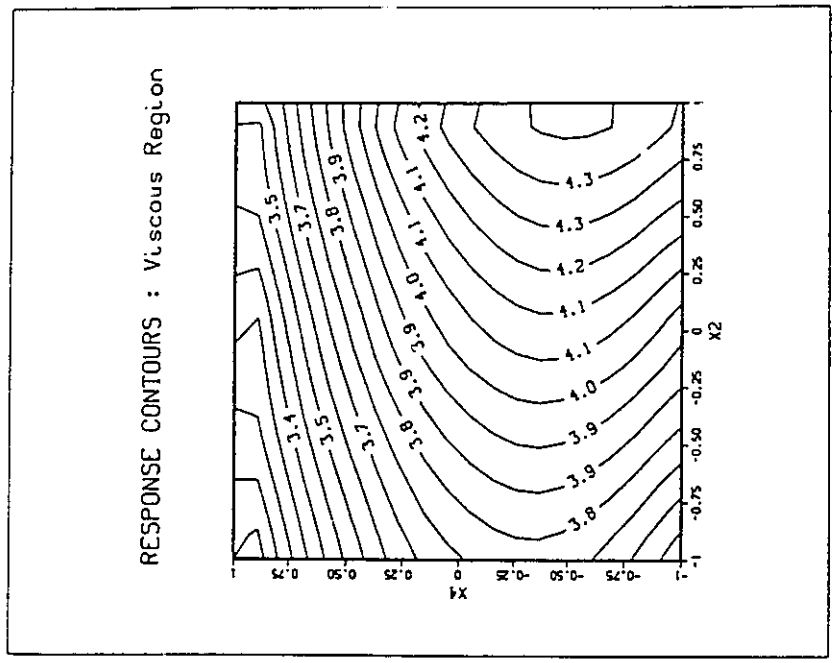

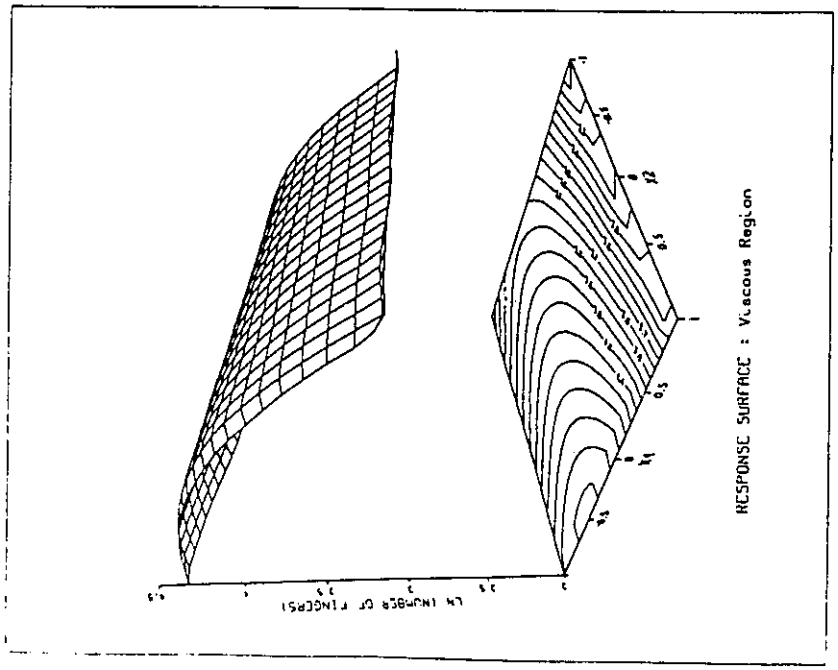

Fig. 49- Response surface and contours for model J.

relative increase of 53%. At the other extreme (favorable conditions for the number of fingers) namely at (X_2, X_4, X_5) = (1, -1, -1), the logarithm of the number of fingers increases by 0.74, a relative increase of 109% in the number of fingers as X_3 is increased from -1 to 1. The ratio of maximum to minimum number of fingers is 10.55. Fig. 48 shows the response surface and contours for the X_2X_3 interaction. The highest number of fingers (keeping $X_4 = X_5 = 0$) occurs at (X_2, X_3) = (1, 1).

Fig. 50 depicts the response surface and contours for the X_3X_4 interaction ($X_2 = X_5 = 0$). At $X_3 = 1$, the maximum is at $X_4 = -0.21$ and at $X_3 = -1$, the maximum passes through $X_4 = -0.61$. For all values of X_4, the number of fingers increases as X_3 is increased. This is again due to increased M, mobility ratio.

Fig. 51 shows the response surface and contours for the X_3X_5 interaction. The logarithm of the number of fingers has a minimum at $X_5 = (0.142 + 0.089\ X_3 - 0.073\ X_4)/0.408$. In this case since $X_4 = 0$, the minimum passes through $X_5 = 0.57$ at $X_3 = 1$ and through $X_5 = 0.13$ at $X_3 = -1$. Again, for all values of X_5, the number of fingers increases as X_3 increases from -1 to 1.

The effect of, X_4, the coded form of permeability, also depends upon the value of the other operating variables, namely, X_2, X_3 and X_5. The location of the maximum is at $X_4 = (-0.384 - 0.097\ X_2 + 0.189\ X_3 + 0.073\ X_5)/0.934$. For instance, at the X_4X_5 plane (i.e. $X_2 = X_3 = 0$), the maximums are at $X_4 = -0.33$ for $X_5 = 1$ and at $X_4 = -0.50$ if $X_5 = -1$ (see Fig. 52).

The effect of X_5, the coded form of IFT, depends on the value of X_3 and X_4. At (X_3, X_4) = (-1, 1), as X_5 increases from -1 to 1, the logarithm of number of fingers is increased by a small factor of 0.04, a relative increase of only 4% in the number of fingers, while at (X_3, X_4) = (1, -1) the logarithm of the number of fingers actually decreases by 0.61, a relative reduction of 46% in the number of fingers, as X_5 increases from -1 to 1. The ratio of the maximum to the minimum number of fingers is 5.88. This conflicting behavior again underscores the importance of interaction

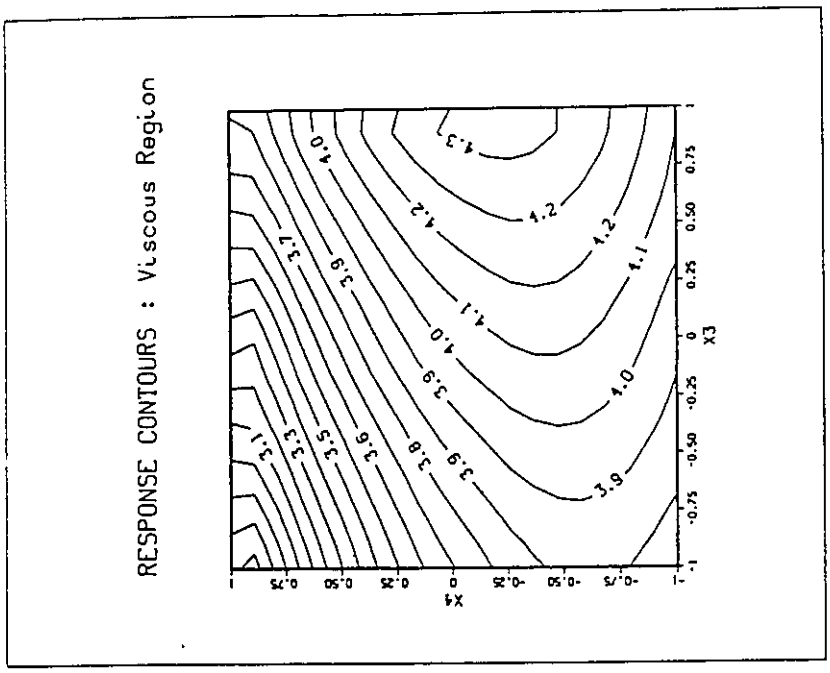

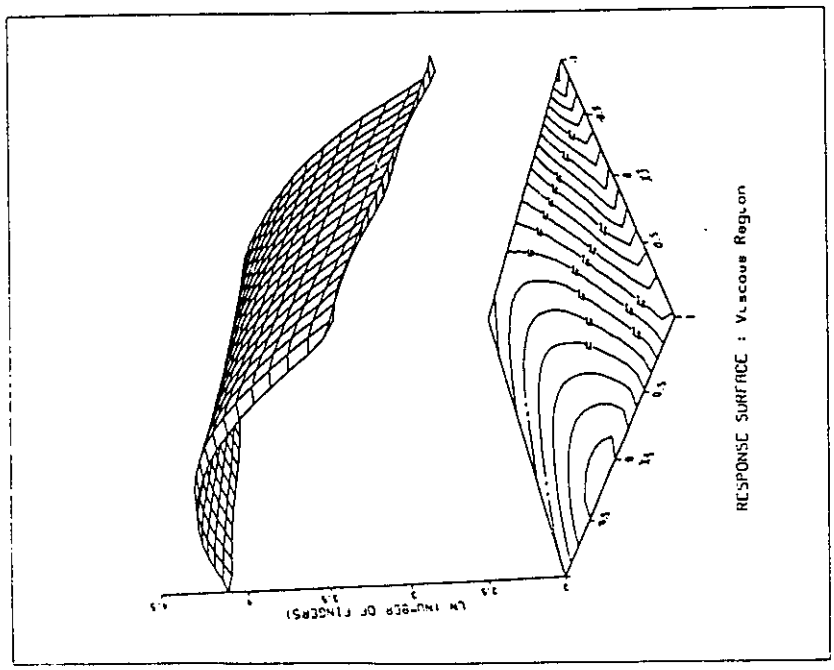

Fig. 50- Response surface and contours for model J.

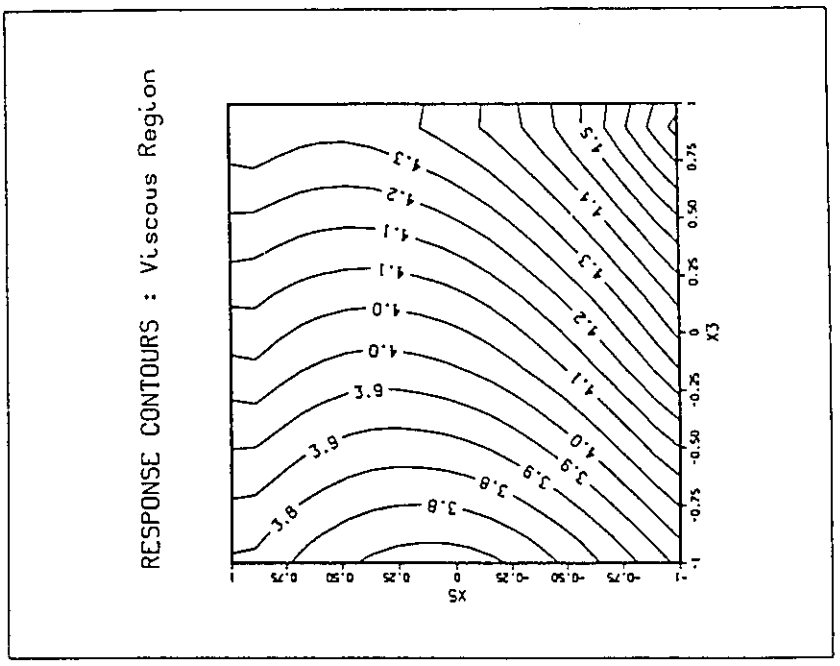

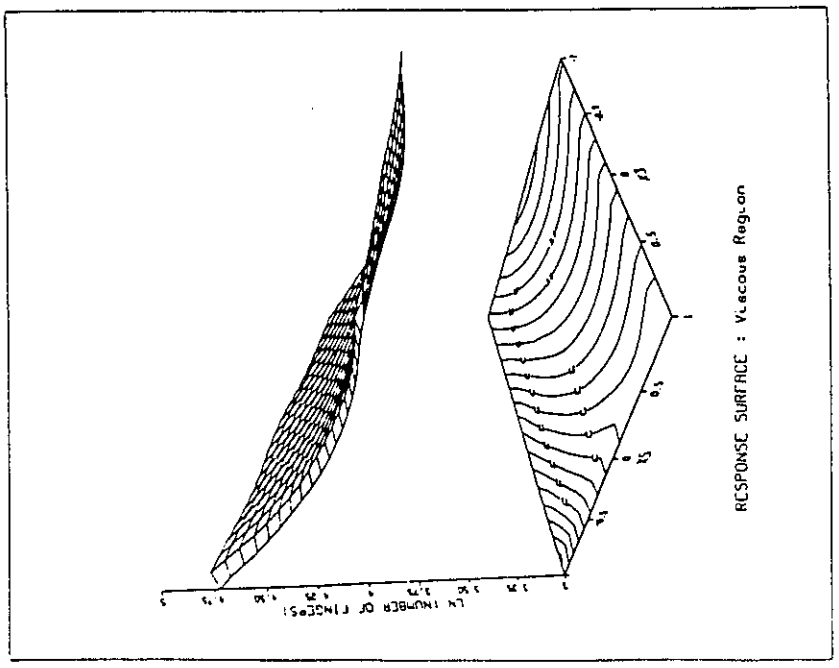

Fig. 51- Response surface and contours for model J.

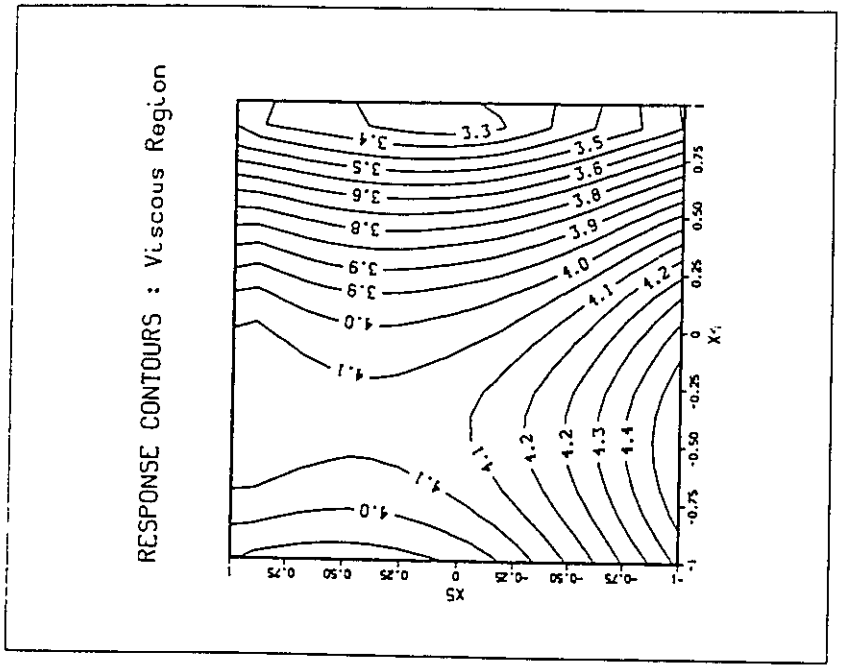

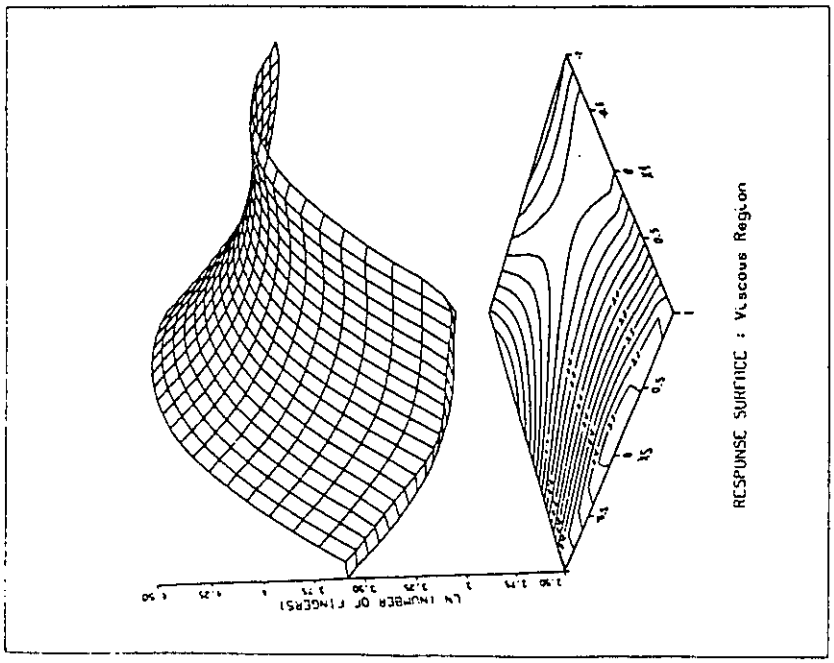

Fig. 52- Response surface and contours for model J.

consideration before generalizing the results obtained from experimental work. Considering the X_4X_5 response surface (Fig. 52), the logarithm of the number of fingers passes through a maximum at $X_5 = 0.17$ for $X_4 = 1$ and at $X_5 = 0.53$, for $X_4 = -1$.

Recovery Model (Model K - Table 12)

In terms of coded dimensionless terms (Eqn. 65), the fitted model for the percent recovery is found to be

$$\text{Ln(Rec \%)} = 2.585 + 0.193\ X_3 - 1.023\ X_4 + 0.227\ X_2X_4 \qquad (101)$$

The coded capillary number X_1 does not affect the logarithm of percent recovery (see Table 12) in any significant way. This could be because the capillary number in this region is very high (even at $X_1 = -1$), therefore, further increases in N_{Ca}, do not produce any significant additional effects.

The effect of the coded form of h $/\sqrt{K}$, X_2, depends on the value of X_4 as indicated by the term $\beta_{24}X_2X_4$. The minimum recovery occurs at $(X_2, X_4) = (-1, 1)$ and the maximum at $(X_2, X_4) = (-1, -1)$. The ratio of maximum to minimum recovery is 12.18. Fig. 53 shows that at $(X_2, X_4) = (1, -1)$ the logarithm of percent recovery is 3.38. In addition, as the coded viscosity ratio is increased from -1 to 1, the percent recovery constantly decreases for all values of X_2. This decrease is more significant at lower X_2 values (higher permeabilities). The percent recovery does not, however, change in a significant way for a given viscosity ratio when the coded form of h $/\sqrt{K}$, X_2, changes from -1 to 1. This conclusion underscores the relative importance of viscosity ratio on the percent oil recovery. The increased mobility ratio, M, at high viscosity ratios causes more fingering and this, in turn, will attenuate the recovery.

The effect of, X_3, the coded form of R/h, is a linear positive one and does not depend on the other dimensionless terms. The maximum recovery is again obtained

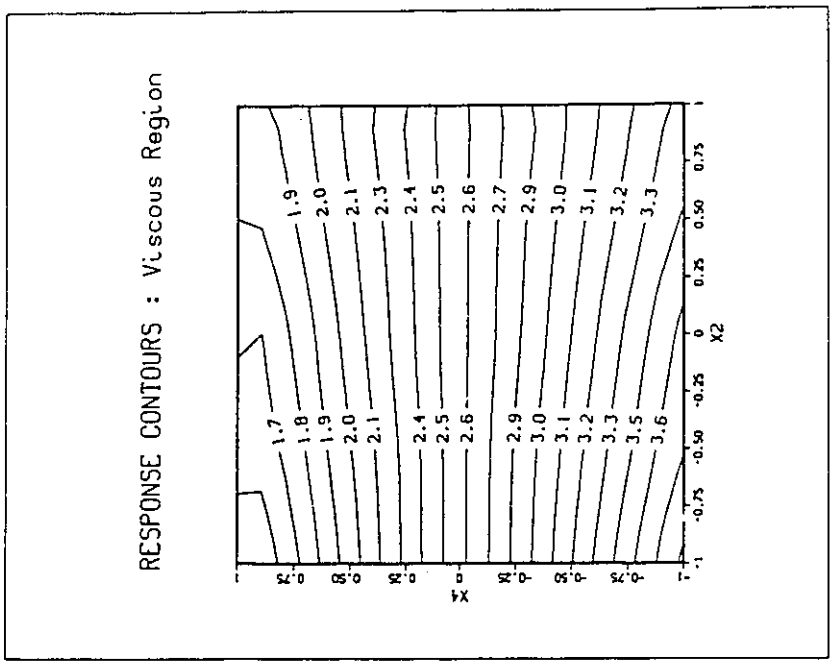

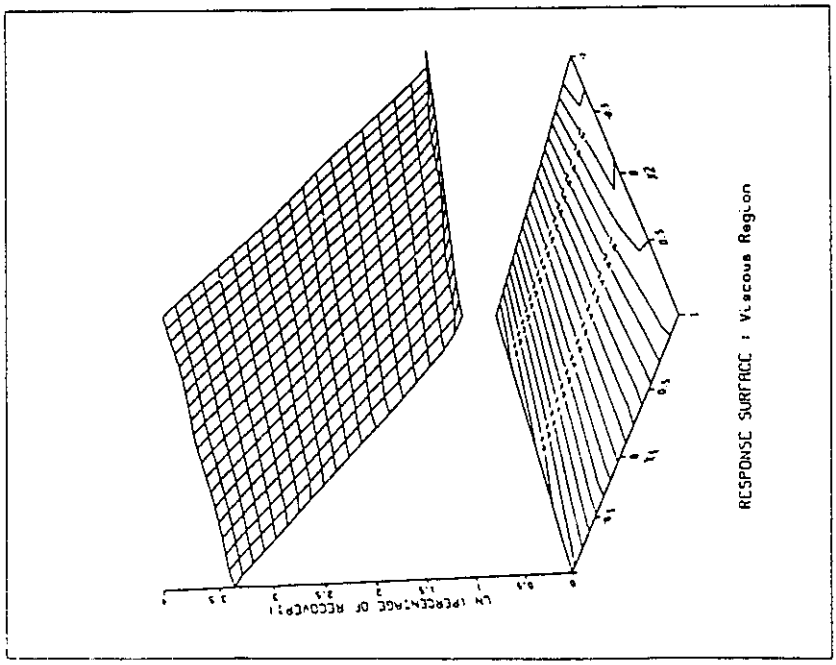

Fig. 53- Response surface and contours for model K.

at $X_3 = 1$ and the minimum at $X_3 = -1$. The ratio of maximum to minimum recovery is 1.47.

Table 12

Parameter Estimates and Pertinent Statistics for Models Based on Eqn. 65 (Models K & L)

Response	Significant Parameters	Parameter Values	Standard Error	$\frac{SSR}{(n-p)}$	$\hat{\sigma}_p^2$	lack of fit ratio (eqn. 70)	$F_{0.05}$	R^2_{adj}
ln(Rec%) N = 40 $N_p = 4$	β_0	2.585	0.048	0.087	0.083	1.066	2.40	0.806
	β_3	0.193	0.061					
	β_4	-1.023	0.085					
Model K	β_{24}	0.227	0.089					
ln (n) N = 40 $N_p = 8$	β_0	3.814	0.036					
	β_1	0.450	0.072	0.047	0.027	2.244	2.48	0.844
	β_2	0.284	0.045					
	β_3	0.298	0.044					
	β_4	0.489	0.069					
Model L	β_{23}	0.100	0.048					
	β_{24}	-0.242	0.065					
	β_{34}	0.150	0.067					

Model for Number of Fingers (Model L - Table 12)

The fitted model relating the total number of fingers to various dimensionless variables (see Eqn. 65) is

$$\text{Ln}(n) = 3.814 + 0.450\, X_1 + 0.284\, X_2 + 0.298\, X_3 + 0.489\, X_4 + 0.100\, X_2X_3 - 0.242\, X_2X_4 + 0.150\, X_3X_4 \qquad (102)$$

The model predicts that all dimensionless terms affect the logarithm of the number of fingers (Table 12).

The coded capillary number, X_1, affects the logarithm of the number of fingers in a linear positive fashion. The maximum number of fingers occur at $X_1 = 1$ and the minimum at $X_1 = -1$. The ratio of maximum to minimum number of fingers is 2.46.

The coded form of $h/\sqrt{K}$, X_2, affects the logarithm of the number of fingers both as a main and an interaction term which depends upon the values of X_3 and X_4 as indicated by terms $\beta_{23}X_2X_3$ and $\beta_{34}X_3X_4$. At $(X_3, X_4) = (-1, 1)$, as the value of X_2 increases from -1 to 1, the logarithm of the number of fingers decreases by 0.12. At the other extreme, namely at $(X_3, X_4) = (1, -1)$, this trend is reversed. In other words, the logarithm of the number of fingers actually sharply increases as the capillary number is increased. This augmentation is by a factor of 1.25. Between these two extremes, the ratio of maximum to minimum number of fingers is 3.50. But the absolute maximum and minimum number of fingers occur at $(X_3, X_4) = (1, 1)$ and at $X_2 = 1$ and $(X_3, X_4) = (-1, -1)$ and $X_2 = -1$, respectively. Here the ratio is 8.52 (an increase of 752%).

Fig. 54, depicts the response surface and contours for the X_2X_3 interaction term. Regardless of X_3, the logarithm of number of fingers constantly increases as coded X_2 increases (or the permeability K, decreases). This increase is intensified at higher values of X_3, the coded form of R/h (at constant $X_4 = 0$). This behavior is quite consistent with theory. On the other hand, as Figure 55 shows (R/h is kept constant, $X_3 = 0$), the number of fingers constantly increases as X_2 is increased for all values of X_4 the coded form of viscosity ratio, $\frac{\mu_o}{\mu_w}$. This increase, however, is more considerable at $X_4 = -1$. This means that at high viscosity ratios, the fingering enhancing effect of $h/\sqrt{K}$ is not very significant as is the case at low values of X_4. This might be due to the fact that, at high X_4 values (high mobility), the number of fingers is already very high (around 100); therefore, further increases of X_2 (reduction of permeability) do not cause further increases in the number of fingers.

As far as the coded form of R/h, X_3, is concerned, its effect depends upon X_2 and X_4. At (X_2, X_4) = (-1, 1), as the value of X_3 increases from -1 to 1, the logarithm of the number of fingers increases by 0.70, a relative increase of 101% in the number of fingers, whereas at (X_2, X_4) = (1, -1) this increase is by 0.50, a relative increase of 64%. Fig. 54 depicts the response surface and contours. The logarithm of the number of fingers increases steadily as X_3 is increased from -1 to 1 for all values of X_2 (for various permeabilities). As discussed earlier, since h, the thickness of the cell is constant, this is due to increased surface area of the oil/water interface at higher R values, which in turn increases the chances of instability and finger formation.

Fig. 56 shows that at constant values of X_2 = 0 (moderate permeability) the logarithm of the number of fingers increases as the coded form of R/h increases from -1 to 1 for all viscosity ratios.

As far as X_4, the coded viscosity ratio is concerned, its effect on the number of fingers depends upon the value of X_2 and X_3. At (X_2, X_3) = (-1, 1), the logarithm of the number of fingers increases sharply by 1.76, a relative increase of 482%. At (X_2, X_3) = (1, -1), this increase is by 0.19, a 21% relative increase in the total number of fingers. Fig. 55 shows that at constant X_3 = 0, as the viscosity ratio is increased, the number of fingers also increases. This is true for all values of $h/\sqrt{K}$, however, this increase is more significant at low values of X_2. That is, at high permeability. On the other hand, at moderate permeabilities (X_2 = 0), the number of fingers again increases as X_4 is increased from -1 to 1. This increased number of fingers due to higher mobility ratio (M) is more significant at lower ratios of R/h. This seems logical because, at low values of X_3, the number of fingers is rather limited, and therefore the enhancing effect of viscosity ratio would seem more noticeable and more obvious.

An attempt was made to fit the data from all experiments for the three regions (159 runs) to linear models similar to Equations 61 and 65. The final models were simplified and tested for their adequacy. The qualitative lack of fit test (residual

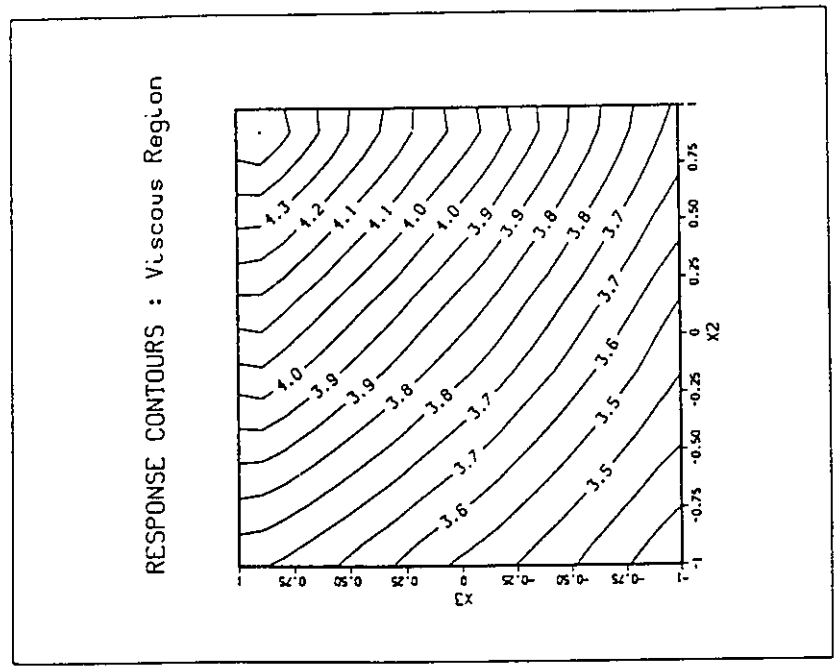

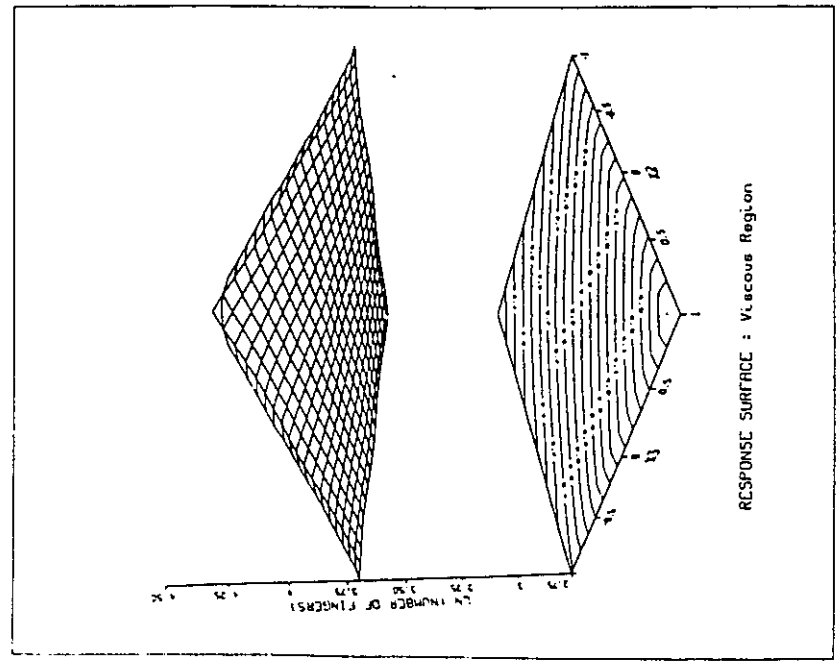

Fig. 54- Response surface and contours for model L.

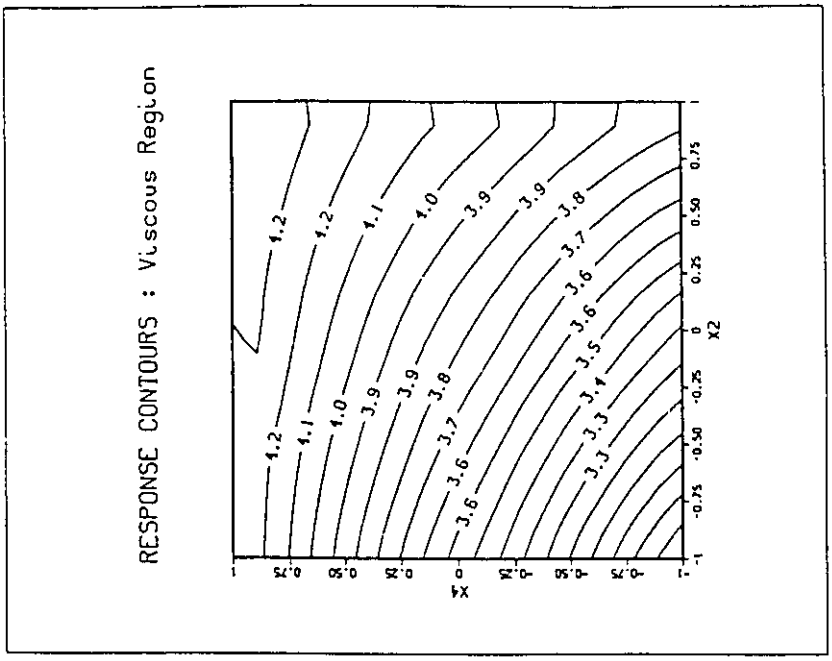

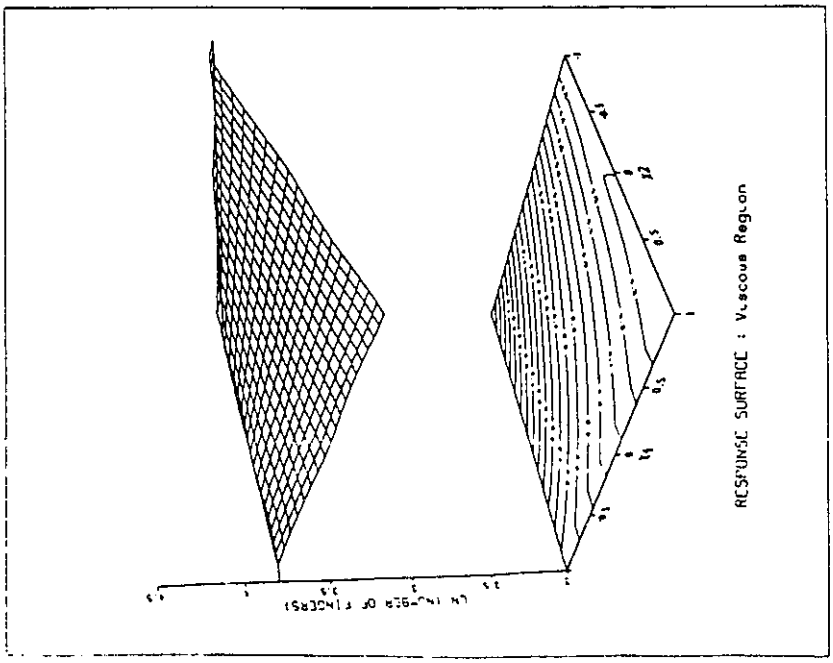

Fig. 55- Response surface and contours for model L.

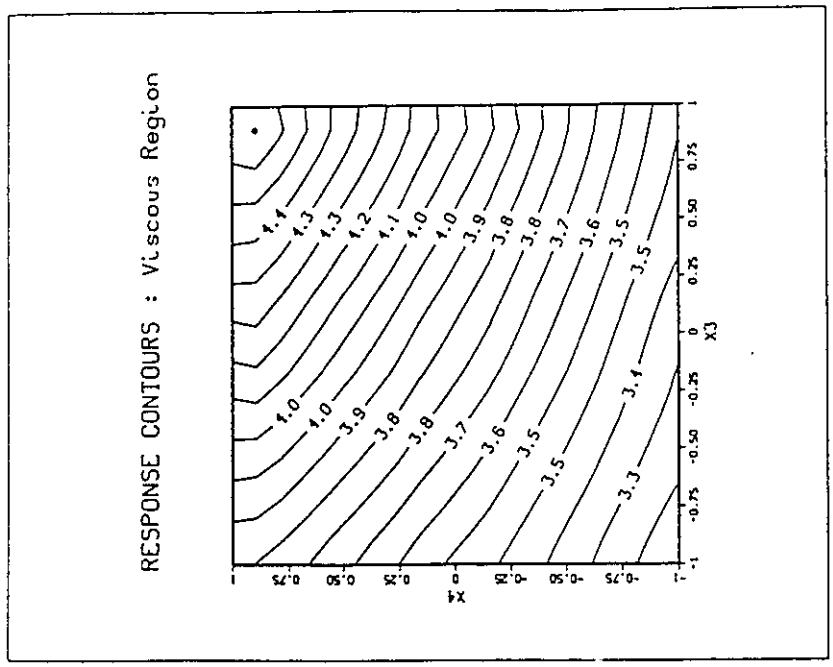

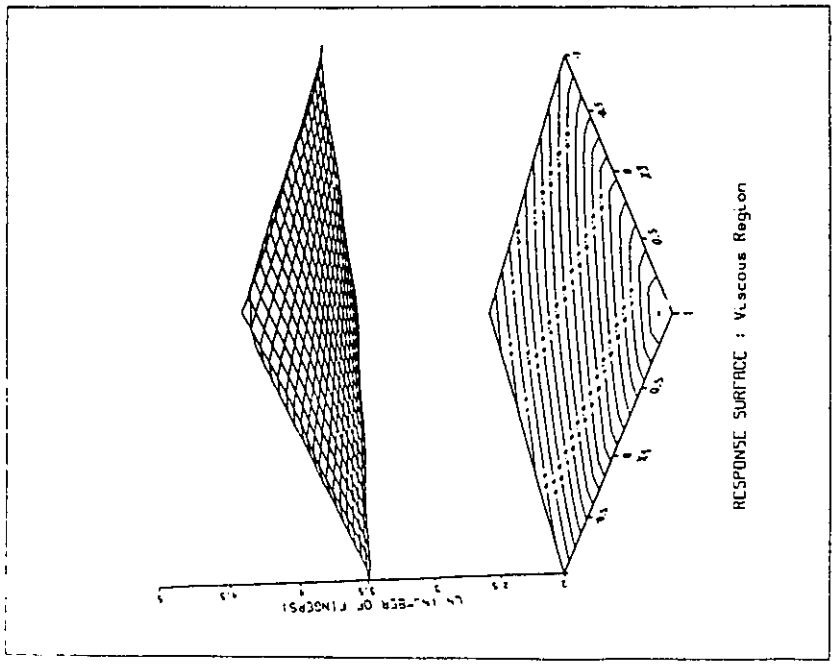

Fig. 56- Response surface and contours for model L.

plots, etc.) did not reveal any lack of fit but the quantitative test (R ratio test) showed that these models cannot adequately represent the process (R ratio > $F_{v_1, v_2, 0.05}$). This means that the errors arising from the model are greater than the experimental errors and could be due to the complexity of the process if all regions are studied together. In other words, one model alone cannot represent the complex behavior of the system over all three regions. In view of the fact that within each of the capillary, intermediate and viscous regions, different forces are dominant and therefore different mechanisms are involved, this finding is not surprising.

The Growth Ratio

As mentioned earlier, one of the biggest problems in past research in the area of viscous fingering has been how to define, identify and count a finger that is at maximum growth rate or stable (not growing or decaying). Obviously there should also be a wide range of other fingers that have a growth rate between these two extreme situations. In linear displacement, comparison of pictures taken of the cell at various times resulted in establishing the number of fingers that are growing at rather high rates. Previous investigators have used this method to come up with a number and attribute it to the number of fingers at maximum growth. In theory, however, there can only be one finger that has the maximum growth rate. The situation becomes more complicated in more practical radial displacements where the number of fingers are much greater and where the interface surface area is constantly increasing. In addition, one finger could be at high growth rate at one moment and at a much lower growth rate just moments later.

Since these important limitations in measuring the number of fingers at various growth rates could result in erroneous results and thus false conclusions, we have based our study on the total number of interfacial perturbations (viscous fingers). Consequently, our models predict a higher number of fingers, and thus a lower value of finger wavelength than the analytical model proposed by Ni et al. (19) namely

$$\lambda_m = \frac{2\pi R^*}{n_m} = \left[\frac{24\pi^3 R^* K h \gamma C^*}{Q(\mu_o - \mu_w)}\right]^{1/2} \qquad (103)$$

Therefore, the value of C*, the wettability number, computed by the above equation using our experimental results would also be much lower than those reported earlier. The wettability number C* depends upon the wettability characteristics of the porous

medium and is a measure of the ability of the fluid to wet the porous medium. (It may also include all of the model errors). Since the interfacial tension is a dynamic variable (aging phenomenon), it is very logical that the effective IFT and therefore C* vary from one experiment to the other. In the absence of any analytical formula to calculate C* from the total number of fingers, it is impossible to compute the true value of C*. However, the ratio of C_t^*, calculated from Eqn. (103) using the total number of fingers and the value of $C_m^* \equiv 300$ (calculated for water-wet systems and based on the number of fingers at maximum growth), should be equal to the square of the ratio of the number of fingers at maximum growth rate to the total number of fingers, i.e.

$$\frac{C_t^*}{C_m^*} = \left(\frac{n_m}{n}\right)^2 \tag{104}$$

This ratio is called the "growth ratio number" and is thought to represent the percentage of those fingers that are growing at maximum rate to the total number of fingers.

$$\frac{n_m}{n}\,\% \simeq \sqrt{\frac{C_t^*}{C_m^*}} \times 100 \tag{105}$$

Table 13

C_t^* Values at Each R for Different Regions Based on Eqn. 103

	REGION			
R_i	CAPILLARY	INTERMEDIATE	VISCOUS	AVERAGE
R_1	2.23	7.81	26.26	12.10
R_2	0.35	1.31	6.85	2.84
R_3	2.51	3.92	37.79	14.74
AVERAGE	1.70	4.35	23.63	9.89
GROWTH RATIO (%)	7.53	12.04	28.07	18.16

Table 13 indicates that C_t^* increases steadily with flowrate Q. On the other hand, with respect to R, there seems to be a minimum C_t^* at R_2. It should be noted that Eqn. 103 is exact for C_m^* (it is based on the number of fingers at maximum growth) and its use to calculate C_t^* is only to give us an approximate value which can be used to calculate the growth ratio according to Eqn. 105. These results are shown in Table 13 and indicate that the ratio of the number of fingers that are growing at high rates to the total number of fingers increases as the flow rate increases. This result seems logical considering that the flow rate increases from 0.65 to 510.0 mL/h (784 fold increase). Since there is a limit to how fast a finger can grow, to absorb this increase in flowrate, a larger number of fingers have to start growing. On the average, for the three regions, only 18.16% of fingers are growing at high rates and the rest are stable. A reported value of $C_m^* = 300$ has been used for these calculations.

II) Non-Linear Models

Single Response Models

The results of fitting the data to models of the general form of Equations 77 and 78 are shown in Tables 14-15 and Tables 16-17, respectively (Appendix C). Computation of the pure error variance and lack of fit ratio, R, was based on the true value of the dependent variable (response) and not its logarithm. As an example, I discuss one of the possible models.

Recovery Model for Viscous Region (Model I' - Table 14)

In terms of the real variables (See Eqn. 77) the fitted model for the recovery is found to be

$$(\text{Rec}\%) = 79.700\ R^{0.267}\ (\mu_o - \mu_w)^{-0.669}\ K^{0.125}\ \gamma^{-0.071} \qquad (106)$$

According to this model, the flow rate does not affect the oil recovery while the radius of breakthrough and permeability seem to enhance the recovery. The IFT and viscosity difference, however, have an attenuating effect on the recovery. The most important operating variable is the viscosity difference. The comparison of lack of fit ratio for model I' to the corresponding $F_{0.05}$ value reveals that the model is not adequate (i.e. the errors arising from lack of fit are greater than the experimental errors). When the R ratio is compared to a $F_{0.01}$ value, the model passes the quantitative lack of fit test and therefore one could conclude that the model is adequate. The residual plots, on the other hand, do not reveal any inadequacy.

The other models, (A'-H' and J'-L') as can be seen from tables 14-17, indicate higher degrees of inadequacy ($R >> F_{0.01}$). Comparison of models I (linear) and I' (non-linear) lead us to conclude that both models indicate a high degree of interac-

tion, but the linear model provides the information in a more easily interpreted form. In any case, the linear model is preferred to the non-linear model because of the better fit.

Multiresponse Parameter Estimation

The data were fitted to three models similar to Eqns. 83, 84 and 85 as described in Chapter 7. In most cases, the multiresponse parameter estimates for θ_2 and θ_3 were not significantly different from zero (the value of θ_4 was included in, and inseparable from θ_1, θ_6 and θ_8). Therefore, unfortunately, the resulting models only included the viscosity ratio, i.e.

$$Y_1 = \theta_1(B_4)^{\theta_5} \tag{107}$$

$$Y_2 = \theta_6(B_4)^{\theta_7} \tag{108}$$

$$Y_3 = \theta_8(B_4)^{\theta_9} \tag{109}$$

Although they are adequate, these models are not very informative since they only reveal information as to the effect of one independent variable (i.e. the viscosity ratio, $\frac{\mu_o}{\mu_w}$). Here, I will only show the results from fitting the data for the intermediate region on the logarithm of percent recovery (similar to single response model G' in Table 16).

$\theta_1 = 46.451 \pm 8.033$ $\qquad$ $\theta_5 = -0.343 \pm 0.059$

$\theta_6 = 56.996 \pm 14.163$ $\qquad$ $\theta_7 = -0.427 \pm 0.091$

$\theta_8 = 95.285 \pm 31.855$ $\qquad$ $\theta_9 = -0.505 \pm 0.128$

The multiresponse estimates of the non-common parameters θ_1, θ_6 and θ_8 are more precise then those obtained by non-linear single response, while the estimates of parameters for viscosity ratio, namely θ_5, θ_7 and θ_9, have almost the same precision as those in Model G'.

These models indicate a hampering effect of viscosity ratio on the logarithm of percent recovery. This rather important hampering effect was also predicted by linear and non-linear single response models. MPE could be used to fit the linearized models to the data.

10 - SUMMARY AND CONCLUSIONS

In this study new results for the recovery of oil and the extent of fingering in radial displacements in water-wet porous media covering a broad range of operating conditions have been presented. Models have been developed to describe the effects of the operating variables on the recovery and the number of fingers. In one case the models were expressed directly in terms of the operating variables; in the other, the models were developed in terms of familiar dimensionless groups. Both approaches provided good descriptions of the data and allowed one to better understand both the magnitude and the form of the effects of the operating variables. They also allowed optimal conditions to be identified and provided evidence as to the adequacy of some theoretical models.

In another approach, the data were analyzed using both non-linear single response and multi-response parameter estimation methods. Due to limitations as to the number of possible parameters being considered, non-linear methods produced models that were not as informative as the linear models. The non-linear models were not as adequate as the linear ones.

In general, as far as the signs and trends are concerned, the results of linear least squares estimation are in good agreement with theory and with previous research. However, one should not forget that during the analytical work (19, 20) many assumptions had to be made that were not necessarily attainable and true during the present experimental study. One good example is the assumption of perfect two-dimensional flow which is rarely obtainable in experimental work. Another example is the difficulty arising from the extension of the Hele-Shaw cell theory to a porous medium; that is the use of macroscopic (continuum) equations and boundary conditions involving pressure at the macroscopic interface to describe interfacial effects which obviously take place at the microscopic level. These points, in addition to those discussed earlier, could explain the differences between the magnitude of the

parameters found in this study and those proposed in previous theoretical work (i.e. Eqn. 57). The present study has accurately quantified the effects of each operating variable and each dimensionless group, and their interactions, on the oil recovery and the number of fingers. This has resulted in determination of the level of importance (relative size) of each of those effects, with respect to each other, on the oil recovery and fingering pattern.

The consideration of all independent variables at the same time and the use of statistical experimental design and various statistical analysis techniques is quite new for these types of systems. It is the only comprehensive and systematic approach which can result in mathematical models that can define the process. These models may be used to predict or to optimize the oil recovery (or the finger formation) process.

The large data set (159 experiments) and experimental design employed extend the validity of these findings over a wide range of values for the other operating variables or dimensionless groups. This could not be said about most past research studies which have only covered one or two variables at a time over a limited range. One very important factor often ignored by many investigators is the nature of the residuals and the experimental errors which can vary from one experiment to another. The models in the present study have taken these factors into consideration.

The resolution of numerous experimental difficulties that were encountered during this study is a positive contribution to the development of this field of research. Furthermore, the concept of favorable ($M < 1$) and unfavorable ($M > 1$) mobility ratios and Haines jumps, although not new, have been well documented and explained. In addition, we have pinpointed the serious shortcomings and limitations that are encountered if the number of fingers at maximum growth rate are considered and instead we have studied the total number of fingers. The concept of

growth ratio, i.e. the ratio of number of fingers at maximum growth rate to the total number of fingers, is introduced and computed for each region. Some of the most important findings of the present study are listed below:

1) Changes of flowrate of the injected fluid within any of the three discussed regions, did not influence the oil recovery. However, low flowrates within the capillary region enhance imbibition and this in turn increased the oil recovery. Low flowrates can also cause end-effects around the cell edges. In my opinion, this phenomenon is responsible for the abnormally high recoveries observed by Nasr-El-Din et al. (20) and Sayyouh et al. (38) at very low flowrates.
2) The flow rate, Q, has an enhancing effect on the number of fingers up to a certain point (viscous region) after which, due to an already high number of fingers, any further increase in the flowrate did not cause any more fingering. This indicates that, at this point, the number of existing fingers is large enough to accommodate and absorb further increases in the flowrate.
3) Distance from the injection point (radius of breakthrough, R) has a positive effect on the percent recovery. However, due to the natural imbibition that occurs when capillary forces are dominant, this effect is the greatest within the capillary region.
4) The number of fingers steadily increases as the distance from the injection point is increased. This is due to the increased surface area of the oil/water interface which increases the possibility of instability occurrence.
5) The viscosity difference (or ratio) has a large negative effect on the oil recovery. This is due to the increased mobility ratio, M, which in turn will enhance fingering and therefore reduce the recovery (decreased sweep efficiency). This phenomenon explains the lower oil recoveries obtained during waterflooding of heavy oil fields. This attenuating effect of viscosity difference (or ratio)

on the oil recovery is more apparent at high flow rates due to the absence of natural imbibition (which has a competing effect with the viscosity difference or the viscosity ratio) within this region.

6) The permeability of the porous medium, K, has a complex effect on the oil recovery which depends upon the values of distance and viscosity difference. In general, more permeable media hamper finger formation (offer small resistance to flow), which results in enhanced recovery.

7) On the other hand, permeability affects the number of fingers in a negative fashion. This effect is influenced by other operating variables within the capillary region due to the interplay of capillary imbibition phenomenon.

8) The interfacial tension, has a negative (attenuating) effect on the oil recovery within the capillary region, and this effect is intensified at small distances and lower viscosity differences.

9) The IFT has a complex effect on the number of fingers which depends upon the value of the other operating variables. The magnitude of these effects, however, is not large.

10) A new capillary number ($N_{Ca} = \frac{Q\mu}{K\gamma}$) has been introduced in this study which has the advantage of remaining constant during the whole experiment. The effect of this capillary number on the oil recovery is very complex at low to moderate flowrates; it does not affect the recovery within the viscous region, most probably because N_{Ca} is already very high at this point and any further increase in the viscous forces does not produce significant changes in oil recovery. However, its effect depends upon the value of other variables. The existence of these interactions explains the already reported but not fully understood results of Taber (9), and it underscores the dangers involved in generalizing conclusions where only one or two variables have been considered.

11) The capillary number has a positive (enhancing) effect on the finger formation process. This is due to the increase in the viscous forces as compared to capillary forces. Since there is an upper limit to how fast any finger can grow, new fingers have to be formed in order to absorb and accommodate the flow.

12) Non-linear single response parameter estimation produces models that are not as adequate as those produced by linear least squares parameter estimation methods. This is due to the form of the models employed and not the method. In addition, non-linear models are less informative as far as the nature and form of the individual interactions is concerned.

13) Multiresponse parameter estimation (MPE) produces models that due to a lower number of parameters are not very informative.

14) The average values of $\tilde{C}_i$ (the wettability constant based on the total number of fingers) for the capillary, intermediate and viscous regions were found to be 1.70, 4.35 and 23.63 respectively. This indicates that previous researchers were probably not justified in using just one value of C* for all of their experiments.

15) The concept of growth ratio (the percentage of the number of fingers that are growing at high growth rates to the total number of fingers) is for the first time introduced. These ratios were found to be 7.53, 12.04 and 28.07 percent for the capillary, intermediate and viscous regions, respectively. This indicates that as the flowrate increases, a larger percentage of the fingers have to start growing in order to accommodate and absorb the increase in the flowrate.

11- RECOMMENDATIONS FOR FUTURE WORK

- The use of experimental design and statistical analysis procedures is strongly recommended for any future work in this field because it is the only comprehensive way by which one can obtain information as to the nature of the main operating (independent) variables and their interactions (joint effects).

- The use of thinner cells (smaller h) could ensure a more two dimensional flow which may lead to results that are closer to available analytical solutions developed for two dimensional flow. However, one should make sure that the wall effects (higher permeability at the vicinity of the plates) are kept to a minimum.

- It is felt that if manufacturing difficulties are resolved, larger cells will probably result in more information as far as the radius of breakthrough (distance from the injection point) is concerned. In other words, a wider operating range for radius would make practical sense.

- If specific information concerning one or several operating variables and/or their interactions is required, these information should be utilized in choosing the type of factorial design. The kind of factorial design should be compatible and appropriate for the type of specific information sought.

- Linear least squares seemed to produce models that are quite adequate and informative. Since non-linear models cannot determine interactions individually, it is recommended that the linear model building process be utilized if preliminary study shows that they are in fact the appropriate type of model for that specific process. However, the multiresponse parameter estimation technique could be used to fit the linearized models to the data.

- The concept of capillary, intermediate and viscous regions is relative and the limits of each of these regions depends on the specifics of the system such as the size and permeability of the porous medium, the flow rate, etc. Therefore, these factors should be studied carefully before determining the boundaries of each region.

- The same type of experiments and modelling could be repeated for strongly oil-wet systems, such as the one studied by Ni et al. (19). The resulting models could be compared with those obtained in this study and this could well reveal information as to the nature of the process and the mechanisms involved.

12 - NOMENCLATURE

a_i = constant

b_i = constant

B_i = dimensionless term

C = Chuoke parameter

C* = wettability constant

C_m^* = wettability constant based on maximum number of fingers

C_t^* = wettability constant based on total number of fingers

d = diameter of the oil droplet in spinning drop tensiometer

d_p = diameter of the solid particles

D = duct diameter

D_o = pore throat diameter

DLA = diffusion-limited aggregation

E_m = microscopic displacement efficiency

E = expected valve

EOR = enhanced oil recovery

f = response function

f_i = fraction of phase i flowing

F = value of probability density function

g = gravitational constant

h = cell thickness

h_o = initial height of liquid

h(t) = height of liquid at time t

I = defining relation

IFT = interfacial tension

K = cell permeability

k_e = effective permeability

k_r = relative permeability

L = distance, core length

L( ) = likelihood function

M = mobility ratio = $(K_w/\mu_w)/(K_o/\mu_o)$

MPE = multiresponse parameter estimation

n = total number of fingers

n_m = number of fingers at maximum (high) growth

N = number of runs

N_{Ca} = traditional capillary number = $\frac{\mu V}{\gamma \varepsilon}$

N_p = number of parameter estimates

OOIP = original oil in place

PV = pore volume

p_c, P_c = capillary pressure

p_o = pressure in the displaced phase

p_w = pressure in the displacing phase

P_i = pressure in phase i

Q = volumetric injection flow rate

q_i = volumetric injection flow rate for fluid i

r = radial distance from the injection point

r = principal radius of curvature of the finger tip (in the plane of the plate)

r' = principal radius of curvature (normal to the plate)

R = radius (radial distance from the injection point) of breakthrough

R* = radius of displacement front in complete absence of fingering

R ratio = used in quantitative lack of fit test

R^2_{adj} = adjusted coefficient of determination (square of correlation between the dependent variables and the predicted value)

R_o = radius of inlet port

R_{wo} = curvature of the interface

Rec% = percentage of volumetric oil recovery

Re = Dimensionless Reynolds number = $\frac{\rho V dp}{\mu \varepsilon}$

S = spreading coefficient

S_i = fractional saturation for fluid i

S_{OR} = residual oil saturation

S_{wi} = irreducible water saturation

Soi = initial oil saturation

$S(\theta)$ = sum of squares of residuals

SSR = sum of squared residuals

S_W = wetting phase saturation

t = time

t_{br} = time at breakthrough

T = inverse of angular velocity

V_{cell} = total volume of the cell

V = superficial velocity

V = variance

V_{solid} = volume of the solid particles

V_p = pore velocity = V/ε

W = work of adhesion or cohesion

w = thickness of the cell

x = distance

x_i = operating variables

X_i	=	coded operating variable
Y_i	=	observed response values
$\overline{Y_i}$	=	mean observed response value
Z_{nm}	=	disturbance term for the mth response and nth run
Z_{ri}	=	difference between observed and predicted response for the mth response and nth run
α	=	probability level
α	=	density difference
β_i	=	parameter estimate for linear least squares parameter estimation
γ	=	interfacial tension
γ^*	=	effective interfacial tension = $C^*\gamma$
ξ	=	operating variable
Π	=	spreading pressure
π	=	3.1416
η	=	expected response
ε	=	porosity
ε_n	=	random error
ρ	=	density
θ	=	contact angle
θ_a	=	advancing contact angle
θ_r	=	receding contact angle
μ_o	=	viscosity of the oil phase
μ_w	=	viscosity of the water phase
$\widetilde{\sigma}_p^2$	=	estimated variance of response
ν_p	=	degrees of freedom associated with the pooled estimate of variance
λ	=	finger wavelength
λ_i	=	parameters for the non-linear model
ϕ_i	=	parameters for the non-linear model

1 3 - BIBLIOGRAPHY

1) Jha, K.N., "Enhanced Oil Recovery - An Introduction", Chemistry in Canada, 34, 19 (1982).

2) Berger, B.D., Anderson, K.E., "Modern Petroleum", Pennwell Books, Oklahoma, (1981).

3) Latil, M., "Enhanced Oil Recovery", Chap. 2, Paris, (1980).

4) Prince, J.P., "Enhanced Oil Recovery Potential in Canada - A Methodological Review", Canadian Energy Research Inst., 9, Calgary (1978).

5) Herbeck, E.F., Heintz, R.C., Hastings, J.R., "Fundamentals of Tertiary Oil Recovery", Energy Communications, (1977).

6) Greenkorn, R.A., "Flow Phenomena in Porous Media", Marcel Dekker Inc., N.Y., 1983.

7) Morrow, N.R., "Physics and Thermodynamics of Capillary Action in Porous Media, in Flow Through Porous Media", Amer. Chem. Soc., Washington, D.C., Chapter 6, (1970).

8) Chatzis, I., Morrow, N., "Correlation of Capillary Number Relationships for Sandstones", SPE AIME 10114 (1981).

9) Taber, J.J., "Research on Enhanced Oil Recovery: Past, Present and Future", Pure & Appl. Chem. Vol. 52, p. 1323-1357, (1980).

10) Taber, J.J., Kirby, J.C., Schroeder, F.U., "Studies on the Displacement of Residual Oil: Viscosity and Permeability Effects", AIChE Symp. Series, 69, 53 (1973).

11) Foster, W.R., "A Low-Tension Waterflooding Process", J. Pet. Technol. 255, 205-210, (1973).

12) Shah, D.O., "Third European Symp. on E.O.R., U.K.", Sept. 1981.

13) Bear, J., "Dynamics of Fluids in Porous Media", Elsevier, N.Y. (1972).

14) Paterson, L., Hornof, V., Neale, G., "Water Fingering into an Oil-Wet Porous Medium Saturated with Oil at Connate Water Saturation", Rev. Inst. Fr. Pétrole, 39, 517-521 (1984).

15) Spanos, T.J.T., "A Stability Analysis of Immiscible Viscous Displacement in a Homogeneous Porous Medium", Can. J. Phys., 58, 138 (1980).

16) Paterson, L., Hornof, V., Neale, G., "Visualization of a Surfactant Flood of an Oil-Saturated Porous Medium" Soc. Pet. Eng. J., 24, 325-327 (1984).

17) Paterson, L., Hornof, V., Neale, G., "A Consolidated Porous Medium for the Visualization of Unstable Displacements", Powder Tech., 33, 265-268 (1982).

18) Stoneberger, M.W. and Claridge, E.L., "Graded Viscosity Bank Design with Pseudoplastic Fluids", SPE 14230 (1985).

19) Ni, L.W., Hornof, V., Neale, G., "Radial Fingering in a Porous Medium", Rev. Inst. Fr. Pétrole, 41, 217-228 (1986).

20) Nasr-El-Din, H., Hornof, V., Neale, G., "Radial Fingering in a Water Wet Porous Medium", Rev. Inst. Fr. Pétrole, 42, 783-796 (1987).

21) Lenormand, R., Zarcone, C., "Two-Phase Flow Experiments in a Two-Dimensional Permeable Medium", Physicochem. Hydrodyn., 6, 497-506 (1985b)

22) Perkins, T.K., Johnston, O.C., "A Study of Immiscible Fingering in Linear Models", SPE 2230, 39-46 (1969).

23) Lenormand, R., Touboul E., Zarcone, C., "Numerical Models and Experiments on Immiscible Displacements in Porous Media", J. Fluid Mech. 189, 165-187 (1988).

24) Melrose, J.C., Brandner, C.F., "Role of Capillary Forces in Determining Microscopic Displacement Efficiency for Oil Recovery by Waterflooding", Can. Pet. Tech., 13, 54 (1974).

25) McLean, J.W., Saffman, P.G., "The Effect of Surface Tension on the Shape of Fingers in Hele-Shaw Cell", J. Fluid Mech., 102, 455-469 (1981).

26) Morgan, J.C., Schechter, R.S., Nade, W.H., "Ultra-low Interfacial Tension and its Implications in Tertiary Oil Recovery"

27) Aronofsky, J.S., "Mobility Ratio: Its Influence on Flood Patterns During Water Encroachment", Pet. Trans. AIME, 195, 15-24 (1952).

28) Sigmund, P.M., Sarma, H., Sheldon, D., Aziz, K., "Flow Instability in Porous Media: Rate Dependence of Unstable Waterfloods", 35th Can. Chem. Eng. Conf., October 1985.

29) Homsy, G.M., "Viscous Fingering in Porous Media", Ann. Res. Fluid Mech., 19 271-311 (1987).

30) Hornof, V., Morrow, N.R., "Gravity Effects in the Displacement of Oil by Surfactant Solutions", SPE Reservoir Eng. 627-633 (1987).

31) Nafeh, A.H., "Stability of Liquid Interfaces in Porous Medium", Phys. Fluids, 15, 1751 (1972).

32) Melrose, J.C., "Interfacial Phenomena as Related to Oil Recovery Mechanisms", Can. Chem. Eng., 48, 638 (1970).

33) Uren, L.C., Fahmy, E.H., "Factors Influencing the Recovery of Petroleum from Unconsolidated Sands by Waterflooding", Trans. AIME 77, 318-335 (1927).

34) Taber, J.J., "The Injection of Detergent Slugs in Water Floods", Trans. AIME 213, 186-192 (1958).

35) Taber, J.J., "Dynamic and Static Forces Required to Remove a Discontinuous Oil Phase from Porous Media Containing Both Oil and Water", Soc. Pet. Eng. J., 9, 3-12 (1969).

36) Saffman, P.J. and Taylor, G.I., "The Penetration of a Fluid into a Porous Medium or Hele-Shaw Cell Containing a more Viscous Liquid", Proc. R. Soc. A245, 312 (1958).

37) Moore, T.F., Slobad, R.L., "The effect of Viscosity and Capillarity on the Displacement of Oil by Water", Prod. Monthly 20, 20-30 (1956).

38) Sayyouh, M.H.M., Farouq Ali, S.M., Stahl, C.D., "Rate Effects in Tertiary Micellar Flooding of Bradford Crude Oil", Soc. Pet. Eng. J., 7639 (1981).

39) Mungan, N., "Interfacial Effects in Immiscible Liquid-Liquid Displacement in Porous Media", Trans. AIME, 237, 247 (1966).

40) Hornof, V., Morrow, N.R., "Gravity Effects in the Displacement of Oil by Surfactant Solutions", SPE AIME 13573, 255-259 (1985).

41) Necombe, J., McGhee, J., and Rzasa, M.J., "Wettability Versus Displacement in Waterflooding in Uncosolidated Sand Columns", Trans. AIME, 204, 227-232 (1955).

42) Sarma, H.K., "Viscous Fingering: One of the Main Factors Behind Poor Flood Efficiencies in Petroleum Reservoirs", Powder Tech., 48, 39 (1986).

43) Chen, J.D., "Radial Viscous Fingering Patterns in Hele-Shaw Cells", Experiments in Fluids, 5, 363 (1987).

44) Jennings, H.Y., "Waterflood behaviour of High Viscosity Crudes in Preserved soft and Unconsolidated Cores", J. Pet. Technol., 116-120 (January 1966).

45) Anderson, W.G., "Wettability Literature Survey: The Effects of Wettability on Waterflooding", J. Pet. Technol., 1605-1622 (Dec. 1987).

46) Peters, E.J., Flock, D.L., "The Onset of Instability During Two-Phase Immiscible Displacement in Porous Media", Soc. Pet. Eng. J., 21, 249-258 (1981).

47) Morrow, N.R., "Wettability and its Effects on Oil Recovery", J. Pet. Tech., 1476-1484 (Dec. 1990).

48) Hebermann, B., "The Efficiency of Miscible Displacement as a Function of Mobility Ratio", SPE, 205-213, (Oct. 1960).

49) Tayal, P., Narayan, K.A., "Visualization of Water and Surfactant Floods in Oil-Saturated Porous Media", Exp. in Fluids, 9, 337-344 (1990).

50) Chuoke, R.L., Van Meurs, P. and Van Der Poel, C., "The Instability of Slow Immiscible, Viscous Liquid-Liquid Displacement in Permeable Media", Trans. Am. Inst. Min. Eng. 216, 188 (1959).

51) Fayers, F.J., Muggeridge, A.H., "Extension to Dietz Theory and Behaviour of Gravity Tongues in Slightly Titled Reservoirs", SPE Reservoir Eng., 487-494 (Nov. 1990).

52) Rachford, H.H., "Instability in Waterflooding Oil from Water-wet Porous Media Containing Connate Water", S.P.E.J., 231, 133-148 (1964).

53) Morrow, N.R., "Viscous Instabilities and Dimensionless Wavelength Based on a Microscopic Length", RRRC 85, May 20 (1985).

54) Spanos, T.J.T., "A General Stability Analysis for Immiscible Viscous Displacement in a Porous Medium", Can. J. Phys., 59, 678 (1981).

55) Jerauld, G.R., Davis, H.T., Scriven, L.E., "Frontal Structure and Stability in Immiscible Displacement", SPE AIME 126, 135-142 (1984).

56) Bataille, J., "Stabilité d'un Déplacement Radial Non-Miscible", Rev. Inst. Fr. Pétrole, 22, 1349-1364 (1968).

57) Bird, R.B., Stewart, W.E., Lightfoot, E.N., "Transport Phenomena", John Wiley and Sons, New York (1960).

58) Muskat, M., Wychoff, R.D., Botset, H.G., Meres, M.W., "Flow of Gas-Liquid Mixtures Through Sands", Pet. Trans. AIME 123, 69 (1937).

59) Buckley, S.E., Leverett, M.C., "Mechanism of Fluid Displacement in Sands", Pet. Trans. AIME 146, 107 (1941).

60) Kiriakidis, D.G., Neale, G.H., Mitsoulis, E., "Numerical Simulations of Radial Displacement of a Wetting Fluid by a Non-Wetting Fluid in a Porous Medium", J. Phys. A: Math Gen. 23, 5089-5094 (1990).

61) Sarma, H.K., Bentsen, R.G., "An Experiment Verification of a Modified Instability Theory for Immiscible Displacement in Porous Media", J. of Can. Pet. Tech. 88-99, (July-August 1987).

62) Box, G.E.P., Hunter, W.G. and Hunter, J.S., "Statistics for Experimenters", J. Wiley (1978).

63) Draper, N., Smith, H , "Applied Regression Analysis", J. Wiley, (1981).

64) Draper, N.R. and Hunter, W.G., "Design of Experiments for Parameter Estimation in Multiresponse Situations", Biometrika, 53, 525-533 (1966).

65) Bacon, D.W., "Collection and Interpretation of Industrial Data", Dept. Chem. Eng. Queen's U. Kingston.

66) SAS User's Guide, SAS Inst., Ed. 5 (1985).

67) Bates, D.M. and Watts, D.G., "Non-Linear Regression Analysis and its Application", J. Wiley & Sons, Chap. 3-4, (1988).

68) Hopkins, J.S., Golding, J.A., Ritcey, G.M., "The Critical Factors Influencing Uranium Precipitation by Hydrogen Peroxide: The Use of Experimental Design Techniques", Hydrometallurgy, 17, 315-334 (1987).

69) Box, M.J. and Draper, N.R., "Estimation and Design Criteria for Multiresponse Non-Linear Models with Non-Homogeneous Variance", App. Statist., 21, 13-24 (1972).

70) Heller, J.P., "The Interpretation of Model Experiments for the Displacement of Fluids Through Porous Media", AIChE Journal, 9,4, 452-459 (1963).

71) Cayias, J.L., Schechter, R.S., Wade W.H., "The Measurement of Low Interfacial Tension Via the Spinning Drop Technique" ACS Symp. Ser. No. 8, 234-247, (1975).

APPENDIX A

Residual Plots

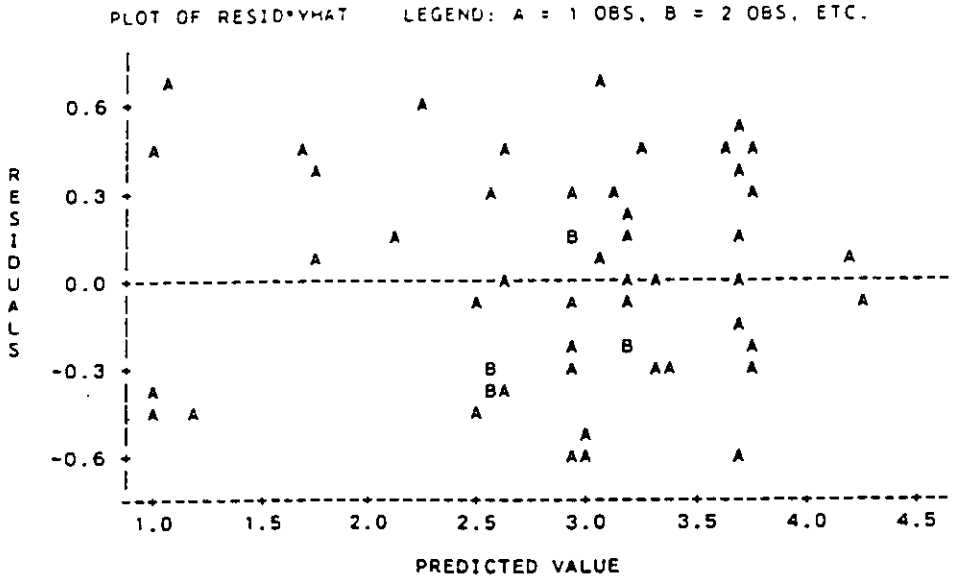

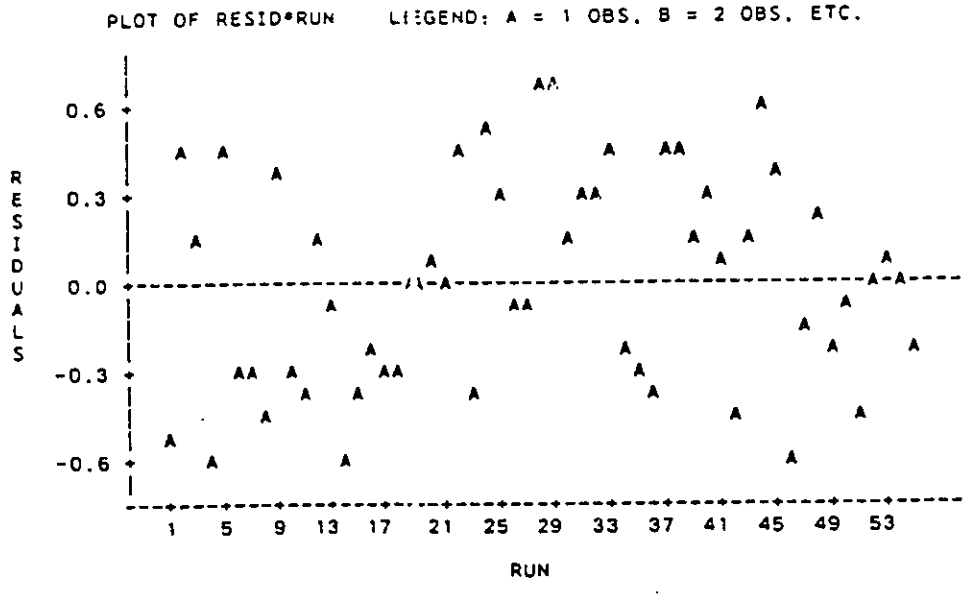

Fig. 57- Residual plots for model A.

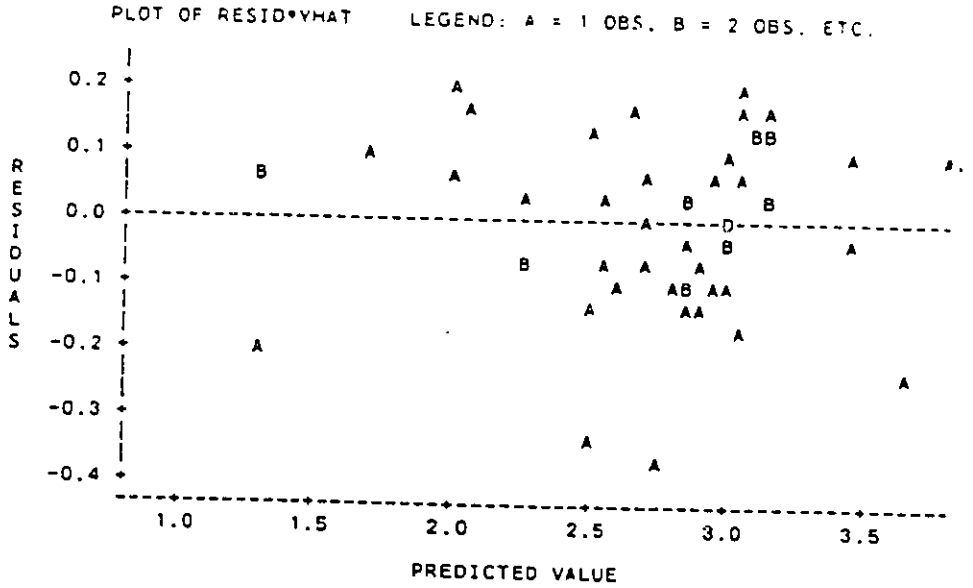

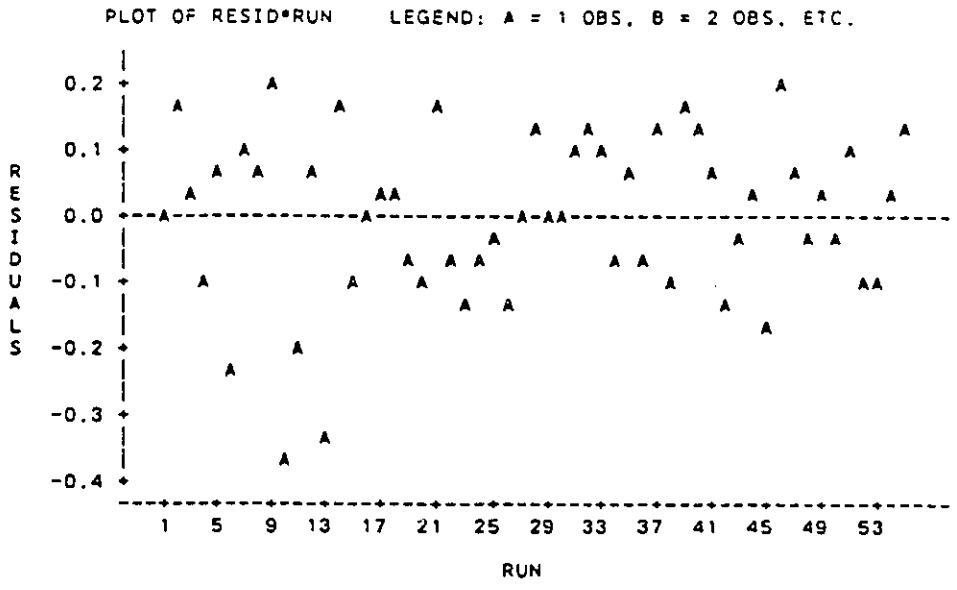

Fig. 58- Residual plots for model B.

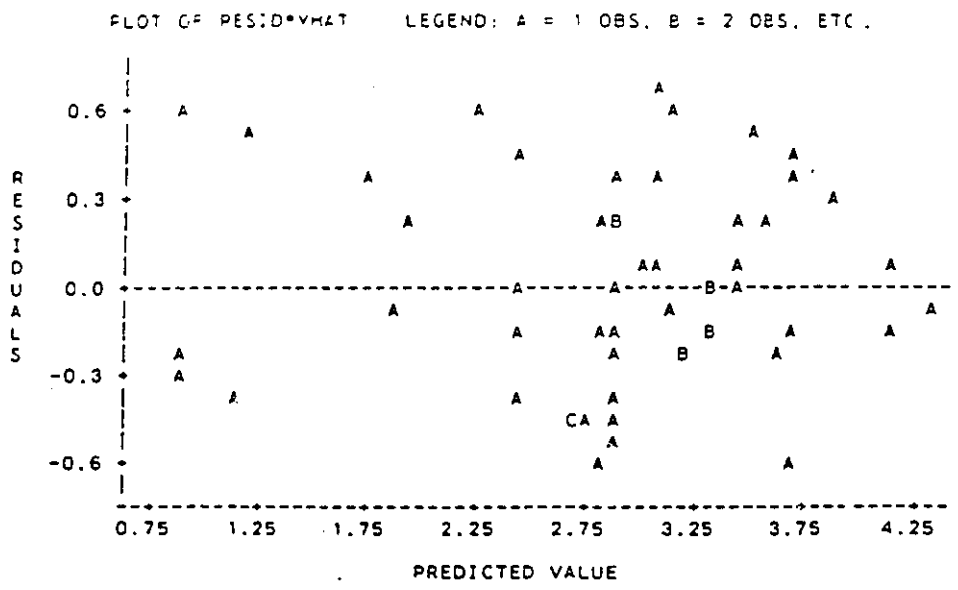

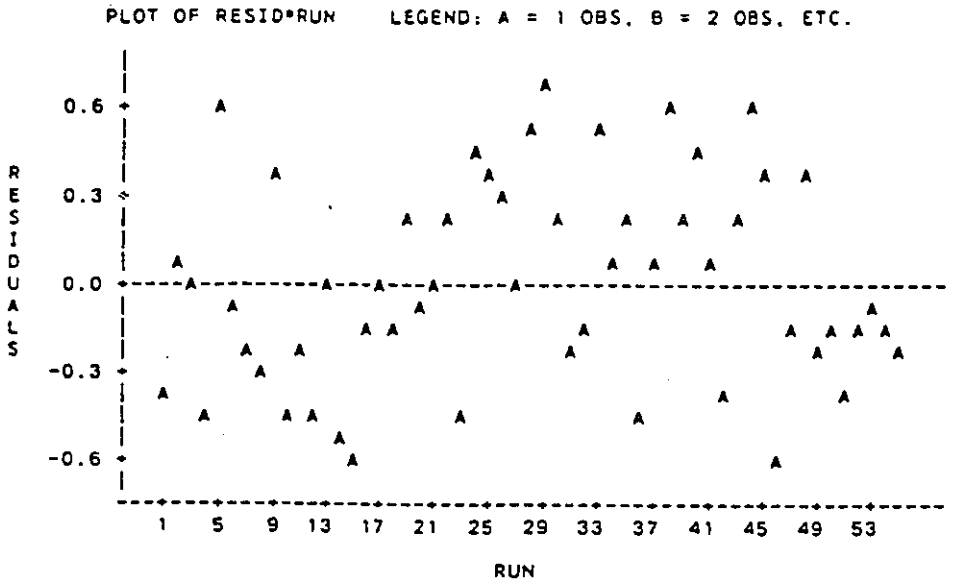

Fig. 59- Residual plots for model C.

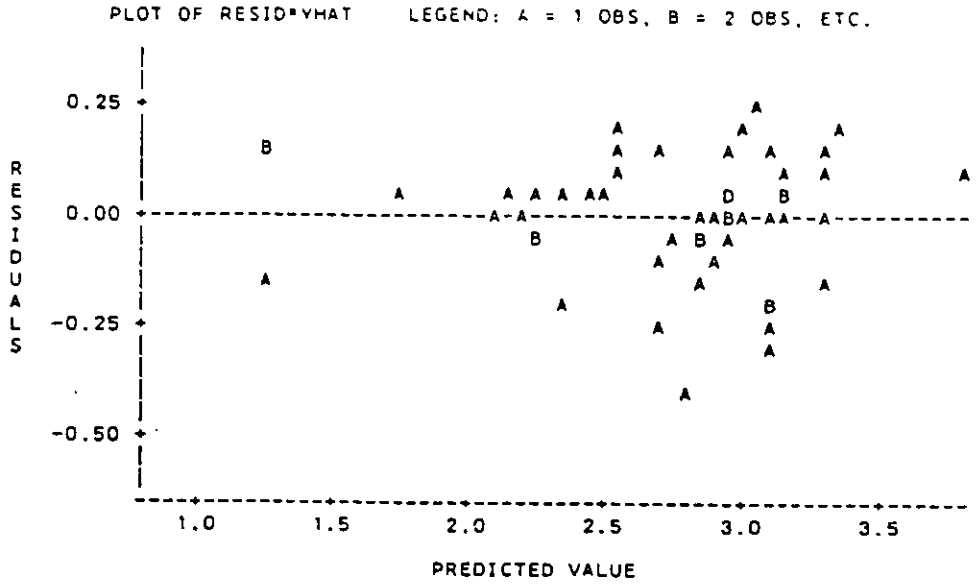

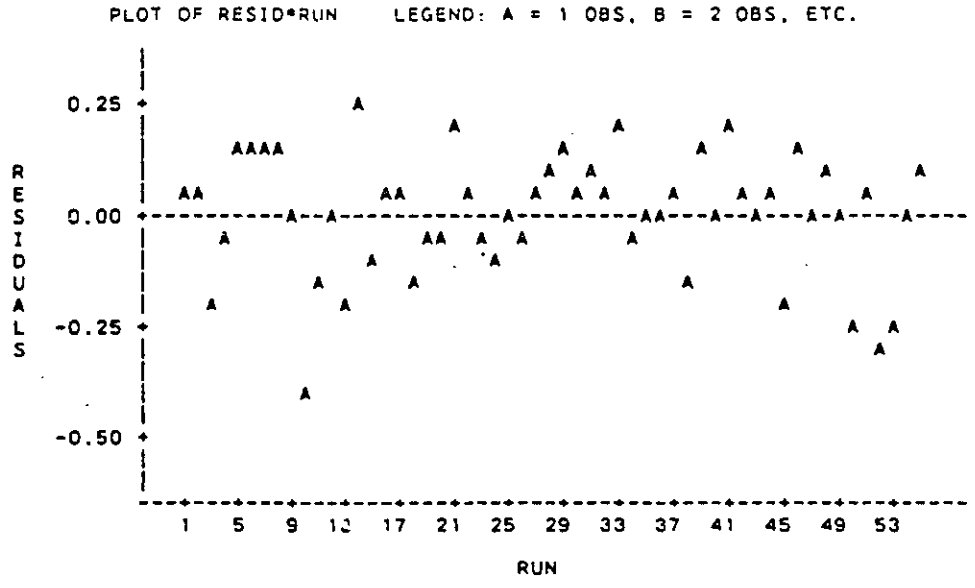

Fig. 60- Residual plots for model D.

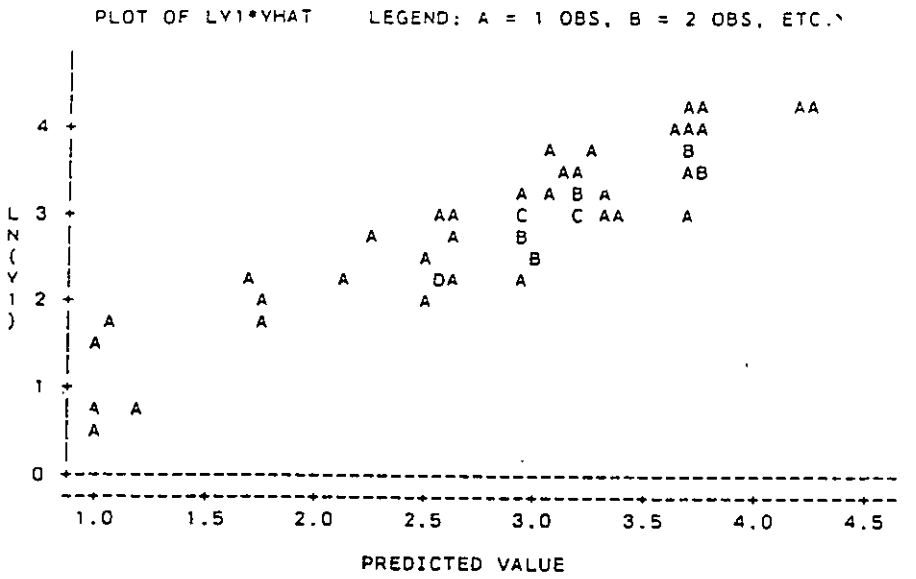

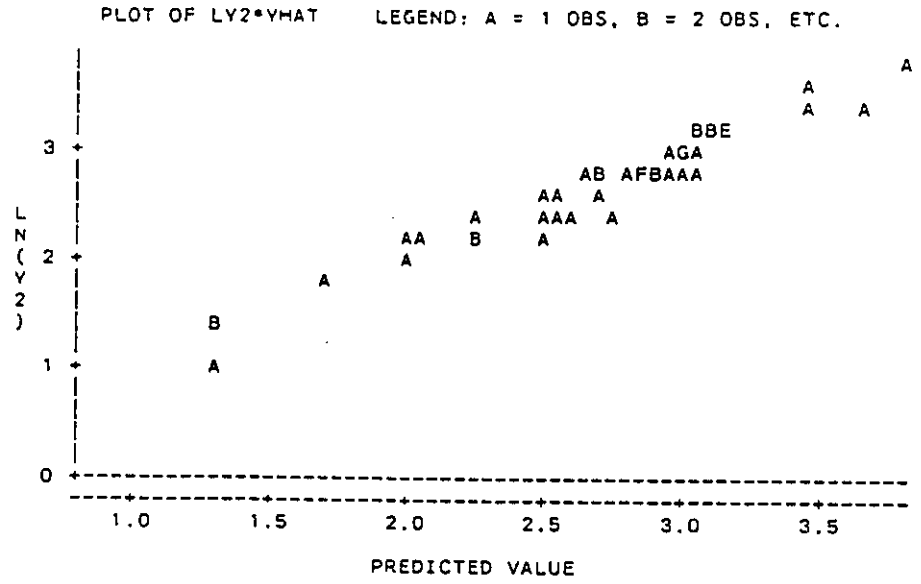

Fig. 61- Plots of observed VS. predicted values for models A and B.

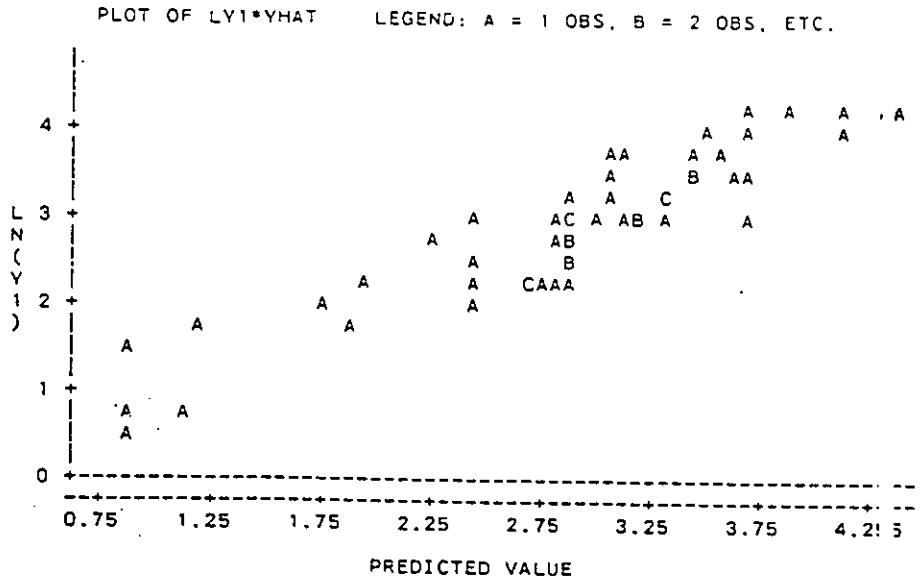

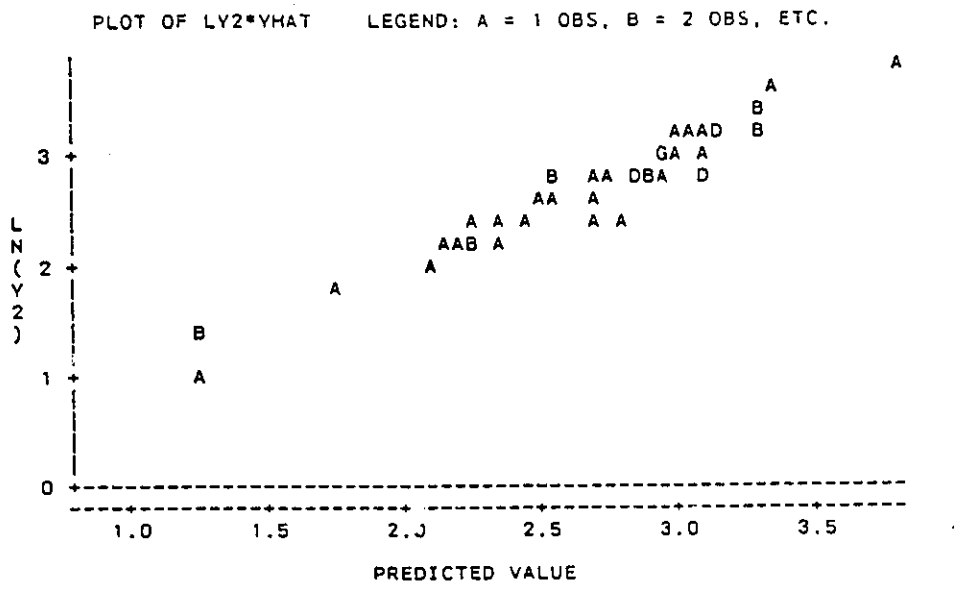

Fig. 62- Plots of observed VS. predicted values for models C and D.

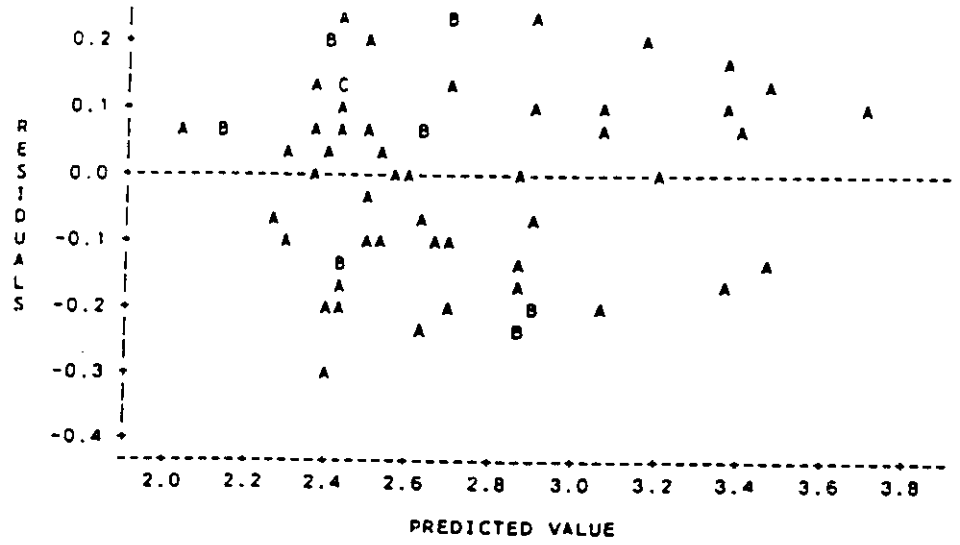

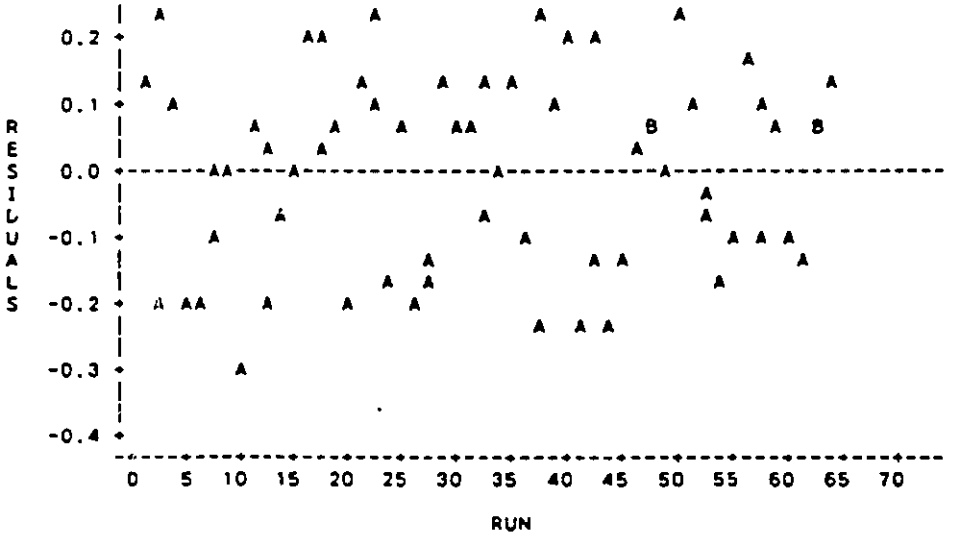

Fig. 63 - Residual plots for model E.*

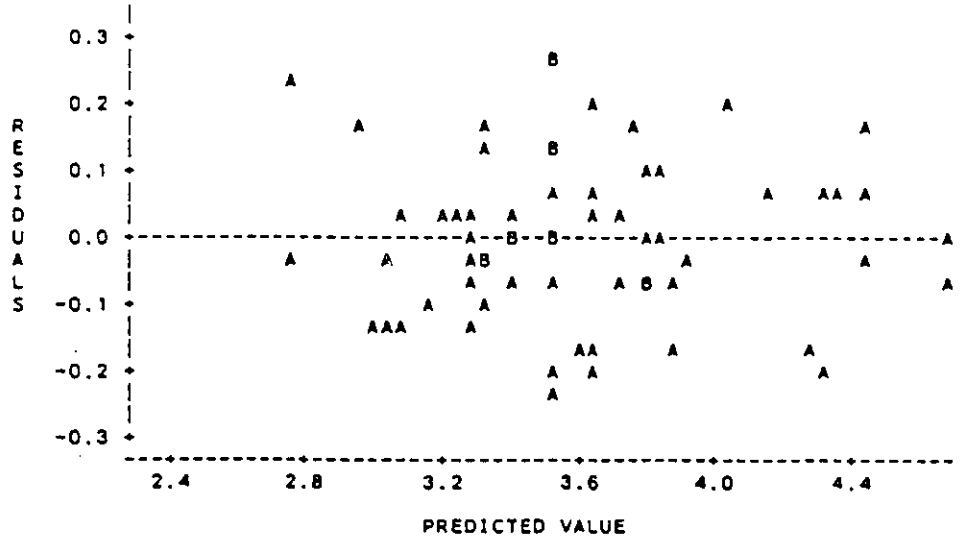

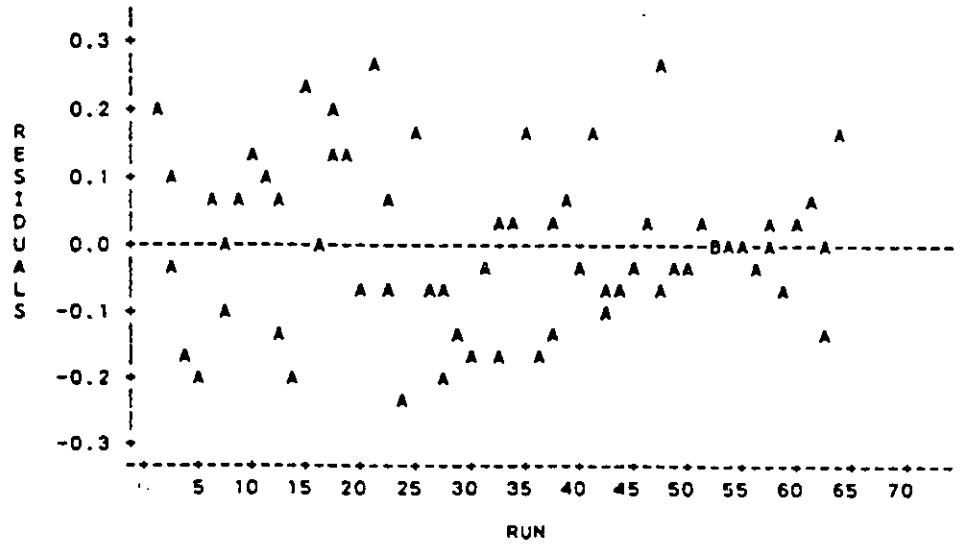

Fig. 64 - Residual plots for model F.*

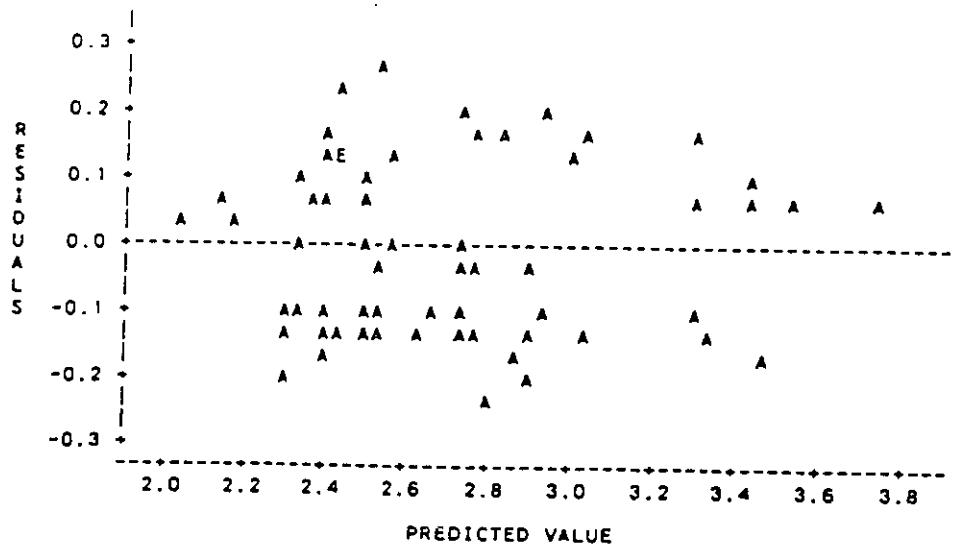

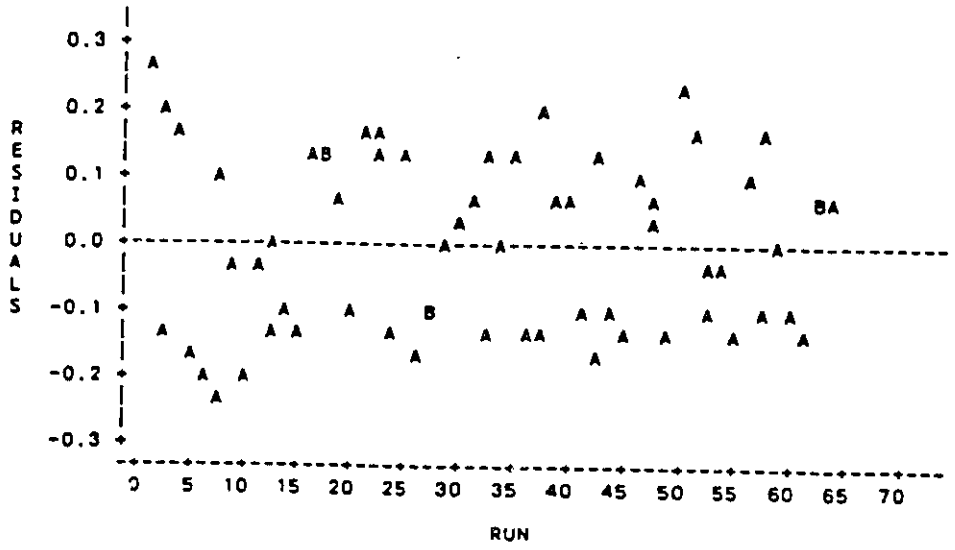

Fig. 65 - Residual plots for model G.*

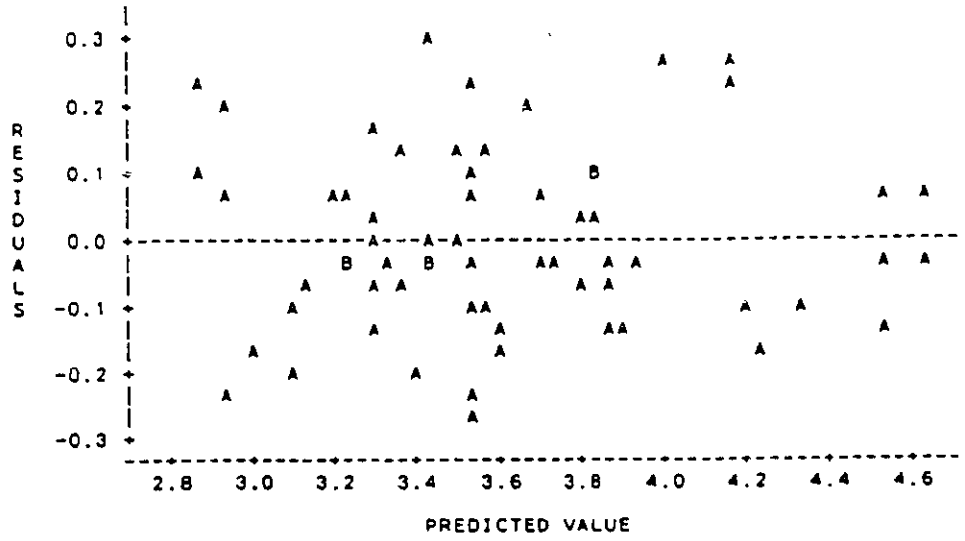

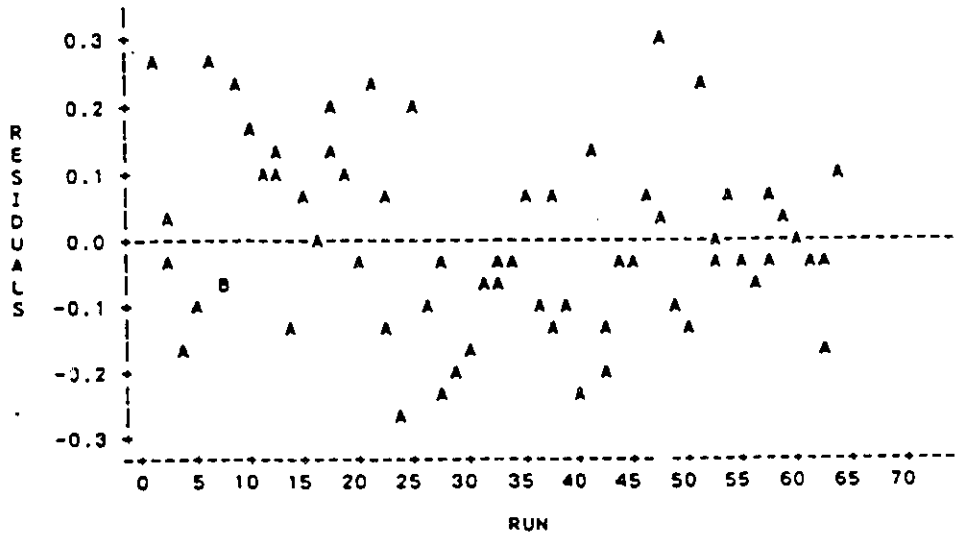

Fig. 66 - Residual plots for model H.

* A: 1 OBS, B: 2 OBS, C: 3 OBS, etc...

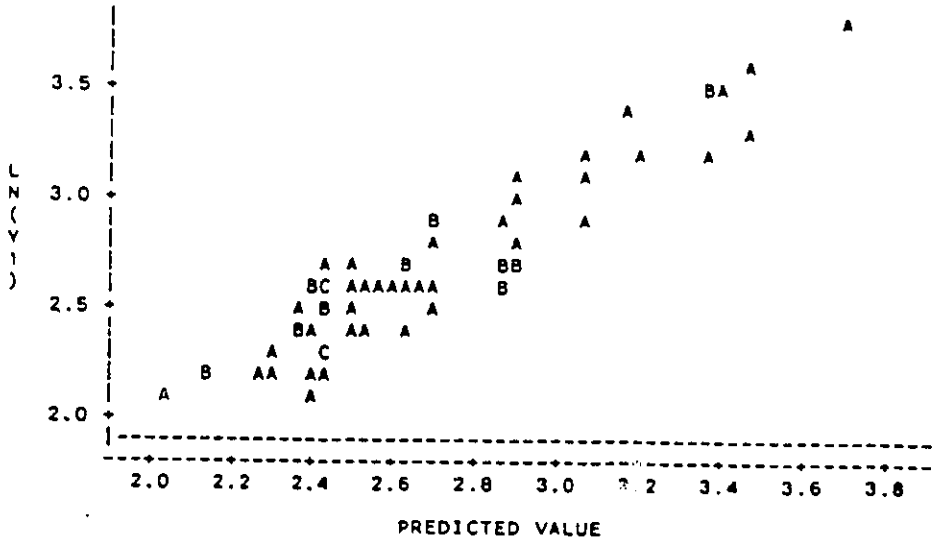

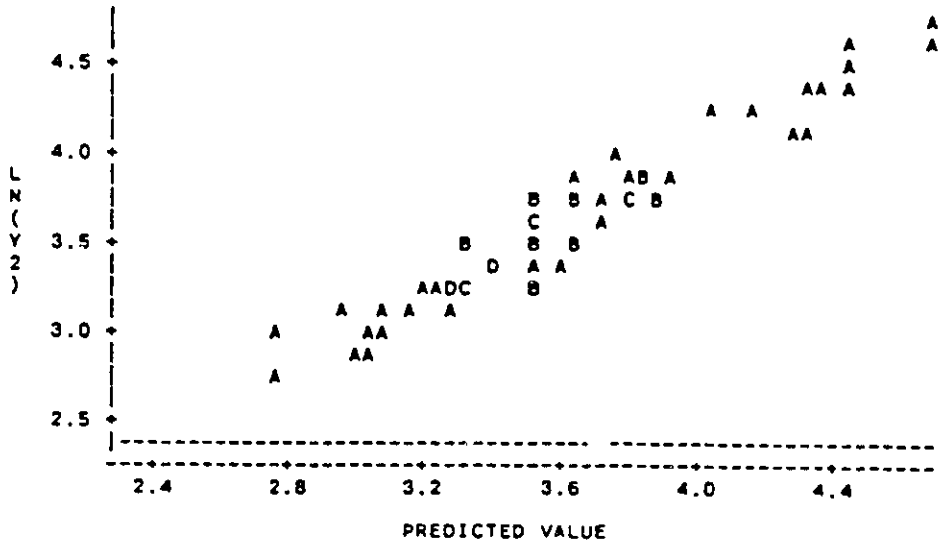

Fig. 67- Plot of observed VS. predicted values for models E and F.*

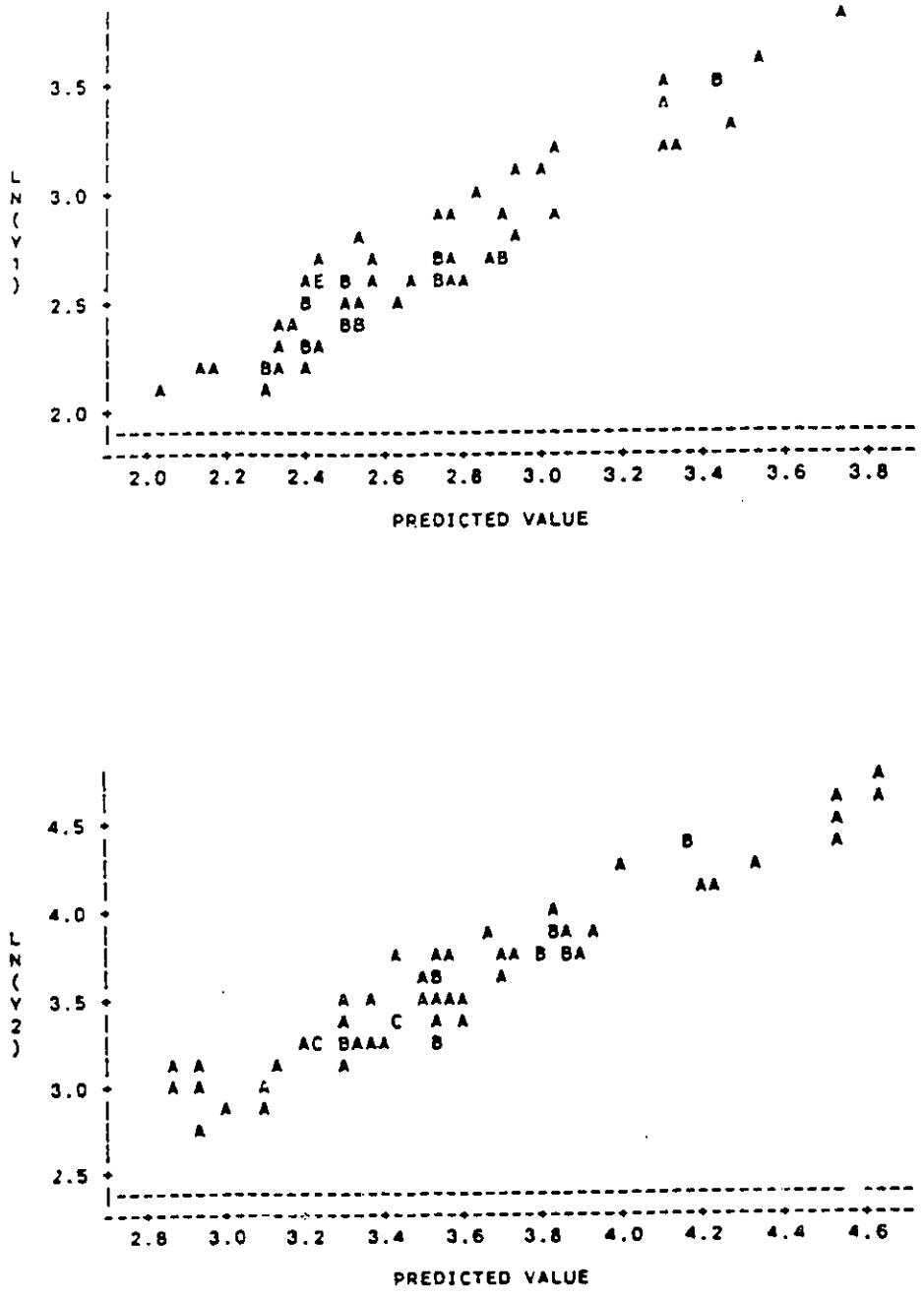

Fig. 68- Plots of observed VS. predicted values for models G and H.*

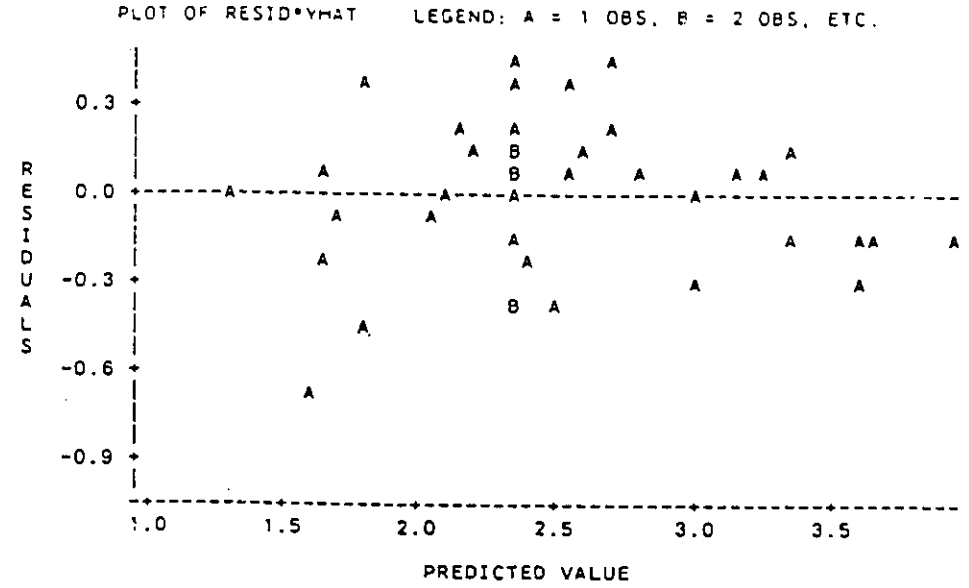

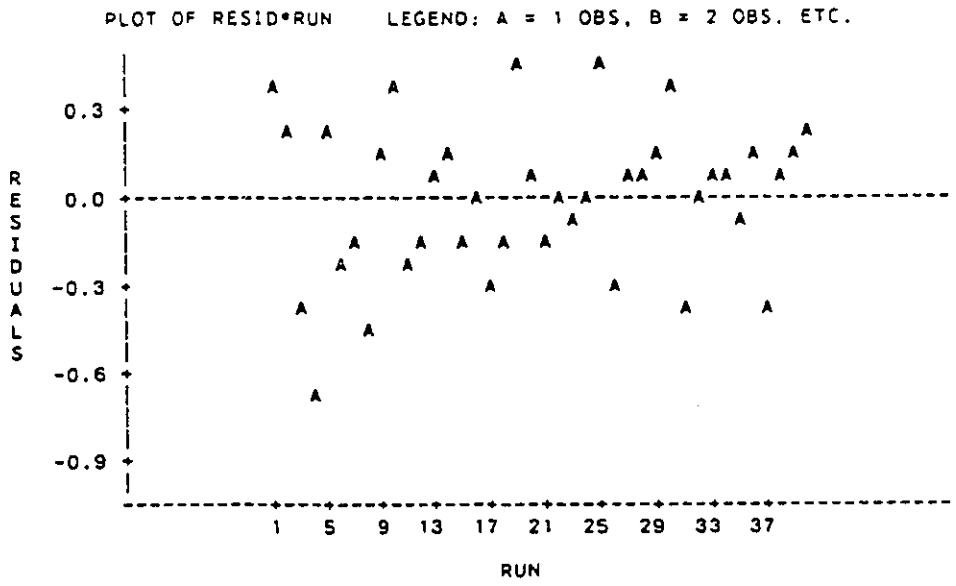

Fig. 69- Residual plots for model I.

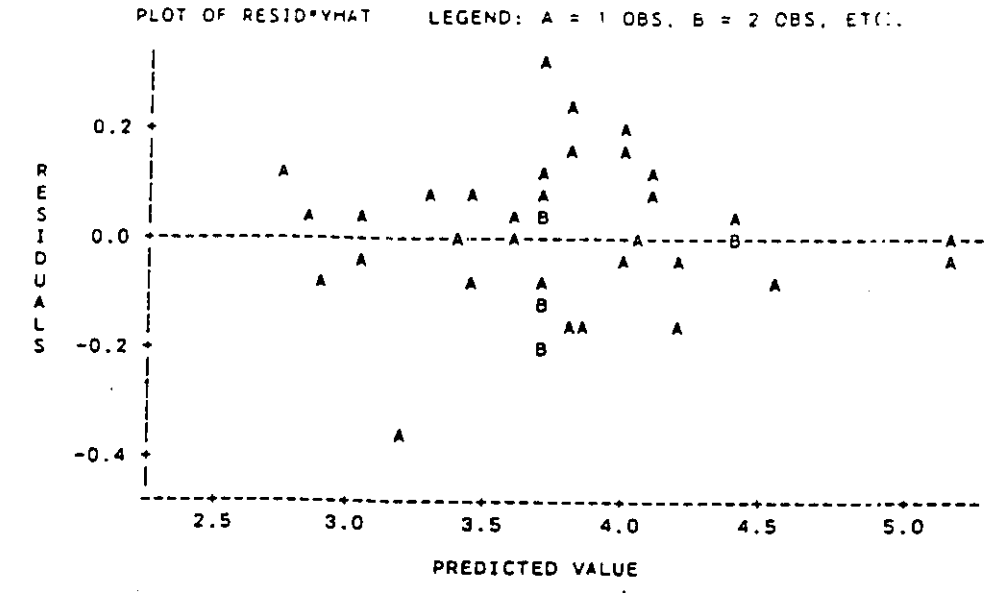

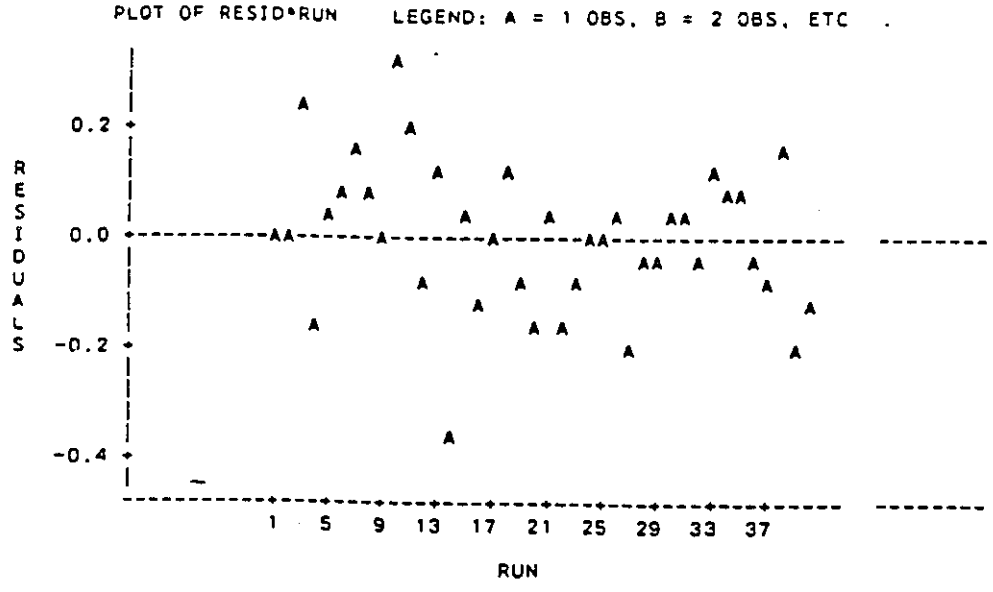

Fig. 70- Residual plots for model J.

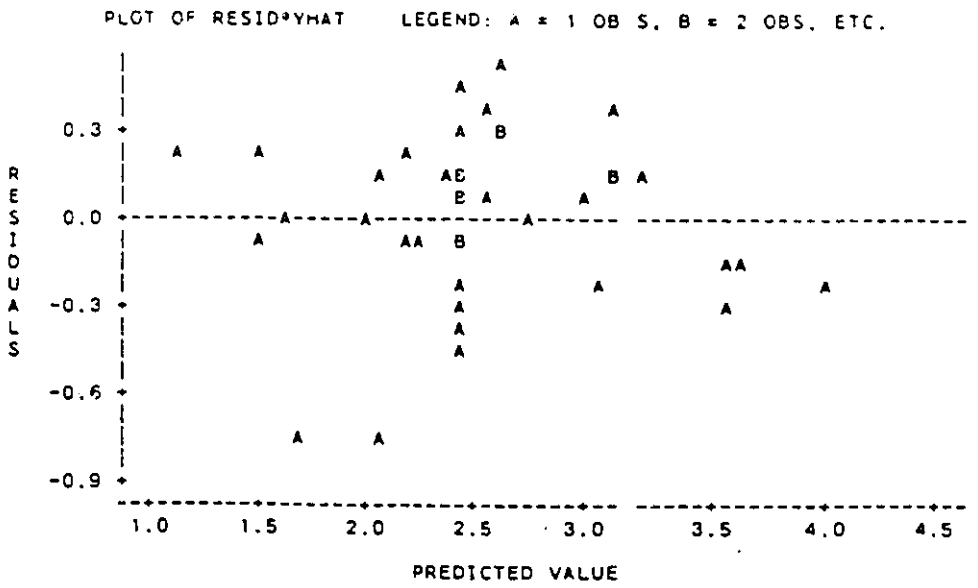

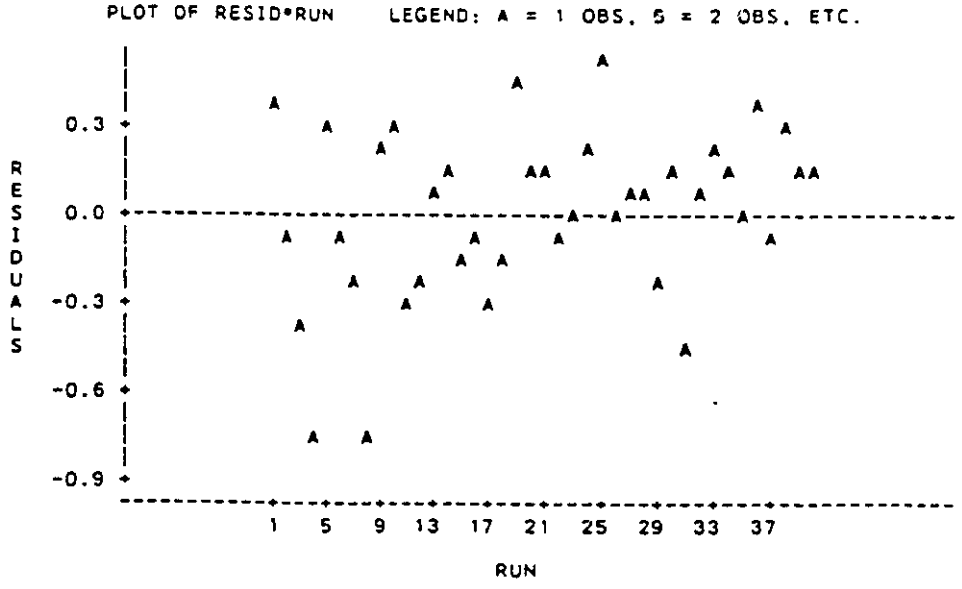

Fig. 71- Residual plots for model K.

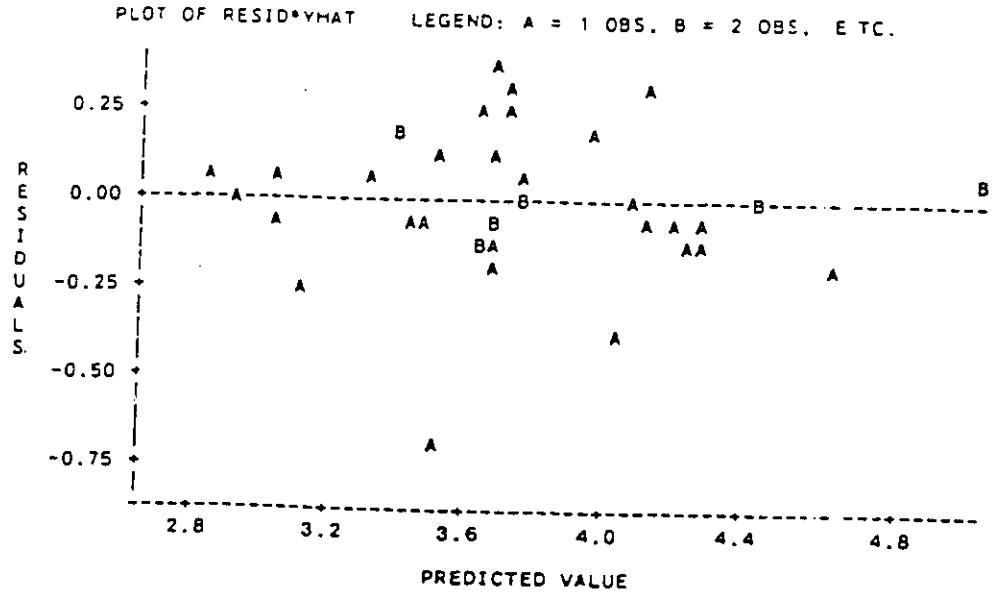

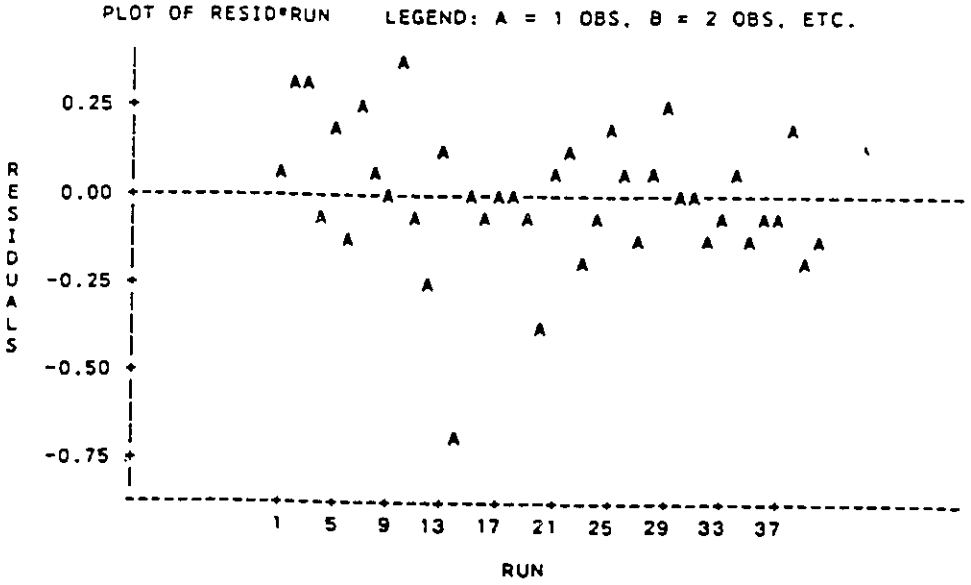

Fig. 72- Residual plots for model L.

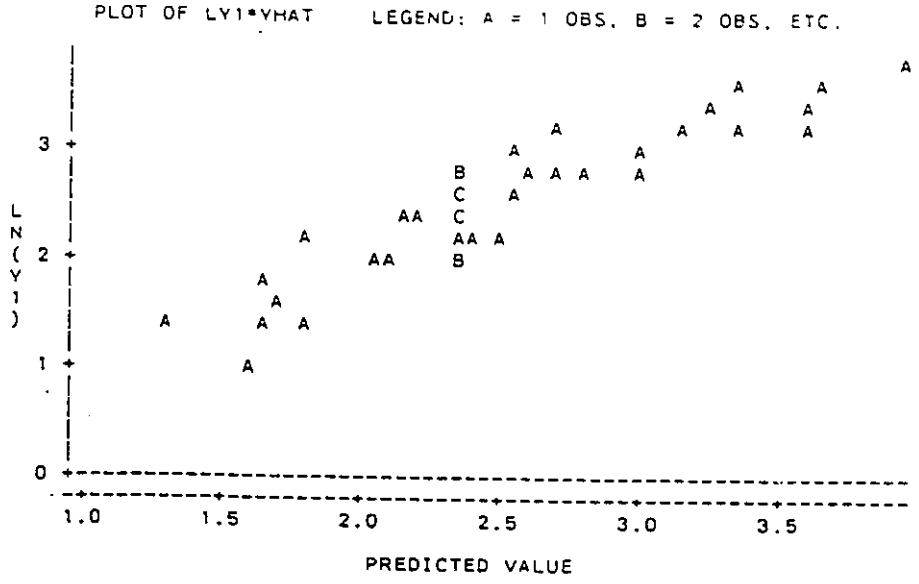

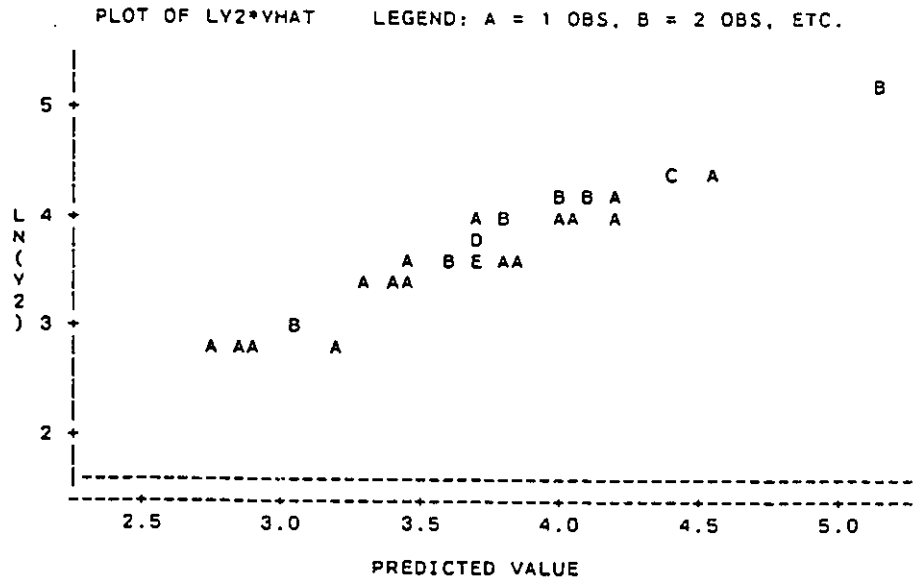

Fig. 73- Plots of observed VS. predicted values for models I and J.

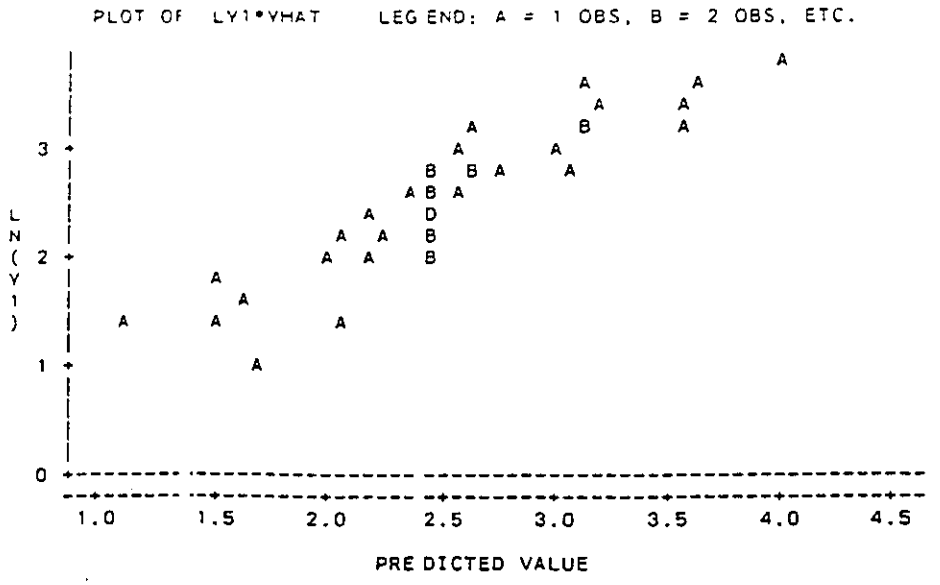

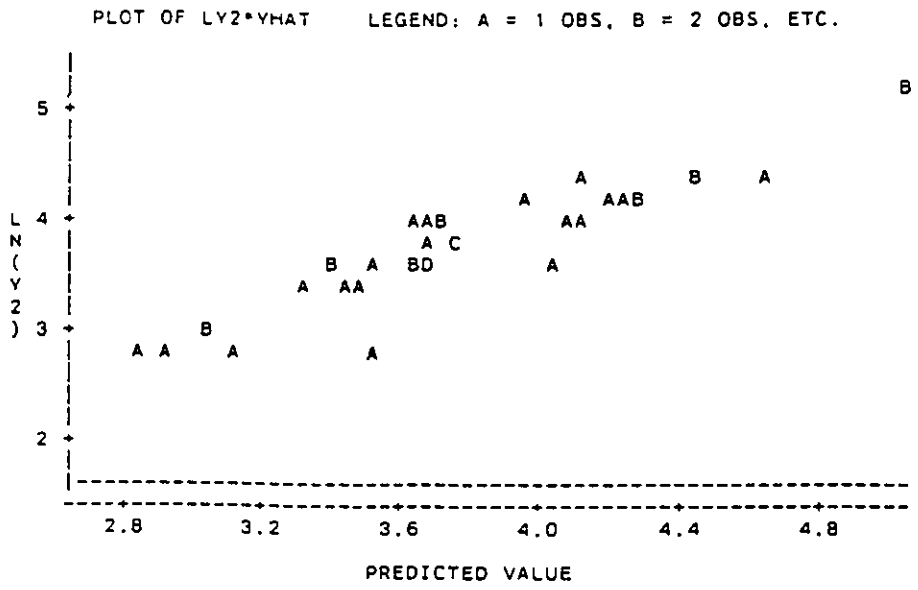

Fig. 74- Plots of observed VS. predicted values for models K and L.

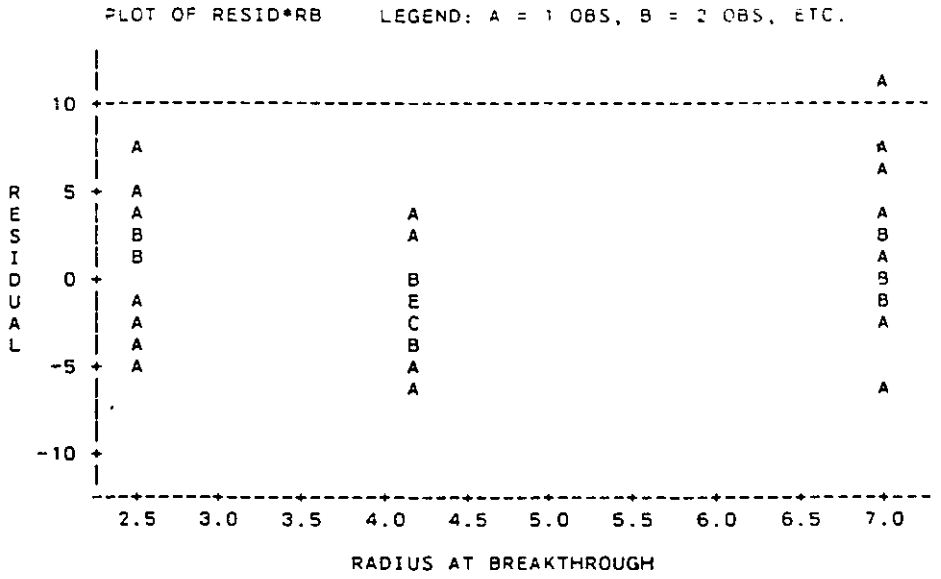

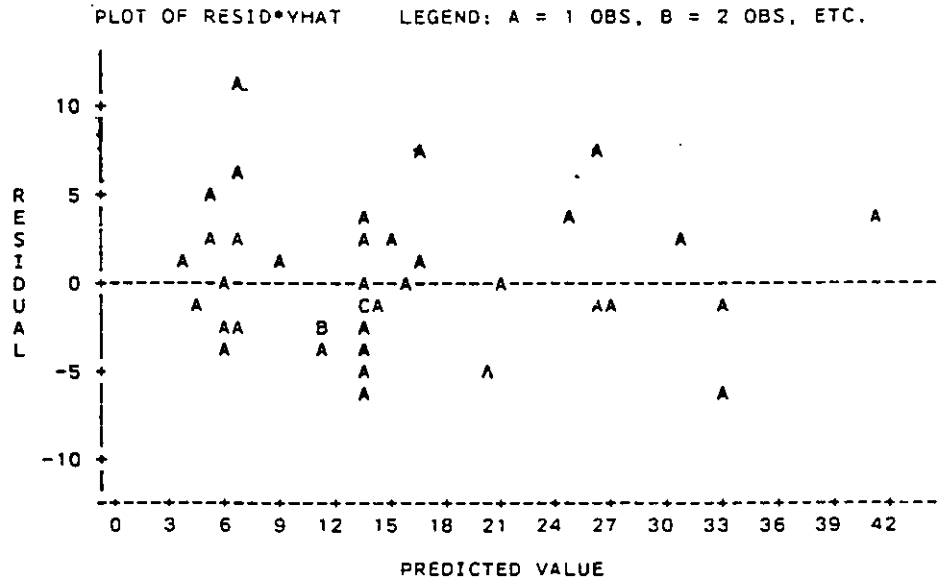

Fig. 75- Residual plots for model I (Non-linear).

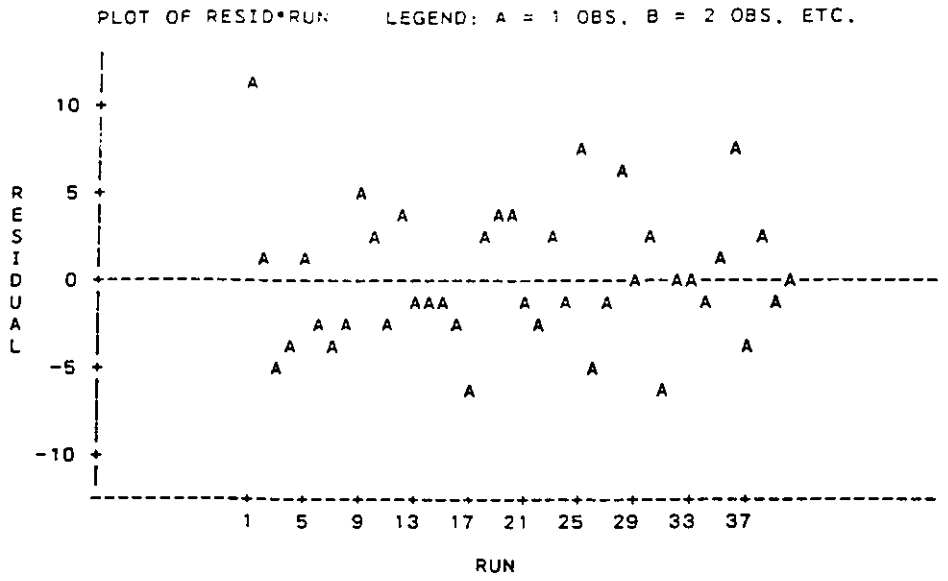

Fig. 76- Residuals vs. run order for model I'.

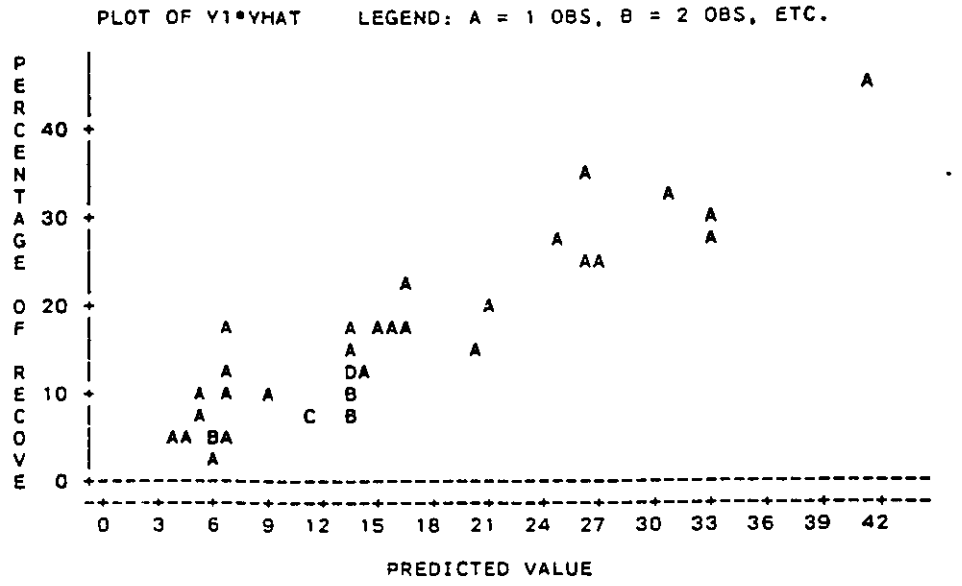

Fig. 77- Observed vs. predicted value for model I'.

APPENDIX B

Absolute Permeability Measurements

Darcy's law was used to develop a formula to predict absolute permeability in the case of radial flow in a cell made of glass beads sandwiched between two glass plates (see Fig. 20)

Darcy's Law:

$$V_r = \frac{Q}{A} = -\frac{k}{\mu}\frac{dP}{dr} \qquad (A)$$

The flow rate Q could be written in terms of h, the liquid light in the small tube and t, the time.

$$Q = -a\frac{dh}{dt} \qquad (B)$$

where $a = \pi R_1^2$ is the area of the small tube.

On the other hand,

$A = W(2\pi r)$

$$\frac{Q(t)}{2\pi W r} = -\frac{K}{\mu}\frac{dP}{dr} \qquad (C)$$

Knowing that $A = f(r)$

$V = f(r)$

$Q = f(t)$

Integration yields

$$\frac{Q(t)}{2\pi W}\int_{R_1}^{R_2}\frac{dr}{r} = -\frac{K}{\mu}\int_{P_1}^{P_2} dP \qquad (D)$$

$$\frac{Q(t)}{2\pi W}\left(\frac{R_2}{R_1}\right) = -\frac{K}{\mu}(P_2 - P_1) \qquad (E)$$

Since only a single fluid is considered, the static pressure p is zero and $P = p - \rho g h = -\rho g h$.

Substitution gives,

$$-\frac{R_1^2}{2w\rho g}\frac{dh}{h}\ln\left(\frac{R_2}{R_1}\right)=\frac{K}{\mu}dt \qquad (F)$$

Integration yields,

$$-\frac{R_1^2}{2w\rho g}\int_{h_o}^{h(t)}\frac{dh}{h}\ln\left(\frac{R_2}{R_1}\right)=\frac{K}{\mu}\int_o^t dt \qquad (G)$$

$$-\frac{R_1^2}{2w\rho g}\ln\ (h(t)/h_o)\ \ln\ (\frac{R_2}{R_1})=\frac{K}{\mu}t \qquad (H)$$

Then K the permeability is

$$K=\frac{R_1^2\mu}{2tw\rho g}\ln\ (\frac{h_o}{h(t)})\ \ln\ (\frac{R_2}{R_1}) \qquad [=]\ L^2 \qquad (I)$$

APPENDIX C

Results For Non-Linear Models

Table 14

Parameter Estimates and Pertinent Statistics for Recovery Models Based on Eqn. 77

Model	θ_0	θ_1	θ_2	θ_3	θ_4	θ_5	$\frac{SSR}{n-p}$	$\tilde{\sigma}_p^2$	lack of fit ratio	$F_{0.05}$ $F_{0.01}$
MODEL A' N = 55 N_p = 5 Capillary region	15.484 ± 12.352	-----	1.147 ± 0.285	-0.481 ± 118	0.147 ± 0.129	-0.065 ± 0.046	93.17	39.26	3.54	1.98 2.66
MODEL E' N = 64 N_p = 4 Intermediate region	57.233 ± 21.420	-----	0.253 ± 0.160	-0.409 ± 0.085	-----	-0.096 ± 0.360	22.016	4.70	8.37	1.84 2.38
MODEL I' N = 40 N_p = 5 Viscous region	79.700 ± 48.18	-----	0.267 ± 0.018	-0.669 ± 0.126	0.125 ± 0.098	-0.071 ± 0.040	17.13	7.75	2.93	2.44 3.63

Table 15

Parameter Estimates and Pertinent Statistics for Models Predicting the Number of Fingers Based on Eqn. 77

Model	θ_0	θ_1	θ_2	θ_3	θ_4	θ_5	$\frac{SSR}{n-p}$	$\hat{\sigma}_p^2$	lack of fit ratio	$F_{0.05}$ $F_{0.01}$
MODEL B' $N = 55$ $N_p = 4$ Capillary region	2.965 ± 1.515	0.178 ± 0.091	0.679 ± 0.210	0.162 ± 0.083	-----	-----	27.49	2.49	19.30	1.97 2.64
MODEL F $N = 64$ $N_p = 5$ Intermediate region	13.904 ± 5.002	0.135 ± 0.057	1.016 ± 0.115	0.088 ± 0.037	-0.366 ± 0.049	-----	39.79	10.85	6.43	1.85 2.39
MODEL J' $N = 40$ $N_p = 5$ Viscous region	18.598 ± 9.076	-----	0.771 ± 0.160	0.289 ± 0.062	-0.347 ± 0.076	-0.103 ± 0.032	102.92	13.47	11.56	2.44 3.63

Table 16

Parameter Estimates and Pertinent Statistics for Recovery Models Based on Eqn. 78

Model	θ_0	θ_1	θ_2	θ_3	θ_4	$\frac{SSR}{(n-p)}$	$\hat{\sigma}_p^2$	lack of fit ratio	$F_{0.05}$ $F_{0.01}$
MODEL C' $N = 55$ $N_p = 4$ Capillary region	5.492 ± 5.434	-0.038 ± 0.037	-----	1.112 ± 0.293	-0.482 ± 0.128	101.441	39.26	3.88	1.97 2.64
MODEL G' $N = 64$ $N_p = 3$ Intermediate region	31.767 ± 14.106	-----	-----	0.250 ± 0.150	-0.412 ± 0.068	20.16	4.70	7.47	1.83 2.37
MODEL K' $N = 40$ $N_p = 4$ Viscous region	96.486 ± 34.049	-0.068 ± 0.033	-----	0.232 ± 0.167	-0.637 ± 0.110	15.71	7.75	2.61	2.43 3.62

Tab. 17

Parameter Estimates and Pertinent Statistics for Models Predicting the Number of Fingers Based on Eqn. 78

Model	θ_0	θ_1	θ_2	θ_3	θ_4	$\frac{SSR}{(n-p)}$	$\hat{\sigma}_p^2$	lack of fit ratio	$F_{0.05}$ $F_{0.01}$
MODEL D' N = 55 $N_p = 4$ Capillary region	1.275 ± 0.978	0.058 ± 0.034	-----	0.675 ± 0.228	0.192 ± 0.106	31.346	2.49	22.11	1.97 2.64
MODEL H' N = 64 $N_p = 5$ Intermediate region	0.012 ± 0.009	0.150 ± 0.064	0.732 ± 0.108	1.029 ± 0.125	0.064 ± 0.040	46.96	10.85	7.77	1.85 2.39
MODEL L' N = 40 $N_p = 3$ Viscous region	-----	0.161 ± 0.028	-----	0.660 ± 0.140	0.277 ± 0.76	184.33	13.47	20.55	2.42 3.59